A STUDY OF RIDE COMFORT PERFORMANCE OF OCCUPANT ON CAR SEAT EXPOSED TO WHOLE-BODY VIBRATION

Tingsheng Tang

A thesis

in

the Department

of

Mechanical Engineering

Presented in Partial Fulfillment of the Requirements

For the Degree of Master of Applied Science at

Concordia University

Montreal, Quebec, Canada

August 2002

ABSTRACT

A Study of Ride Comfort Performance of Occupant on Car Seat

Exposed to Whole-Body Vibration

Tingsheng Tang

The perception of whole-body vibration and automotive driver/passenger comfort is strongly influenced by the static and dynamic properties of the seat. The analysis of comfort performance of the polyurethane foam (PUF) seats poses considerable challenges due to nonlinear properties of PUF and complex biodynamic response behavior of the human body. In this dissertation, the static and dynamic properties of three PUF seats are characterized in the laboratory under a wide range of preloads and excitation conditions. The measured data are analyzed to determine the stiffness and damping models of the seats as a function of the preload, and relative deflection and relative velocity of the cushion. The models thus derived are analyzed to study the vibration transmission performance of PUF seats loaded with a rigid mass under broadband as well as road-measured random excitation. Laboratory experiments are performed to evaluate vibration responses of the seat-rigid mass system and the data are used to examine the validity of the proposed models under the wide range of conditions considered. The analytical model of the seat-rigid mass system resulted in good agreements with the measured data in terms of acceleration transmissibility. A number of performance measures are formulated to assess the vibration isolation effectiveness of the seat. These included the true and frequency weighted rms acceleration, S.E.A.T. (Seat Effective Amplitude Transmissibility) values, and peak acceleration. A parametric study is carried out to study the influence of stiffness and damping gains, body-weight, frequency and relative

deflection dependence of the PUF stiffness and damping on the vibration isolation effectiveness. Analytical models of the seat-occupant systems are developed by incorporating four different biodynamic human body models, reported in the literature, into the nonlinear seat model. Laboratory experiments are also performed with one subject to experimentally derive the vibration transmissibility characteristics of the seat-occupant system. The analytical response characteristics of the seat-occupant systems are compared with the measured response to assess the validity of the models. The results revealed reasonably good agreement between the measured and computed response characteristics under certain excitations, but considerable deviation was observed under other excitation. The three degree-of-freedom seated human body model, proposed in the literature, is further tuned to satisfy the measured apparent mass (APMS) and seat transmissibility characteristics in order to account for the body coupling with the deformable cushion. The validity of the proposed model is demonstrated by comparing its response characteristics with the measured data.

ACKNOWLEDGEMENTS

I must first express my sincere gratitude to my supervisors, Dr. Subhash Rakheja and Dr. Paul-Émile Boileau, for their initiation of the project and their constant guidance and dedication throughout the realization of the thesis work, including experimental work, valuable advice and contributions, as well as patience I shall not forget.

I would like to acknowledge the support provided by the technicians, the friends and the colleagues during the test and data processing.

I wish to thank various researchers whose data and conclusions have been employed in this study.

Financial support provided by Concordia Graduate Fellowship and the Institut de recherche Robert-Sauvé en santé et en sécurité du travail du Québec (IRSST) scholarship are gratefully acknowledged.

Finally, I would like to express my appreciation to my wife, Guangli, who provides general encouragements, understanding and assistance in the completion of this thesis work, especially in the final stage. I dedicate this thesis to her and my son Yinan.

TABLE OF CONTENTS

LIST OF FIGURES

LIST OF TABLES

LIST OF ABBREVIATIONS AND SYMBOLS

ABBREVIATIONS

APMS	Apparent mass
BS	British Standard Institution
D/A	Digital to Analog
dB	Decibel
DPMI	Driving-point mechanical impedance
DOF	Degree-of-freedom
DRI	Dynamic Response Index
FFT	Fast Fourier Transform
HP	High pass
ISO	International Standard Organization
LP	Low pass
LVDT	Linear variable differential transformer
MTVV	Maximum transient vibration value
PSD	Power spectral density
PUF	Polyurethane foam
rmq	Root-mean-quad
rms	Root-mean-square
SAE	Society of Automotive Engineers
S.E.A.T.	Seat Effective Amplitude Transmissibility
STHT	Seat-to-head transmissibility
WBV	Whole-Body Vibration

WBVVS	Whole-Body Vehicular Vibration Simulator

SYMBOLS

A	the excitation amplitude (m)
A_i	the deflection amplitude of the i^{th} measured data (m)
a_1	stiffness gain
a_2	the preload dependence of the stiffness
a_3	relative velocity and deflection dependence of the stiffness
a_4	the relative deflection dependence of the stiffness constant
a_{rms}	The rms of acceleration (m/s^2)
a_{rms_time}	The rms of acceleration in the time domain (m/s^2)
a_{rms_freq}	The rms of acceleration in the frequency domain (m/s^2)
$a_{w\cdot rms}$	The rms of frequency-weighted acceleration (m/s^2)
$a_{w\cdot peak}$	The peak value of frequency-weighted acceleration (m/s^2)
$a_{w\cdot rms\_time}$	The rms of frequency-weighted acceleration in the time domain (m/s^2)
$a_{w\cdot rms\_freq}$	The rms of frequency-weighted acceleration in the frequency domain (m/s^2)
b_1	damping coefficient gain
b_2	preload dependence of the seat damping

b_3	relative velocity and deflection dependence of the seat damping
b_4	the relative deflection dependence of the seat damping
C	the damping coefficient of a seat cushion (Ns/m)
c_{den}	the damping in the case of big deflection (Ns/m)
c_{eq}	the equivalent viscous damping coefficient (Ns/m)
d_1 to d_7	the model parameters coefficients of frequency response function
f	frequency of excitation (Hz)
f_c	the center frequency of the frequency band (Hz)
f_i	the frequency of the i^{th} measured data (Hz)
f_l	the lower limits of the frequency band (Hz)
f_u	the upper limits of the frequency band (Hz)
F(x)	the measured cushion force (N)
$H(j\omega)$	the complex transfer function of the seat
$H(jf)$	frequency response function
$H^*(s)$	a model of frequency response function
K	stiffness coefficient of a seat cushion (N/m)
k_{den}	the stiffness in the case of big deflection (N/m)
k_{eq}	the equivalent stiffness coefficient (N/m)
k_i	the stiffness of the i^{th} measured data (N/m)
n	the number of measured data

$S_{\ddot{x}_o}$	the auto power spectral density of the seat acceleration response $\ddot{x}_o$ ($(m/s^2)^2/Hz$)
$S_{\ddot{x}_o\ddot{x}_i}$	the cross-spectral density of the seat acceleration response and seat pan acceleration $\ddot{x}_i$ ($(m/s^2)^2/Hz$)
$S_x(jf)$	the power spectral density of the measured/synthesized acceleration ($(m/s^2)^2/Hz$)
$S_y(jf)$	the power spectral density of the white noise excitation ($(m/s^2)^2/Hz$)
T	the measurement duration (s)
$\ddot{x}_o$	the seat acceleration response (m/s^2)
$\ddot{x}_i$	seat pan acceleration (m/s^2)
$\ddot{x}_w(t)$	the instantaneous frequency-weighted acceleration (m/s^2)
W	preload (N)
W_i	the preload of the i^{th} measured data (N)
λ_1	the weighting factors applied to the apparent mass modulus
λ_2	the weighting factors applied to the apparent mass phase
ψ	the weighting factor applied to the seat-to-body transmissibility
ΔE	the energy dissipated per cycle of vibration (Nm)
ω	the excitation frequency (rad/s)

1 INTRODUCTION AND SCOPE OF DISSERTATION

1.1 General

The assessment of automotive seating comfort characteristics is a highly complex task due to excessive inter-subject variations, such as the body sizes, weights and preference, and variation in the driving environments. The subjective perception experienced by the driver/passenger is associated directly with the level of comfort. Since the driver's/passenger's perception of comfort is related to the seat design, the enhancement of comfort properties of automotive seats forms an important design objective. However, many factors, which include design factors, environment factors and subjects' factors, affect the comfort performance of automotive seats. The comfort performance of the seat may be further influenced by the seat-occupant interactions and the surrounding environment, such as visual field, ability to reach control panel, interior space, hand hold, temperature and humidity of environment, noise, vibration, individual factors, subject posture and so on. Among all of these factors, vibration transmitted to the occupant through the seat is one of the most important factors related to the overall perception of the comfort.

Whole-body vibration (WBV) occurs when the body is supported on a surface which is vibrating. The human occupant on a car seat is the most typical example of exposure to whole-body vibration. The vibration transfers to the seated occupant from the supporting seat surface, the seat-back, the steering wheels, and the feet, along all three translational and rotational axes [1]. A good seat has been defined as one that (i) gives good support to the driver and passengers in every driving situation; (ii) reduces the

transmission of vibration from the car to the body of the driver and the passengers; and (iii) provides comfortable seating with respect to temperature and humidity [2]. It has been reported that the vertical component of vibration transmitted to the seat is usually the highest after the frequency and the axis weightings are applied [3,4]. Paddan and Griffin [5] studied vibration affects on the different human subjects and the same human subject in different directions. The study concluded that seat to body transmissibility is greatest along the z-axis, as shown in Figure 1.1.

Consequently, the assessment of vertical vibration transmission performance of the seat under representative excitations arising from the tire-road interactions is vital to achieve the design objective of enhancing the occupant comfort. The ride comfort performance in this dissertation thus refers to the nature of vertical vibration transmitted to the occupant on the car seat and exposed to the whole body vibration. In view of the quality of the road surface on which the people have to travel, they may be submitted to significant levels of vibration and shock that arise primarily from the tire-terrain interactions, the intensity of which is dependent on the road profile, the speed, the quality of the vehicle primary suspension and of the seat ability to attenuate the vibration. Even though the tolerance of the humans to the same level of vibration varies from individual to individual, the frequency dependence shows the same functional dependence and displays a marked increase in the sensitivity in the region of 2 –10 Hz [57]. It is well known that vibration in most automotive vehicles is predominant in the 0.5 to 10 Hz frequency range and that levels of exposure of as high as 1 m/s^2 may be encountered.

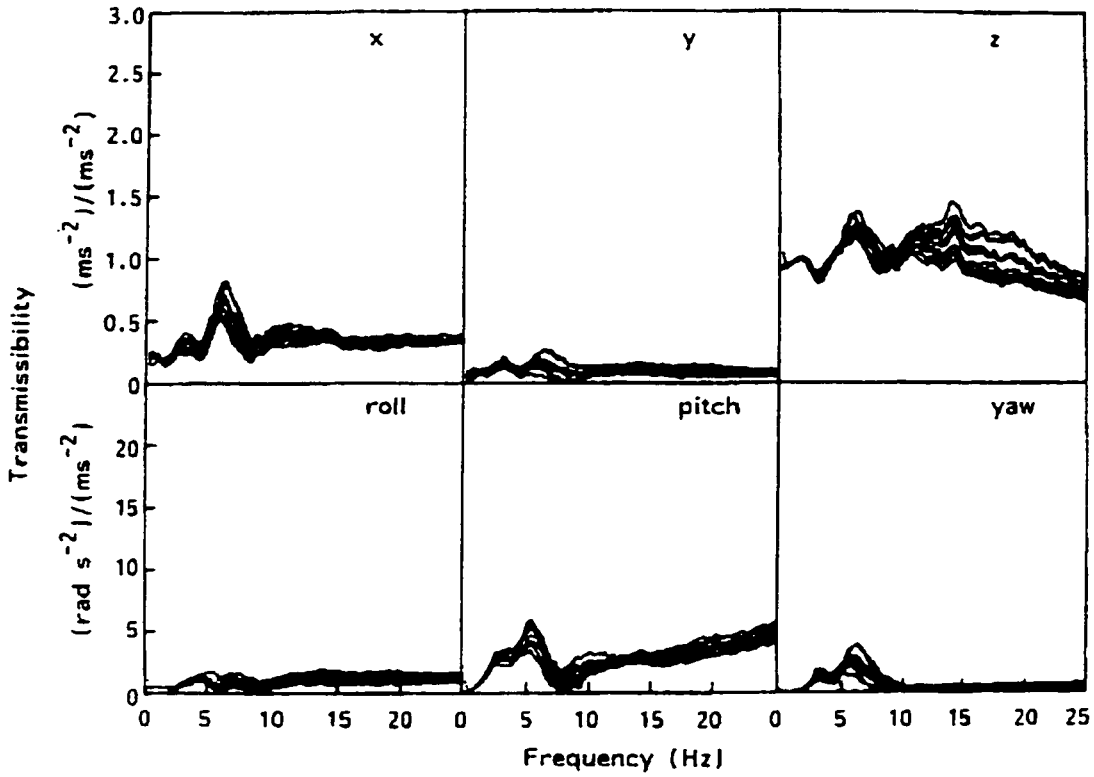

Figure 1.1: Variations in the transmission of vertical seat vibration to the body of a single subject measured on 12 separate occasions [5] respectively.

Exposure to such vertical whole body vibration has been known to interfere with the occupant's comfort, work efficiency and health. Many chronic health effects have been associated with prolonged exposure to whole-body vibration. These include disorders of the spine, abdominal pain, digestive and vision problems, etc. [1,4,6,7].

The dynamic responses of the human body on the seats to vertical whole-body vibration and shock have been investigated experimentally for more than four decades. The development of an understanding of the side effects of whole-body vibration on the human body involves study of the mechanical, psychological, physiological and pathological responses. Even so, complex nature of the human body and complicated

visco-elastic properties of seats have prevented a clear understanding of the form of the dynamic response of the body. Understanding of the mechanical responses of the human body and nonlinear properties of the seats are essential to reduce the undesirable effects on the ride comfort and the feelings of occupants caused by vibration. A number of studies have investigated the dynamic properties of the human body and the seat. One of the objectives of the seat designer is to achieve an overall reduction in vibration discomfort of the seat-occupant compared with the discomfort that would be experienced with a rigid seat [4].

Owing to the complexities associated with the human perception of comfort and response to vibration, and static and dynamic properties of polyurethane foam (PUF) seats, the comfort assessments are mostly performed through subjective and objective tests [4,24]. The latter is frequently considered more desirable since the former yields inconsistent results due to excessive variations in the individuals' preferences. The objective methods are employed in to the field as well as laboratory measurements. The field measurement methods, however, involve high cost, lack of repeatability, and uncontrolled conditions, and thus are justified when only limited number of tests is required. Alternatively, the laboratory-based methods yield more consistent measures under controlled conditions.

In general, subjective evaluations yield considerable data on relative ride ranking and don't provide quantitative information to the designer. Furthermore, it is considered to be complex and expensive, specifically when repetitive tests need to be performed with a large number of seats. The subjective evaluations, however, can be effectively used to obtain ride perception when relatively small number of prototype seats is involved. This

method is used to obtain general qualitative view for ride comfort as the first step in design procedure.

Objective methods propose direct measures of physical quantities, such as displacement, force, and acceleration [4,24], often yield quantitative information for the designer. The experiment-based objective methods, however, also pose considerable difficulties and concerns. These include the high cost associated with repetitive tests with large number of subjects and data analysis, and ethical concerns related to human exposure to vibration. Alternatively, few attempts have been made to develop analytical models of automotive seats, such that the number of field and laboratory trials could be limited to a minimum.

In an effort to improve the vibration comfort of automobile occupants, many car manufacturers have been made increasingly aware of the importance of better designing the car seats to reduce exposure to vibration. While several efforts have been made to identify polyurethane foams with better vibration attenuation properties, an objective assessment of vibration attenuation performance of such seats requires the consideration of contribution due biodynamics of the seated occupant to whole-body vibration. It is thus vital to assess the comfort performance of seats loaded with human occupant when either field or laboratory methods are used. For the design purposes, such a procedure may be considered cumbersome, since any alterations of the seat would most likely be followed by a series of measurements to assess the influence of the changes on the overall attenuation performance. Alternatively, development of suitable models representing both the seat and the occupant offers the possibility to assess the impact of any modifications on the basis of simulation results, that may be supplemented by only

few tests. Development of an analytical model of the seat involves two distinct tasks: (i) modeling the static and dynamic properties of the PUF seat; and (ii) modeling the seated occupant.

While modeling techniques have been successfully applied to represent the biodynamic responses of the human body exposed to whole-body vibration, suitable biodynamic models capable of representing automobile occupants and postural constraints are still lacking. The biodynamic response characteristics of the human body are known to be influenced by several factors, including subject weight, posture, backrest support, feet and hand position, vibration excitation type and level, etc. While most current biodynamic models have been derived on the basis of measured biodynamic response functions, the conditions associated with the development of these models have often been very different from those that would apply to automobile drivers. Most of the seated occupant models have been derived from biodynamic response of subjects seated with no back support, exposed to relatively high magnitudes of vibration. The reported models may thus be considered not likely applicable to automobile occupants which involve a seated posture with fully supported back with an inclined backrest and seat pan, with hands either in lap or in a driving position, subjected to significantly lower vibration excitation levels.

The PUF seat cushions are known to yield highly nonlinear static and dynamic properties that are highly dependent upon the seated body weight and nature of excitation (frequency and stroke). Although a number of studies have attempted to characterize the static and dynamic properties of PUF cushion, only limited evidence exist on the validity of the resulting models.

In this dissertation research, the static and dynamic properties of selected PUF cushion are explored to derive nonlinear models, which are validated for a range of selected body weights and excitations. The reported biodynamic models are applied to derive a couple seat-occupant model. The validity of the resulting model is explored through comparisons with the measured data. A modified biodynamic model is proposed to effectively carry out the vibration attenuation performance of automotive seats.

1.2 Literature Review

The reported studies relevant to human comfort perception, assessment methods, characterization of PUF seats and biodynamics of the seated occupant are reviewed. The highlights of these studies are briefly discussed below in order to gain knowledge and formulate the scope of the dissertation research.

1.2.1 Analysis of comfort performance

The comfort performance of a seat is mostly evaluated through either laboratory or field measurements. The 'measurement' involves the assignment of numerical values according to some rules, while the 'evaluation' results in some indication of the relative or absolute worth, value or severity. Vibration measurement may therefore make use of mathematical procedures which do not necessarily indicate vibration severity or discomfort. The evaluation of vibration with respect to human response involves the use of procedures which, by some means, provide an indirect measure of severity of vibration exposure. Conceptual illustration of the measurement and evaluation of vibration with respect to human response is shown in Figure 1.2. The evaluation, however, may involve

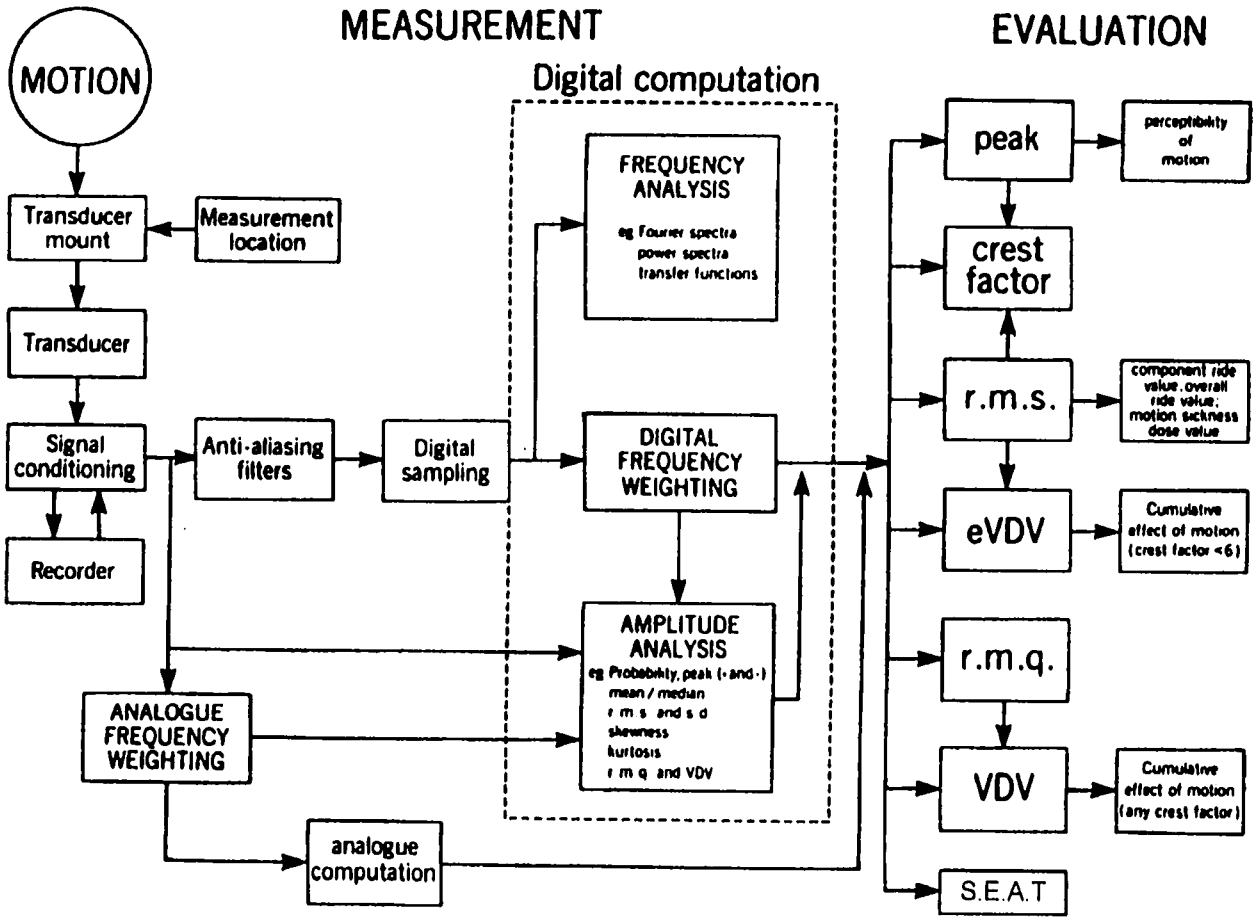

Figure 1.2: Conceptual illustration of the measurement and evaluation of vibration with respect to human response.

Different objective measures are defined in terms of frequency-weighted root mean square (rms) or root-mean-quad (rmq) acceleration, and seat-effective amplitude transmissibility (S.E.A.T.). The methods for deriving these measures and their interpretation are documented in standards, which are briefly summarized below.

International Standard ISO 2631-1

Presently, the most commonly used standard for evaluating human exposure to WBV and shock is the International Standard ISO 2631-1 (1997) developed by the International Standards Organization (ISO). This standard defines the frequency weighting functions, which account for the variation of human sensitivity to vibration frequency. The frequency weighting procedure implies that human response to WBV is not only related to magnitude but also to the frequency of the vibration. The purpose of the frequency weighting procedure is to compensate and to normalize for differences in human susceptibility and sensitivity at different frequencies. Figure 1.3 presents the frequency-weighting curve for principal weighting, W_k, which applies to vibrations in the vertical direction in order to assess health and comfort effects on seats. The standard also presents the main vibration exposure assessment methods based on frequency-weighted rms acceleration measured at the point of entry of the vibration in the body. This method must be complemented with additional assessment methods including a fourth power vibration dose value of acceleration (VDV), and /or a maximum transient vibration value (MTVV) to emphasize the added influence of transient vibration and high amplitude shock events. Evidently, the International Standard ISO 2631-1 (1997) [1] provides guidance on comfort and health risk based on the frequency-weighted rms

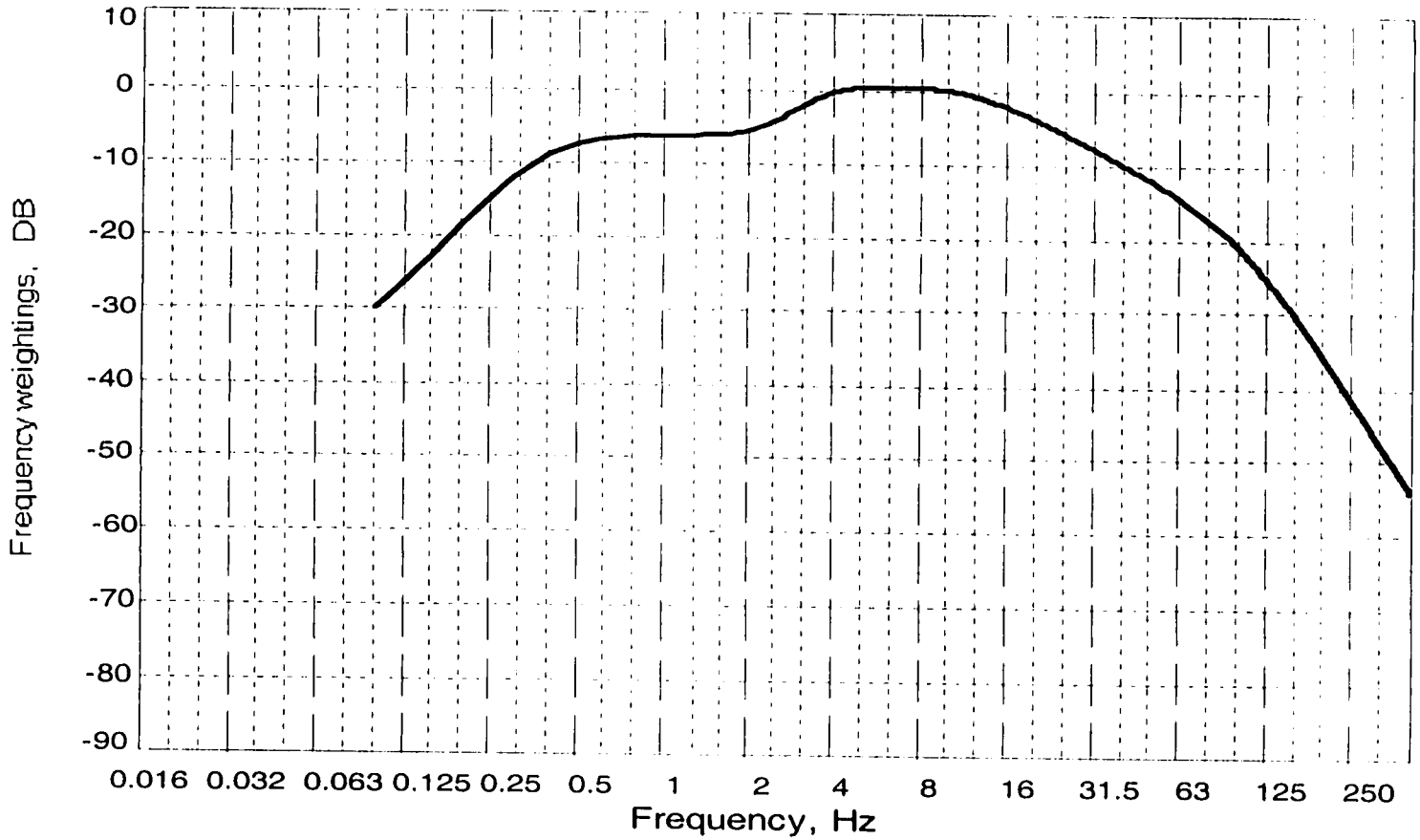

Figure 1.3: Frequency weighting curve for principal weighting, W_k, proposed in ISO 2631-1 (1997).

acceleration measured within the frequency range of 0.5 to 80 Hz at the seat-subject interface for a seated individual subjected to continuous broad-band vibration. On that basis, it must be supposed that the amount of vibration measured at the interface is a good indicator of the vibration transmitted to the body.

The effects of vibration on the comfort of a person exposed to periodic, random or transient vibration are assessed in the frequency range 0.5 to 80 Hz. When assessing the effects on comfort, all the relevant vibration directions should be included to obtain the overall total value of vibration at each point of entrance of vibration within the body (i.e. seat, feet, backrest) neglecting angular motion, the point vibration total value is defined as:

$$a_{wT} = \left(k_x^2 a_{wx}^2 + k_y^2 a_{wy}^2 + k_z^2 a_{wz}^2\right)^{1/2} \tag{1.1}$$

where $a_{wx} = \sqrt{\sum_i (w_{xi} a_{xi})^2}$, $a_{wy} = \sqrt{\sum_i (w_{yi} a_{yi})^2}$, and $a_{wz} = \sqrt{\sum_i (w_{zi} a_{zi})^2}$ are frequency-weighted rms accelerations with respect to the orthogonal axes x, y, z, respectively; k_x, k_y, and k_z are multiplying factors; w_{xi}, w_{yi}, and w_{zi} are the weighted factors for the i th one-third octave band with respect to the orthogonal axes x, y, z, respectively; a_{xi}, a_{yi}, and a_{zi} are the rms acceleration for the i th one-third octave band in the orthogonal axes x, y, z, respectively.

The overall rms value of the frequency-weighting acceleration ($a_c = \left(\sum_i a^2_{wT}\right)^{1/2}$) can be then compared with the following guidance:

$a_c < 0.315$ m/s²	Not uncomfortable
$0.315 < a_c < 0.63$ m/s²	A little uncomfortable
$0.5 < a_c < 1$ m/s²	Fairly uncomfortable
$0.8 < a_c < 1.6$ m/s²	Uncomfortable
$1.6 < a_c < 2.5$ m/s²	Very uncomfortable
$a_c > 2.5$ m/s²	Extremely uncomfortable

The standard cautions that before making this comparison, it is important to remember that reactions to various magnitudes of vibration depend on various factors such as comfort expectations, annoyance and tolerance. Therefore, the above figures should be treated only as guidance.

Frequency weighting

Many studies have concluded that the vibration energy absorbed by the human body is strongly related to the frequency of vibration, with peaks being in the range of 4-6 Hz [4,29]. Human body exhibits different sensitivity to vibration within different frequency ranges. The weighting factor has thus been introduced within the standardized evaluation procedures to account for the human sensitivity to vibration. The frequency weightings are defined in the form of filter transfer functions or weighting factors corresponding to center frequencies of the one-third octave bands, that could be directly applied in the frequency-domain analyses. Figure 1.3 illustrates the transfer function of the W_k-filter defined in ISO 2631-1 [1]. The weighting factors represent the magnitude

ratio of the transfer function corresponding to specific frequencies, which are the highest within the frequencies of 4-12 Hz.

Vibration discomfort assessment of occupants is primarily based on laboratory evaluations of subjects' judgment when exposed to various vibration stimuli. Equivalent sensitivity contours express the vibration magnitude required to produce equivalent discomfort for each vibration frequency, axis and input position, especially in frequency. Consequently, frequency-weighting functions in the time domain are defined to express the differences in discomfort at different vibration frequencies.

For the assessment of health and comfort effects due to vertical vibration transmitted at the seat level, a frequency weighting function, Wk, is defined in the 0.5 to 80 Hz frequency range [1]. The frequency weighting function is defined as a combination of a series of transfer functions. Mathematically, the transfer function of the weighting filter is as a combination of high-pass, low-pass, acceleration-velocity transition and upward step transfer function, given by:

i) High pass filter:

$$H_h(s) = \frac{1}{1 + \omega_1 /(Q_1 s) + (\omega_1 / s)^2} \tag{1.2}$$

where $\omega_1 = 2\pi f_1$, $f_1 = 0.4$ Hz, $s = jf$, and $Q_1 = 1/\sqrt{2}$.

ii) Low pass filter:

$$H_l(s) = \frac{1}{1 + s/(Q_2 \omega_2) + (s/\omega_2)^2} \tag{1.3}$$

where $\omega_2 = 2\pi f_2$, $f_2 = 100$ Hz, and $Q_2 = 1/\sqrt{2}$.

iii) Acceleration-velocity transition (proportionality to acceleration at lower frequencies, proportionality to velocity at higher frequencies):

$$H_t(s) = \frac{1 + s/\omega_3}{1 + s/(Q_4\omega_4) + (s/\omega_4)^2} \tag{1.4}$$

where $\omega_3 = 2\pi f_3$, $f_3 = 12.5$ Hz and $Q_4 = 0.63$; $\omega_4 = 2\pi f_4$, and $f_4 = 12.5$ Hz.

iv) Upward step (steepness approximately 6 dB per octave, proportionality to jerk):

$$H_s(s) = \frac{1 + s/(Q_5\omega_5) + (s/\omega_5)^2}{1 + s/(Q_6\omega_6) + (s/\omega_6)^2}\left(\frac{\omega_5}{\omega_6}\right)^2 \tag{1.5}$$

where $\omega_5 = 2\pi f_5$, $f_5 = 2.37$ Hz, and $Q5 = 0.91$; $\omega_6 = 2\pi f_6$, $f_6 = 3.35$ Hz, and $Q_6 = 0.91$.

The total frequency weighting function is expressed as:

$$H(s) = H_h(s) \cdot H_l(s) \cdot H_t(s) \cdot H_s(s) \tag{1.6}$$

S.E.A.T.

The S.E.A.T. (Seat Effective Amplitude Transmissibility) has been defined as a measure of the efficiency of a seat in isolating the body from · ation [53]. It provides a simple numerical assessment of the seat isolation efficiency. An un-weighted S.E.A.T. value of a seat represents the ratio of the un-weighted rms acceleration measured on the seat to the un-weighted rms acceleration measured on the seat base along the same direction, given by

$$S.E.A.T. = \frac{a_{rms}\ \ of\ \ seat\ \ vibration}{a_{rms}\ \ of\ \ base\ \ vibration} \qquad (1.7)$$

where the rms acceleration may be computed either from the time domain or from the acceleration spectra in the following manner:

$$a_{rms\_time} = \sqrt{\frac{1}{T}\int_0^T \ddot{x}^2(t)\,dt}$$

$$a_{rms\_freq} = \sqrt{\int_{f_1}^{f_2} S_{\ddot{x}}(f)\,df} \qquad (1.8)$$

where $\ddot{x}(t)$ is the acceleration time history and $S_{\ddot{x}}(f)$ is its power spectral density. T is the sample or measurement duration, and f_1 *and* f_2 define the frequency limits of the analysis.

A frequency-weighted S.E.A.T. value represents the ratio of the frequency-weighted rms acceleration measured on the seat to the frequency-weighted rms acceleration measured on the seat base along the same direction, given by:

$$S.E.A.T._w = \frac{a_{w.rms}\ \ of\ \ seat\ \ vibration}{a_{w.rms}\ \ of\ \ base\ \ vibration} \qquad (1.9)$$

where the frequency-weighted rms acceleration $a_{w,rms}$ may be computed either in the time-domain or in the frequency-domain

$$a_{w.rms\_time} = \sqrt{\frac{1}{T}\int_0^T \ddot{x}_w^{\,2}(t)\,dt}$$

$$a_{w.rms\_freq} = \sqrt{\sum_{i=1}^{n}\left[a_{rms\_freq}(f_i)w_k(f_i)\right]^2} \qquad (1.10)$$

where $\ddot{x}_w(t)$ is the frequency-weighted acceleration time history obtained through application of the weighting filter, defined in Equation (1.6). $w(f_i)$ is the weighting factor corresponding to center frequency f_i of the i^{th} third-octave band, and n is the number of frequency bands considered in the analysis.

1.2.2 Characterization of Automotive Seats

The continuous pressure from the automobile industry for cost saving has resulted in greater demands for car seat weight together with improved posture and vibration comfort. This has led to a number of studies on the characterization of the flexible polyurethane seating foam and their contribution to the ride comfort [2,8-10]. Various studies have attempted to study the relationship between PUF characteristics and the seat comfort. It is widely concluded that the polyurethane foam widely used in seat cushion design has complex mechanical properties and the ride comfort is closely related with these properties [8]. The highly nonlinear visco-elastic properties of the polyurethane foam cushion depend not only on the composition, density and geometry of the cushion, but also on the excitation magnitude and frequency content, the seated posture and subjects' physical characteristics.

A number of studies have reported the constitutive properties of cellular foams used in automotive seats [9-11]. Lee and Ferraiuolo [12] studied and reported that foam thickness and foam hardness were important parameters affecting seat ride comfort. In the context of the foam properties, the study characterized the force-deflection curves of the foam cushion to identify parameters, such as the linearity and gradient of the curve. Diebschlag et al. [13] recommended polyurethane foam with linear characteristics between applied force and compression ratio by optimizing the force and pressure distribution on the contact surface between a human body and the seat cushion.

Many different models of seat cushion have been proposed with varying objectives. All the reported models tend to characterize the properties through lumped spring and damping elements constrained along vertical direction, while the elements may possess different characteristics, either linear or nonlinear. The majority of the studies on human-seat or seat cushion dynamics, however, consider a linear seat cushion model to predict the comfort of seat and to investigate the optimum seat cushion parameters so as to minimize the transmission of vibration magnitude from the floor to the interface between the seat and the human body [14-17]. These linear models are presented in the force-deflection and force-velocity properties of the cushion along the vertical axis with an equivalent linear spring and a parallel viscous damper, as shown in Figure 1.4. Although the linear cushion model provides good representation of polyurethane foam seats when the magnitude of input vibration is small and the frequency of the input is above 4 Hz, it tends to yield large error when the magnitude of input vibration is large and the frequency of the input is below 4 Hz. Thus, the

applicability of the linear cushion model is when the magnitude of input vibration is small and the frequency of input vibration is above 4 Hz.

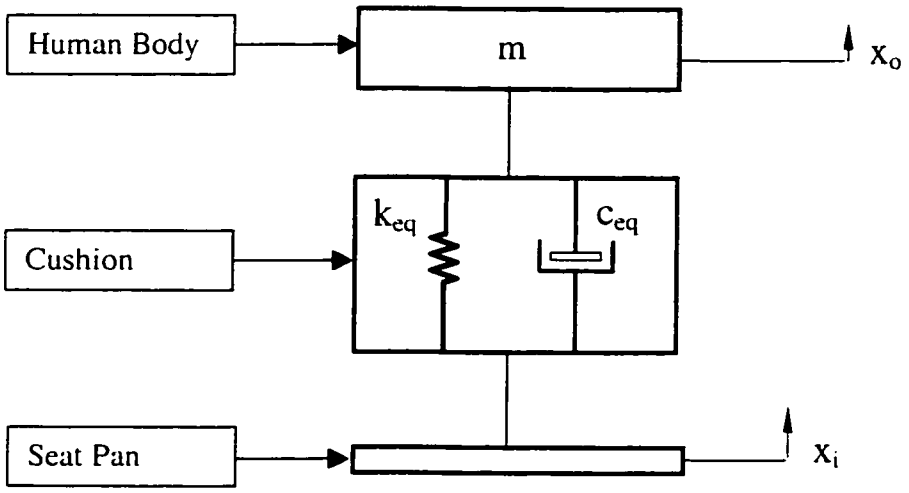

Figure 1.4: Cushion model with an equivalent spring and an equivalent damper representation.

Rakheja et al. [35,46] presented the laboratory characterization of selected automotive seat cushions in terms of force-displacement and force-velocity characteristics as function of the preload (seated body weight), excitation amplitude and excitation frequency. The study also evaluated the equivalent stiffness and damping coefficients as function of the preload, and excitation conditions. The study concluded that the stiffness coefficients of the seat cushion varies most significantly with the preload, and excitation magnitude and frequency. The damping coefficient, however, was found to be less sensitive to variations in body weight and excitation frequency at frequencies above 3 Hz.

Based on the interface pressure distribution measured between the seated subjects and the seat cushion, Wu [18] developed a nonlinear seat cushion model to account for the body hop motion and cushion bottoming, occurring under either large preload or large magnitudes of vibration excitation. Although the proposed model behaves like a conventional linear element when the dynamic deflection is in the vicinity of the static equilibrium position, it demonstrates progressively hardening/softening behavior over a wider range of deflections to account for the body hop and cushion bottoming phenomena. The proposed seat cushion model consists of a parallel nonlinear spring and a linear viscous damper. The force-motion relationship at the human-seat interface of the seat cushion model was expressed as:

$$F_{cushion}(x) = \begin{cases} F_{c0} + k_{c1}(x - x_s) + f(x) + k_{c3}(x - x_1)^3 + c_{eq}\dot{x}, & x_1 \le x < T_c \\ F_{c0} + k_{c1}(x - x_s) + f(x) + c_{eq}\dot{x} & 0 \le x < x_1 \\ 0 & x \le 0 \end{cases} \quad (1.11)$$

In the above, F_{c0} is the static preload on the seat cushion under which the seat cushion undergoes a static deformation of x_s. x is the deflection of the seat cushion with reference to the free thickness of the seat cushion, which should not exceed its free thickness, T_c. c_{eq} is equivalent viscous damping coefficient which can be estimated from vibration transmission characteristics of the human-seat system. $\dot{x}$ is the relative velocity due to foam deformation. The parameters k_{c1} and k_{c3} include linear and nonlinear (cubic) contents of stiffness coefficient, respectively, when cushion bottoming is initiated beyond the deflection threshold of the seat cushion, x_1. The deflection threshold of the seat cushion x_1 should be greater than the cushion deflection at the equilibrium position x_s.

The model incorporates nonlinear restoring property, using linear and cubic dependencies on displacement. f(x) is a nonlinear force function, which mostly relates to the nonlinearity associated with body hop motion. The mass of the seat cushion is further assumed to be negligible, since the density of the polyurethane foam is quite low (in the order of 50 kg/m^3). The proposed model incorporates the influence of body weight through consideration of the static deflection x_s.

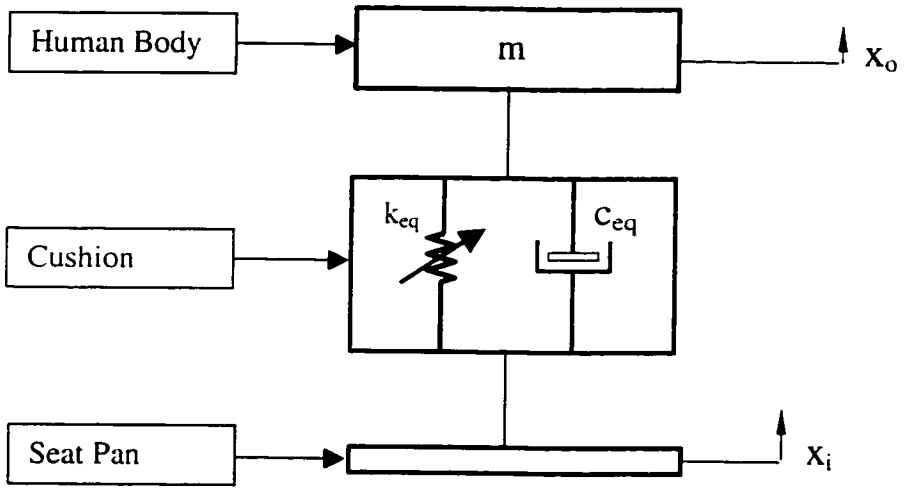

Figure 1.5: Cushion model with a nonlinear spring and an equivalent viscous damper .

By simplifying a continuous shape function that characterize the piecewise continuous stress-strain characteristic of flexible open-celled foam, Patten et al. [19,20] developed a non-linear automotive seat cushion model, which relies explicitly on the

constitutive properties of polyurethane foams and on the geometry of the seat cushion. The model includes the influence of pneumatic damping attributed to air flows within the open-celled foam and matrix polymer. The proposed seat cushion model consists of a parallel nonlinear spring and a non-linear viscous damper, as shown in Figure 1.6. The major assumptions of the model include: (1) the motions relative to static equilibrium are small; (2) the motion occurs along the vertical direction only; (3) the foam consists of an assemblage of cells; (4) the top and bottom sides of the foam cushion are covered with a material that prevents flow though these faces; (5) the air in the foam matrix is treated as a Newtonian fluid; and (6) flow is assumed incompressible, which is justified with low Reynolds numbers.

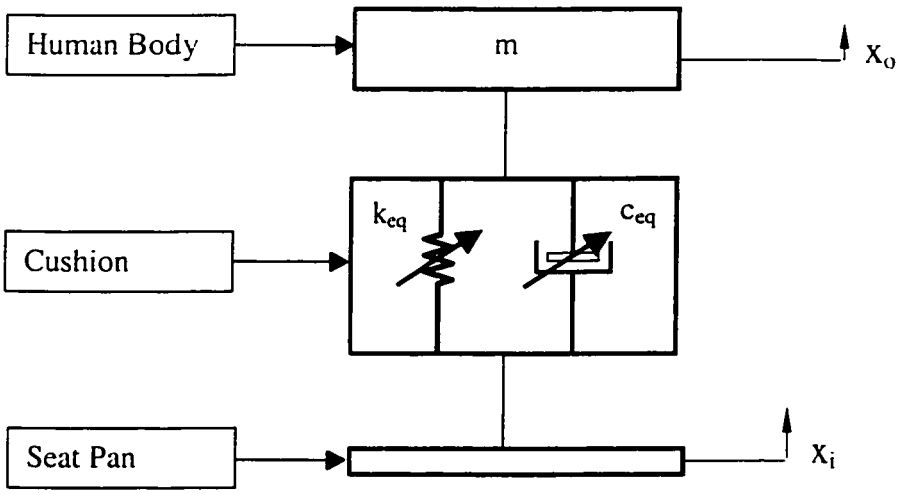

Figure 1.6: Cushion model with a nonlinear spring and a nonlinear damper [19,20].

The nonlinear stiffness and damping coefficients of the seat cushion are described as:

$$K(x) = \frac{K_0}{1 + K_1 x} \tag{1.12}$$

$$C(\dot{x}) = C_0 + C_1 |\dot{x}| \tag{1.13}$$

where K_0, K_1, C_0, and C_1 are constants. It is found that the spring stiffness of the seat cushion is a function of the relative deflection (x) alone, while the damping coefficient is a function of the relative velocity ($\dot{x}$). The study does not consider the influence of seated body weight or the excitation frequency.

Tchernychouk [21] developed a non-linear automotive seat cushion model on the basis of laboratory-measured static and dynamic properties of the polyurethane foam cushions. The proposed seat cushion model consisted of a parallel combination of a nonlinear spring and a non-linear viscous damper, similar to that as illustrated in Figure 1.6. The stiffness and damping properties were established as function of frequency and amplitude of excitation and preload, using a look up table. These tables represented the cushion behavior in the selected ranges of frequency, excitation amplitude and preload. The interpolation was employed to derive the spring stiffness and the damper coefficient of the seat cushion according to specific excitation and body weight.

Leenslag et al. [22] introduced a small-scale dynamic creep test to derive the foam dynamic creep behavior and related vibration properties. The results of the small-scale test were analyzed to evaluate the contribution of non-linear foam behavior to ride comfort and were further employed to model seat behavior. A finite-element based analytical (FEA) model for the polyurethane foam cushion was proposed to study the

quasi-static and dynamic behaviors. Figure 1.7 shows an example of the computed vibration transmissibilities at different percentage level of ILD (preload). In general, minimum values for natural frequency were observed in the 20 to 35 percent ILD range, reflecting the foam's non-linear behavior.

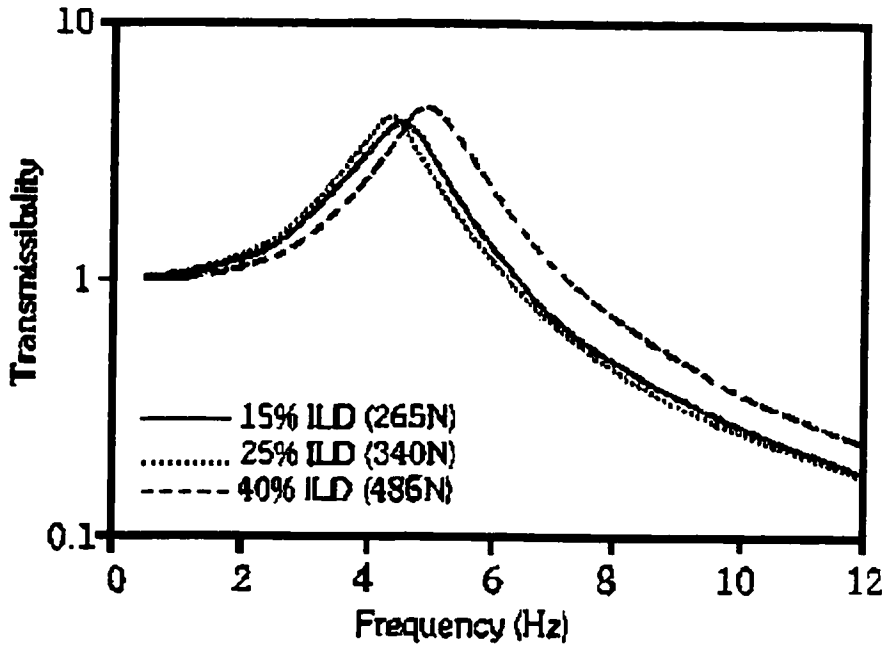

Figure 1.7: Vibration transmissibility of the FEA seat cushion model [22].

All of the above-mentioned studies focus on the characterization of PUF cushion, while the contribution due to biodynamic properties of the human occupant are mostly ignored. The reported studies, however, have established that the vibration attenuation

performance of a seat is strongly dependent upon the mechanical properties of the PUF and the body weight, and that the mechanical properties are complex function of excitation condition. The reported studies, in general, may be grouped in these categories on the basis of the study objective. These are summarized below:

1. The first group of studies includes very limited number of studies, which focus on the development of new materials with superior static and dynamic properties. Murakamiet et al. [23] developed a new MDI (diphenylmethane diisocyanate) - based polyurethane flexible foam for automotive seat cushions having superior static and dynamic properties. The improved MDI-based polyurethane flexible foam provided good pressure distribution properties with increased contact area, and lower maximum and average interface pressure. The variations in the interface pressure were evaluated in terms of coefficient of variation (cv) of the pressure and it was suggested that a lower value of cv would provide favorable pressure distribution [23]. The proposed MDI-based foams also showed lower vibration transmissibility over a wide range of frequency range, especially at the resonance frequency.
2. The second group of studies includes those focusing on the static as well as combination of static and dynamic comfort. With the increasing demand for comfort, not only the dynamic comfort should be studied, but also the static comfort. 'Static comfort' refers to the sitting impressions of the occupants in the absence of dynamic motions. Ebe and Griffin [24] discussed factors affecting static seat cushion comfort. When considering the characteristics of polyurethane foam, the foam hardness feeling and bottoming appear to be important factors that influence the static seat comfort. When changing foam characteristics, such as composition, hardness and thickness,

bottoming will affect static seat comfort, and the stiffness could be a useful indicator of static seat comfort. Pressure around the ischial bones may also reflect both comfort factors: the foam hardness feeling and bottoming [18, 24]. The seat cushions resulting in low pressure around the ischial bones were evaluated as more comfortable than those giving high pressure. Many other factors, such as seat shape, subject posture and seat covers, may also affect the static comfort. Leenslag et al. [22] also considered also the quasi-properties in their FEA analysis of the polyurethane foam cushion.

3. The third group of studies includes those with a focus on development of comprehensive models of the seat cushion for ride quality assessment. The studies conducted by Wu [18], Tchernychouk [21], Patten et al [19,20], Lee and Ferraiuolo [12], and others [9-11] would fall within this group. The highlights of these studies based on the lumped-parameter models have already been discussed in this section. The distributed-parameter FEA-based model developed by Leenslag et al [22] also falls within this group.

1.2.3 Biodynamic Response Functions

The comfort performance of an automotive seat is strongly influenced by the dynamic responses of the seated human occupant. Experimental studies conducted on seats loaded with a passive mass and human subject clearly establish the significant contributions to the overall seat-human system vibration transmissibility [5,21,52]. Figure 1.8 [52] illustrates a comparison of the measured vibration transmissibility characteristics of a seat loaded with a passive mass and human subjects. It is thus vital to consider the

biodynamic response of the human body to whole-body vibration in assessing the comfort performance of the seats.

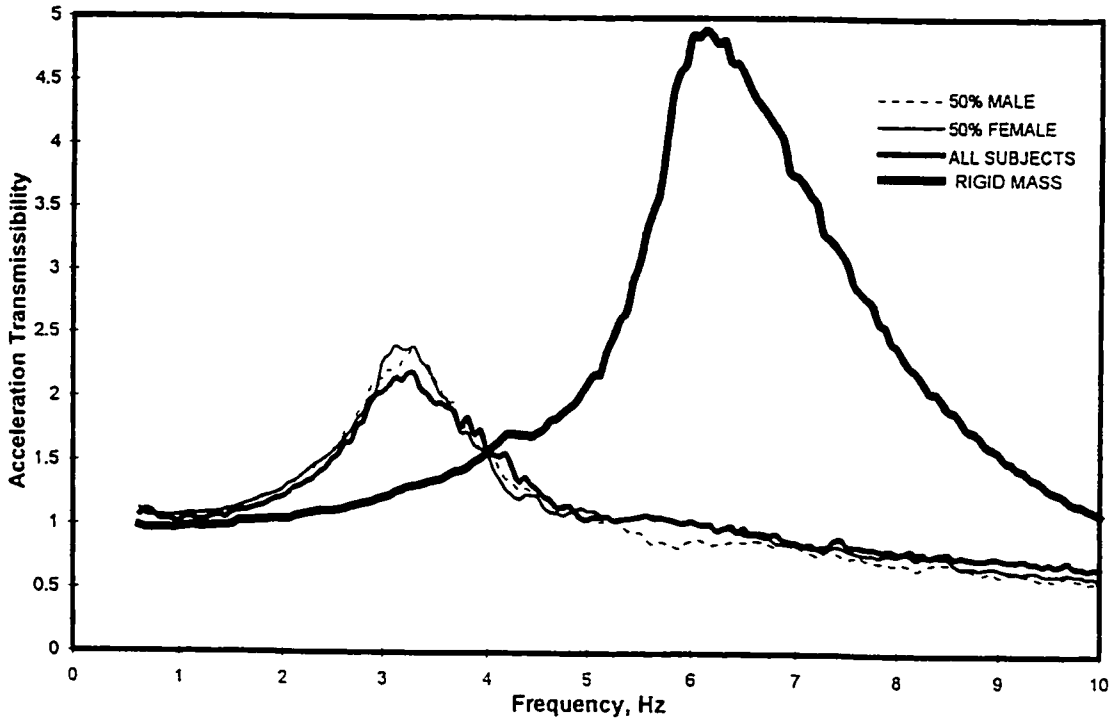

Figure 1.8: Comparison of acceleration transmissibility of the seat loaded with human subjects and a rigid mass [52].

The biodynamic response behavior of the seated human body exposed to whole body vibration may be characterized by three different biodynamic response functions: driving-point mechanical impedance (DPMI), apparent mass (APMS) and seat-to-head transmissibility (STHT). While the first two functions have often been used

interchangeably to describe "to the body" force-motion relationship at the interface between the human body and the seat ("to the body" transfer function), the third function refers specifically to the transmission of motion through the body ("through the body" transfer function) [4,25]. A number of studies have reported the measured biodynamic response functions of human subjects seated on a rigid platform [18,26,27,29]. A vast number of these studies have also proposed a number of biodynamic analytical models of the seated human body on the basis of the measured driving-point mechanical impedance and seat-to-head transmissibility magnitude and phase responses.

The driving-point mechanical impedance DPMI, the complex ratio of applied periodic excitation force $F(j2\pi f)$ at frequency f to the resulting vibration velocity $v(j2\pi f)$ at that frequency measured at the same point and in the same direction as the applied force, is given by:

$$Z(j2\pi f) = \frac{F(j2\pi f)}{v(j2\pi f)} \tag{1.14}$$

where $Z(j2\pi f)$ is the complex DPMI. $F(j2\pi f)$ *and* $v(j2\pi f)$ are the driving force and response velocity at the driving point, respectively. f is the frequency in Hz and $j = \sqrt{-1}$. Under random vibration, the DPMI is derived from:

$$Z(j2\pi f) = \frac{G_{fv}(j2\pi f)}{G_{vv}(j2\pi f)} \tag{1.15}$$

where $G_{fv}(j2\pi f)$ is the cross-spectral density of force and velocity. $G_{vv}(j2\pi f)$ is the auto-spectral density of the velocity.

The apparent mass APMS, the complex ratio of applied periodic excitation force $F(j2\pi f)$ at frequency f to the resulting vibration acceleration $a(j2\pi f)$ at that frequency

measured at the same point and in the same direction as the applied force, is formulated as:

$$M(j2\pi f) = \frac{F(j2\pi f)}{a(j2\pi f)} = \frac{Z(j2\pi f)}{j2\pi f} \tag{1.16}$$

where $M(j2\pi f)$ is the apparent mass and $a(j2\pi f)$ is the driving point response acceleration. The quantity apparent mass has the advantage that it can be obtained directly from the signals provided by accelerometers and force transducers. Moreover, Newton's second law of motion gives apparent mass a simple intuitive meaning: a force applied to a body accelerates the body by an amount proportional to the force, the constant of proportionality being the apparent mass of the body. When the human body is effectively rigid, the apparent mass of the body is equal to its static mass, and the driving force and the acceleration response remain in phase. For the human body, the APMS magnitude at low frequencies is observed to be similar to that of the body weight supported by the seat, and increases with increase in the frequency until the resonant frequency. At higher frequencies the upper body segments are loosely coupled and the human body will no longer be rigid, the apparent mass decreases and is less than the mass of the human body.

The seat-to-head transmissibility STHT is a complex non-dimensional ratio of response acceleration of the head to the forced vibration acceleration at the seat-body interface, and is expressed as:

$$H(j2\pi f) = \frac{\ddot{X}_h(j2\pi f)}{\ddot{X}_0(j2\pi f)} \tag{1.17}$$

where $H(j2\pi f)$ is the complex seat-to-head transmissibility function, and $\ddot{X}_h(j2\pi f)$ is the acceleration responses of the head and $\ddot{X}_0(j2\pi f)$ is the acceleration at the seat-body interface.

The biodynamic response functions have been widely employed to characterize the human biodynamic response. A number of human body models have been proposed in the literature based on the measured data under a variety of test conditions [17,18,27,30,48]. Majority of the measurement conditions used in some investigations, however, cannot be considered representative of those likely to prevail while driving a car [29,76]. The applicability of a proposed biodynamic model to driving situations may thus be questioned without analyzing the test conditions used for deriving the data on which the model relies because the biodynamic response of the human body subjected to vibration is strongly related to a wide range of intrinsic, such as body posture and mass, and extrinsic, such as intensity and type of excitation variables [3,26,64,65,77].

1.2.4 Review of Biodynamic Models

The characterization of vibration isolation performance of seats necessitates the consideration of biodynamic response characteristics of the seated occupant. A number of lumped-parameter models, ranging from single-degree-freedom (DOF) to multi-DOF, have been proposed. A comparative study of these models, conducted by Boileau et al. [26], concluded that these models yield considerably different biodynamic response characteristics. The different models used to characterize the biomechanical response to whole-body vibration employ considerably different idealizations of the body structure. The reported models can be categorized into three types: lumped parameters, continuum

models and discrete models. In the lumped parameter models, the mass of the body structure is concentrated into a few lumped masses interconnected by springs and dampers. The majority of the reported models fall within this group of models. The discrete and continuum models consider distributed parameters of the human body and component characteristics in two-and three-dimension.

In an early study, Coerman [27] proposed a SDOF model of the human body, shown in Figure1.9. The mass of the subject, due to upper torso and the head, supported by the seat is lumped and linked to the base through parallel spring and damping elements. Stiffness coefficient k represents the restoring property of the spine; damping coefficient c is due to the spine and the adjacent tissues. The model parameters were identified to fit the DMPI data measured with subjects sitting without their feet and back supported under sinusoidal excitation only. Payne [28] presented an improved Dynamic Response Index (DRI) model (Figure 1.10) comprising four parallel and uncoupled single-DOF models, which was realized upon combining the DRI model, also known as "spinal" or "shock response" model, with additional single-DOF models: "visceral"; "body vibration"; and "low frequency".

Fairly and Griffin [29] proposed a single-DOF model, as shown in Figure 1.11. This seated body involved two masses: m_1 being the mass of the upper body moving relative to the platform, and m_2 being the mass of the lower body and the legs supported on the platform but not moving relative to the platform. The mass of the legs m_3 was included in the model only when the feet were supported on a stationary footrest. The model parameters were identified to fit the measured mean APMS of 60 subjects,

including male, female and children, sitting erect without back support. The APMS was measured under 1.0 m/s^2 random vibration.

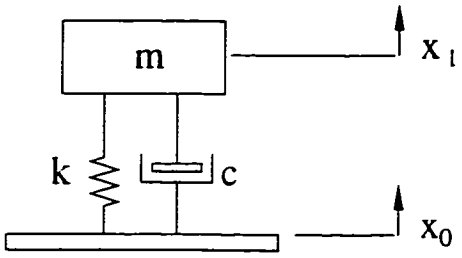

$f_n = 6.3\ Hz \qquad \xi = 0.57 \qquad k = 131181 N/m \qquad for\ "Seated\ \ Erect"$

$f_n = 5.2\ Hz \qquad \xi = 0.65 \qquad k = 84180 N/m \qquad for\ "Relaxed"$

Figure 1.9: SDOF model by Coerman [27].

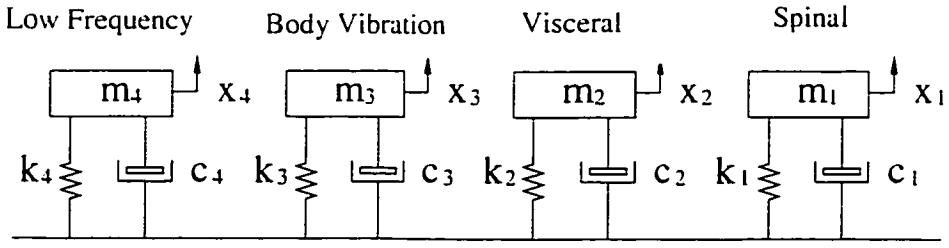

$\omega_{n4} = 1.57\ rad/s \qquad \omega_{n3} = 52.9\ rad/s \qquad \omega_{n2} = 25.1\ rad/s \qquad \omega_{n1} = 52.9\ rad/s$

$\xi_4 = 1.0 \qquad \xi_4 = 1.0 \qquad \xi_4 = 0.4 \qquad \xi_4 = 0.2245$

Figure 1.10: Improved DRI model proposed by Payne [28].

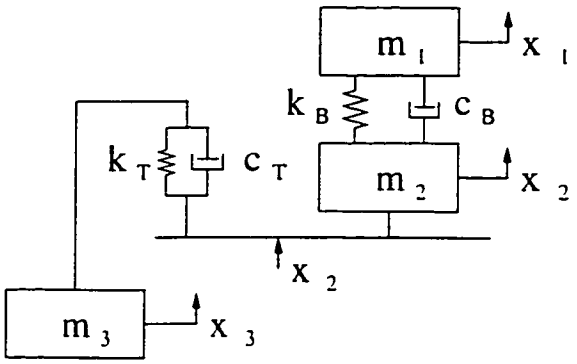

$m_1 = 45.6\ kg \qquad m_2 = 6\ kg \qquad m_3 = 11.5\ kg$

$\xi = 0.475 \qquad c_B = 1360\ Nm/s \qquad f_{nB} = 5\ Hz \qquad c_T, k_B = 0$

Figure 1.11: SDOF model proposed by Fairly and Griffin (1989) [29].

Suggs et al. [30] proposed a two-DOF biodynamic model of the human body to characterize the human body response behavior over a frequency range comprising the first two resonant frequencies of the body (Figure 1.12). The model parameters were identified from the measured DPMI characteristics of 11 male subjects seated upright with feet supported, hands in lap, and exposed to sinusoidal vibration of 2.54 mm amplitude in the 1.75 to 10 Hz frequency range. The lumped masses of the model consisted of m_1, representing the pelvis and the abdomen; m_2, representing the head and the chest; and m_0, representing the spinal column. Similarly, Allen [32] developed another two-DOF biodynamic model of the human body, as shown in Figure 1.13. This model characterizes the upper response and the head response. The lumped masses m_0 and m_1 represent the upper and the head of the body, respectively.

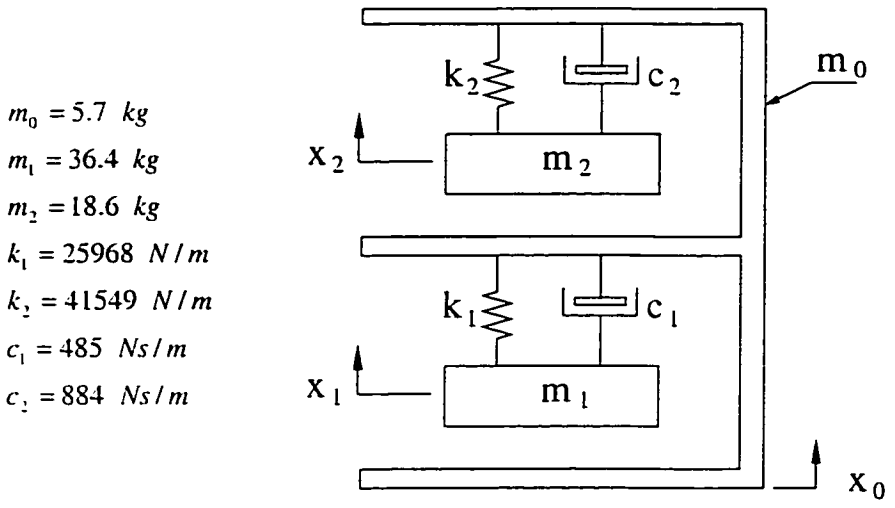

Figure 1.12: 2-DOF model proposed by Suggs *et al.* [30].

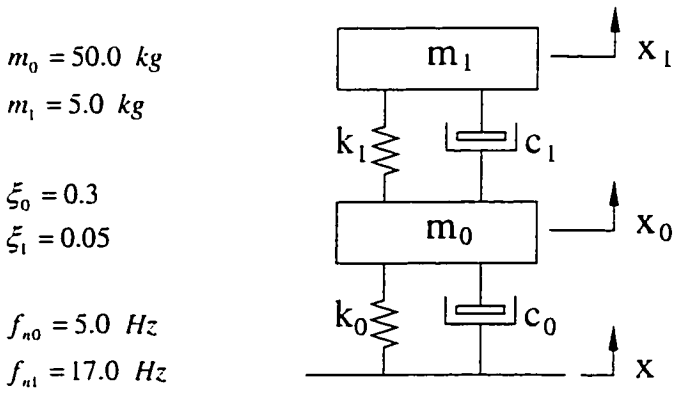

Figure 1.13: 2-DOF model proposed by Allen [32].

A number of multi-degree-of-freedom models have also been developed, ranging from 3-DOF to 10 or more–DOF. Wu [18] proposed a three-DOF model (Figure 1.14), which consists of four masses, coupled by linear elastic springs and viscous-damping elements. The masses m_o to m_3 have no explicit physical meaning. The masses m_1 to m_3 are introduced with an objective to describe the biodynamic behavior related to two resonant peaks observed in the APMS and STHT magnitude responses near frequencies of 5 Hz and 10 Hz, respectively. The lower mass m_o is used to increase the flexibility for tuning the model parameters without increasing the number of DOF. This mass specifically affects the APMS response with only negligible effect on the STHT response. A parametric optimization technique was employed to determine the model parameters. An objective function was defined to minimize the weighted sum of errors in the magnitude and phase responses of the model and the measured data of the two biodynamic response functions APMS and STHT over a specific frequency range.

Boileau [17] proposed a four-DOF model, as shown in Figure 1.15, consisting of four masses, coupled by linear elastic spring and viscous-damping elements. In this model, the mass m_1 represents the head and neck; the mass m_2 represents the chest and upper torso; the mass m_3 represents the lower torso; and the mass m_4 represents the thighs and pelvis in contact with the seat. The mass of lower legs and the feet are not considered in this model, assuming their negligible contributions to the biodynamic response of the seated human body. The model is proposed for a seated subject maintaining en erect posture without back support. The model parameters were identified such that the model response correlates with both the target DPMI and STHT magnitude and phase. Payne and Band [37] proposed another 4-DOF lumped-parameter biodynamic model, as shown

$m_0 = 2\ kg$

$m_1 = 6\ kg$

$m_2 = 2\ kg$

$m_3 = 45\ kg$

$k_1 = 9.99 \times 10^3\ N/m$

$k_2 = 3.44 \times 10^4\ N/m$

$k_3 = 3.62 \times 10^4\ N/m$

$c_1 = 387\ Ns/m$

$c_2 = 234\ Ns/m$

$c_3 = 1.39 \times 10^3\ N/m$

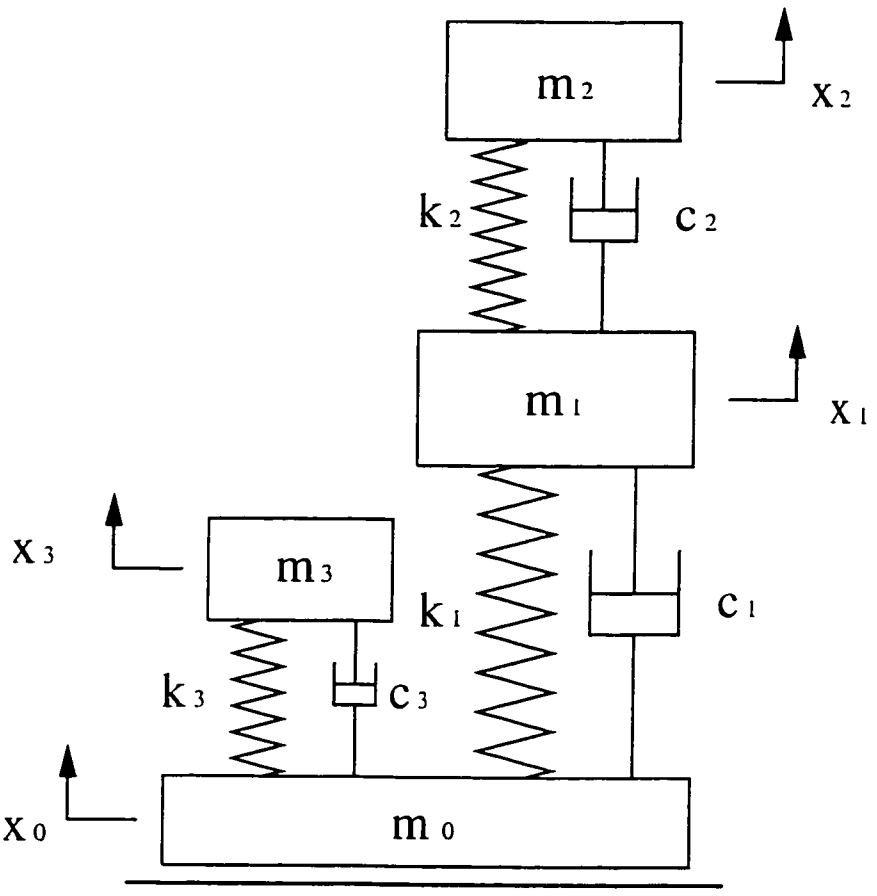

Figure 1.14: Three-DOF model proposed by Wu [18] and included in the ISO 5982 [25].

$m_1 = 5.31\ kg$

$m_2 = 28.49\ kg$

$m_3 = 8.62\ kg$

$m_4 = 12.78\ kg$

$\sum_{i=1}^{4} m_i = 55.2\ kg$

$k_1 = 310\ kN/m$

$k_2 = 183\ kN/m$

$k_3 = 162.8\ kN/m$

$k_4 = 90\ kN/m$

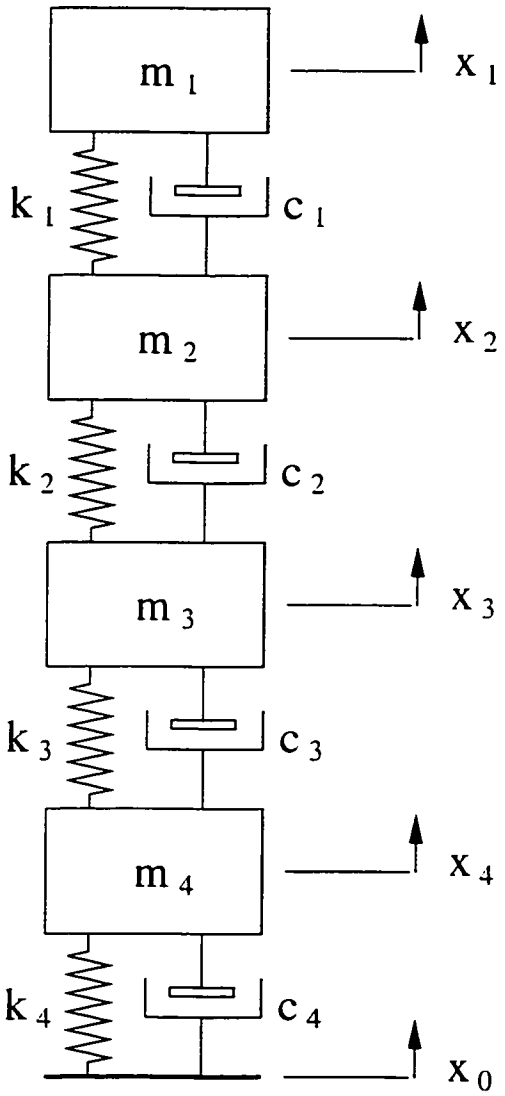

Figure 1.15: 4-DOF linear model proposed by Boileau [17].

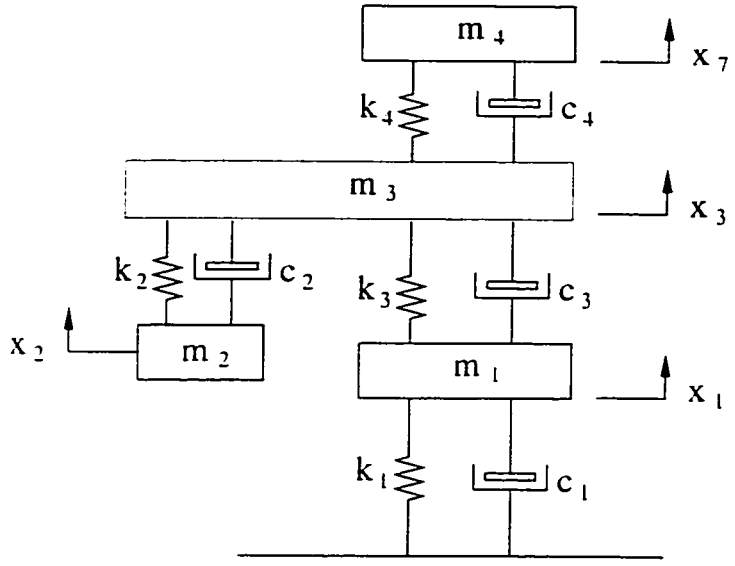

Figure 1.16: 4-DOF model proposed by Payne and Band [37].

in Figure 1.16, as an extension of the "spinal model" described in Figure 1.9. The proposed model comprises mass m_1 representing the buttocks and pelvis; m_2 representing the viscera; and m_4 representing the neck and the head. The model parameters were identified from the DPMI.

Smith [47] proposed a 5-DOF mathematical model based on the measured DPMI and transmissibility of major anatomical structures contributing to the observed resonance behavior. The model, as shown in Figure 1.17, was relatively effective in simulating the vibration responses of the male body. The five lumped masses represented spine, torso/chest, pelvis, lower legs and upper legs, respectively. The model was further modified to represent the leg as a two-DOF structure uncoupled to the torso and spine [48]. The model coefficients were adjusted to produce the best match for the major

resonance peaks observed in both the DPMI and transmissibility profiles for the female and male. The model was again refined for evaluating the effectiveness in simulating the major resonance observed in the DPMI and transmissibility frequency responses [49]. In the modified model, the upper and lower legs were coupled, as suggested by the data.

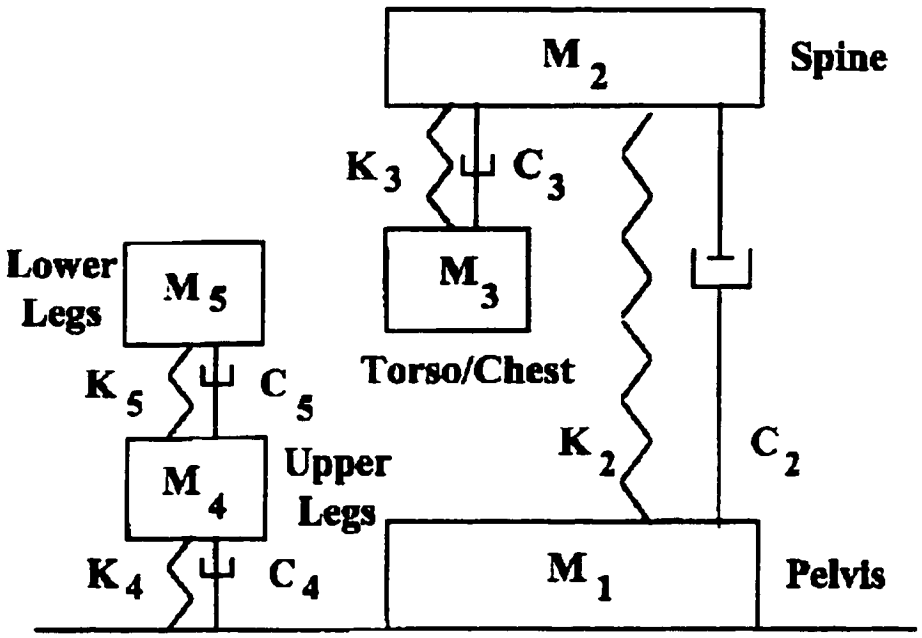

Figure 1.17: 5-DOF mechanical model of the human body by Smith, S.D. [48].

A few nonlinear models have also been reported in the literature. Demic [39] proposed a three-DOF nonlinear model of the human body to account for nonlinear body response to high intensity shock excitations (Figure 1.18). The parameters, k_1 to k_3 and c_1 to c_3, include linear and nonlinear (cubic) contents, respectively. The model incorporates nonlinear restoring and dissipative force, using linear and cubic dependencies on

displacement and velocity, respectively. Matching the model response with the measured transfer functions only identified the model parameters.

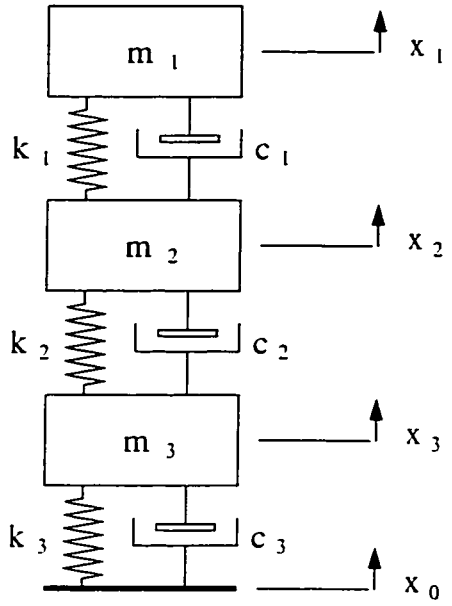

Figure 1.18: 3-DOF non-linear model proposed by Demic [39].

The majority of lumped parameter models are one-dimensional. In order to predict motion of the human body in the two-dimensional space or the three-dimensional space, finite element models of the human body has also been formulated. Discrete models and continuum models are both distributed parameter models. The discrete models treat the spine as a layered structure of rigid elements, representing the vertebral

bodies, and deformable elements representing the inter-vertebral discs. The continuum models treat the spine as a homogeneous rod beam. Belytschko and Privitzer [40] developed a three-dimensional head-spine model using finite element method. Kitazaki and Griffin [41] proposed a two-dimensional space finite element model of the human body, shown in Figure 1.19. This biomechanical model, which evolved from those developed by Belytschko and E. Privitzer [40], was used to model the spine, viscera, head, pelvis and buttocks tissue, using beam, spring and mass elements. This model was entirely linear and includes 134 elements and 87 masters degrees-of-freedom. The model was developed by comparison of the vibration mode shapes with those measured in the laboratory. The spinal column was modeled by 24 beam elements, representing all the inter-vertebral discs between the vertebral C1 and the sacrum S1. Mass elements for the torso were located anterior to the spine in the region between the T1 and T10 levels by massless rigid links, so as to model the eccentric inertial loading of the torso on the spine. Below the T10 level (the diaphragm level), the spinal masses and the visceral masses were modeled by separate mass elements. The sum of the spinal and the visceral masses at each vertebral level corresponded to the torso mass, with its mass center also located anterior to the spine. The visceral column in the abdominopelvic cavity was modeled by seven mass elements at the levels from T11 to L5 interconnected by spring elements. The bottom of the visceral column was connected to the pelvis mass by a massless rigid link, and top connected to the spinal beam at the T10 level, also by a massless rigid link representing the pair of the lowest complete ribs. The interaction between the visceral and the spine was modeled by horizontal spring elements interconnecting the visceral masses and the spinal beams. The head was simply modeled by connecting to the top of the

spinal beam at the C1 level by a beam element representing the atlanto-occipital joint. The pelvis was modeled by a mass element and connected to the bottom of the spinal beam at the S1 level by a massless rigid link. A total of seven modes were calculated for a normal body posture below 10 Hz, and the mode shapes of the model coincided well with those obtained from measurements. Various response of the proposed model were compared below 10 Hz with experimental data reported in the literature. The model responses generally show good agreement with the experimental data in the apparent mass, transmissibility to the vertical spinal motion and the transmissibility to vertical head motion.

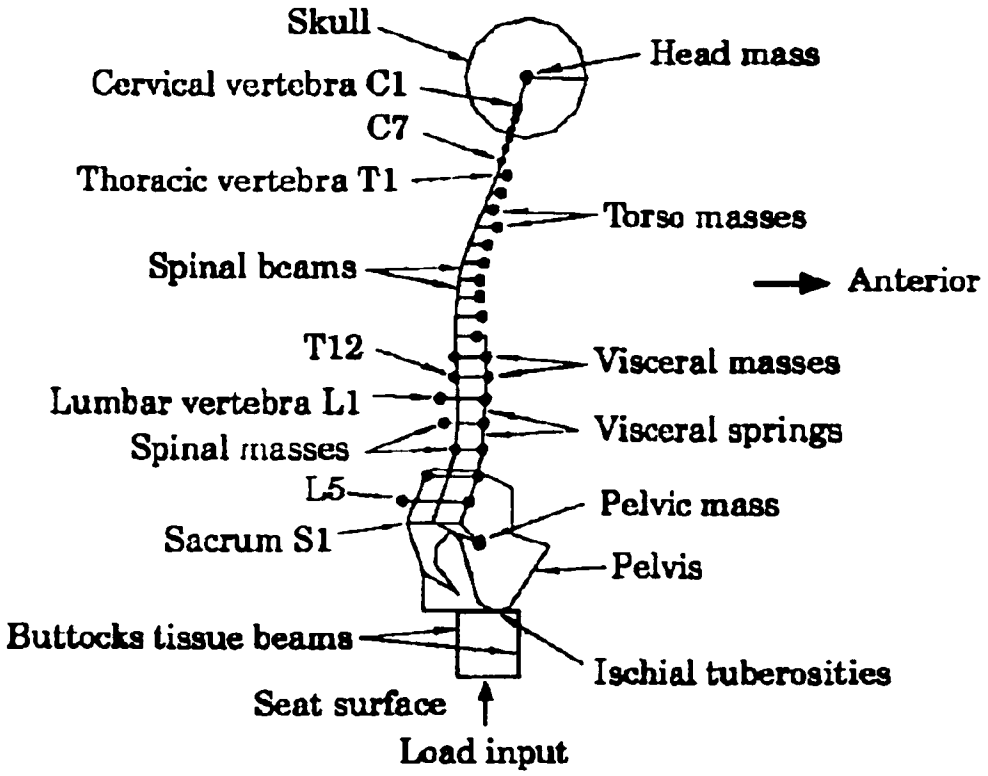

Figure 1.19: The two-dimensional biomechanical model in the normal posture [40].

1.3 Scope of the Dissertation Research

The automotive seats are designed to accommodate subjects of different weights and different vibration environments. From the review of literature, it is apparent that the vibration comfort performance of an automotive seat is strongly influenced by the static and dynamic characteristics of the seat cushion and the biodynamic behavior of the seated human body. Although the comfort performance of the automotive seats can be reliably assessed through experiments with human subjects, when representative subjects sample and test conditions are determined, this approach involves high cost and certain ethical concerns. The assessment methods based on proven analytical models, which either eliminate or reduce the involvement of human subjects and repetitive tests, are thus considered highly desirable.

The development of analytical model for vibration comfort assessment of seats requires modeling of the static and dynamic properties of PUF cushions, and the human occupant, and their integration. Although a number of automotive seat and occupant models have been proposed, their effectiveness in assessing the comfort performance has not yet been proven. Moreover, only limited efforts have been made to derive analytical models of the coupled human occupant and automotive seat model.

From the review of the published studies on the characterization of PUF cushion, it is apparent that mechanical properties are strongly influenced by the preload, excitation frequency and deflection magnitude. The models developed thus far mostly consider the deflection magnitude, while only two of the models attempt to consider the deflection magnitude, preload and frequency. The validity of these models, however, has not been proven even with a rigid mass representing the human occupant.

The biodynamic models of the seated occupant exposed to WBV are known to be formulated under condition that is not representative of the automobile environment. The application of the models to the PUF model, performed in one study, thus yields unsatisfactory results [35,21]. The large degree of error observed between the coupled model response and the measured data may be attributed to two major factors: (i) lack of proven model of the PUF cushion; and (ii) inapplicability of the biodynamic model of the occupant. It should also be pointed out that the biodynamic models are invariably desired from the measured biodynamic response functions that are acquired for the human subject seated on a rigid platform. The automotive seats provide a flexible interface and coupling between the seat and the occupant, which may affect the biodynamic response and the distribution of body weight on the seat. This would raise additional concerns on the applicability of the reported models.

This dissertation research focuses on the development of automotive seat cushion model and the human occupant model for effective assessment of the coupled system. The measured static and dynamic properties of PUF cushion are analyzed to study the influence of seated weight, frequency and amplitude of excitation. An analytical model is then derived and validated when coupled with a passive mass representing the human occupant. Vibration comfort performance of the coupled seat-occupant system is attempted by integrating the selected biodynamic models to the validated seat cushion model. Optimization method is used to identify the human occupant model parameters that would satisfy both the biodynamic response of the occupant seated on a rigid platform and the vibration transmissibility of the coupled seat-occupant system.

The dissertation research is expected to yield considerable contributions to the knowledge in view of vibration response of human occupants seated under automotive postures and vibration conditions. The outcome of the research work will provide a design and analysis tool for enhancement of human comfort and safety under automotive vibration environment.

1.4 Objectives of the Dissertation Research

The overall objective of this dissertation is to develop methodologies for objective assessment of vibration performance characteristics of the car seats subjected to whole-body vibration, such that the human exposure to transmitted vibration during evaluations is reduced.

As part of this study, it is proposed to derive models of a car seat and of a seated automobile occupant, as a means of predicting the influence of seat design parameters on its vibration attenuation performance. While the seat model is derived on the basis of measured dynamic stiffness and damping characteristics of a car seat cushion, the biodynamic model is derived on the basis of reported models and apparent mass response data. The seat as well as the combined models are analyzed and validated on the basis of measurements carried out in the laboratory to assess the vibration transmissibility characteristics of a car seat loaded with passive load and subjects. For that purpose, sinusoidal vibration, white noise and typical acceleration time traces are used as inputs to the seat. In summary, the specific objectives of the study are summarized as follow, which also comply with some of the recommendation for future work outlined in [6]:

1. Acquire essential data to characterize static and dynamic properties of automotive seat cushions from the laboratory tests and published studies.
2. Perform laboratory measurements to derive vibration transmissibility characteristics of a car seat loaded with rigid mass and human subjects.
3. Derive a seat cushion model for different preloads corresponding to 5^{th}, 50^{th} and 95^{th} percentile body weight for automobile occupants based on the measured static and dynamic properties; and perform simulation to examine the model validity when loaded with a rigid mass.
4. Perform parametric sensitivity analysis to study the influence of the seat design parameters on the vibration attenuation performance of the seat with different body masses.
5. Develop a coupled occupant-seat model by integrating a published biodynamic model of the occupant to the validated seat model; perform simulation and examine the validity of the coupled model.
6. Formulate an optimization problem to identify the biodynamic model to be applied to automotive seats, such that the biodynamic response correlates with the measured data acquired for the subjects seated on a rigid platform, and the vibration transmissibility of the coupled system correlates with that derived from the laboratory measurements.
7. Explore the validity of the coupled seat-occupant model.

1.5 Thesis Organization

This dissertation is organized into six chapters to describe the research methodology in realizing the above objectives. The literature is reviewed in chapter 1 highlighting the research contributions on the various subjects so as to formulate the scope of the work.

Chapter 2 presents the test matrix and test methodology for characterizing the static and dynamic properties of automotive seat cushion. The static and dynamic force-deflection data are analyzed to identify the dependency on the preload, excitation frequency and deflection magnitude. Nonlinear seat cushion models are developed and validated using the measured data.

In Chapter 3, the test and data analysis methodologies are described for deriving the vibration transmissibility characteristics of an automotive seat loaded with rigid mass and human subjects. A non-linear vertical vibration model of the car seats is derived on the basis of the analytical model formulated in chapter 2. The seat model includes linear and nonlinear stiffness, and linear and nonlinear damping components. Finally, the model with a rigid mass representing the human occupant is analyzed to derive the vertical acceleration transmissibility of the seat under selected excitations. The validity of the model is demonstrated by comparing the model results with the measured data.

In chapter 4, an acceleration time history characterizing the typical vibration environment of automobiles synthesized using MATLAB Optimization Toolbox is used to evaluate the vibration attenuation performance of the seat. The analyses are performed to study the influence of various model parameters on the ride comfort performance of seats.

A coupled human-seat model is formulated in chapter 5 by integrating a human occupant model to the validated model of the seat. The validity of the model is examined by comparing the model results with the measured data. The occupant model is refined using optimization techniques. The validity of the modified human-seat model is demonstrated.

Finally, the highlights of the dissertation research, conclusions and the recommendations for the future work are presented in Chapter 6.

2 CHARACTERIZATION AND MODEL OF SEAT CUSHION

2.1 Introduction

The automotive seats are designed to provide adequate postural support and to further attenuate the whole body vehicular vibration arising primarily from the tire-terrain interactions, even though the automobile suspension is designed to provide as good a ride quality as possible [44]. Automotive driver/passenger seating comfort is strongly influenced by the perception of whole-body vibration. The comfort assessment of the car seats can be performed through accurate characterization of static and dynamic properties of the seat and the seated human body.

The polyurethane foam (PUF) is widely used in seat cushion design, which possesses complex mechanical properties. It has been established that the stiffness and damping properties of air-filled polymeric foams are nonlinear functions of the seated body weight, force-deflection and force-velocity properties of foam cushions, which primarily arise from the nonlinear stress relaxation behavior and viscous-elastic non linearity present in the stress-strain curves [21,35,45]. The dynamic characterization of an automotive seat cushion involves determination of dynamic stiffness and damping properties. These properties may depend upon various internal factors, such as material, and construction, and external factors, such as seated body weight, and amplitude and frequency of excitation. The seat properties may be identified in the laboratory through measurement of the static and dynamic force deflection characteristics under representative test conditions. The static and dynamic tests are performed on a candidate seat, which is referred to as seat "C". The reported data for two other seats, referred to as

seat "A" and seat "B" [46], is further considered for general characterization. Analytical models are formulated to describe both static and dynamic properties as function of the preload and excitation conditions. This chapter presents the test methodology employed to characterize the static and dynamic properties of PUF seat cushions.

2.2 Test Methodology

2.2.1 Test setup

Few studies have shown that the stiffness and damping characteristics of PUF seat cushions are strongly dependent upon frequency and amplitude of excitation and body mass [21,35]. The experiment is thus designed to acquire the force-deflection and force-velocity data under a wide range of these important parameters, namely, preload (body weight), and excitation amplitude and frequency. Figure 2.1 illustrates the schematic of the test setup designed as recommended in the SAE J1051 [42] to perform the static and dynamic tests. The test setup comprises a vibration platform mounted on an electro-hydraulic vibration exciter. An indenter comprising 20 cm diameter disk and fixed to an inertial frame through a force sensor is used to apply the desired preload. The initial position of the vibration exciter is adjusted to achieve a desired preload. The vibration exciter is operated in the position feedback mode to generate sinusoidal displacement motion. The static and dynamic characteristics of the components under varying loads and displacement excitations are measured in terms of instantaneous force, displacement and velocity response using a Sensotech load cell, a built-in Schaevitz LVDT, and a velocity transducer (LVT), respectively. The load cell and LVT are installed between a fixed inertial frame and the component, which is mounted on a vibration platform. The

LVDT is built within the electric-hydraulic exciter to measure the excitation displacement [35].

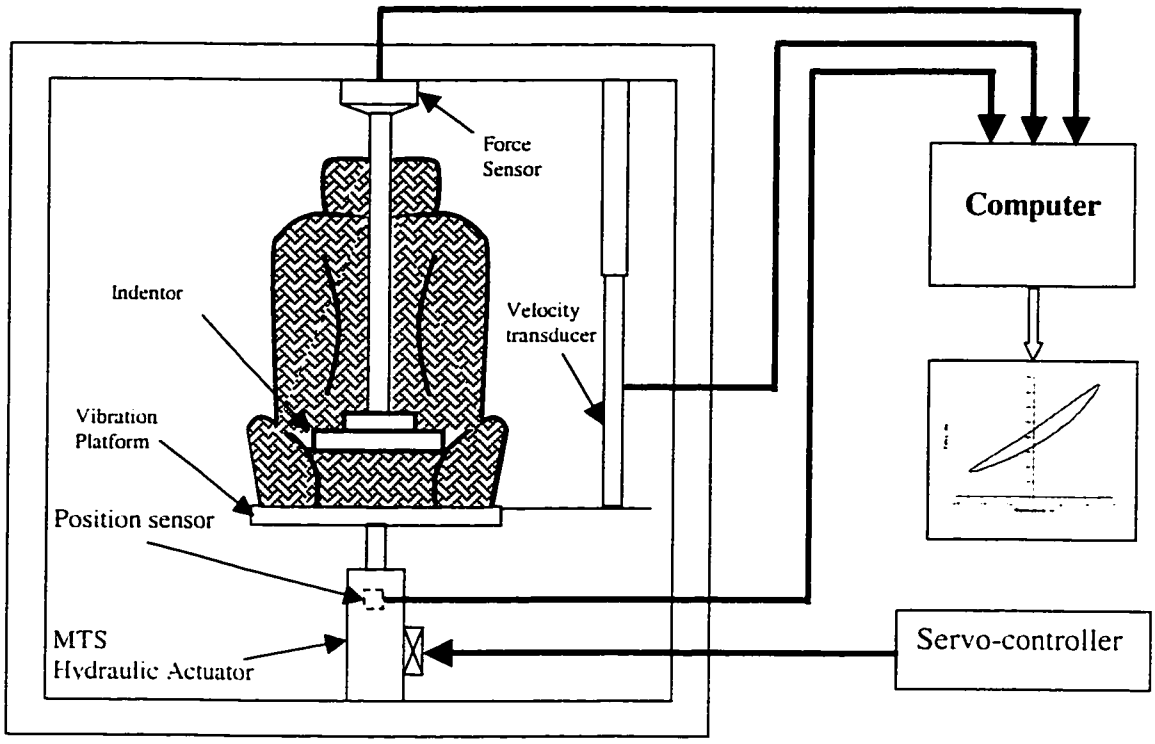

Figure 2.1: Schematic of the test setup for measurement of static and dynamic properties of seat cushion.

2.2.2 Test Matrix

The experiment is designed to conduct experimental characterizations under a wide range of representative conditions. The range of test variables is derived from the following:

- Preload: The static and dynamic characterizations of the seat are performed for different preloads representing the 5^{th}, 50^{th} and 95^{th} percentile adult population. Considering that a seat cushion supports approximately 73% of the total body weight [43], three different preloads of 358 N, 537 N and 716 N are selected, which represent the body masses of 50kg, 75kg, and 100 kg, respectively.
- Amplitude of Excitation: The vehicle seats are subject to varying levels of displacement excitations depending upon various vehicle and road factors. In the dynamic characterization test of the seat, the input excitations of amplitudes ranging from 0.254 mm to 19 mm are considered to represent the range of displacements that may be encountered in the automobiles.
- Frequency of Excitation: The automobile vibration predominates in the vicinity of the sprung mass natural frequencies (≈ 1 Hz) and the unsprung mass natural frequencies (≈ 9-12 Hz). The test matrix is thus formulated to vary the excitation frequency from 0.5 to 12 Hz. The amplitude of excitation at higher frequencies, however, is limited to ensure safety of the experiment and prevent the failure of the seat cushion.

Based on practical driving conditions the test matrix, illustrating the range of preloads, amplitudes and frequencies, are shown in Table 2.1.

Apart from the dynamic test, the static properties of the seat cushion are also evaluated under gradual loading and unloading of the seat. The loading and unloading is achieved through a large amplitude and low frequency (0.0833 Hz) displacement signal.

Table 2.1: Test Matrix Describing the Range of Preloads, Excitation Strokes and Excitation Frequencies.

Preload (N)	**Excitation Amplitude (mm)**	**Excitation Frequency (Hz)**						
		0.5	**1**	**2**	**4**	**8**	**10**	**12**
358 & 537	0.254	–	–	–	–	×	×	×
	0.635	–	–	–	–	×	×	×
	1.270	–	–	–	–	×	×	×
	1.905	–	–	–	–	×	×	×
	2.54	×	×	×	×	×	–	–
	6.35	×	×	×	×	–	–	–
	12.7	×	×	×	×	–	–	–
	19.05	×	×	×	×	–	–	–
716	0.254	–	–	–	–	×	×	×
	0.635	–	–	–	–	×	×	×
	1.270	–	–	–	–	×	×	×
	1.905	–	–	–	–	×	×	
	2.54	×	×	×	×	–	–	–
	6.35	×	×	×	×	–	–	–
	12.7	×	×	×	×	–	–	–
	19.05	×	×	×	×	–	–	–

Notes: the conditions marked with × are used in the experiments;
and the conditions marked with – are not used in the experiments.

2.2.3 Data acquisition

The dynamic properties of the car seats are derived from the force-deflection characteristics, measured under different vibration frequencies, preloads and excitation amplitudes. The input displacement signal is configured and controlled by servo-controller. The force, deflection and velocity signals are acquired in an analog DMA (Direct Memory Access) block of the PC comprising an 8-channel data acquisition board PC-1-204228W-1. The DMA block is linked to a DDE (Dynamic Data Exchange) server block. The analog signals are converted into digital signals by A/D (Analog/Digital) conversion, and transferred into the MS-EXCEL worksheet, using Visual Designer software. Figure 2.2 illustrates the schematic of test and data acquisition system.

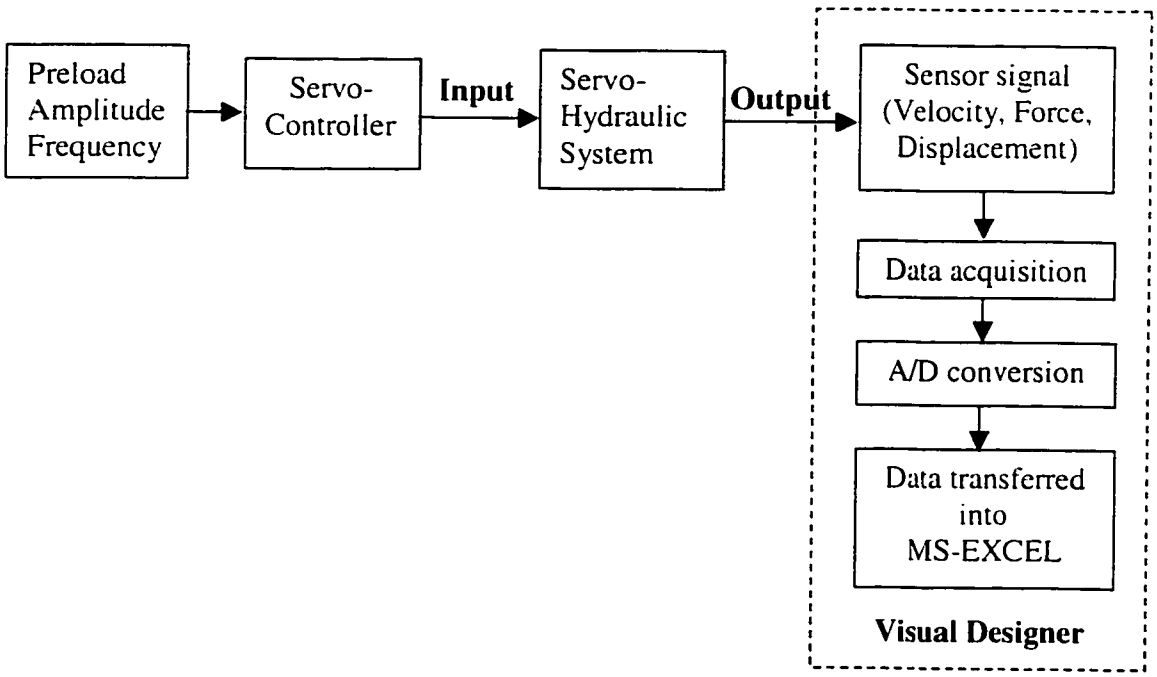

Figure 2.2: The schematic of the test and data acquisition system.

The sampling rate of the data acquisition is configured within the Visual Designer acquire 360 samples/cycle for each channel. The selection of this sampling rate allows for desirable variations in the sampling rate with variations in the excitation frequency. The sampling rate satisfies the equation

$$\text{Sampling rate} = 360 * f \text{ (samples/s)} \tag{2.1}$$

The acquired data is used to generate on-line force-deflection and force-velocity characteristics of the seat cushion within the EXCEL environment. The measured data and the curves are further analyzed to derive the static and dynamic properties and their dependence upon the preload, frequency and deflection.

2.3 Static Characteristics of car seat cushion

Figure 2.3 illustrates the static force-deflection characteristics of the seat "C", acquired under cycle loading at a very low frequency of 0.0833 Hz. The measured data exhibit considerable hysteresis. The mean force attained during loading and unloading is clearly a nonlinear function of the cushion deflection x. The curve is fitted by polynomial and the order of polynomial is determined by the tolerance between the measured data and fitting curve. The polynomial may be expressed as:

$$F(x) = 6\times10^{-5}x^4 - 5.4\times10^{-3}x^3 + 0.2353x^2 + 3.4056x + 3.7248; \quad x > 0 \tag{2.2}$$

where F(x) the force in N and x is cushion deflection in mm.

From the figure, if can be clearly seen that the static stiffness of the seat increases considerably with increasing preload and deflection. Equation (2.2) may be used to

compute the static stiffness coefficients at different magnitudes of static deflections by differentiation of the force F with respect to the deflection x, namely,

$$\text{stiffness} = \left.\frac{\partial F}{\partial x}\right|_{x=x_i} = 24\times10^{-5}x_i^{\,3} - 1.62\times10^{-2}x_i^{\,2} + 0.4706x_i + 3.4056 \qquad (2.3)$$

In the above, x_i is the static deflection corresponding to a specific preload F_i. The static deflection can be computed from Equation (2.2) by letting $F(x) = F_i$.

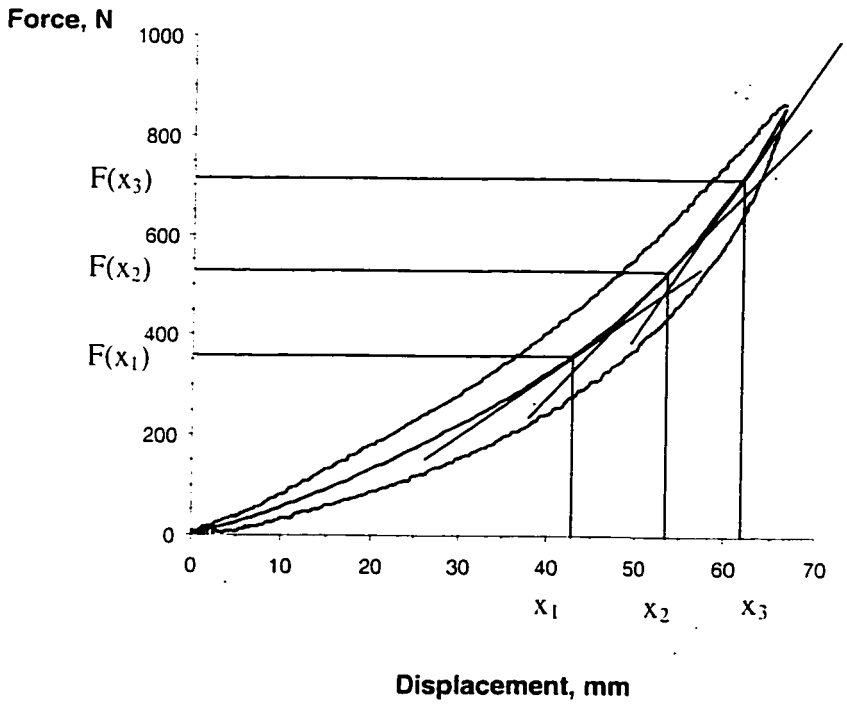

Figure 2.3: Measured static force-deflection characteristics of the seat "C" cushion.

In addition to the measured data for seat "C", the data acquired for the other two seats ("A" and "B") during an earlier study [46] were analyzed to compute their static

stiffness corresponding to different preloads. Table 2.2 summarizes the static stiffness characteristics of all three seats for specific values of preload. Owing to the available data the static stiffness values for seats "A" and "B" were determined for lower preloads. Moreover, seat "B" was reported to have failed under the higher preload set at 627N. The results clearly show that the seat stiffness increases considerably with increasing preload. This property may yield relatively less variation in the seat natural frequency with varying preload. The stiffness values further suggest that seat "C" yields much higher stiffness under larger preload, when compared with that of seats "A" and "B".

Table 2.2: Static Stiffness of all three seats.

Seat	Preload (N)	Deflection (mm)	Static Stiffness* (N/m)
"C"	358	42.76	12700
	537	54.17	19500
	716	61.89	27400
"A"	347	54	12000
	480	65	14000
	627	74	17700
"B"	347	60	10000
	480	71	14500

* Stiffness values are rounded to nearest hundreds.

2.4 Dynamic characteristics of car seat cushions

2.4.1 Dynamic stiffness coefficients

The dynamic stiffness coefficient of a seat is known to differ from its static stiffness value [35]. It is derived from the measured dynamic force-deflection data, as a function of the preload, excitation frequency and excitation amplitude. The measured dynamic force-deflection is an enclosed loading/unloading curve, where the static equilibrium position under a given preload is defined as the reference position. The dynamic stiffness coefficients are then derived from the mean curves around the operating point representing the static equilibrium [35]. In order to simplify calculation of dynamic stiffness, Figure 2.4 illustrates, as an example, the force-deflection characteristics of seat "C" corresponding to 358 N preload, and subject to 12.7 mm peak displacement excitation at a frequency of 1 Hz. The mean force may be expressed as a cubic function in deflection:

$$F(x) = 0.012x^3 + 0.3415x^2 + 18.763x + 353.88 \qquad (2.4)$$

where F is in N and x is in mm.

The dynamic stiffness corresponding to the defined preload and excitation is derived as:

$$\frac{\partial F}{\partial x}\Big|_{x=0} = 0.036x^2 + 0.683x + 18.763\Big|_{x=0} = 18763 \qquad N/m$$

According to the method described above, the dynamic force-deflection characterization measured for seat "C" are analyzed to derive the dynamic stiffness coefficients, which are listed in Table 2.3. The dynamic stiffness for seats "A" and "B", reported in a previous study, are listed in Table 2.4 [46]. The data in Tables 2.3 and 2.4

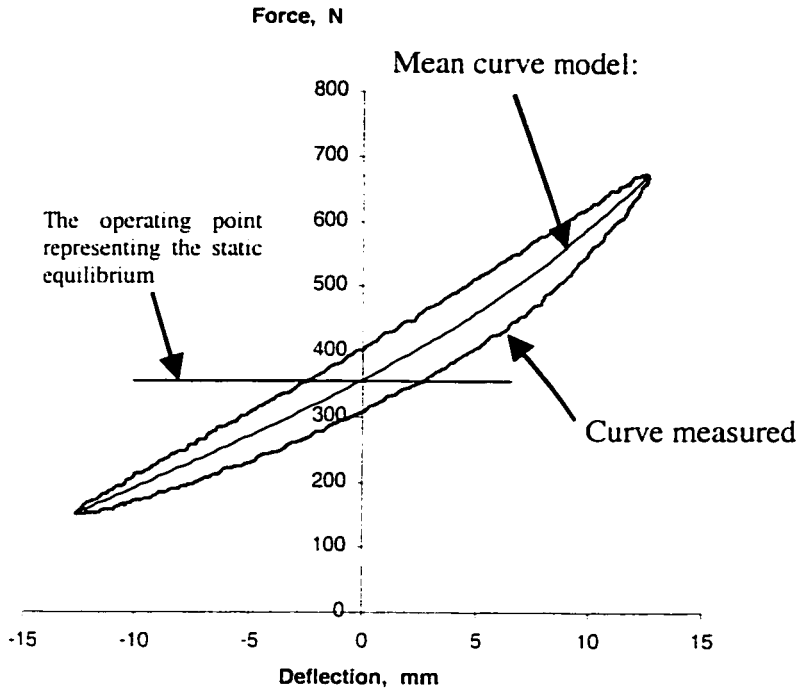

Figure 2.4: Dynamic Force-Deflection Characterization (Preload = 358 N, Stroke = 12.7mm, and Excitation Frequency = 1 Hz).

clearly show that the dynamic force-deflection characteristics and thus the dynamic stiffness of seat cushions are a function of the preload, amplitude and frequency of excitation. The results are plotted graphically in Figures 2.5 to 2.25.

The dynamic force-deflection characteristics of seat "C", presented in Figures 2.5-2.7, clearly illustrate that excitation frequency and amplitude influence the dynamic stiffness when the preload is constant. The dynamic stiffness quickly approaches a higher value as the frequency is increased to 0.5 Hz. The stiffness characteristics of the cushion then increase only slightly with further increase in the excitation frequency, and decrease greatly with the increase in the amplitude of the excitation. The dynamic stiffness increases from 42000 N/m to 45000 N/m, when the frequency of excitation is increased

from 2 Hz to 8 Hz at an amplitude of excitation of 2.54 mm under preload of 537 N. The dynamic stiffness increases just 7 % when the frequency increases from 2 Hz to 8 Hz. The dynamic stiffness decreases from 42000 N/m to 24000 N/m, when the amplitude of excitation is increased from 2.54 mm to 19.05 mm at frequency of excitation of 2 Hz under preload of 537 N. This decrease is most likely attributed to increased air flow.

Results are summarized:

i) when f increases, k increases for similar amplitude;

ii) when amplitude of excitation increases, k decreases;

iii) when preload increases, k increases.

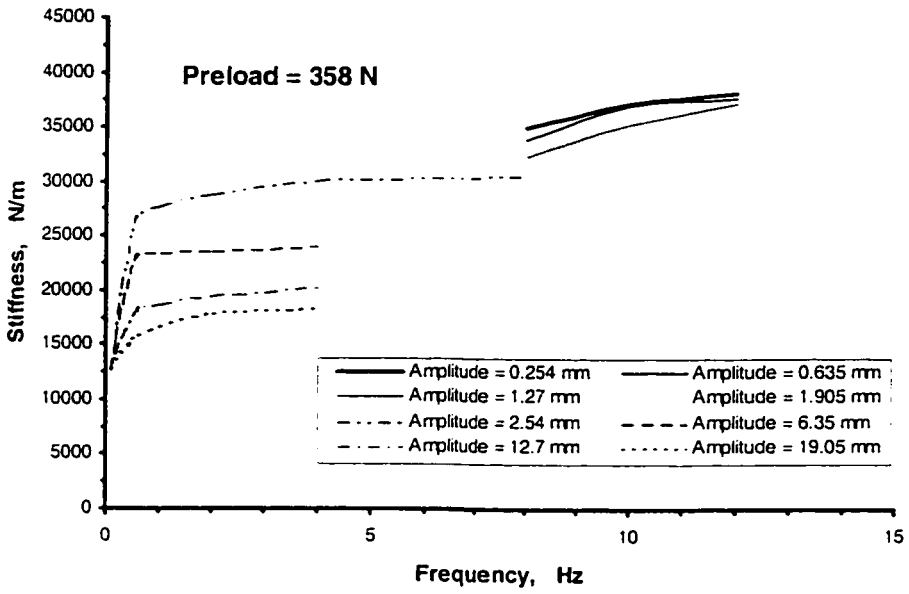

Figure 2.5: Influence of the Excitation Frequency and Amplitude on Dynamic Stiffness at Constant Preload of 358 N for Seat "C".

Table 2.3: The dynamic stiffness coefficients and equivalent damping coefficients for seat "C".

Preload (N)	Deflection (mm)	Frequency (Hz)	Stiffness (N/m)	Damping (Ns/m)
358	2.54	0.5	26195	1260.72
	6.35		22647	1265.97
	12.7		17823	1156.54
	19.05		15455	1064.61
	2.54	1	27727	714.41
	6.35		23434	700.40
	12.7		18760	619.85
	19.05		16582	576.08
	2.54	2	28781	385.22
	6.35		23602	385.22
	12.7		19455	339.69
	19.05		17397	308.18
	2.54	4	30180	210.12
	6.35		24096	210.12
	12.7		20126	189.11
	19.05		17909	175.10
	0.254	8	34988	140.08
	0.635		33899	112.06
	1.27		32372	112.06
	1.905		31562	112.06
	2.54		30509	196.11
	0.254	10	37270	70.04
	0.635		37146	87.55
	1.27		35298	105.06
	1.905		33891	105.06
	0.254	12	38219	63.04
	0.635		37675	84.05
	1.27		37209	105.06
	1.905		35771	126.07

Preload (N)	Deflection (mm)	Frequency (Hz)	Stiffness (N/m)	Damping (Ns/m)
537	2.54	0.5	38564	1968.12
	6.35		29842	2039.04
	12.7		24924	1776.39
	19.05		21884	1587.28
	2.54	1	39573	1040.09
	6.35		30562	1062.86
	12.7		24883	903.52
	19.05		22593	808.96
	2.54	2	41021	542.81
	6.35		31297	612.85
	12.7		25936	469.27
	19.05		23304	427.24
	2.54	4	43497	273.16
	6.35		33076	294.17
	12.7		26801	252.14
	19.05		23351	231.13
	0.254	8	47536	238.14
	0.635		47044	168.10
	1.27		45473	196.11
	1.905		43385	182.10
	2.54		42956	238.14
	0.254	10	52674	140.08
	0.635		52388	140.08
	1.27		49867	140.08
	1.905		46920	140.08
	0.254	12	53313	147.08
	0.635		50972	126.07
	1.27		48685	147.08
	1.905		45151	168.10

Preload (N)	Deflection (mm)	Frequency (Hz)	Stiffness (N/m)	Damping (Ns/m)
716	2.54	0.5	49212	2390.99
	6.35		37580	2515.31
	12.7		30558	2236.90
	19.05		26804	2002.27
	2.54	1	51999	1302.74
	6.35		39721	1397.30
	12.7		31574	1188.93
	19.05		28209	1061.11
	2.54	2	54568	703.90
	6.35		40986	735.42
	12.7		33392	626.86
	19.05		28941	546.31
	2.54	4	55867	385.22
	6.35		42029	406.23
	12.7		33677	336.19
	19.05		29497	308.18
	0.254	8	61567	350.20
	0.635		59961	266.15
	1.27		58888	336.19
	1.905		58863	336.19
	0.254	10	70254	105.06
	0.635		70098	157.59
	1.27		64945	175.10
	1.905		63353	192.61
	0.254	12	72575	126.07
	0.635		71807	168.10
	1.27		68781	189.11

Table 2.4: The dynamic stiffness coefficients and equivalent damping coefficients for seat "A" and seat "B".

Preload	Amplitude	Frequency	Stiffness (N/m)		Damping (Ns/m)	
			Seat "A"	Seat "B"	Seat "A"	Seat "B"
347	6.35 (for seat "A") 2.54 (for seat "B")	0.1/0.5	19050.88	20434.17	656.5	
		1	20101.48	23743.56	411.485	584.834
		1.5	20714.33	25249.42	315.18	402.73
		2	20574.25	25547.09	245.14	322.184
		4	20889.43	26632.71	154.1	243.389
		6	21729.91	27193.03	124.3	171.598
		8	22115.13	27350.62	117.317	155.839
		10	22290.23	28138.57	99.761	136.578
	12.7	0.1/0.5	16757.07	17194.82	605.8	
		1	17422.45	19296.02	401	462.264
		1.5	17912.73	20311.6	297.67	348.449
		2	17807.67	20206.54	232.9	288.915
		4	18227.91	21187.1	157.6	194.361
		6	18893.29	21764.93	120.8	159.341
		8	18998.35	22447.82	113.8	140.08
		10	19401.08	22307.74	94.6	105.06
	19.05	0.1/0.5	14936.03		528.8	
		1	15443.82		360.7	
		1.5	15864.06		260.9	
		2	15899.08		201.4	
		4	16214.26		131.3	
		6	16757.07		105.1	
		8	17299.88		91.1	
		10	18000.28		91.1	
480	6.35 (for seat "A") 2.54 (for seat "B")	0.1/0.5	20959.47	27525.72	558.6	
		1	21554.81	29802.02	371.2	730.167
		1.5	21519.79	30747.56	253.895	464.015
		2	21659.87	30905.15	218.875	358.955
		4	22447.82	32638.64	154.1	266.152
		6	23025.65	33128.92	98.1	236.385
		8	23936.17	33198.96	61.3	187.357
		10	23638.5	33304.02	80.5	168.096
	12.7	0.1/0.5	18858.27	21992.56	605.8	
		1	19453.61	23498.42	394.01	565.573
		1.5	19471.12	24251.35	301.22	435.999
		2	19663.73	24549.02	239.9	339.694
		4	20346.62	25669.66	164.6	234.634
		6	21064.53	26282.51	110.3	197.863
		8	21502.28	26493.34	91.1	182.104
		10	21607.34	26702.75	94.6	148.835
627	6.35	0.1/0.5	22412.8		590.1	
		1	22903.08		376.5	
		1.5	22833.04		262.65	
		2	23165.73		192.61	
		4	23848.62		154.1	
		6	24128.78		80.5	
		8	24934.24		101.6	
		10	25196.89		91.1	
	12.7	0.1/0.5	19646.22		576.1	
		1	21677.38		376.5	
		1.5	21677.38		310	
		2	22010.07		255.6	
		4	22517.86		157.6	
		6	23095.69		110.3	
		8	24163.8		113.832	
		10	24058.74		105.1	

Notes: 0.1/0.5 means 0.1 Hz for seat "A" and 0.5 Hz for seat "B"

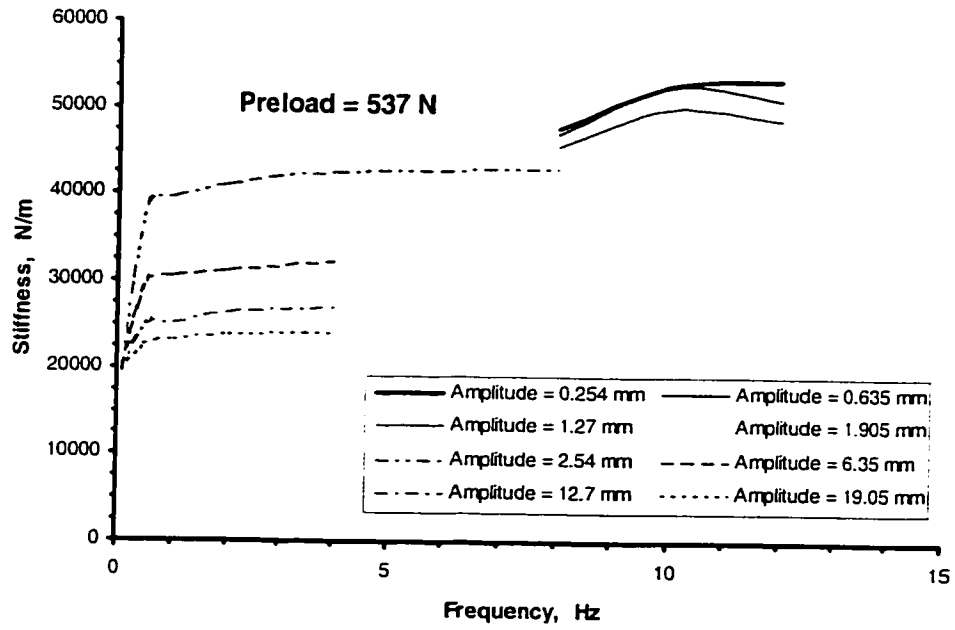

Figure 2.6: Influence of the Excitation Frequency and Amplitude on Dynamic Stiffness at Constant Preload of 537 N for Seat "C".

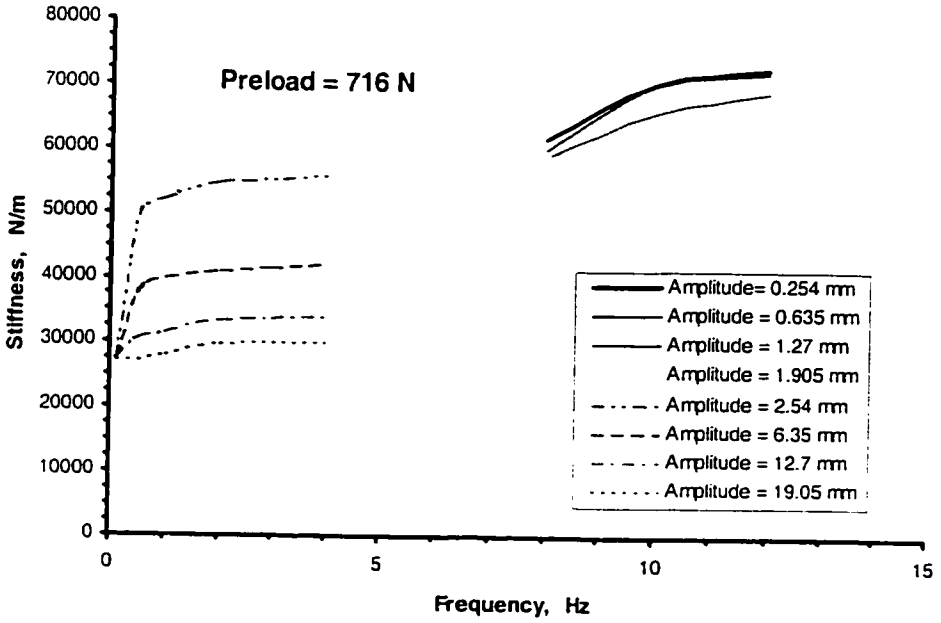

Figure 2.7: Influence of the Excitation Frequency and Amplitude on Dynamic Stiffness at Constant Preload of 716 N for Seat "C".

The dynamic force-deflection characteristics of seats "A" and "B", shown in Figure 2.8-2.12, also reveal similar trends as those of seat "C". For seat "A", the stiffness increases just 4.8 % (from 21000 N/m to 22000 N/m) when the frequency increases from 2 Hz to 8 Hz under the preload of 347 N and amplitude of excitation of 6.35 mm; the dynamic stiffness decreases up to 74% (from 21000 N/m to 15500 N/m) when the amplitude increases by 300% (from 6.35 mm to 19.05 mm) at frequency of excitation of 2 Hz under the preload of 347 N. For seat "B", the stiffness increases just 6.5 % (from 31000 N/m to 33000 N/m) when the frequency increases from 2 Hz to 8 Hz under the preload of 480 N and amplitude of excitation of 2.54 mm; the dynamic stiffness decreases up to 77.5% (from 31000 N/m to 24000 N/m) when the amplitude increases 400 % (from 2.54 mm to 12.7 mm) at frequency of excitation of 2 Hz under the preload of 480 N.

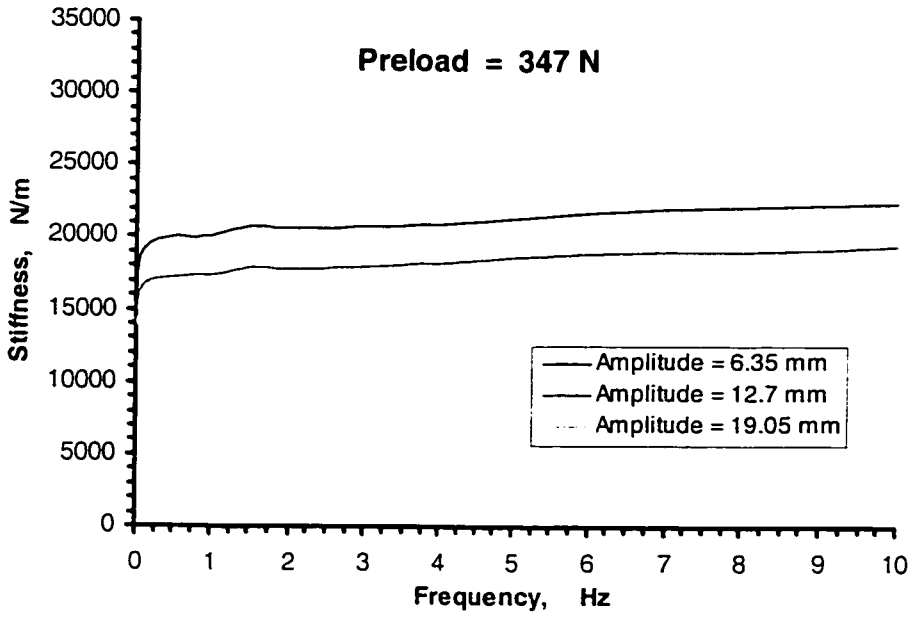

Figure 2.8: Influences of the Excitation Frequency and Amplitude on Dynamic Stiffness at Constant Preload of 347 N for Seat "A".

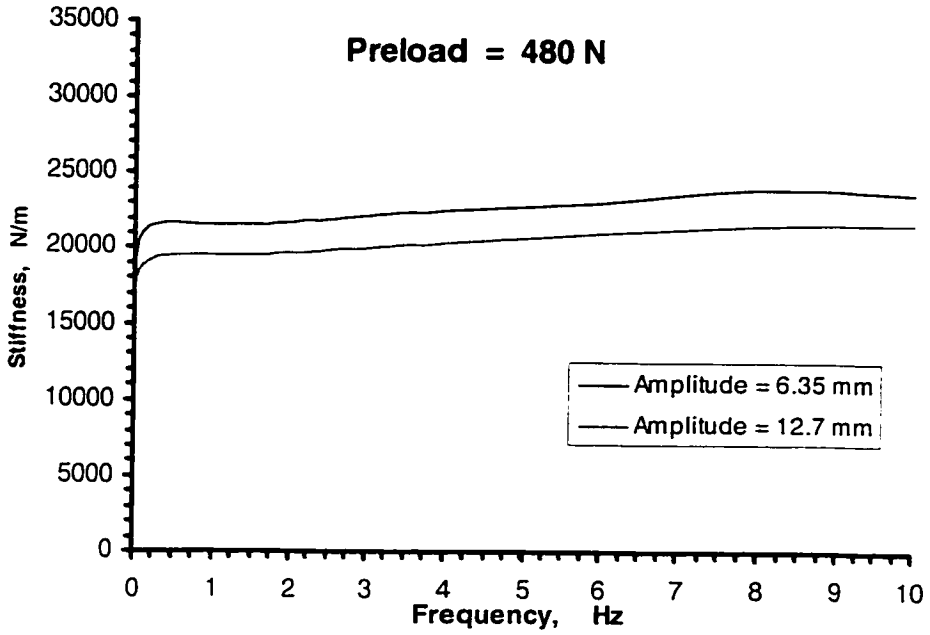

Figure 2.9: Influences of the Excitation Frequency and Amplitude on Dynamic Stiffness at Constant Preload of 480 N for Seat "A".

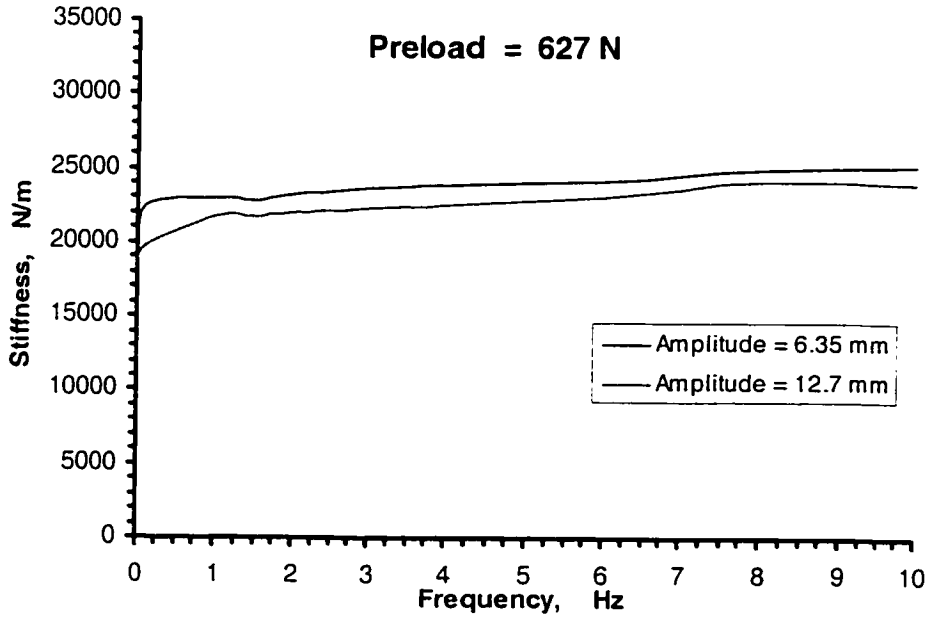

Figure 2.10: Influences of the Excitation Frequency and Amplitude on Dynamic Stiffness at Constant Preload of 627 N for Seat "A".

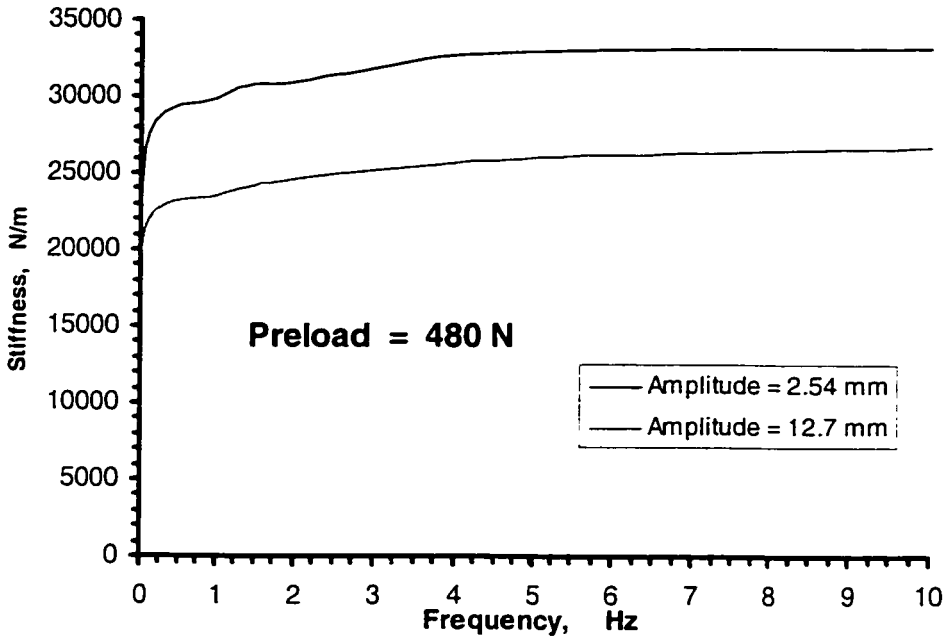

Figure 2.11: Influence of the Excitation Frequency and Amplitude on Dynamic Stiffness at Constant Preload of 480 N for Seat "B".

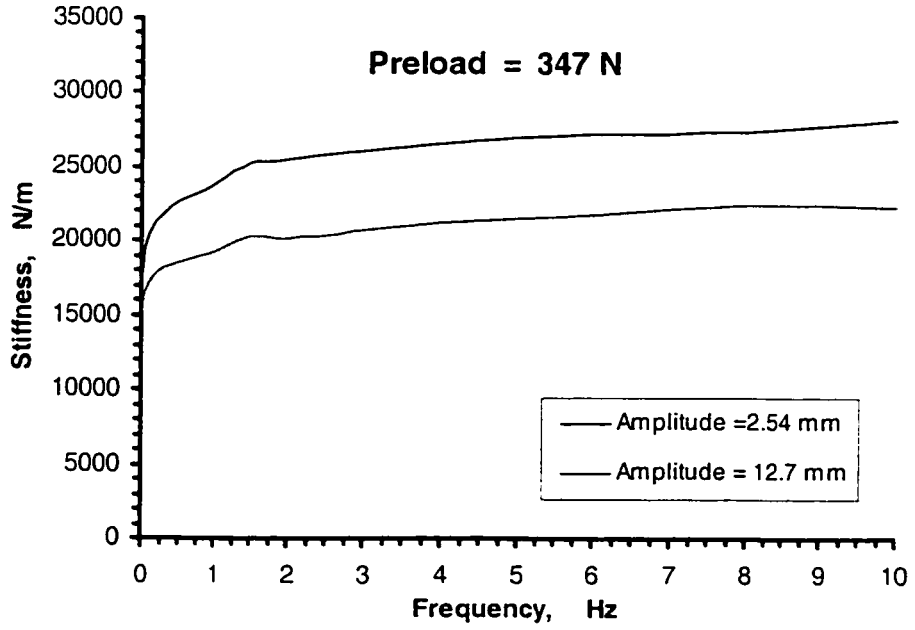

Figure 2.12: Influences of the Excitation Frequency and Amplitude on Dynamic Stiffness at Constant Preload of 347 N for Seat "B".

In summary, the increase in the excitation amplitude yields a considerably lower stiffness, while an increase in the excitation frequency causes a slight increase. The results also suggest that the influence of excitation frequencies on the dynamic stiffness of all three seats is very similar. The influence of amplitude, however, is most significant influence on Seat "A", and the least on Seat "C".

The dynamic force-deflection characteristics of seat "C" are further evaluated to study the influence of preload. Figures 2.13-2.20 illustrate the cushion stiffness as function of excitation frequency for different values of preload and amplitude. The results clearly show that the preload affects the stiffness most significantly, at all frequencies and

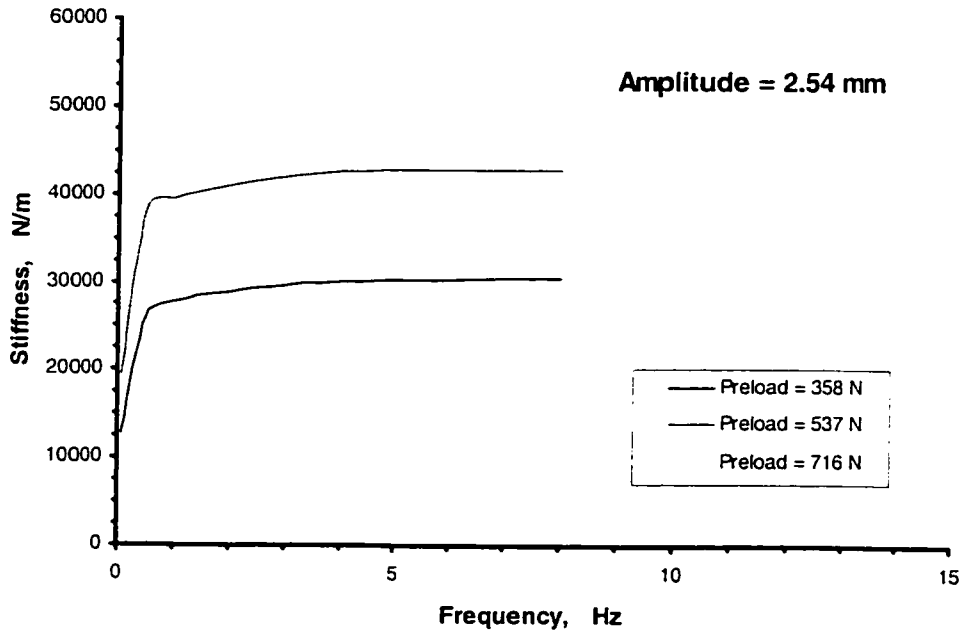

Figure 2.13: Influence of the Excitation Frequency and Preload on Dynamic Stiffness at Constant Stroke of 2.54 mm for Seat "C".

amplitudes of excitation. While the stiffness characteristics of the cushion increase only slightly with increase in the excitation frequency, the stiffness values increase greatly with increase in the preload. The dynamic stiffness increases from 55000 N/m to 58500 N/m, when the frequency of excitation is increased from 2 Hz to 8 Hz at amplitude of excitation of 2.54 mm under preload of 716 N. The dynamic stiffness increases from 27500 N/m to 55000 N/m, when the preload is increased from 358 N to 716 N at a frequency of excitation of 2 Hz under the amplitude of excitation of 2.54 mm. The dynamic stiffness increases up to 100 % when the preload increases by 100 %.

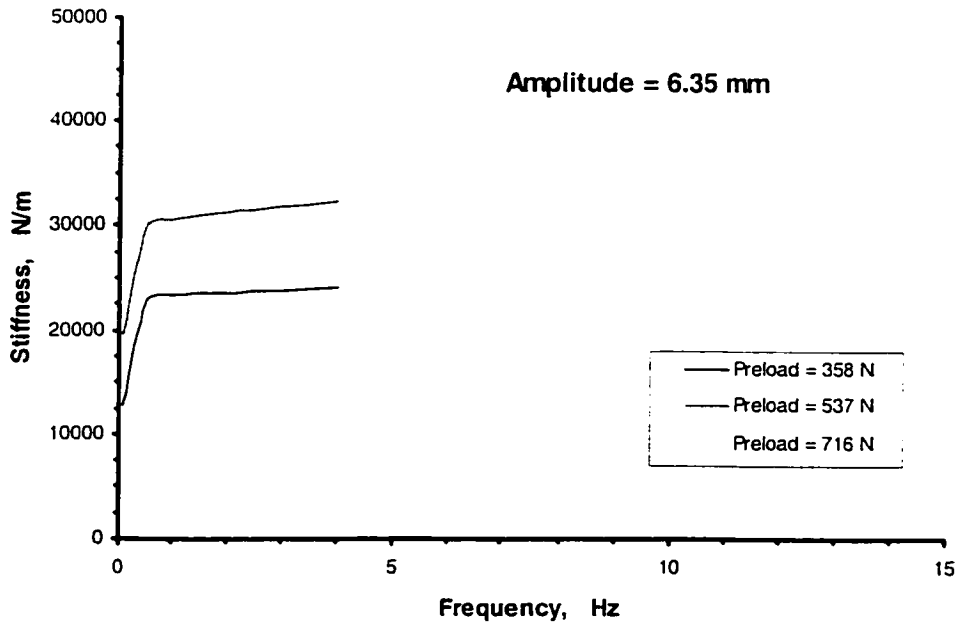

Figure 2.14: Influence of the Excitation Frequency and Preload on Dynamic Stiffness at Constant Stroke of 6.35 mm for Seat "C".

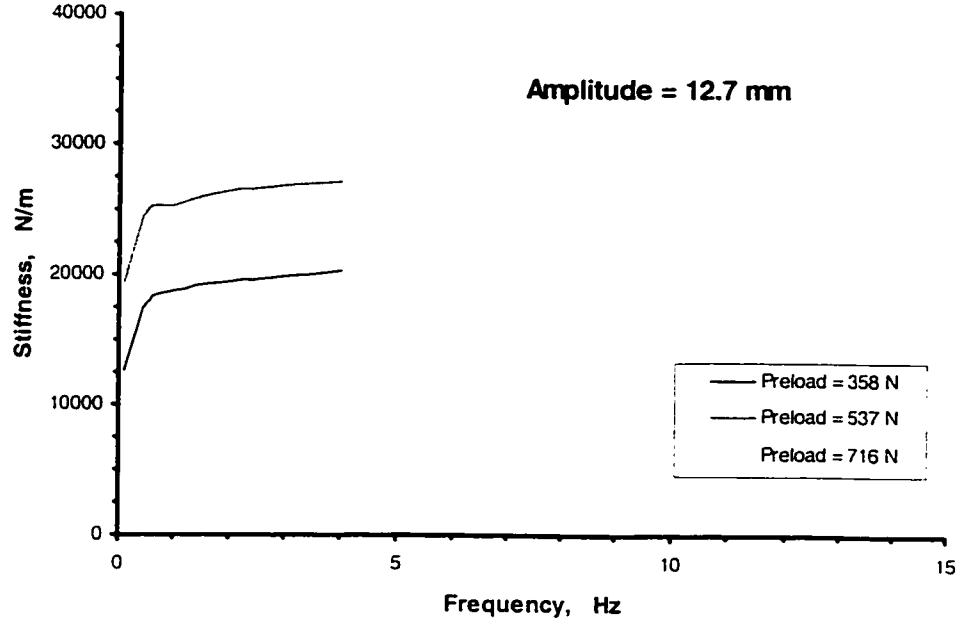

Figure 2.15: Influence of the Excitation Frequency and Preload on Dynamic Stiffness at Constant Stroke of 12.7 mm for Seat "C".

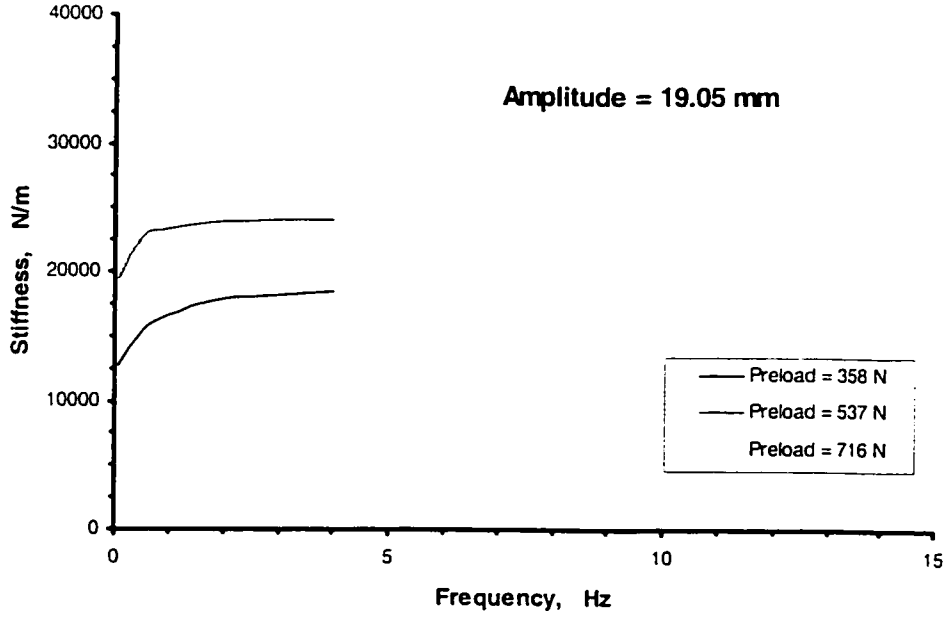

Figure 2.16: Influence of the Excitation Frequency and Preload on Dynamic Stiffness at Constant Stroke of 19.05 mm for Seat "C".

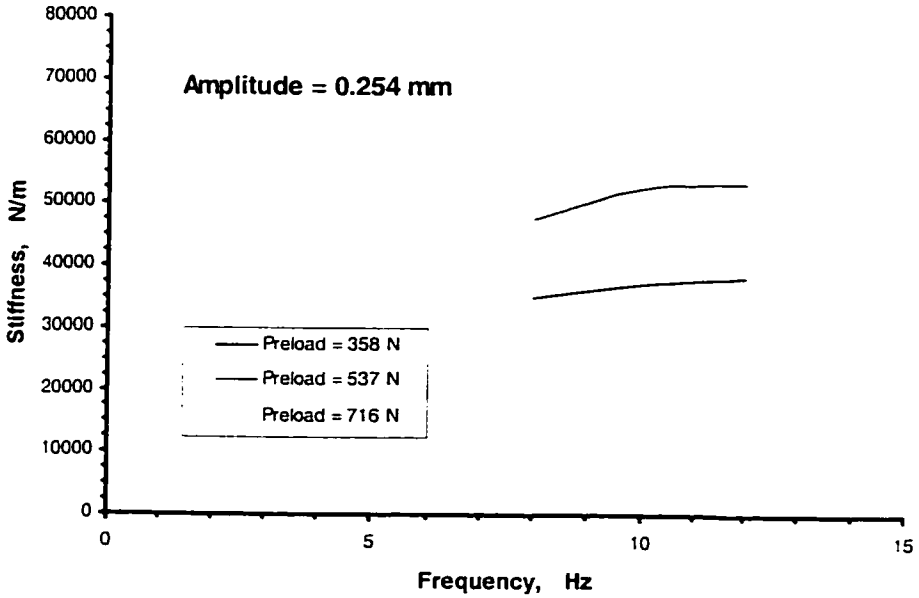

Figure 2.17: Influence of the Excitation Frequency and Preload on Dynamic Stiffness at Constant Stroke of 0.254 mm for Seat "C".

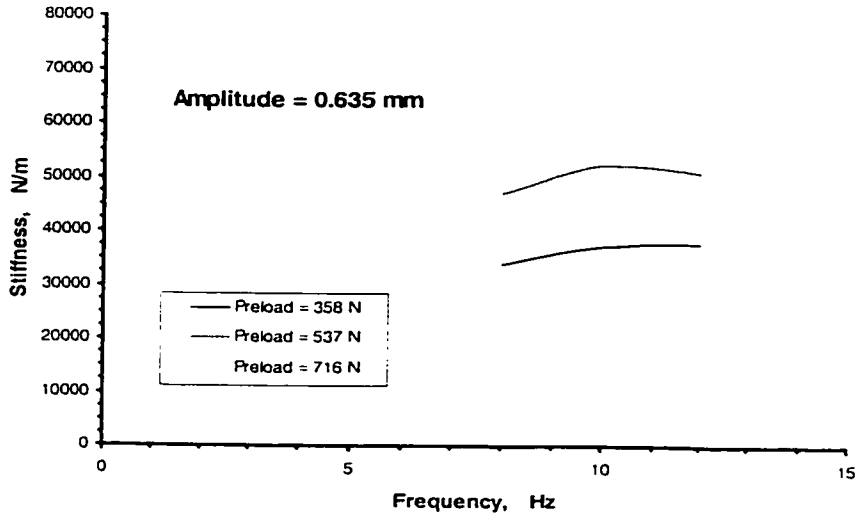

Figure 2.18: Influence of the Excitation Frequency and Preload on Dynamic Stiffness at Constant Stroke of 0.635 mm for Seat "C".

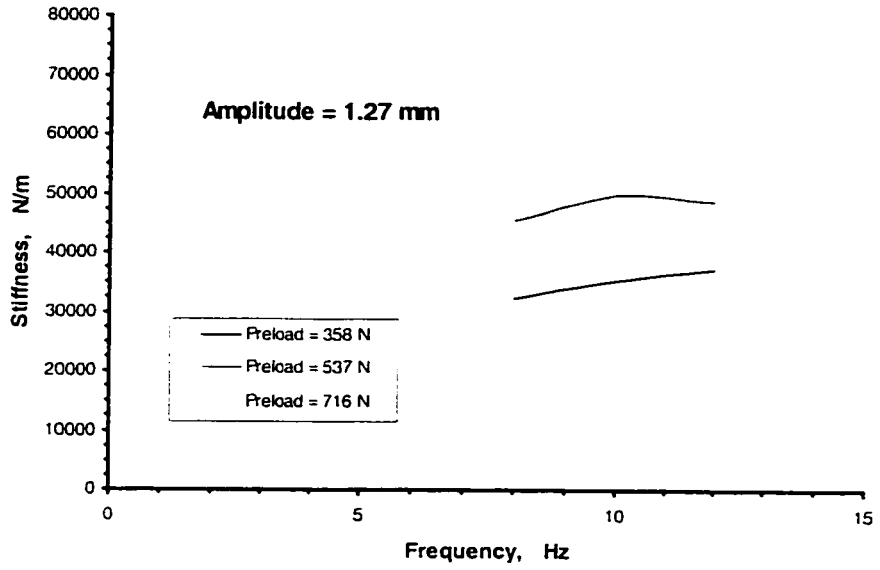

Figure 2.19: Influence of the Excitation Frequency and Preload on Dynamic Stiffness at Constant Stroke of 1.27 mm for Seat "C".

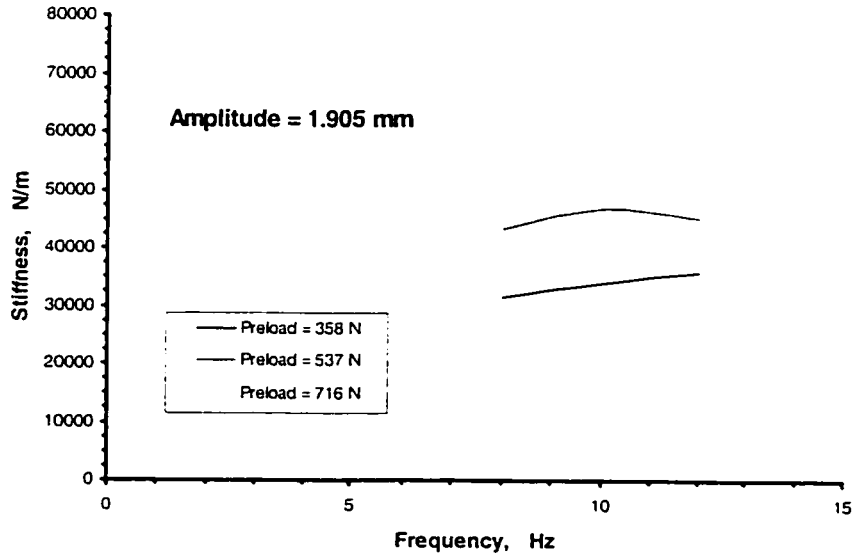

Figure 2.20: Influence of the Excitation Frequency and Preload on Dynamic Stiffness at Constant Stroke of 1.905mm for Seat "C".

The dynamic force-deflection characteristics of seats "A" and "B", shown in Figures 2.21-2.25, also reveal similar trends in preload as those observed for seat "C". For seat "A", the stiffness increases just 6.4 % (from 23500 N/m to 25000 N/m) when the frequency increases from 2 Hz to 8 Hz under the preload of 627 N and amplitude of excitation of 6.35 mm; the dynamic stiffness increases up to 14.6 % (from 20500 N/m to 23500 N/m) when the preload increases by 80 % (from 347 N to 627 N) at a frequency of excitation of 2 Hz under the amplitude of excitation of 6.35 mm. For seat "B", the stiffness increases just 7.2 % (from 31000 N/m to 33500 N/m) when the frequency increases from 2 Hz to 8 Hz under the preload of 480 N and amplitude of excitation of 2.54 mm; the dynamic stiffness increases up to 19 % (from 26000 N/m to 31000 N/m) when the preload increases by 38 % (from 347 N to 480 N) at a frequency of excitation of 2 Hz under the amplitude of excitation of 2.54 mm.

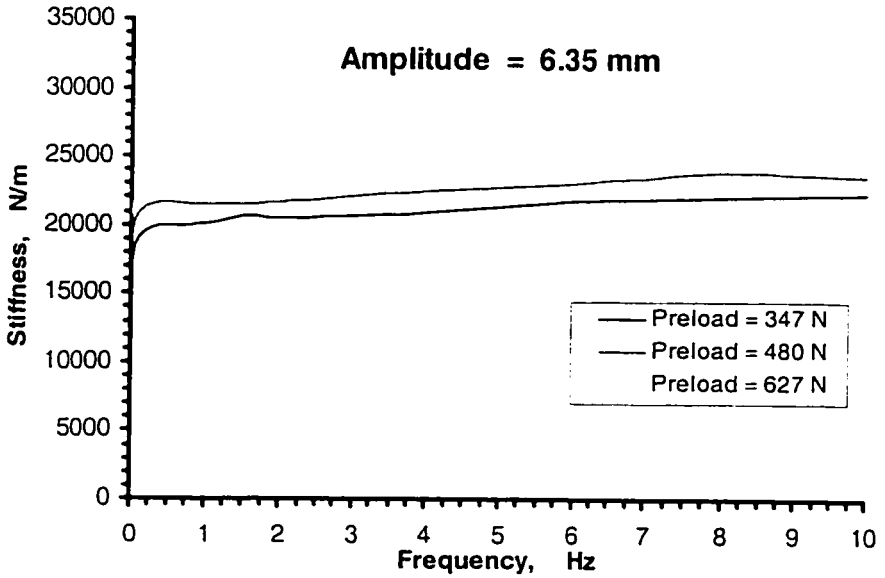

Figure 2.21: Influence of the Excitation Frequency and Preload on Dynamic Stiffness at Constant Stroke of 6.35 mm for Seat "A".

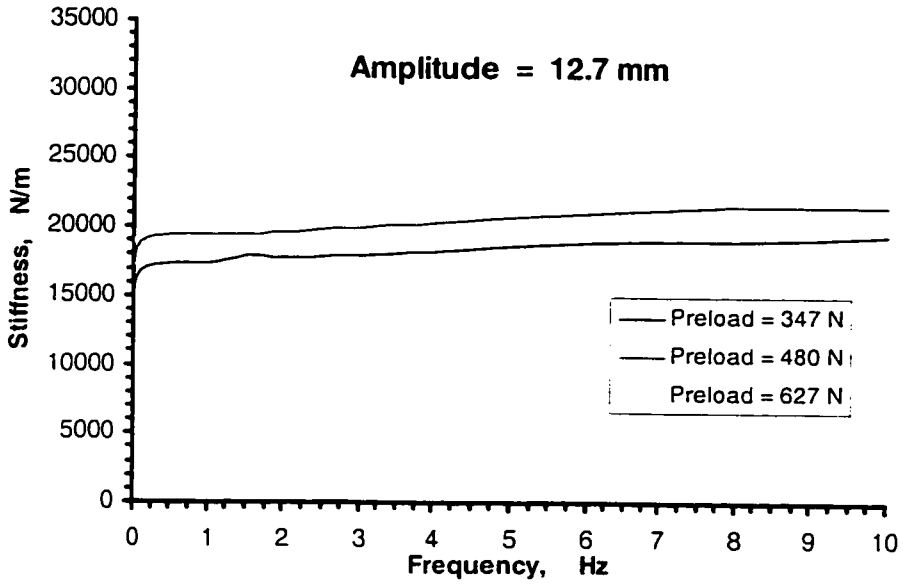

Figure 2.22: Influence of the Excitation Frequency and Preload on Dynamic Stiffness at Constant Stroke of 12.7 mm for Seat "A".

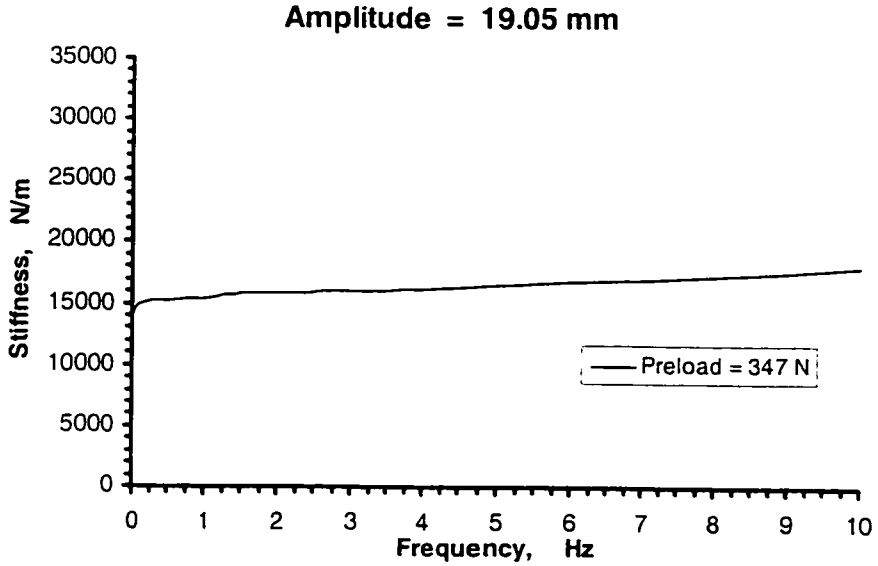

Figure 2.23: Influence of the Excitation Frequency and Preload on Dynamic Stiffness at Constant Stroke of 19.05 mm for Seat "A".

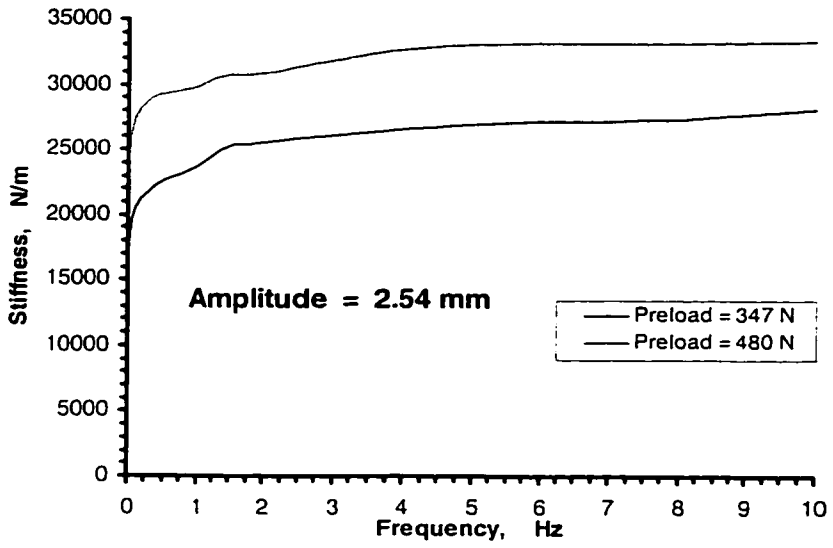

Figure 2.24: Influence of the Excitation Frequency and Preload on Dynamic Stiffness at Constant Stroke of 2.54 mm for Seat "B".

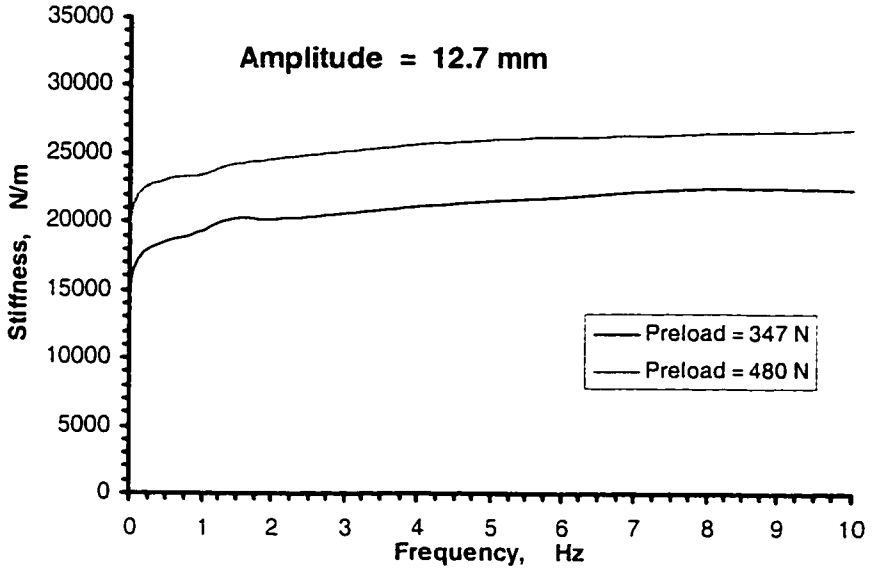

Figure 2.25: Influence of the Excitation Frequency and Preload on Dynamic Stiffness at Constant Stroke of 12.7 mm for Seat "B".

In summary, the observations made from Figure 2.5 - 2.25 can be summarized as follows:

i) The dynamic stiffness increases slightly with increase excitation frequency beyond 0.5 Hz, irrespective of the preload and magnitude of deflection.

ii) The dynamic stiffness decreases greatly with increase in the amplitude of the excitation, irrespective of the preload and frequency of excitation.

iii) The dynamic stiffness increases greatly with increase in the preload, irrespective of the amplitude and frequency of excitation.

2.4.2 Equivalent damping coefficients

The equivalent damping coefficient of a seat can be derived from the measured force-deflection data, as a function of the preload, excitation frequency and excitation amplitude, using the principle of energy similarity or dissipation [33]. Referring to the dynamic force-deflection characteristics under cyclic loading and unloading (Figure 2.26), the energy dissipated ΔE, due to cyclic deformation of the cushion can be derived from [33]:

$$\Delta E = \oint F dx \tag{2.5}$$

where F is the force and x is the deflection.

The equivalent viscous damping coefficient may be derived by equating the dissipated energy to that of a viscous damper, given by:

$$\Delta E = \pi c_{eq} \omega A^2 \tag{2.6}$$

where ω is the excitation frequency, in rad/s, A is the excitation amplitude in m, and c_{eq} is the equivalent viscous damping coefficient in Ns/m that may be considered valid in the

vicinity of the selected excitation frequency and amplitude, and the preload.

The energy dissipated per cycle by the seat cushion is determined from the area enclosed within the loading and unloading curves, as shown in Figure 2.26. The equivalent damping coefficient is then derived from Equation (2.6) as:

$$c_{eq} = \frac{\Delta E}{\pi \omega A^2} \tag{2.7}$$

The equivalent damping coefficients for seat "C" computed corresponding to each preload and excitation frequency and amplitude are listed in Table 2.3. Table 2.4 presents the corresponding damping coefficients derived from the force-deflection data for seats "A" and "B". The results show that the equivalent damping coefficients for all three seats vary considerably with the preload and excitation condition. These variations are presented in Figures 2.27 to 2.43.

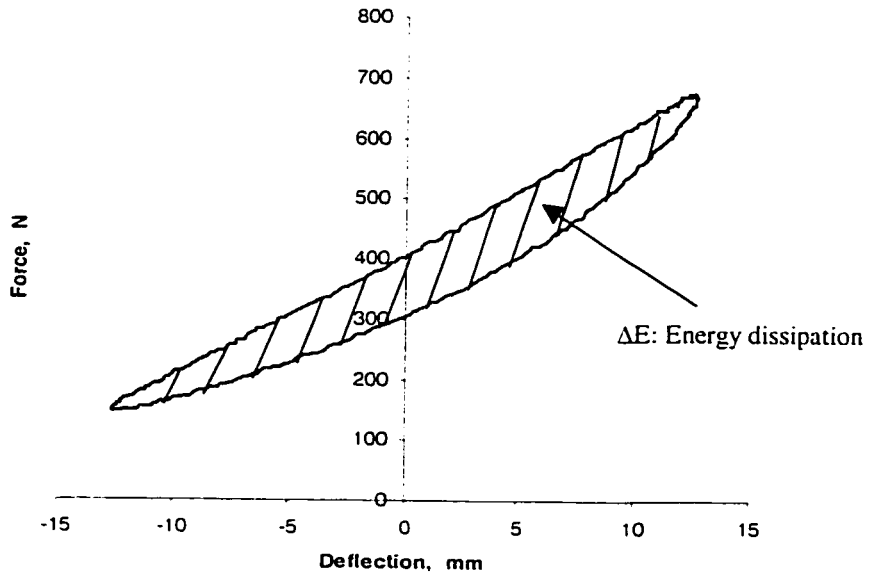

Figure 2.26: Dynamic Force-Deflection Characteristics of seat "C" (Preload = 357 N, Stroke = 12.7 mm, and Excitation Frequency = 1 Hz).

The damping characteristics of seat "C", presented in Figures 2.27-2.29, clearly illustrate that excitation frequency and amplitude influence the coefficients when the preload is a constant. The increase in the excitation frequency causes a decrease in the equivalent damping coefficient which tends to be most drastic at lower frequencies. The equivalent damping coefficient decreases from 1260 Ns/m to 210 Ns/m, when the frequency of excitation is increased from 0.5 Hz to 4 Hz at an amplitude of excitation of 2.54 mm under preload of 358 N. The equivalent damping coefficients approach similar values at frequencies above 4 Hz. The equivalent damping coefficient decreases from 340 Ns/m to 310 Ns/m, when the amplitude of excitation is increased from 12.7 mm to 19.05 mm at frequency of excitation of 2 Hz under preload of 358 N, which may be considered to be relatively small when compared to the effects of the frequency.

The PUF cushions dissipate energy through two mechanisms: (i) the hysteretic properties of the material; and (ii) the air inflow and outflow through the open cell structure. At lower frequencies, the open cell structure permits large air flow. Moreover, the hysteresis is known to yield relatively high damping coefficient at lower frequencies, which diminishes considerably at higher frequencies [8,9]. Consequently, the PUF cushions yield relatively higher damping coefficient at lower excitation frequencies. Higher excitation frequencies limit the breathing ability of the PUF; the damping coefficient at higher frequencies may thus be mostly attributed to air flows.

The damping characteristics of seats "A" and "B", shown in Figures 2.30-2.33, also demonstrate trends that are similar to those observed for seat "C". For seat "A", the equivalent damping coefficient decreases up to 74 % (from 660 Ns/m to 154 Ns/m) when the frequency increases from 0.5 Hz to 4 Hz under the preload of 347 N and amplitude of

excitation of 6.35 mm, and it continues to decrease from 154 Ns/m to 100 Ns/m when the frequency increases from 4 Hz to 10 Hz; the equivalent damping coefficient decreases only 13 % (from 230 Ns/m to 200 Ns/m) when the amplitude increases by 50 % (from 12.7 mm to 19.05 mm) at a frequency of excitation of 2 Hz under the preload of 347 N. For seat "B", the equivalent damping coefficient decreases up to 58 % (from 580 Ns/m to 240 Ns/m) when the frequency increases from 1 Hz to 4 Hz under the preload of 347 N and amplitude of excitation of 2.54 mm, and it continue to decrease from 240 Ns/m to 140 Ns/m when the frequency increases from 4 Hz to 10 Hz; the equivalent damping coefficient decreases only 10 % (from 320 Ns/m to 290 Ns/m) when the amplitude increases from 2.54 mm to 12.7 mm at a frequency of excitation of 2 Hz under the preload of 347 N.

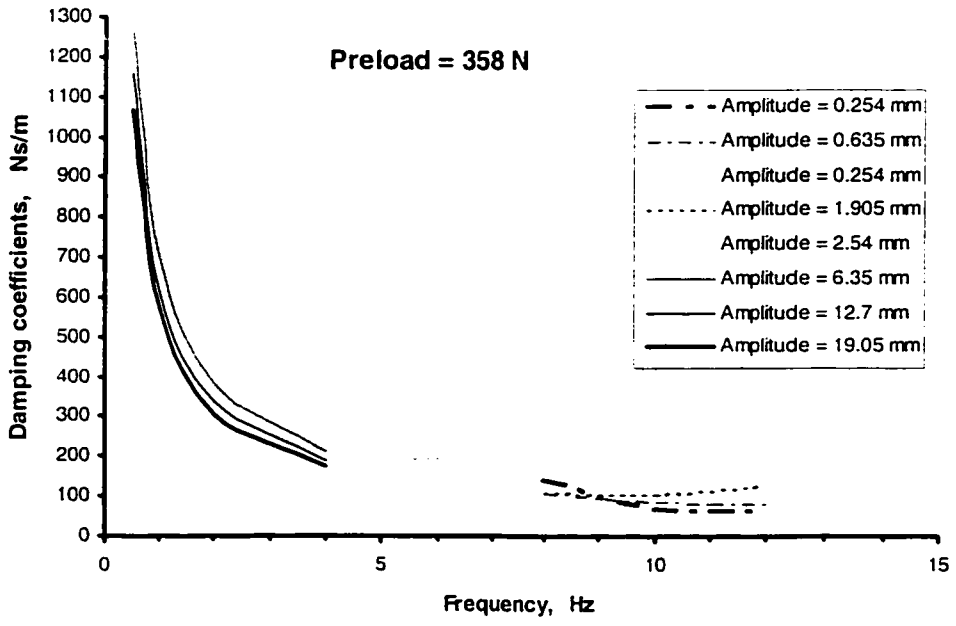

Figure 2.27: Effects of the Excitation Frequency and Amplitude on Equivalent Damping Coefficients at constant Preload of 358 N for Seat "C".

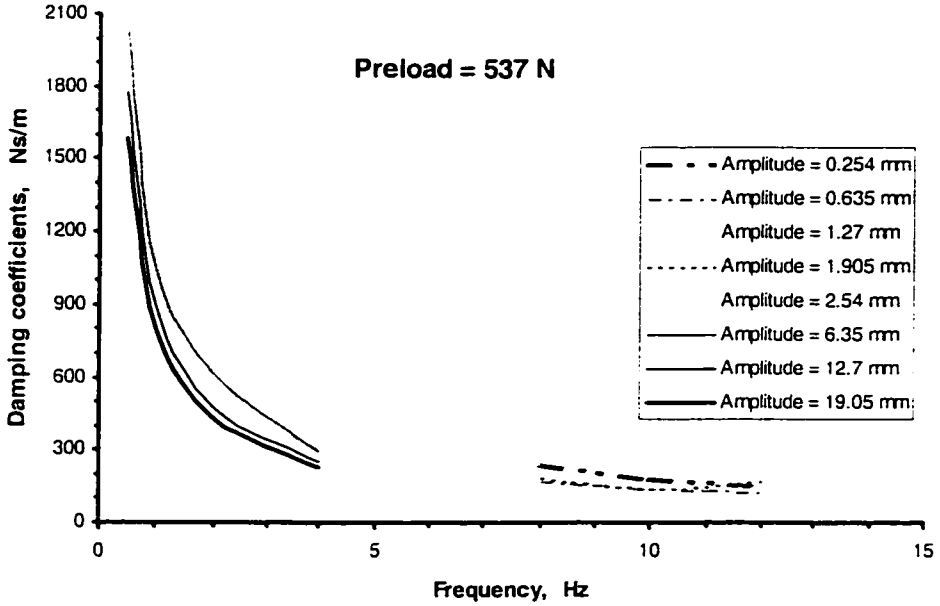

Figure 2.28: Effects of the Excitation Frequency and Amplitude on Equivalent Damping Coefficients at constant Preload of 537 N for Seat "C".

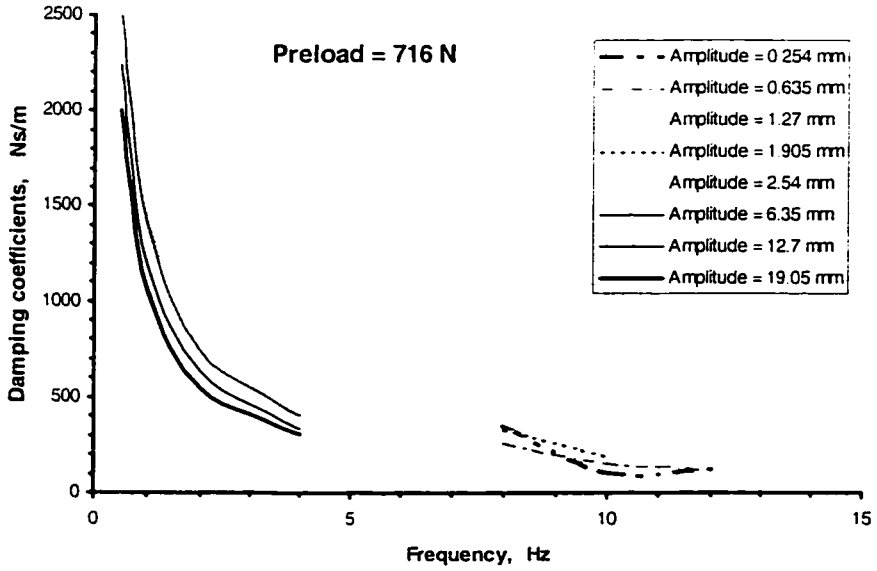

Figure 2.29: Effects of the Excitation Frequency and Amplitude on Equivalent Damping Coefficients at constant Preload of 716 N for Seat "C".

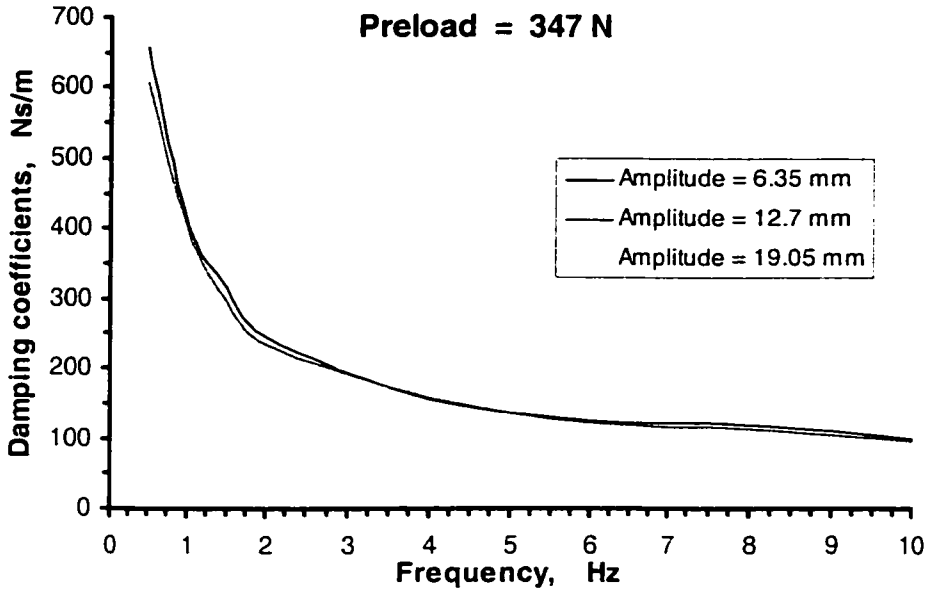

Figure 2.30: Effects of the Excitation Frequency and Amplitude on Equivalent Damping Coefficients at constant Preload of 347 N for Seat "A".

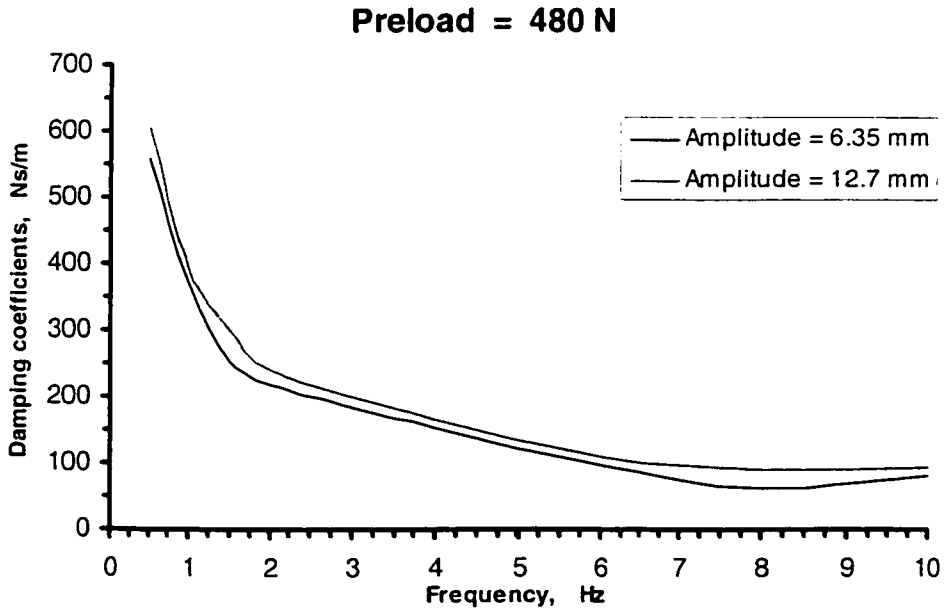

Figure 2.31: Effects of the Excitation Frequency and Amplitude on Equivalent Damping Coefficients at constant Preload of 480 N for Seat "A".

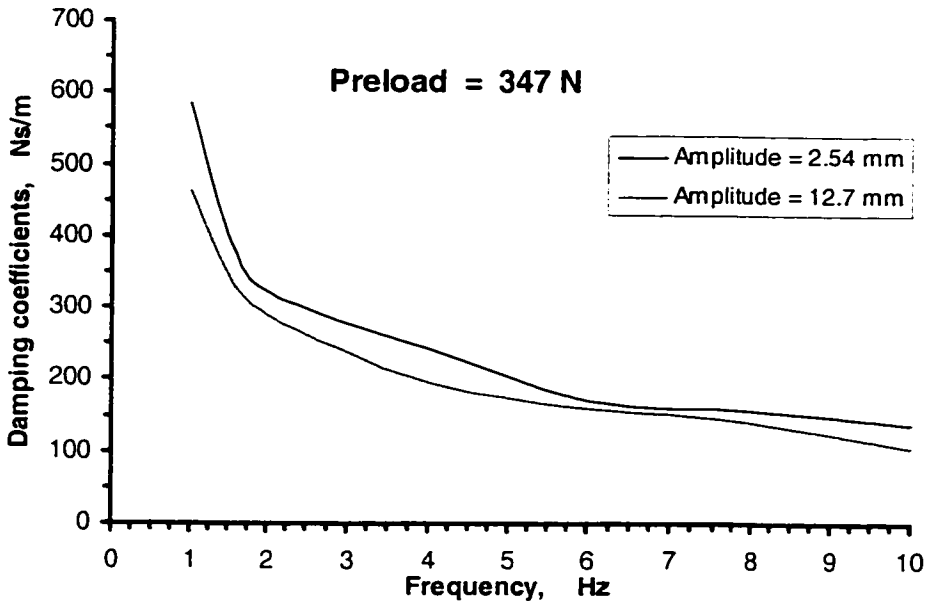

Figure 2.32: Effects of the Excitation Frequency and Amplitude on Equivalent Damping Coefficients at constant Preload of 347 N for Seat "B".

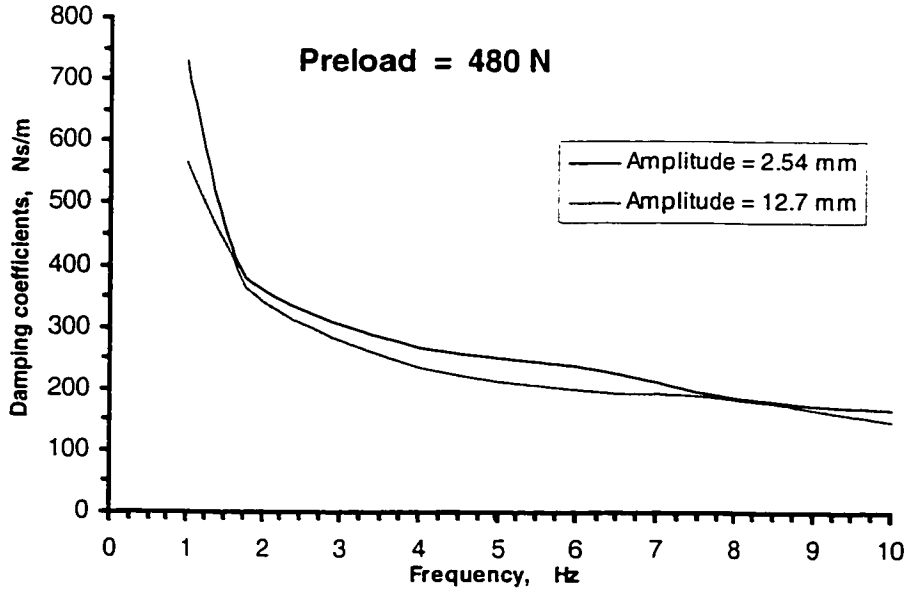

Figure 2.33: Effects of the Excitation Frequency and Amplitude on Equivalent Damping Coefficients at constant Preload of 480 N for Seat "B".

Figures 2.34 to 2.43 illustrate the effects of the preload and excitation frequency on the equivalent damping coefficient. The dynamic force-deflection characteristics of seat "C", presented in Figures 2.34 to 2.41, clearly illustrate that excitation frequency and preload affect the damping coefficients in a significant manner. An increase in the preload yields higher damping coefficients, mostly attributed to increased internal friction and reduced air flow passage. The equivalent damping coefficient increases from 340 Ns/m to 630 Ns/m, when the preload is increased from 347 N to 627 N at a frequency of excitation of 2 Hz under the excitation amplitude of 12.7 mm. The equivalent damping coefficient of the seat cushion increases up to 86 % when the preload increases by 100 %.

The damping characteristics of seat "B", shown in Figure 2.43, illustrate similar trends in the preload. The equivalent damping coefficient, however, increases only 21 % (from 290 Ns/m to 340 Ns/m) when the preload increases by 38 % (from 347 N to 480 N) at a frequency of excitation of 2 Hz under the excitation amplitude of 12.7mm. The results suggest that the seat "C" yields considerably higher damping coefficients, which are more sensitive to variations in the preload. The damping coefficients derived for seat "A", shown in Figure 2.42, show negligible effect of preload.

In summary, the observations made from Figures 2.27 to 2.43 may be summarized as follows: i) The equivalent damping coefficients decrease rapidly with increase in the excitation frequency in the low frequency range under 4 Hz and the rate of decay diminishes considerably at frequencies above 4 Hz. ii) The equivalent damping coefficients increase with increase in the preload. iii) The equivalent damping coefficients decrease only slightly with increase in the amplitude of excitation. Its effect can be considered to be insignificant when compared to those of the other two factors.

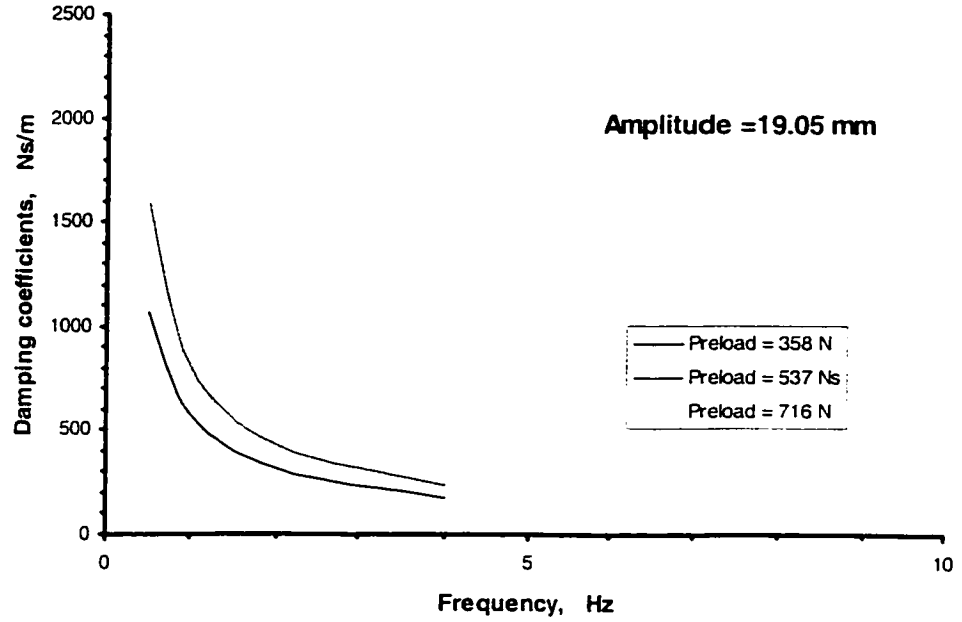

Figure 2.34: Effects of the Excitation Frequency and Preload on Equivalent Damping Coefficients at Constant Amplitude of 19.05 mm for Seat "C".

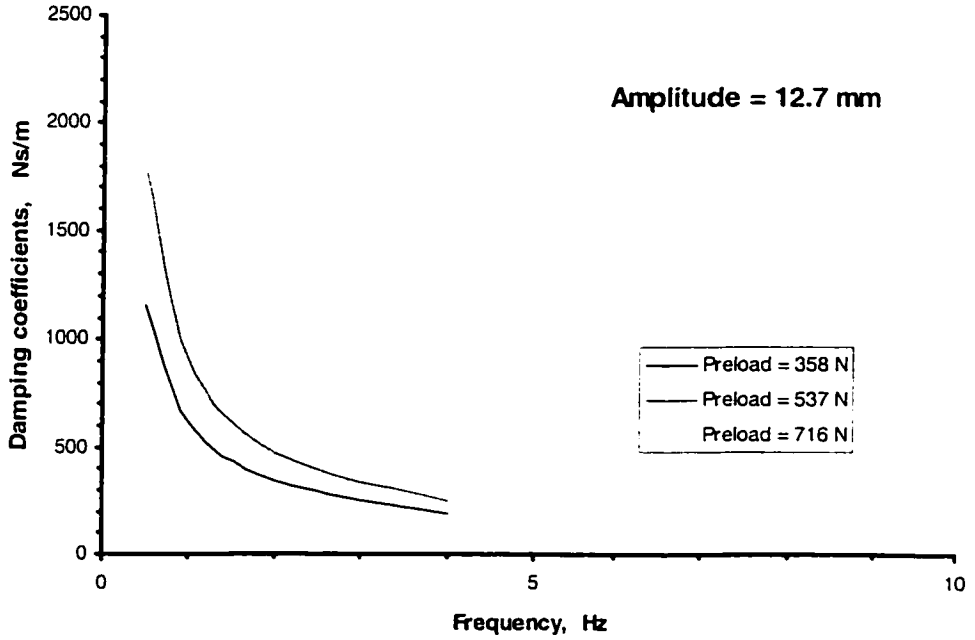

Figure 2.35: Effects of the Excitation Frequency and Preload on Equivalent Damping Coefficients at Constant Amplitude of 12.7 mm for Seat "C".

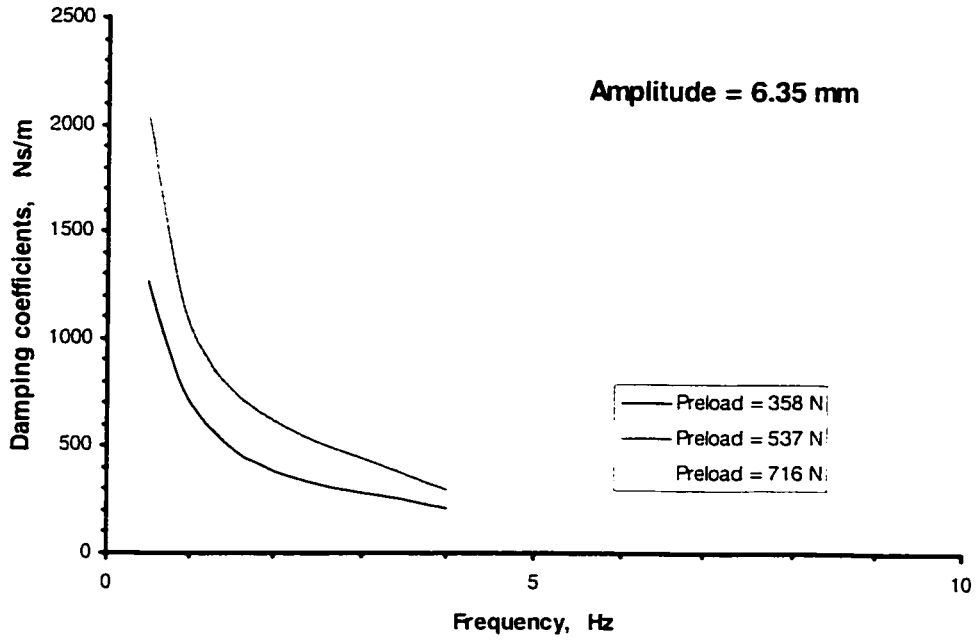

Figure 2.36: Effects of the Excitation Frequency and Preload on Equivalent Damping Coefficients at Constant Amplitude of 6.35 mm for Seat "C".

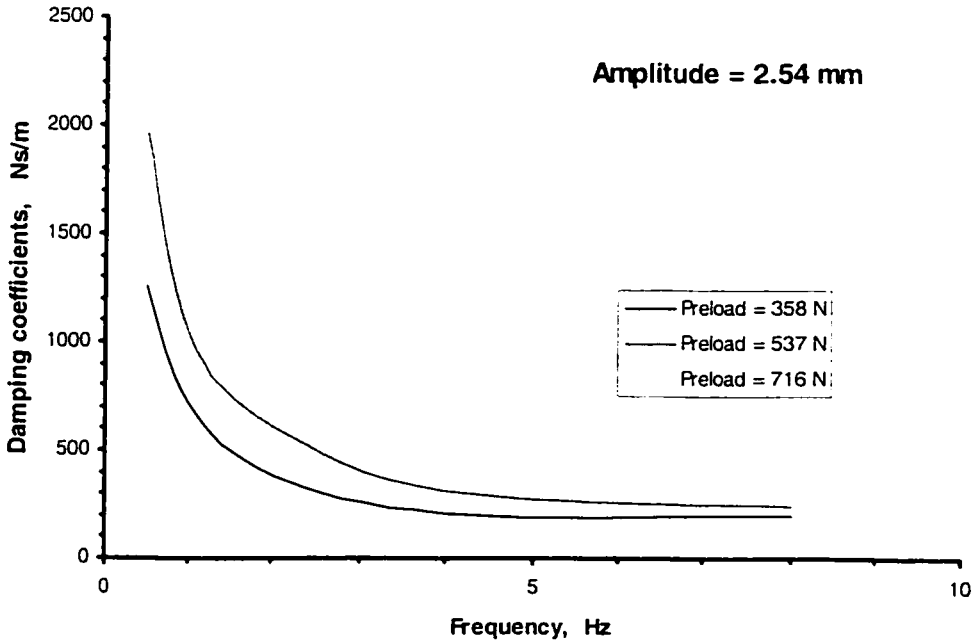

Figure 2.37: Effects of the Excitation Frequency and Preload on Equivalent Damping Coefficients at Constant Amplitude of 2.54 mm for Seat "C".

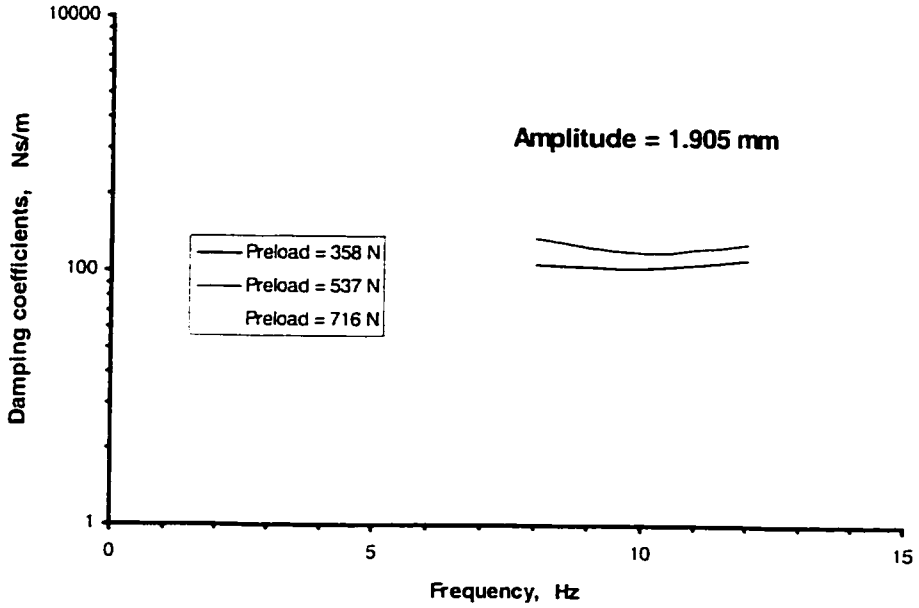

Figure 2.38: Effects of the Excitation Frequency and Preload on Equivalent Damping Coefficients at Constant Amplitude of 1.905 mm for Seat "C".

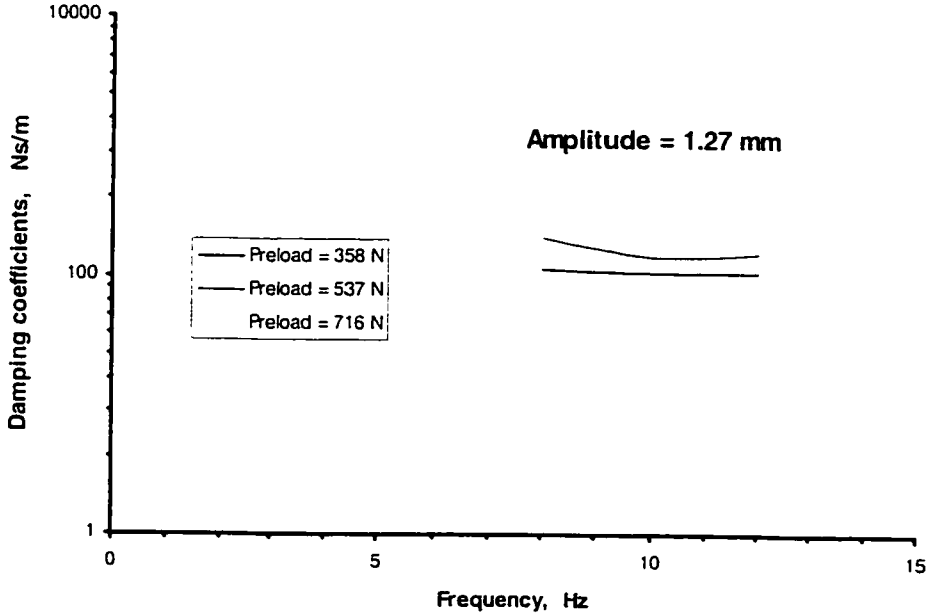

Figure 2.39: Effects of the Excitation Frequency and Preload on Equivalent Damping Coefficients at Constant Amplitude of 12.7 mm for Seat "C".

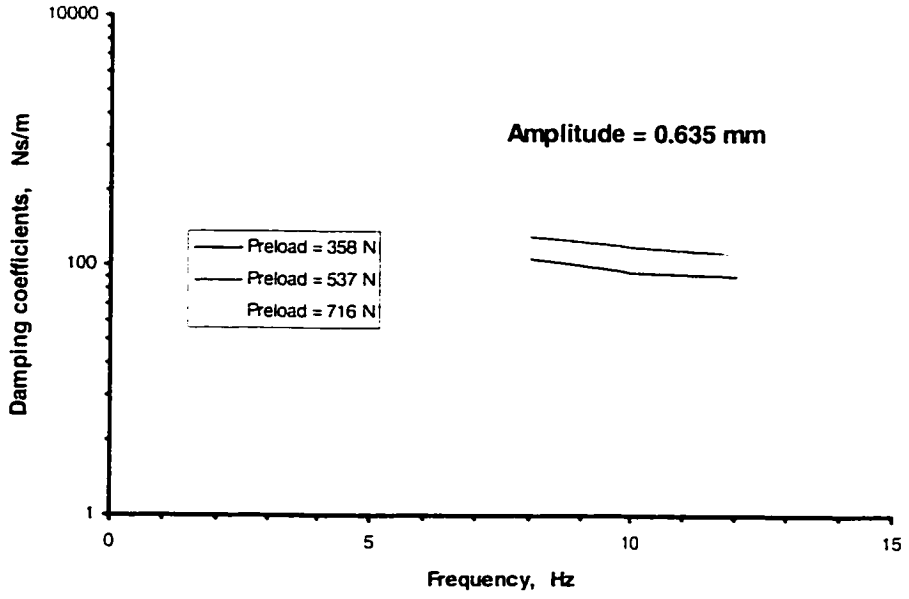

Figure 2.40: Effects of the Excitation Frequency and Preload on Equivalent Damping Coefficients at Constant Amplitude of 0.635 mm for Seat "C".

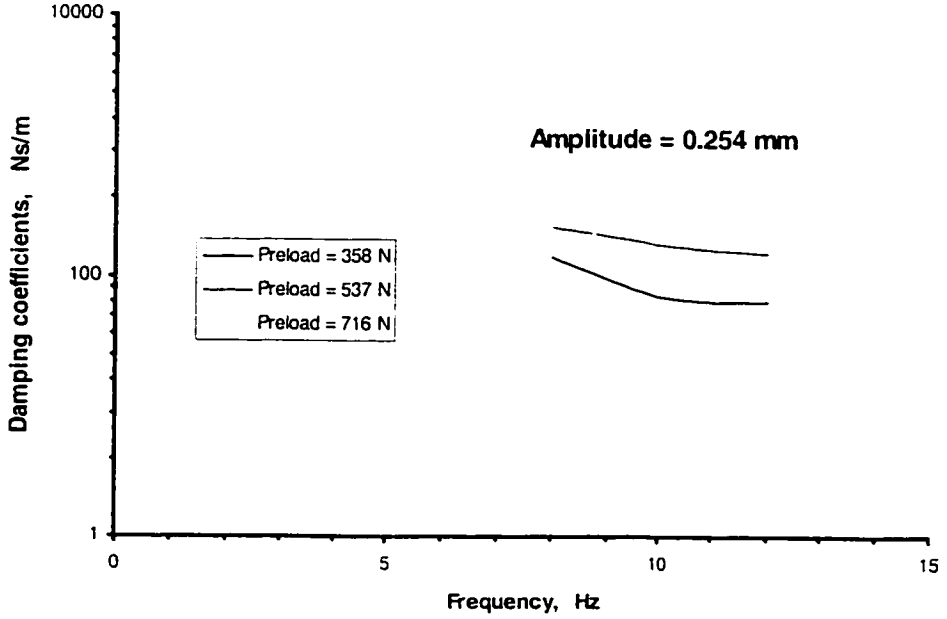

Figure 2.41: Effects of the Excitation Frequency and Preload on Equivalent Damping Coefficients at Constant Amplitude of 0.254 mm for Seat "C".

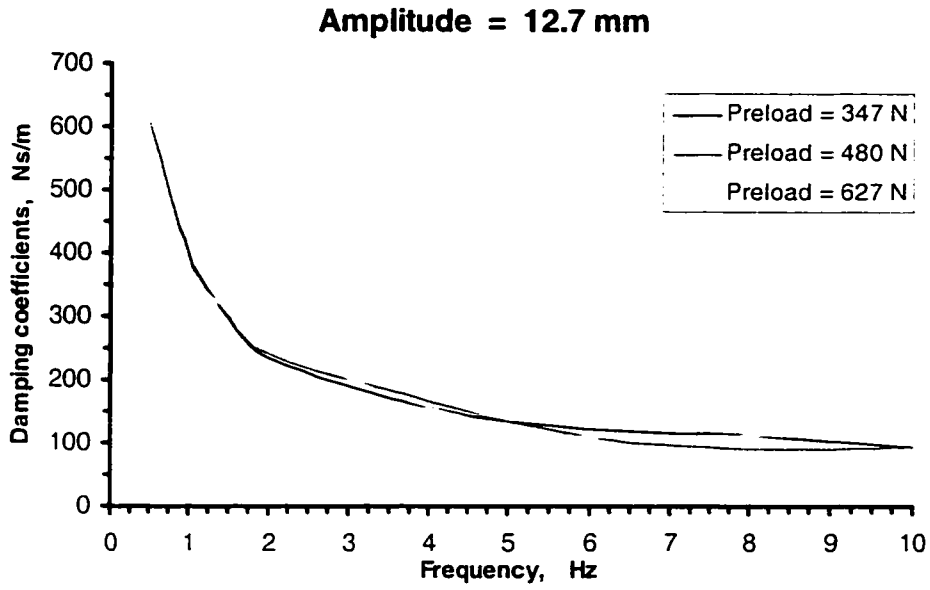

Figure 2.42: Effects of the Excitation Frequency and Preload on Equivalent Damping Coefficients at Constant Amplitude of 12.7 mm for Seat "A".

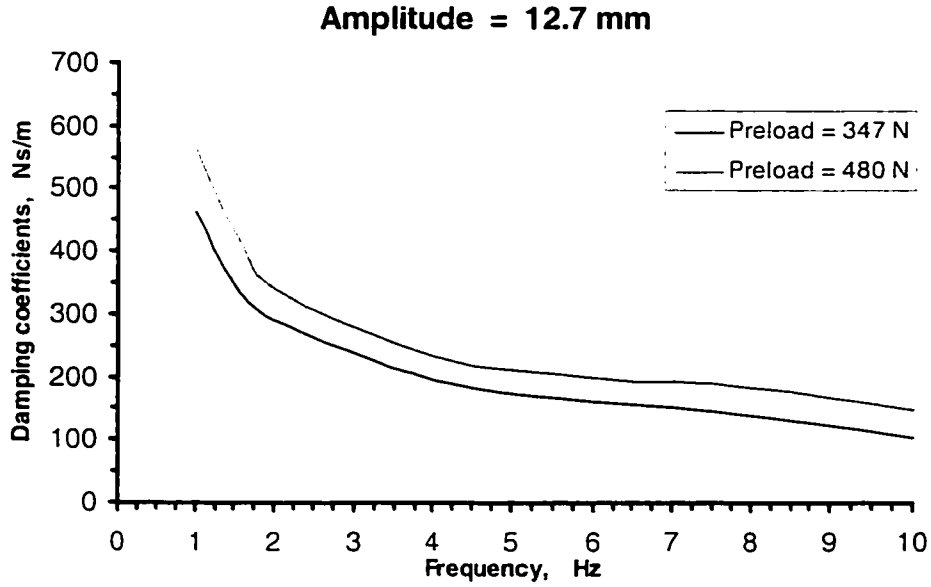

Figure 2.43: Effects of the Excitation Frequency and Preload on Equivalent Damping Coefficients at Constant Amplitude of 12.7 mm for Seat "B".

2.5 Modeling the dynamic properties of PUF seat cushion

Owing to the strong nonlinearities and complex dependence upon the nature of excitation and preload, the PUF cushions are widely characterized by an equivalent linear stiffness coefficient and a viscous damping coefficient. The equivalent linear stiffness coefficient is mostly derived from the static force-deflection curve, acquired using SAE J1051 [42] method, while the energy dissipation property is characterized by light vision damping on the basis of measured force-deflection properties [21,35,46]. The equivalent stiffness coefficient can be considered valid in the vicinity of a specific preload and deflection, while it can not account for the dependence of the force on nature of excitation and preload. Although a number of nonlinear models have been proposed to characterize the stiffness and damping properties, these models also do not account for variation in excitation frequency and preload [19,20,22].

2.5.1 Modeling the stiffness characteristics

The dynamic stiffness properties of the automotive seat cushion show that the stiffness coefficient of a cushion depends upon the preload W, the deflection amplitude A and the frequency, f, *of* excitation. The measured data suggest that the dynamic stiffness coefficients may be described by a power function, such that:

$$K = a_1 W^{a_2} f^{a_3} A^{a_4} \tag{2.8}$$

where K is stiffness coefficient of a seat cushion in N/m; W is preload in N; f is frequency of excitation in Hz; A is deflection amplitude in m; and a_1, a_2, a_3 *and* a_4 are model parameters.

The method of least squares is used to identify the coefficients a_1, a_2, a_3 and a_4 by minimizing the sum of squared error between the measured and predicted stiffness coefficients. Equation (2.8) can be rewritten as:

$$\ln K = \ln a_1 + a_2 \ln W + a_3 \ln f + a_4 \ln A \tag{2.9}$$

The target function of the squared error is expressed as:

$$E = \sum_{i=1}^{n} (\ln k_i - \ln a_1 - a_2 \ln W_i - a_3 \ln f_i - a_4 \ln A_i)^2 \tag{2.10}$$

where k_i is the stiffness, W_i is the preload, f_i is the frequency, and A_i is the deflection amplitude of the i^{th} measured data, and n is the number of measured data.

The values of a_1, a_2, a_3 and a_4 are derived so as to minimize the sum of squared errors. Differentiating the squared error with respect to a_1, a_2, a_3 and a_4, respectively, and equating them to zero, yields the following algebraic expressions:

$$\sum_{i=1}^{n} 2(\ln k_i - \ln a_1 - a_2 * \ln W_i - a_3 * \ln f_i - a_4 * \ln A_i)(-1) = 0 \tag{2.11}$$

$$\sum_{i=1}^{n} 2(\ln k_i - \ln a_1 - a_2 * \ln W_i - a_3 * \ln f_i - a_4 * \ln A_i)(-\ln W_i) = 0 \tag{2.12}$$

$$\sum_{i=1}^{n} 2(\ln k_i - \ln a_1 - a_2 * \ln W_i - a_3 * \ln f_i - a_4 * \ln A_i)(-\ln f_i) = 0 \tag{2.13}$$

$$\sum_{i=1}^{n} 2(\ln k_i - \ln a_1 - a_2 * \ln W_i - a_3 * \ln f_i - a_4 * \ln A_i)(-\ln A_i) = 0 \tag{2.14}$$

Equations (2.11) to (2.14) can be written in the matrix form as follows:

$$\begin{bmatrix} \sum_{i=1}^{n} & \sum_{i=1}^{n} \ln W_i & \sum_{i=1}^{n} \ln f_i & \sum_{i=1}^{n} \ln A_i \\ \sum_{i=1}^{n} \ln W_i & \sum_{i=1}^{n} (\ln W_i)^2 & \sum_{i=1}^{n} \ln f_i * \ln W_i & \sum_{i=1}^{n} \ln A_i * \ln W_i \\ \sum_{i=1}^{n} \ln f_i & \sum_{i=1}^{n} \ln f_i * \ln W_i & \sum_{i=1}^{n} (\ln f_i)^2 & \sum_{i=1}^{n} \ln A_i * \ln f_i \\ \sum_{i=1}^{n} \ln A_i & \sum_{i=1}^{n} \ln A_i * \ln W_i & \sum_{i=1}^{n} \ln A_i * \ln f_i & \sum_{i=1}^{n} (\ln A_i)^2 \end{bmatrix} \begin{Bmatrix} \ln a_1 \\ a_2 \\ a_3 \\ a_4 \end{Bmatrix} = \begin{Bmatrix} \sum_{i=1}^{n} \ln K_i \\ \sum_{i=1}^{n} \ln K_i * \ln W_i \\ \sum_{i=1}^{n} \ln K_i * \ln f_i \\ \sum_{i=1}^{n} \ln K_i * \ln A_i \end{Bmatrix} \tag{2.15}$$

Equation (2.15) is solved in conjunction with the stiffness coefficients derived from the measured data (Figures 2.5 to 2.12) to identify the model coefficients a_1, a_2, a_3 and a_4. The measured data attained for seat "C" revealed distinctly different stiffness values for two different ranges of deflection. The seat exhibits relatively higher stiffness for deflections below 2.54 mm and considerably smaller stiffness under deflection above 2.54 mm, as shown in Figures 2.5 to 2.7. Two sets of model coefficients are thus identified to characterize the stiffness properties of seat "C", which are summarized in Table 2.5.

Table 2.5: The optimum parameters of dynamic stiffness model.

Seat	Deflection amplitude range	a_1	a_2	a_3	a_4
A	0.254 to 19.05 mm	24.27	0.30	0.03	-0.18
B	0.254 to 19.05 mm	5.99	0.65	0.05	-0.08
C	< 2.54 mm	86.983	0.8657	0.0271	- 0.0397
	≥ 2.54 mm	49.534	0.8120	0.0463	- 0.0266

It should be noted that the coefficients a_1, a_2, a_3 and a_4 describe the dependence of the seat stiffness on preload, frequency and deflection amplitude, respectively, while the coefficient a_1 can be interpreted as a constant gain value. The derived model coefficients suggest the following:

i) The influence of preload on the seat stiffness is determined from parameter a_2. The stiffness values of all three seats increase with increase in the preload ($a_2>0$). The stiffness of seat "C" is most sensitive to variation in the preload,

while that of seat "A" is least sensitive.

ii) The influence of excitation frequency on the seat stiffness is determined from the parameter a_3. The parameter values suggest that stiffness coefficients of all three seats increase with increase in frequency. The increases in stiffness values, however, are small. Furthermore, the results suggest that the sensitivity of stiffness of all three seats to variations in excitation frequency is comparable.

iii) The effect of deflection amplitude on stiffness of a PUF seat is determined from parameter a_4. The stiffness values of all three seats decrease with increase in deflections amplitude ($a_4<0$). The results suggest that the influence of deflection amplitude on the stiffness value is small relative to that due to variations in the preload. The seat "A" exhibits most sensitivity to variations in deflection amplitude.

2.5.2 Validation of the stiffness model

The validity of the proposed stiffness models is examined by comparing the model results with the corresponding measured data over the range of excitation amplitudes, excitation frequencies and preloads. Equation (2.8) is solved to derive the stiffness constants for each of the three seats under excitations in the 0 to 10 Hz frequency range, and values of preload and amplitude used in the experimental characterization.

Figures 2.44 to 2.55 present a comparison of the results of models of all the three seats with the corresponding measured data over the range of test conditions considered

in the study. In general, the model results are observed to be in close agreement with the measured stiffness coefficients. For seat "A", the results attained from proposed model agree very well with measured data, shown in Figures 2.44-2.47. Some derivation between the model results and the measured data, however, are observed under a_1 large preload of 627 N and a large deflection of 19.05 mm. These deviations may be attributed to possible bottoming of the seat. The model results attained for seat "B" agree very well with the measured data for the entire range of test conditions considered, as shown in Figures 2.48 to 2.51. Figures 2.52 to 2.55 illustrate the comparison of model results with the corresponding measured data for seat "C". The results generally show a reasonably good agreement between the measured and computed results, except for extreme preload (716N) and small deflection amplitudes (<2.54 mm).

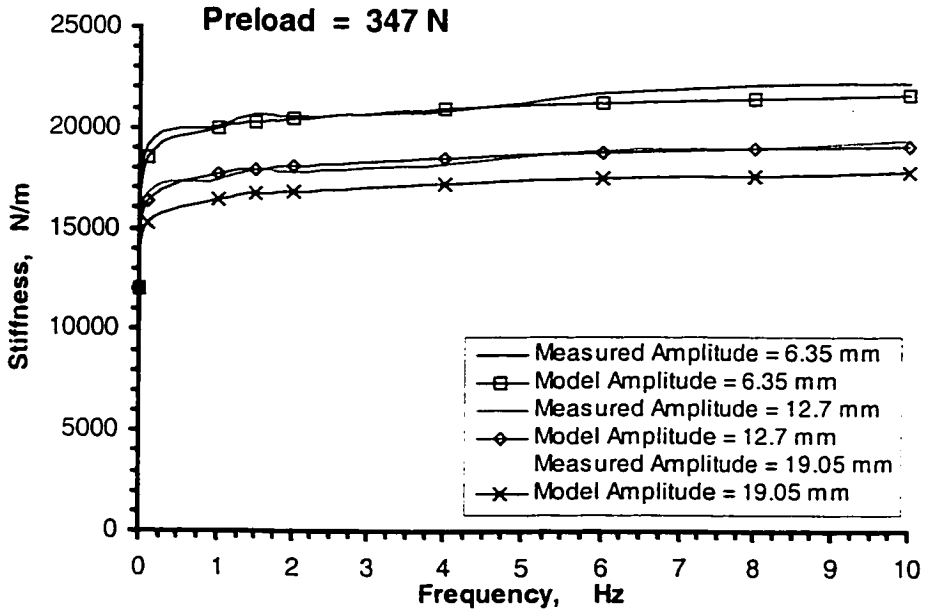

Figure 2.44: The comparison of the modeled stiffness with the measured data at constant preload of 367 N for Seat "A".

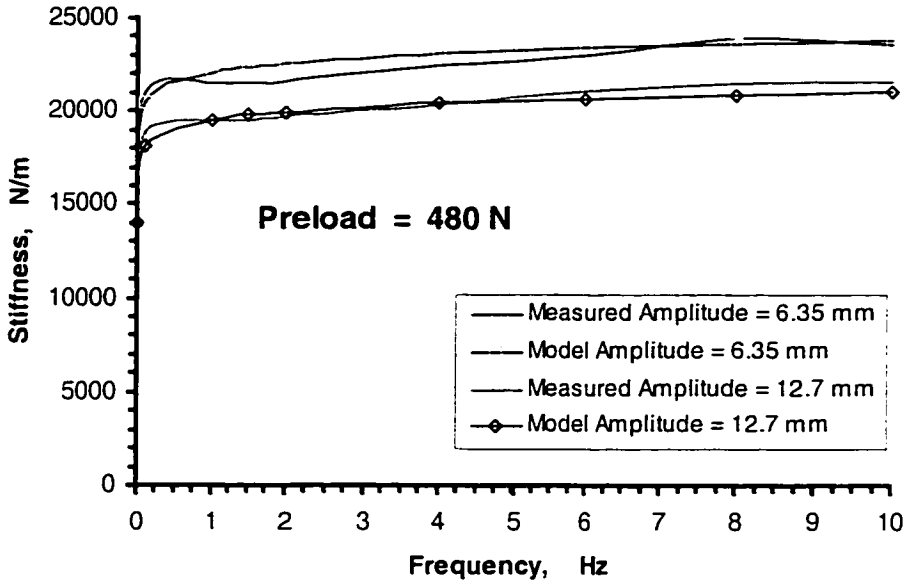

Figure 2.45: The comparison of the modeled data with the measured data at constant preload of 480 N for Seat "A".

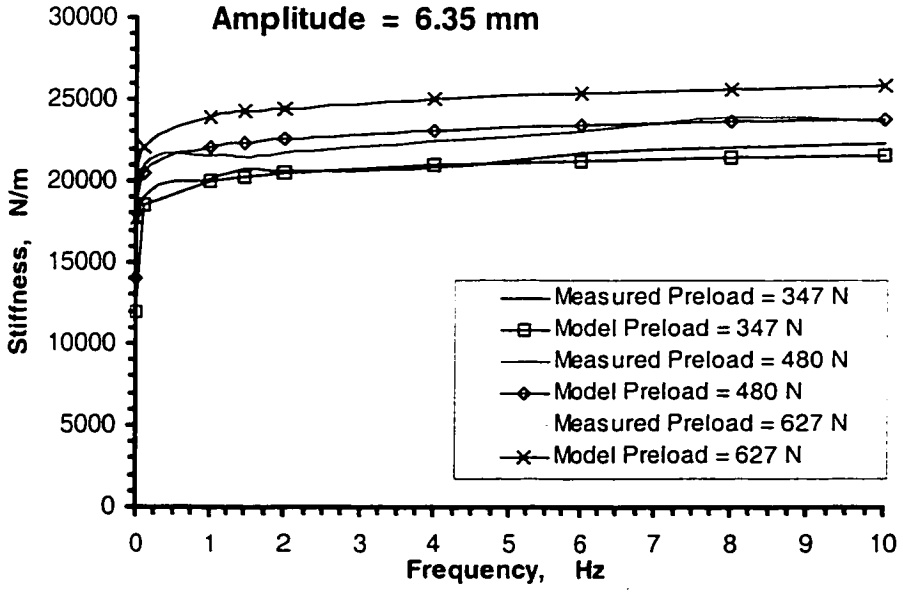

Figure 2.46: The comparison of the modeled stiffness with the measured data at constant amplitude of 6.35 mm for Seat "A".

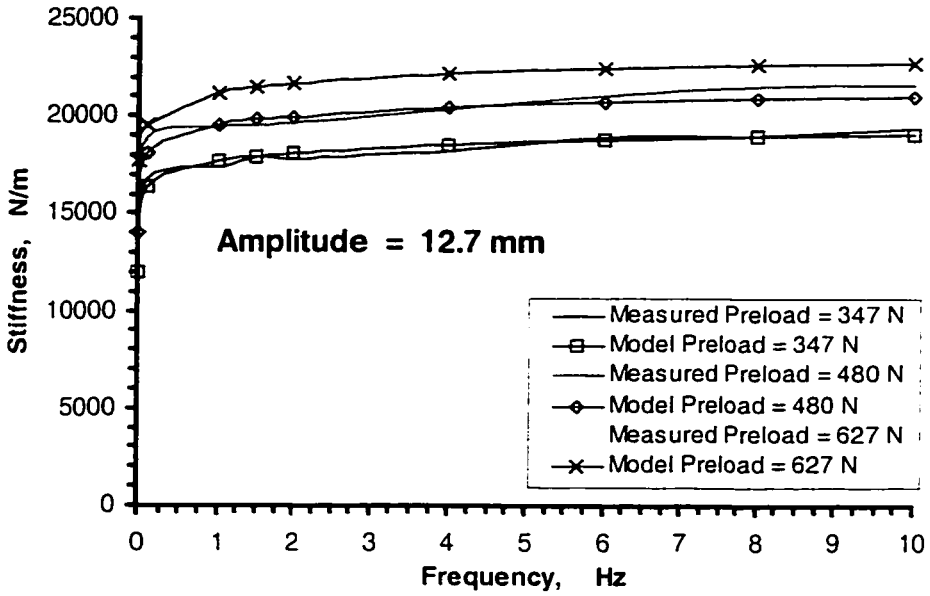

Figure 2.47: The comparison of the modeled stiffness with the measured data at constant amplitude of 12.7 mm for Seat "A".

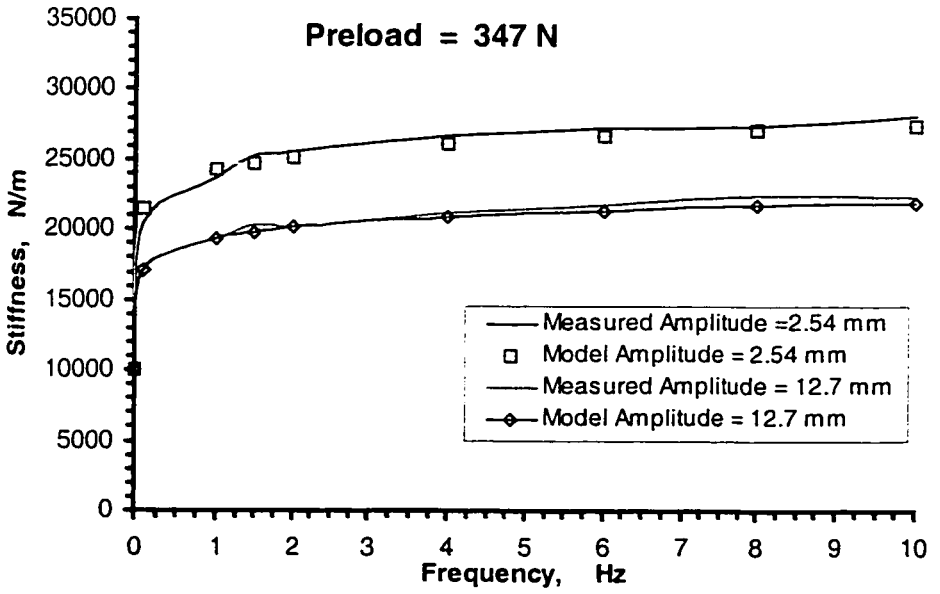

Figure 2.48: The comparison of the modeled stiffness with the measured data at constant preload of 4347 N for Seat "B".

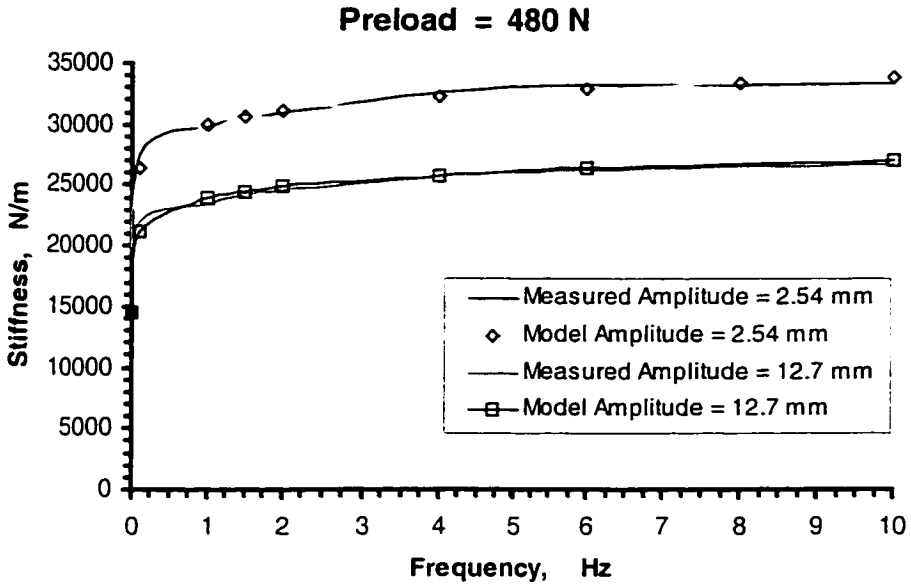

Figure 2.49: The comparison of the modeled stiffness with the measured data at constant preload of 480 N for Seat "B".

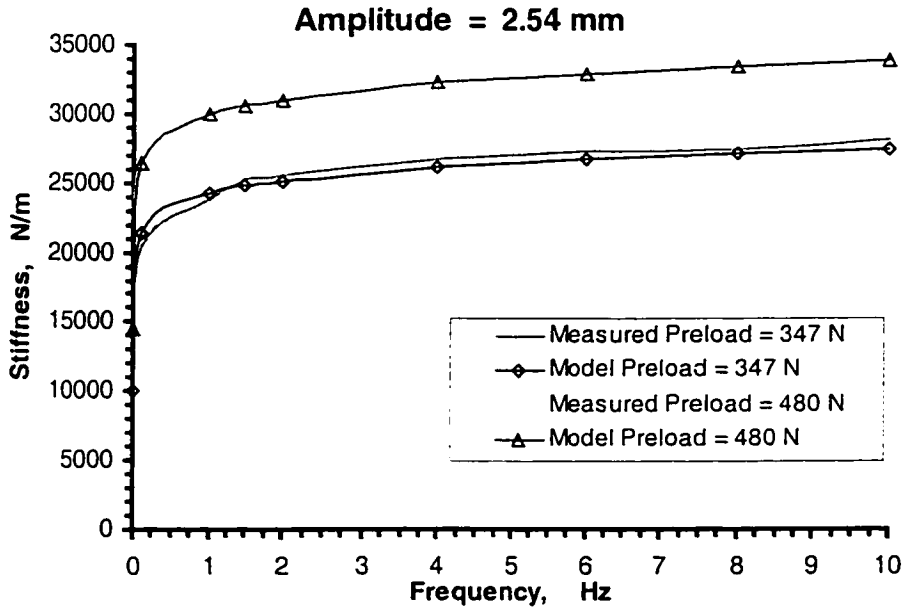

Figure 2.50: The comparison of the modeled stiffness with the measured data at constant amplitude of 2.54 mm for Seat "B.

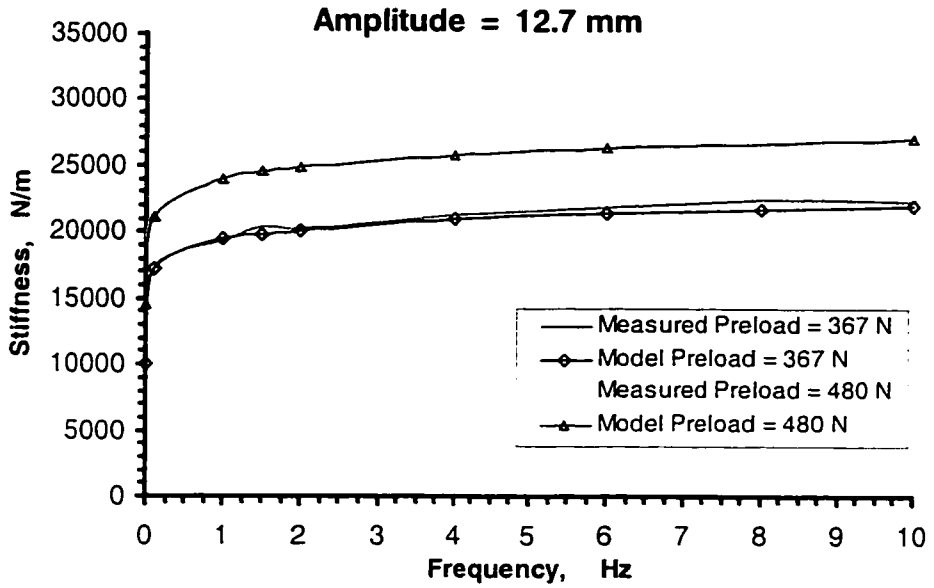

Figure 2.51: The comparison of the modeled stiffness with the measured data at constant amplitude of 12.7 mm for Seat "B.

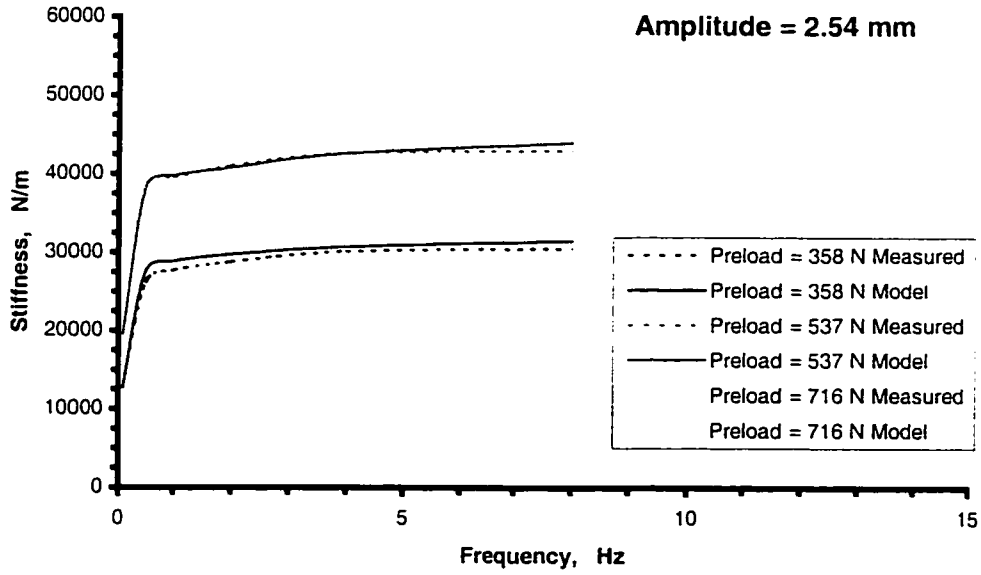

Figure 2.52: The comparison of the modeled stiffness with the measured data at constant amplitude of 2.54 mm for Seat "C".

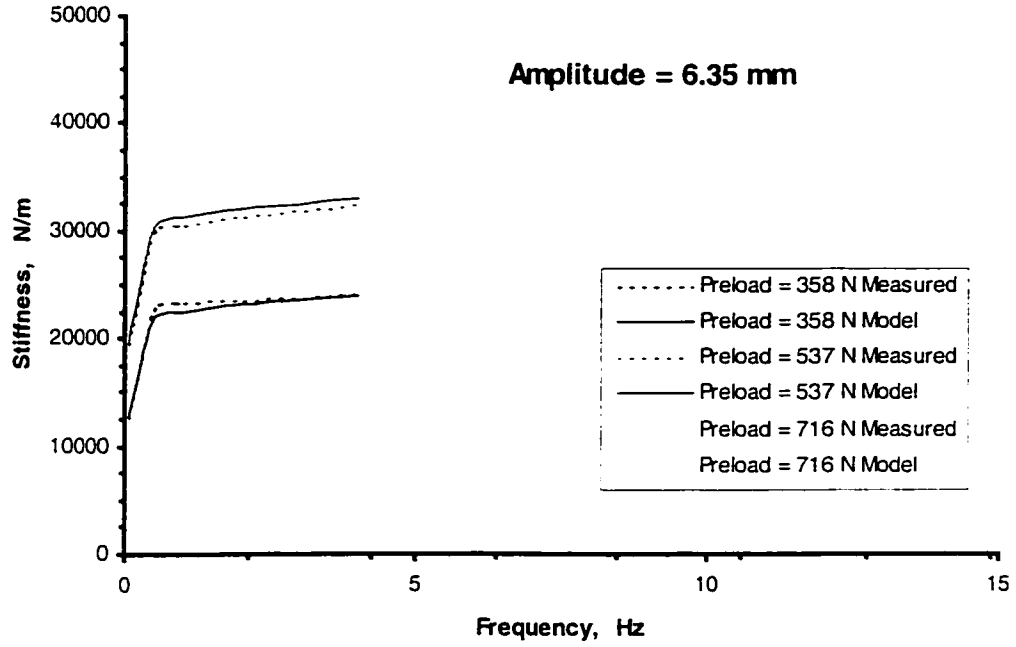

Figure 2.53: The comparison of the modeled stiffness with the measured data at constant amplitude of 6.35 mm for Seat "C".

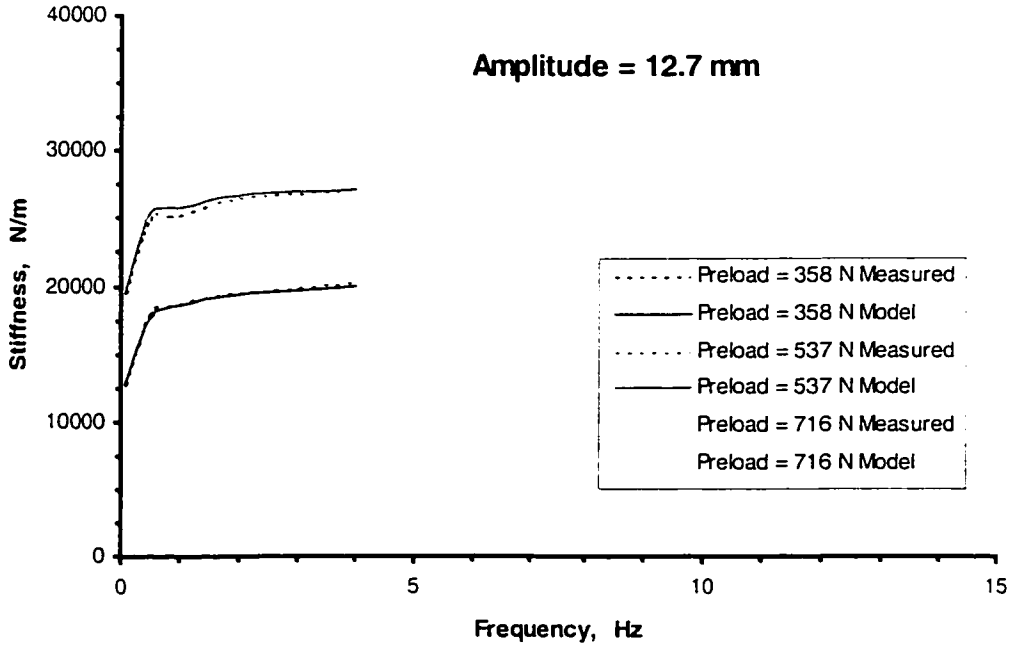

Figure 2.54: The comparison of the modeled stiffness with the measured data at constant amplitude of 12.7 mm for Seat "C".

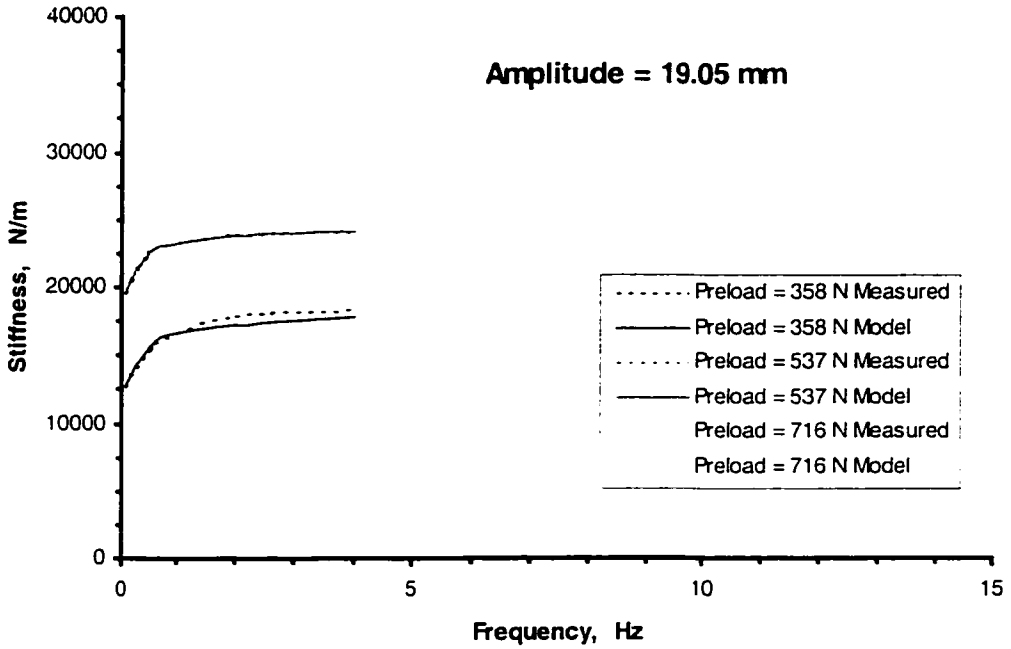

Figure 2.55: The comparison of the modeled stiffness with the measured data at constant amplitude of 19.05 mm for Seat "C".

2.5.3 Modeling the damping characteristics

The energy dissipation properties of the automotive seat cushions show that the damping coefficient of a cushion depends upon the preload, the deflection amplitude and the frequency of excitation. The measured data suggest that the damping coefficients may be described by a power function, such that:

$$C = b_1 W^{b_2} f^{b_3} A^{b_4} \tag{2.16}$$

where C is the damping coefficient of a seat cushion in Ns/m; W is preload in N; f is frequency of excitation in Hz; A is deflection amplitude in m; and b_1, b_2, b_3 *and* b_4 are model parameters. The method of least squares is used to identify the coefficients b_1, b_2, b_3 and b_4 by minimizing the squared error between the measured and predicted damping

coefficients. For simplifying, equation (2.16) can be rewritten

$$\ln C = \ln b_1 + b_2 \ln W + b_3 \ln f + b_4 \ln A \tag{2.17}$$

The target function of the squared error is expressed as

$$E = \sum_{i=1}^{n} (\ln c_i - \ln b_1 - b_2 \ln W_i - b_3 \ln f_i - b_4 \ln A_i)^2 \tag{2.18}$$

where c_i is the stiffness, W_i is the preload, f_i is the frequency, and A_i is the deflection amplitude of the i^{th} measured data, and n is the number of measured data.

The values of b_1, b_2, b_3 and b_4 are obtained in a similar manner so that used for identifying the parameters a_1, a_2, a_3 and a_4. Following this approach, we obtained the optimum parameters, as shown in Table 2.6.

Table 2.6: The optimum parameters of damping model.

Seat	b_1	b_2	b_3	b_4
A	2.65	0.04	-0.66	-0.04
B	0.16	0.62	-0.59	-0.08
C	2.2226	0.9318	-0.8490	- 0.0438

It should be noted that the coefficients b_1, b_2, b_3 and b_4 describe the dependence of the seat damping on preload, frequency and deflection amplitude, respectively, while the coefficient b_1 can be interpreted as a constants gain value. The derived model coefficients suggest the following:

i) The influence of preload on the seat damping coefficients is determined from parameter b_2. The damping coefficients of all the three seats increase with increase in the preload (b_2>0). The stiffness of seat "C" is most sensitive to

variation in the preload, while that of seat "A" is least sensitive.

ii) The influence of excitation frequency on the seat damping is determined from the parameter b_3. The parameter values suggest that damping coefficients of all three seats decrease with increase in frequency (b_3<0). The decreases in damping values, however, are large. Furthermore, the results suggest that the sensitivity of stiffness of all three seats to variations in excitation frequency is very different. The damping of seat "C" is most sensitive to variation in the frequency of excitation, while that of seat "A" is least sensitive.

iv) The effect of deflection amplitude on damping of a PUF seat is determined from parameter b_4. The damping values of all three seats decrease with increase in deflections amplitude (b_4<0). The results suggest that the influence of deflection amplitude on the damping value is small relative to that due to variations in the preload and frequency of excitation. The seat "B" exhibits most sensitivity to variations in deflection amplitude. Furthermore, the results suggest that the sensitivity of damping of the other two seats to variations in deflection amplitude is comparable.

2.5.4 Validation of the damping model

The validity of the proposed damping models is examined by comparing the model results with the corresponding measured data over the range of excitation amplitudes, excitation frequencies and preload. Equation (2.16) is solved to derive the damping constants for each of the three seats under excitations in the 0 to 10 Hz frequency range, and values of preload and amplitude used in the experimental characterization.

Figures 2.56 to 2.63 present a comparison of the results of models of all the three seats with the corresponding measured data over the range of test conditions considered in the study. In general, the model results are observed to be in close agreement with the measured damping coefficients. For seat "A", the results attained from proposed model agree very well with measured data, shown in Figures 2.56 and 2.57. Some derivation between the model results and the measured data, however, are observed under higher frequencies of above 7 Hz. The model results attained for seat "B" agree very well with the measured data for the entire range of test conditions considered, as shown in Figures 2.58 and 2.59. Figures 2.60 to 2.63 illustrate the comparison of model results with the corresponding measured data for seat "C". The results generally show a good agreement between the measured and computed results, except for higher frequencies (>6Hz) and small deflection amplitudes (<2.54 mm).

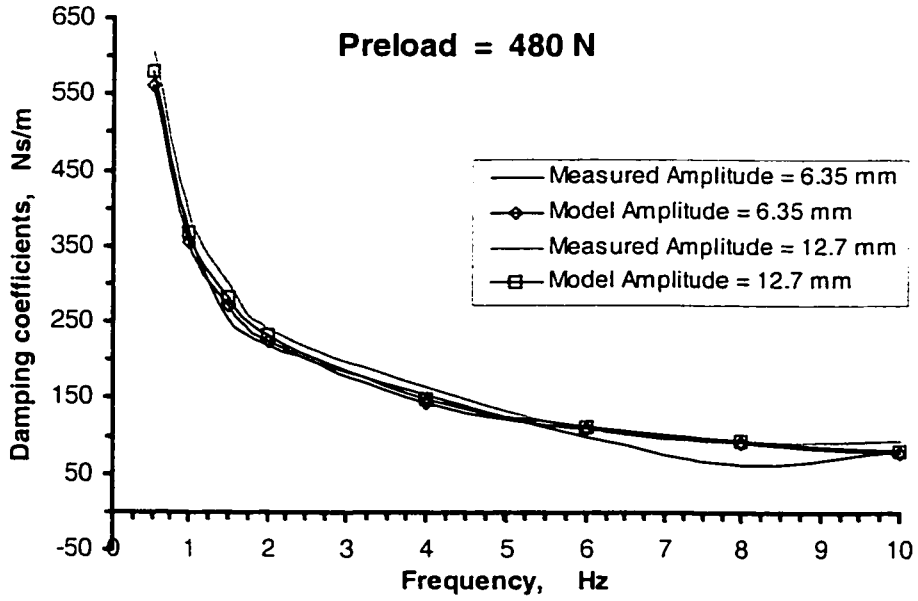

Figure 2.56: The comparison of the modeled damping with the measured data at constant preload of 480N mm for seat "A".

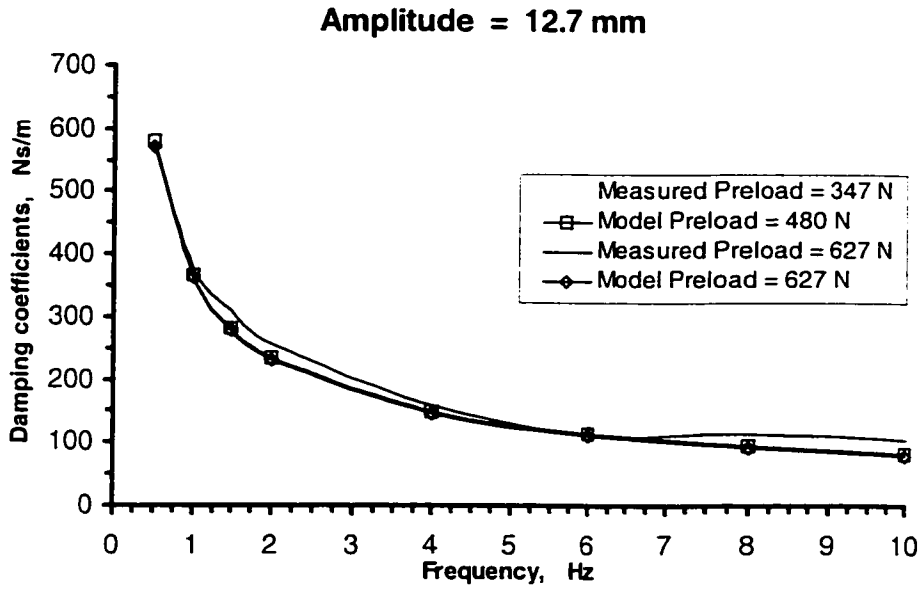

Figure 2.57: The comparison of the modeled damping with the measured data at constant amplitude of 12.7 mm for seat "A".

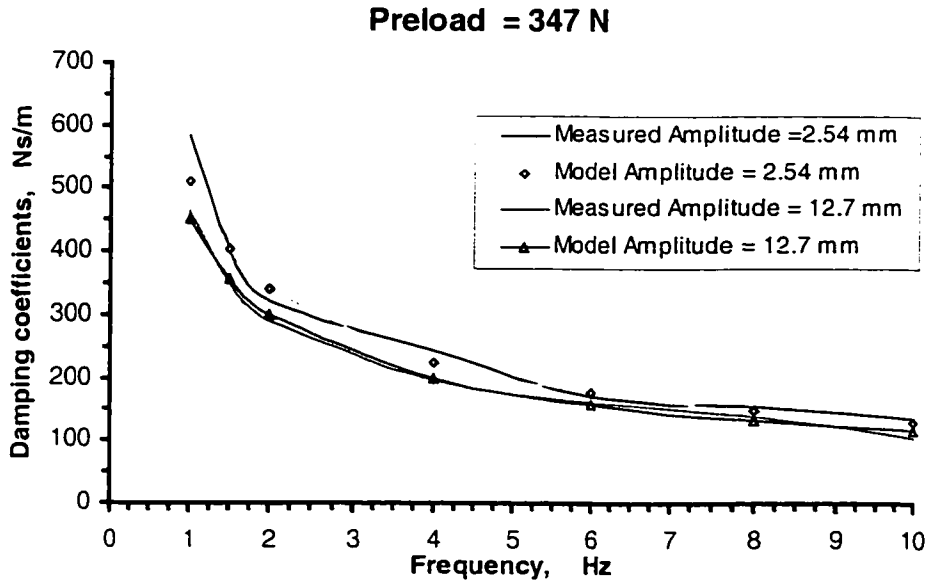

Figure 2.58: The comparison of the modeled damping with the measured data at constant preload of 347N mm for seat "B".

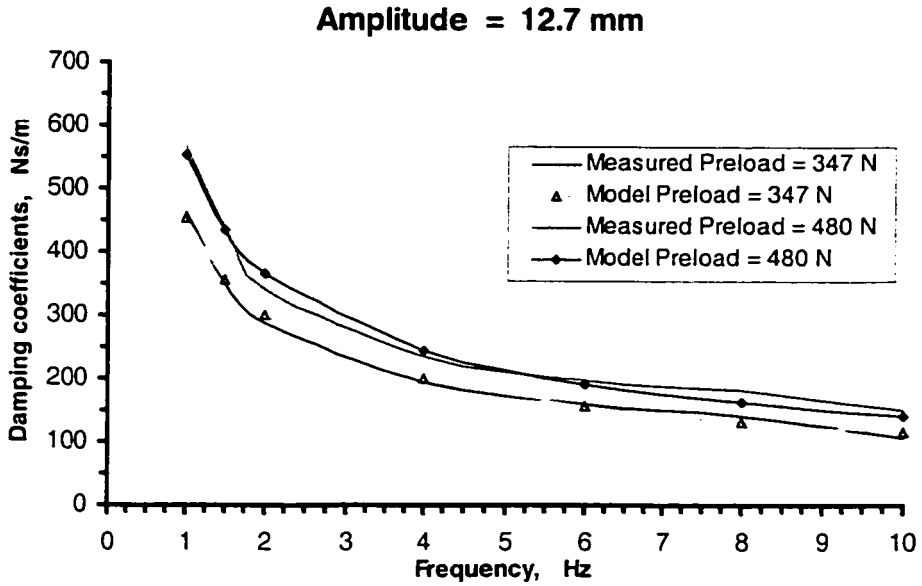

Figure 2.59: The comparison of the modeled damping with the measured data at constant amplitude of 12.7 mm for seat "B".

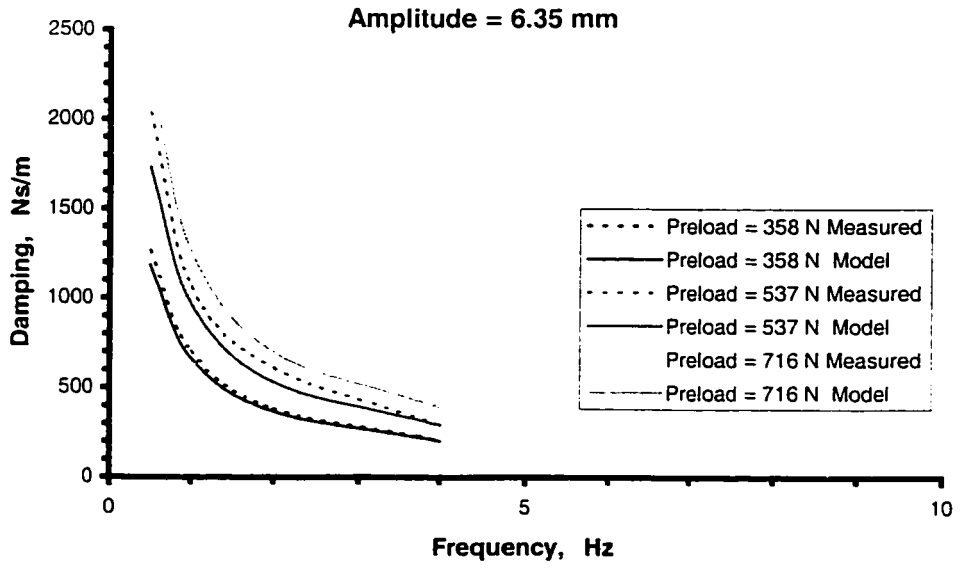

Figure 2.60: The comparison of the modeled damping with the measured data at constant amplitude of 6.35 mm for seat "C".

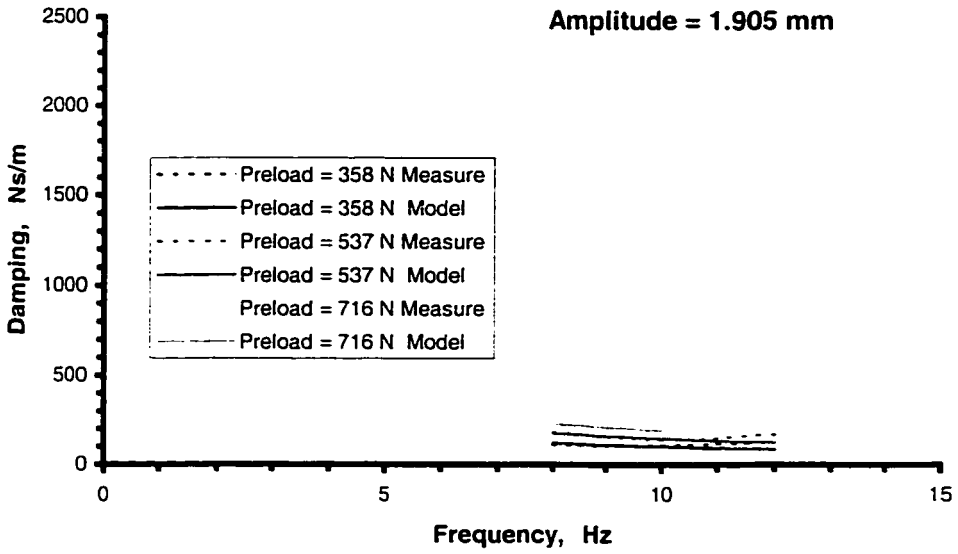

Figure 2.61: The comparison of the modeled damping with the measured data at constant amplitude of 19.05 mm for seat "C".

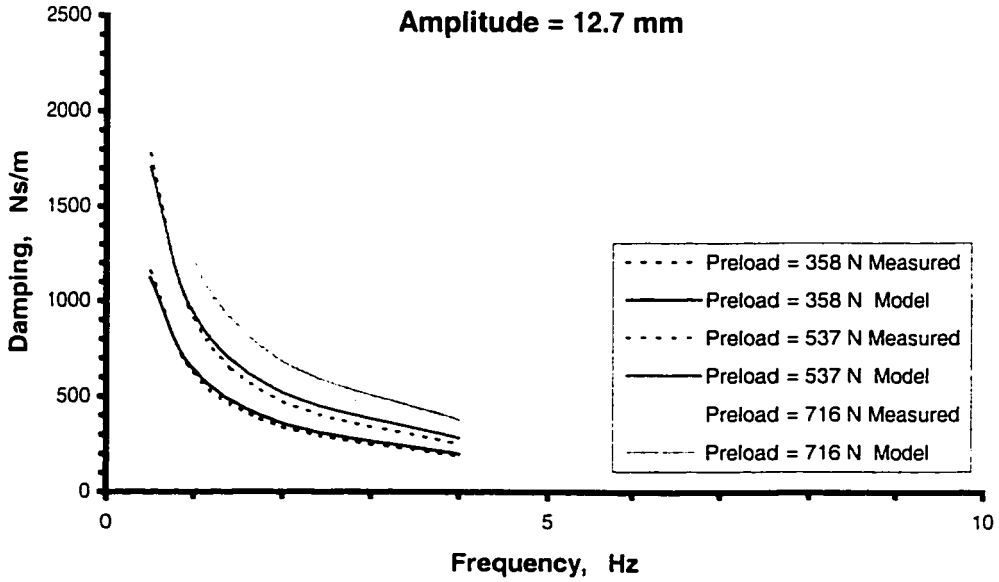

Figure 2.62: The comparison of the modeled damping with the measured data at constant amplitude of 12.7 mm for seat "C".

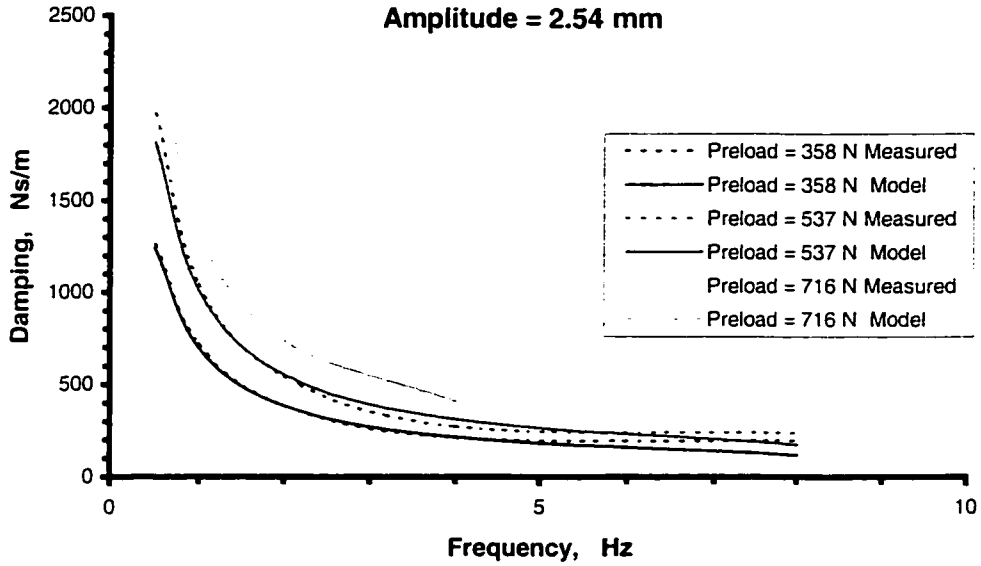

Figure 2.63: The comparison of the modeled damping with the measured data at constant amplitude of 2.54 mm for seat "C".

2.6 Development of Seat Cushion Models for General Application

In subsection 2.5, the dynamic properties of the seat cushions are characterized in equations (2.8) and (2.16). These models describing the dynamic properties of the seat cushions are proposed as functions of the preload, deflection amplitude and excitation frequencies. The validity of the proposed stiffness and damping models is also demonstrated by comparing the predicted force-deflection, force-velocity, and stiffness and damping coefficients with the corresponding measured data over the range of excitation amplitudes, excitation frequencies and preloads. The model results attained for all the three seats agree reasonably well with the measured data over most of the range of test conditions considered.

The proposed models, however, pose limitation for general application. Considering that the models are derived as the basis of the data acquired under sinusoidal excitations, the use of models requires prior knowledge of deflection amplitude A and excitation frequency f. In general application, a seat cushion deformation is time dependent and it may contain various spectral components in a relatively wide frequency band. The proposed models, therefore, need to be modified in order to utilize them for comfort analysis under representative random excitations encountered in an automobile. The changes are realized into two steps. The deflection amplitude of A in the seat cushion models is replaced by absolute value of the instantaneous relative deflection response of the seat cushion, such that the stiffness and damping coefficients may be expressed as:

$$K = a_1 W^{a_2} f^{a_3} |x(t)|^{a_4} \tag{2.19}$$

$$C = b_1 W^{b_2} f^{b_3} |x(t)|^{b_4} \tag{2.20}$$

where $x(t)$ is the instantaneous relative deflection of the seat cushion.

Furthermore, the excitation frequency used in the models could be derived from the instantaneous relative velocity and displacement responses, such that:

$$f = \frac{|\dot{x}(t)|}{2\pi |x(t)|} \tag{2.21}$$

Equations (2.19) and (2.20) can thus be rewritten:

$$K = \frac{a_1}{(2\pi)^{a_3}} W^{a_2} |\dot{x}(t)|^{a_3} |x(t)|^{(a_4 - a_3)} \tag{2.22}$$

$$C = \frac{b_1}{(2\pi)^{b_3}} W^{b_2} |\dot{x}(t)|^{b_3} |x(t)|^{(b_4 - b_3)} \tag{2.23}$$

Equations (2.22) and (2.23) describe the stiffness and damping properties of the

seat cushions for general application as function of preload, relative deflection and relative velocity. These relations are used in the subsequent section to derive analytical models of automotive seats and occupant-seat system.

2.7 Summary

In this chapter, the procedures for laboratory characterization of the static and dynamic properties of seat cushions are described. The static and dynamic properties of these different seats are identified from the measured data, which are observed to be strongly dependent preload, amplitude and frequency of excitation. While all the three seats revealed similar trends in relation to the preload, and amplitude and frequency of excitation, the relative influences of these parameters varied for different seats. Both of the stiffness and equivalent damping coefficients increased with the increase in the preload. An increase in the excitation frequency caused a rapid decrease in the equivalent damping coefficient, and a slight increase in the stiffness coefficient. Both of the stiffness and equivalent damping coefficients decreased with the increase in the excitation amplitudes. Owing to strongly nonlinear properties and lack of adequate stress-strain models for varying material properties, such as hysteresis, rebound index and resilience, curve-fitting methods are applied to derive stiffness and damping models of the seat cushions. A general structure of the models is proposed to characterize the dynamic stiffness and damping coefficients as function of the preload, and excitation and frequency. The validity of the models is demonstrated by comparing the model results with the measured data. The proposed models are further refined for general application involving vibration comfort analysis of the seats.

3 DEVELOPMENT AND VALIDATION OF SEAT MODELS

3.1 Introduction

It is well known that seats form an integral part of the automobile and strongly influence the perception and sensation of the ride comfort and safety. The design of an automotive seat for comfort is presently a more practiced art than an application of engineering tools. Automotive manufacturers are beginning to explore the little understood connection between seat design and comfort [23]. At the same time, a number of fundamental studies have attempted to study the relationships between the seat design and properties and the seating comfort. The human perception of comfort is complex function of many factors, such as postural support, seated height, vision, temperature, humidity, vehicle handling, noise and vibration. While many studies have investigated the ergonomic design consideration, only a limited number of studies have reported the vibration comfort performance and analyses.

Owing to strongly nonlinear properties of the seat and high degree of individual variability with regard to vibration comfort performance, the vibration comfort analyses are mostly conducted through either laboratory or field measurements. These studies involve repetitive measurements with relatively large number of subjects and seats, and yield poor repeatability [35,46]. Alternatively, the comfort performance of a seat could be objectively assessed through analysis of the analytical model that could be conveniently formulated from the stiffness and damping coefficient models presented in the previous chapter.

The open cell polyurethane foam (PUF) has become the preferred cushion material for automotive seats because of its good performance/cost ratio and mechanical properties. Open cell PUF foam consists of a polymer matrix with entrained fluid or gas. The gas is able to flow through the polymer matrix under the action of an imposed load. The movement of the gas through the polymer matrix can affect the mechanical properties of the foam. The stiffness of the polymer matrix is also variable, which affects the physical properties of PUF. The stiffness characteristics of PUF are inherently related to the level of loading. The stiffness properties under light loads are mostly determined from the linear elastic bending behaviors, while the loads beyond the linear-elastic range produce elastic buckling of the PUF foam. Low-order and lumped parameter models have been widely developed to describe the vertical vibration properties of automotive seats on the basis of such mechanical properties of the PUF foam.

3.2 Experimental Methods

The vibration comfort performance of automotive seats is typically performed either in the field or by using a motion simulator in the laboratory. The former method offer yields poor repeatability due to variation in the test conditions and the test subjects. The laboratory-based method is widely applied to assess the performance under representative and repeatable test conditions. In this study, the vibration isolation performance characteristics of three different automotive seats are measured in the laboratory under different levels of preload and vibration excitation. This data is used to verify the model.

A Whole-Body Vehicular Vibration Simulator (WBVVS) is employed to evaluate the vibration transmission characteristics of the seats in the laboratory. The WBVVS consists of a vibration platform supported on two servo-hydraulic motion actuators, a PC-based servo-control system and a data acquisition system. The setup also includes a signal conditioning system and a real time signal analyzer (B&K 2035), as shown in Figure 3.1. The motion actuators can replicate signals recorded on the floor or seat base of a car. The feedback control performance of the seat simulator is characterized by both flat amplitude and a flat phase response over a bandwidth of near 40 Hz [50]. The experiments are initially performed on the seat loaded with a rigid mass in order to examine the validity of the model while neglecting the influence that may cause the dynamics of the human subjects. Two piezo-electric accelerometers are placed, one directly on the top surface of the seat cushion, the other at the seat base in order to measure the vertical acceleration at cushion rigid load (sand bag) interface and at the seat pan, respectively. The measured signals are amplified by charge amplifiers and transferred into the signal analyzer.

In this study, the vibration attenuation characteristics of seat "C" are measured, while those for seats "A" and "B" are taken from a previous study. The candidate seat "C" was installed on the WBVVS platform and loaded with a sand bag weighing 56.5 kg, as shown in Figure 3.1. The seat preload is selected as 56.5 kg for representing 50^{th} percentile adult population of mean mass of 75kg.

3.2.1 Test Matrix

The vibration transmissibility characteristics of the seat "C" are investigated in the laboratory using the whole-body vehicular vibration simulator (WBVVS) under

harmonic excitations. The experiments are performed under different amplitudes of excitation in the 0.625 to 10 Hz frequency range. A swept sinusoidal signal is synthesized to provide different amplitudes of peak displacement: 2.54 mm, 6.36 mm and 12.7 mm, in the frequency range from 0.625 to 2 Hz. These correspond to peak acceleration amplitudes of 0.4 m/s^2, 1.0 m/s^2, and 2.0 m/s^2, respectively. In the frequency range from 2 to 10 Hz, the displacement amplitude is decreased to maintain constant the acceleration amplitude at the values established at 2 Hz. The test matrix, illustrating the range of preloads, vibration amplitudes and frequencies, is summarized in Table 3.1.

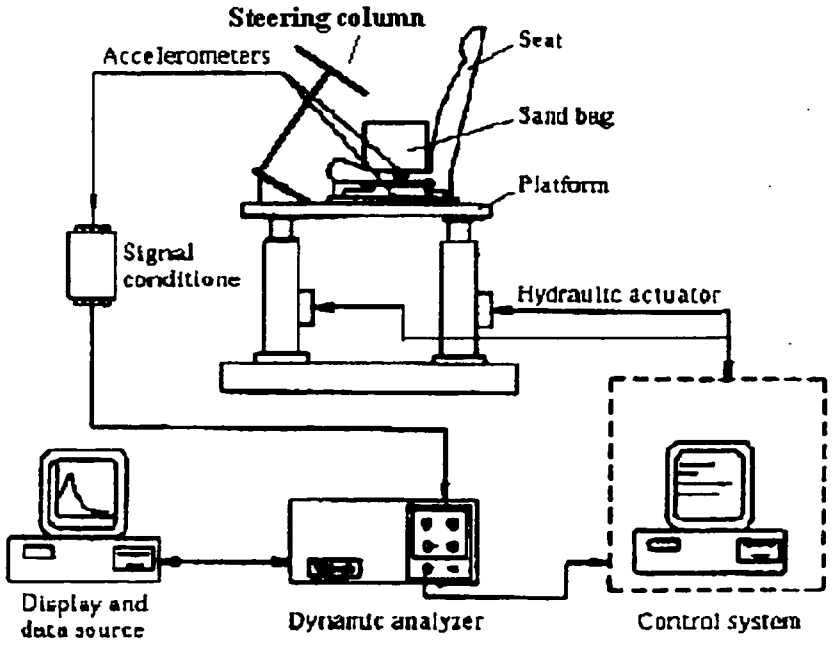

Figure 3.1: Schematic of the experimental setup for measuring the vibration transmissibility characteristics of the seats.

Table 3.1: Test Matrix Describing the Range of Preloads, Excitation Strokes and Excitation Frequencies.

Excitation	Preload	Displacement Amplitude (mm)	Frequency Range (Hz)	Acceleration Amplitude (m/s^2)	Frequency range (Hz)
Swept Sinusoidal	56.5 kg	2.54	0.625 – 2	0.4	2 – 10
		6.35	0.625 – 2	1.0	2 – 10
		12.7	0.625 – 2	2.0	2 – 10

3.2.2 Data acquisition

The measured signals acquired from the two accelerometers mounted on the top surface of the seat cushion and on the seat pan are amplified and fed into the signal analyzer B&K2035. The analyzer-based software is used to compute the vertical acceleration transmissibility of the seat in the following manner:

$$H(j\omega) = \frac{S_{\ddot{x}_o \ddot{x}_i}}{S_{\ddot{x}_i}} \tag{3.1}$$

Where $H(j\omega)$ is the complex transfer function of the seat, $S_{\ddot{x}_i}$ is the auto power spectral density of the seat pan acceleration $\ddot{x}_i$ and $S_{\ddot{x}_o \ddot{x}_i}$ is the cross-spectral density of the seat acceleration response $\ddot{x}_o$ and seat pan acceleration, and ω is the angular frequency ($\omega = 2\pi f$) and $j = \sqrt{-1}$.

The measured transfer function is expressed in terms of transmissibility magnitude and phase response of seat "C", as shown in Figure 3.2. The results show that

the vibration transmissibility characteristics of the seat "C" with a rigid mass under three different amplitudes of excitations vary with the excitation amplitude. The magnitudes of the transmissibility are very similar below 3 Hz for all the excitations. The transmissibility magnitude rapidly increases and reaches the resonant peak value of 4.4 at the resonant frequency of around 4.75 Hz under the excitation displacement amplitude of 12.7 mm, and it decreases above 4.75 Hz. Under the excitation displacement amplitude of 6.35 mm, the magnitude of the transmissibility increases slower than that under the excitation displacement amplitude of 12.7 mm and reaches the resonant peak value of 4.9 at the resonant frequency of around 5.25 Hz, and it decreases faster than that under the excitation displacement amplitude of 12.7 mm above 5.25 Hz. Under the excitation displacement amplitude of 2.54 mm, the magnitude of the transmissibility increases and reaches the resonant peak value of 5.5 at the resonant frequency of around 6 Hz, and decreases afterwards.

Figure 3.2 also shows that the excitation amplitudes lay obvious effects on the phase properties of the transmissibility. The phases of the transmissibility are very close under 3.5 Hz and above 7 Hz, but exhibit obvious differences between 3.5 Hz and 7 Hz under the three excitation displacement amplitudes. The phases of the transmissibility decay rapidly at almost same rate, but occur over different frequency ranges, under three excitation amplitude displacements.

The experimental results indicate that both the resonant peak amplitude and the resonant frequency decrease with increase in the displacement or acceleration of the inputs. This conclusion is coincident with the trends obtained from the static and dynamic properties of the seat cushions. The trends indicate that with the increase in the amplitude

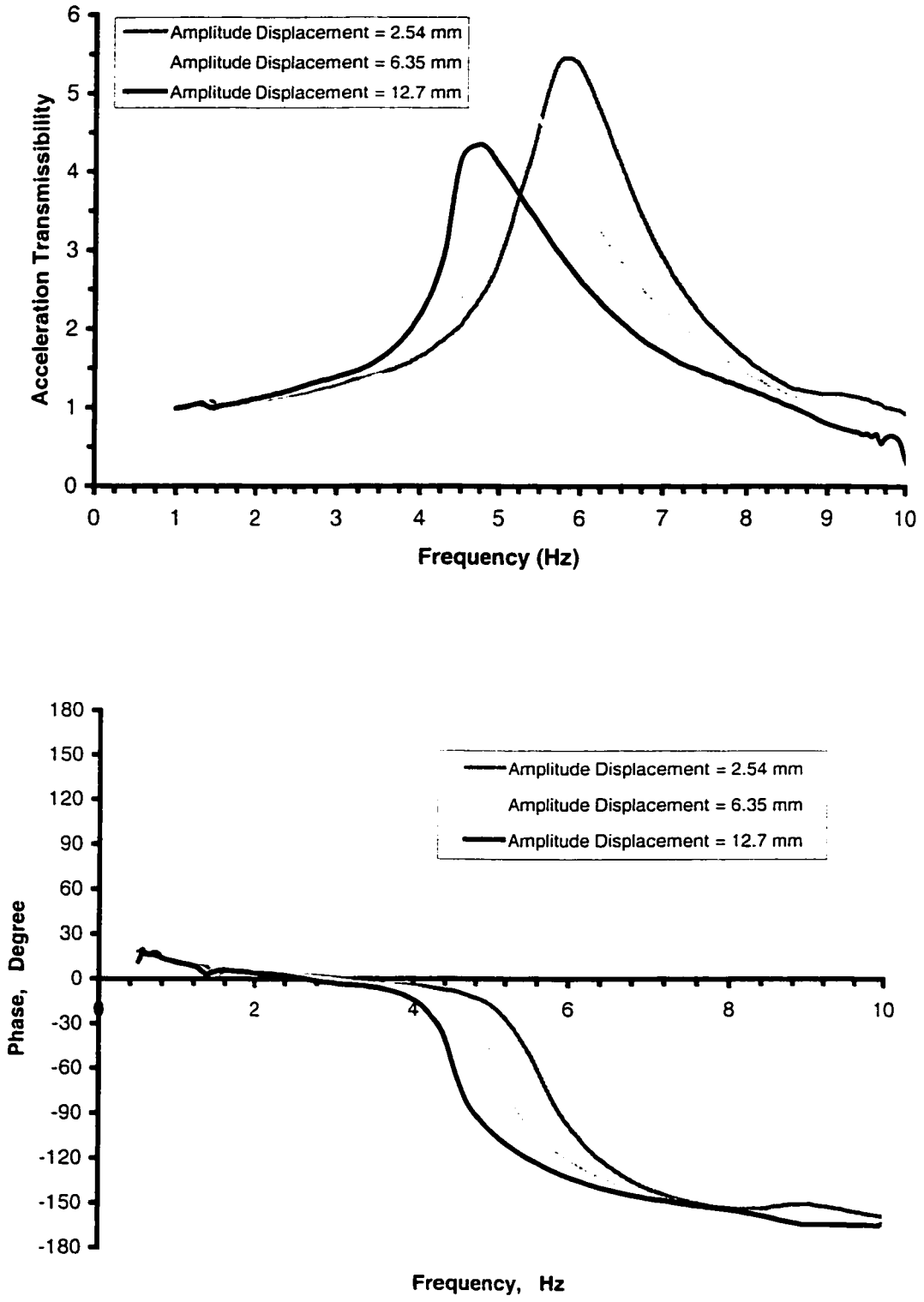

Figure 3.2: Vibration transmissibility characteristics of seat "C" with rigid mass 54.5 kg, as measured under different excitation magnitudes.

of the excitation, the equivalent damping coefficients decrease slightly, but the dynamic stiffness decreases most significantly. The increase in excitation amplitude displacement leads to the decrease in the resonant frequency. The increase in excitation amplitude displacement leads to an increase in the damping ratio $\xi = c/\sqrt{4km}$, and thus lower resonant peak response. The results clearly show the nonlinear vibration transmission characteristics of the seat.

Figures 3.3 and 3.4 illustrate the measured transmissibility magnitude response of seats "A" and "B", respectively, reported under displacement excitation of 6.35 mm [52].

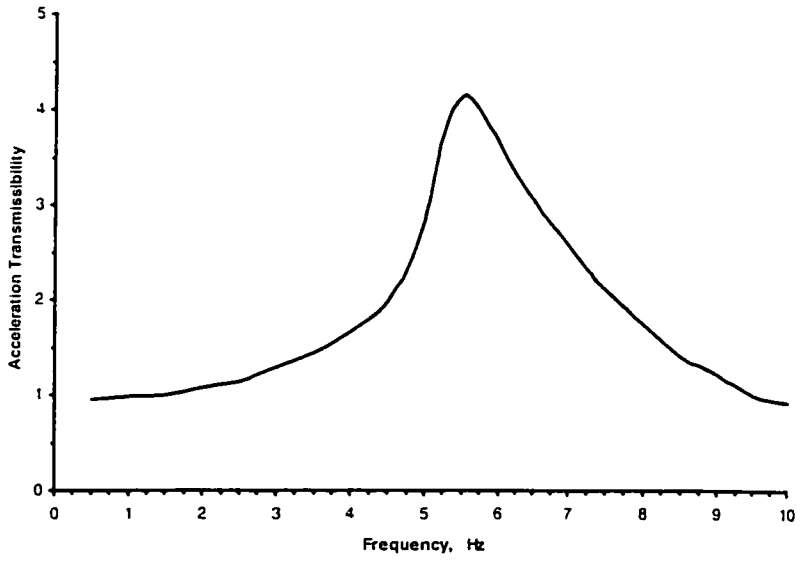

Figure 3.3: Vibration transmissibility of seat "A" with a rigid mass (55 kg) and constant amplitude displacement 6.35 mm [52].

The results show resonant peak response close to 4.35 occurring at a frequency of around 5.5 Hz for seat "A", and close to 3.7 occurring at a frequency of around 5.0 Hz for seat "B". A comparison of Figures 3.2 to 3.4 reveals that seat "B" yields the lowest resonant transmissibility, which occurs at a relatively lower frequency of 5 Hz. Although the vibration transmissibility characteristics of seats "A" and "B" have not been reported for different amplitudes of excitations, the dependence upon the amplitude of excitation is expected to be similar to that observed for seat "C". This is attributed to the nonlinear trends observed from the equivalent damping and stiffness coefficients.

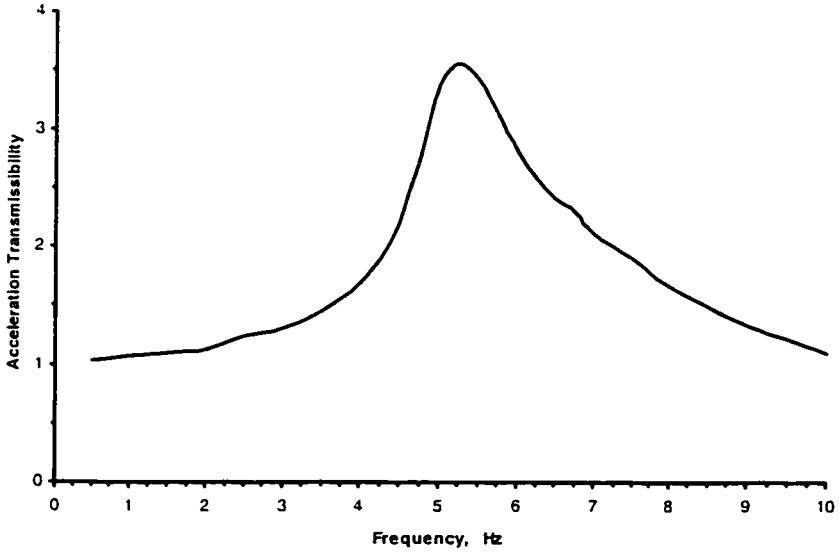

Figure 3.4: Vibration transmissibility of seat "B" with a rigid mass (55 kg) and constant amplitude displacement 6.35 mm [52].

3.3 Development of the seat model with a rigid mass

3.3.1 Analyses of the seat model

The modeling of an automotive seat with a rigid mass involves accurate characterization of the mechanical properties of the open-cell PUF seat cushion. Figure 3.5 depicts the mechanical properties of the open-celled PUF in terms of typical stress-stain relationship [19]. The stress-strain curve reveals three distinct phases. In the first phase ($\varepsilon < 0.05$), the mechanical properties could be characterized by any linear elastic material [51]. This phenomenon is also evident from the measured stiffness characteristics of the seat cushion presented in Figures 2.5 to 2.7. In this phase the walls

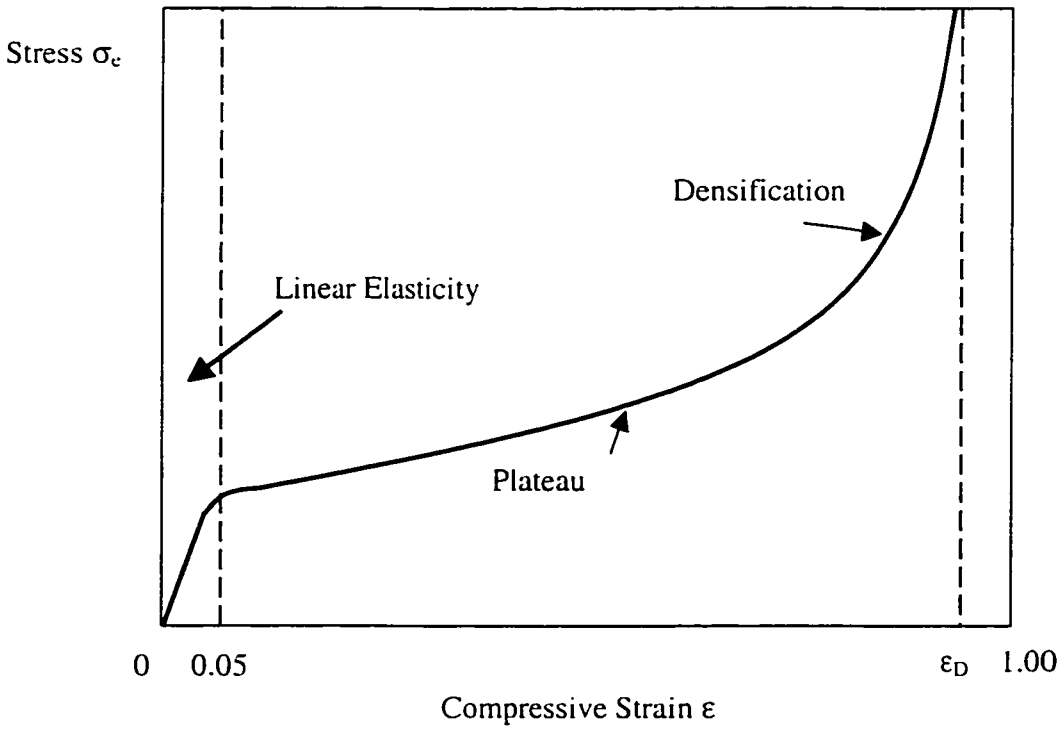

Figure 3.5: Stress-strain curves for open cell foam [19

of the open celled foam provide simple bending resistance to loads. In the second phase, corresponding to higher strains, the walls of the cellular structure suffer progressive buckling. This phase is typified by softening of the foam or reduction in the stiffness of the foam structure. This phenomenon is also evident from the measured stiffness characteristics of the seat cushion presented in Figures 2.5 to 2.7, i.e. the stiffness decreases with the increase in the strain (deflection). Under extreme strains, the PUF undergoes densification due to total buckling and expulsion of the entrained gas from the matrix structure. This last phase is evidenced by steeply increasing stiffness in Figure 3.5, which can also be observed from the measured stiffness data corresponding to extreme deflection.

The modeling of a seat may also require considerations of the seating components, such as the frame, trim covers, and some adjusters in addition to the PUF. A seat cushion model is developed on the basis of stiffness and damping coefficient models derived in Chapter 2. The stiffness model, derived from the measured data, represents mostly the stress-strain relationship within the Plateau region shown in Figure 3.5.

The automotive seats are exposed to vertical vibration and shocks arising primarily from the tire-terrain interactions. The relative deflection and relative velocity response of the seat cushion strongly depend on the seat load, displacement and velocity of the input. The deflection behavior of the seat cushion spans over all the three phases characterized in the stress-strain characteristic. The seat model should thus cover all the three phases, rather than the second phase alone as characterized by the experimental data. The automotive seat cushion is presented by its viscous-elastic properties along the

vertical axis; an equivalent nonlinear spring and a parallel nonlinear viscous damper, as shown in Figure 3.6.

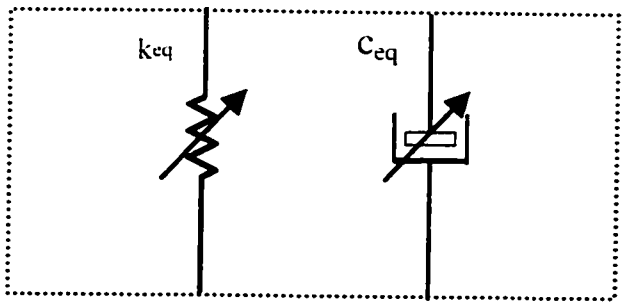

Figure 3.6: Proposed seat model.

Owing to $a_4 - a_3 < 0$ in the stiffness model shown in formula (2.23) and Table 2.5, when the relative deflection of cushion is less than x_v, which is assumed 10^{-5} m in order to avoid that formula (2.23) leads to infinity, it is considered as x_v. In this case, the stiffness and damper are considered as those when the relative deflection of cushion is x_v. Owing to $b_4 < 0$ in the damping model shown in formula (2.24) and Table 2.6, when the relative velocity of cushion is less than $\dot{x}_s$, which is assumed 10^{-5} m/s in order to avoid that formula (2.24) leads to infinity, it is considered as $\dot{x}_s$. In this case, the damper is considered as the one when the relative velocity of cushion is $\dot{x}_s$. When the relative deflection of cushion is greater than the number x_l, which is determined by specific experimental condition, the stiffness and damper are increased by a constant respectively. This constant is caused by the deflection of spring inside the frame of seat. Based on the

formula (2.23) and (2.24) in Chapter 2, the seat models are described as formula (3.2) and (3.3).

$$k = \begin{cases} \dfrac{a_1}{(2\pi)^{a_3}} W^{a_2} |\dot{x}|^{a_3} |x|^{(a_4 - a_3)} & |x| < x_l \ when |\dot{x}| < \dot{x}_s, \dot{x} = \dot{x}_s \\ \dfrac{a_1}{(2\pi)^{a_3}} W^{a_2} |\dot{x}|^{a_3} |x|^{(a_4 - a_3)} + k_{den} & |x| \geq x_l \end{cases} \tag{3.2}$$

$$c = \begin{cases} \dfrac{b_1}{(2\pi)^{b_3}} W^{b_2} |\dot{x}|^{b_3} |x|^{(b_4 - b_3)} & |x| < x_l ; when |\dot{x}| < \dot{x}_s, \dot{x} = \dot{x}_s \\ \dfrac{b_1}{(2\pi)^{b_3}} W^{b_2} |\dot{x}|^{b_3} |x|^{(b_4 - b_3)} + c_{den} & |x| \geq x_l ; when |\dot{x}| < \dot{x}_s, \dot{x} = \dot{x}_s \end{cases} \tag{3.3}$$

Where x and $\dot{x}$ are relative deflection and velocity, respectively; k_{den} and c_{den} are the stiffness and damping in the case of big deflection, respectively.

From the above formulae, the seat possesses a linear elastic phase in which the stiffness is constant for small deflections that can be associated with the region of small strain. With the increase of the deflection, the stiffness shows non-linearity and the seat cushion characteristics enter the second phase. In this phase, the velocity influences slightly on the stiffness. The higher the relative deflection, the bigger the stiffness will be. The change of the entrained amount of the gas and the moving speed of the gas in the foam cause the change of the stiffness. A final stress-strain phase that follows the buckling is the compaction phase, in which the voids within the foam have been almost completely eliminated. In this last phase the foam exhibits a significant hardening characteristic. In this phase, the spring component at the bottom of the seat plays an important role in stiffness and damper, frame bending also, represented by k_{den} and c_{den} in the formulae.

From formulas (3.2) and (3.3), it can be seen that the model parameter a_1 represents the stiffness gain, a_2 describes the preload dependence of the stiffness, a_3 relates to relative velocity and deflection dependence of the stiffness, and a_4 describes the relative deflection dependence of the stiffness constant. The parameter b_1 can be interpreted as a damping coefficient gain, while b_2 describes the load dependence of the damping coefficient. The constants b_3 and b_4 describe the relative velocity and deflection dependence of the seat damping coefficient.

3.3.2 Identification of nonlinear stiffness and damping coefficients

A simple and low order lumped parameter model of the car seat is formulated using Equations (3.2) and (3.3) together with a rigid mass, as shown in Figure 3.7. The equation of motion for the seat-load system can be expressed as:

$$m\ddot{x}_0 + c(\dot{x}_0 - \dot{x}_i) + k(x_0 - x_i) = 0 \tag{3.4}$$

Where x_0 and $\dot{x}_0$ are the displacement and velocity responses of the rigid mass, respectively; and x_i and $\dot{x}_i$ are the displacement and velocity of input at the seat track, respectively. c and k are nonlinear damping and stiffness coefficients described in Equations (3.2) and (3.3), respectively. m is the mass representing the body mass or the sand bag employed in laboratory characterization.

The equation of motion of the seat is solved under sinusoidal excitation used in the laboratory tests, and the resulting responses are compared with the measured data corresponding to specify preloads and excitations.

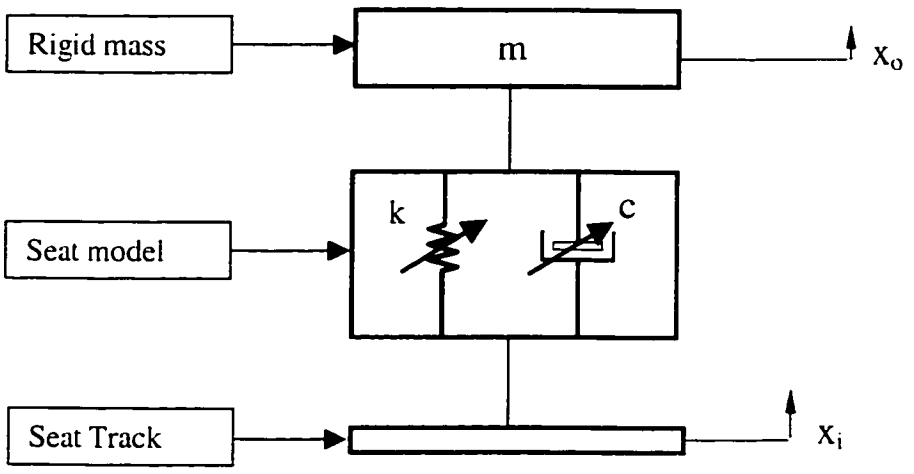

Figure 3.7: Seat –load system.

The trial and error method is used to identify the coefficients k_{den} and c_{den} by minimizing the error between the measured and predicted vertical acceleration transmissibility of the seat-load system. The parameters of k_{den} and c_{den} identified for the three seats are summarized in Table 3.2.

Table 3.2: Linear stiffness and damping parameters of the seat structure.

Seat	K_{den} (N/m)	C_{den} (Ns/m)
A	4400	280
B	2000	270
C	6000	130

3.4 Validation of the seat-load model

The equation of motion of the seat-mass system model, shown in Figure 3.7 is solved using Simulink software under harmonic excitations of varying magnitudes. The stiffness and damping coefficients identified for all the three candidate seats are applied using equations (3.2) and (3.3) together with the parameters presented in tables 2.5, 2.6, and 3.1. The predicted acceleration transmissibility is compared with the measured data and the results are presented in Figures 3.8 to 3.12. The simulations for seats "A" and "B" are performed under 6.35 mm peak displacement excitation in the 0.625 to 2 Hz range, and under constant acceleration 1.0 m/s^2 excitation in the 2 to 10 Hz frequency range, as described earlier in Section 3.2. The simulation for seat 'C' is carried out under three different levels of excitations (2.54 mm, 6.35 mm and 12.7 mm), as described in section 3.2. The simulation results are presented in terms of acceleration transmissibility, the ratio of peak acceleration response of the mass to that of the seat pan ($|\ddot{x}_u / \ddot{x}_i|$). The validity of the proposed model for all three seats is examined by comparing the model results with the measured data.

Figures 3.8 and 3.9 illustrate the comparison of acceleration transmissibility magnitude response derived from the models of seat "A" and "B", respectively, with the corresponding measured data. The results represent the vibration transmissibility of seat "A" and "B" with preload of 55 kg and subject to 6.35 mm displacement excitation. Figure 3.8 shows reasonably good agreement between the model results and the measured data over the entire frequency range.

Figure 3.9 depicts the predicted and measured acceleration transmissibility of seat "B" with preload of 55 kg under the excitation displacement amplitude of 6.35 mm. The

predicted and measured data are very close below 2 Hz. The predicted transmissibility increased more rapidly than the measured value after the excitation frequency is equal to 2 Hz. The predicted transmissibility increased afterwards more slowly than the measured value. The two values finally become identical at 5 Hz. The largest error is 10% in the range from 2 to 5 Hz. The predicted transmissibility agrees with the measured data very well within the resonant frequency range between 5 and 6.25 Hz. at frequencies above, the model predicts a more pronounced attenuation than the measured data where the error can be as high as 40 %.

The model response for both seats "A" and "B" reveals very good agreement with

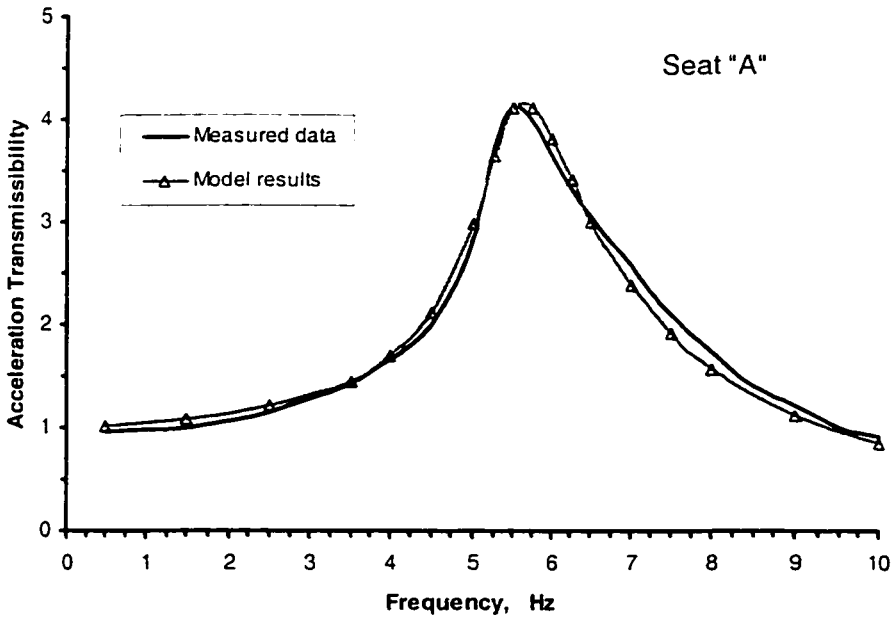

Figure 3.8: Comparison between modeled and measured acceleration transmissibility amplitude and phase of seat "A" under excitation displacement amplitude of 6.35 mm and preload of 55 kg.

the measured data in terms of peak acceleration transmissibility and the resonant frequency. The model response, however, trends to be lower than the measured data at frequencies above 6.5 Hz. The deviation at high frequency excitation could be mostly attributed to intermittent jumping of the load from the seat surface, which is often encountered in laboratory tests. It should be noted that the passive load employed in assessment of seats is often unrestrained to ensure that the visco-elastic properties of the seat are not altered by the restraint. The unrestrained load may encounter hopping motion under high magnitude or high frequency excitations, which could contribute to relatively high transmissibility at higher frequencies.

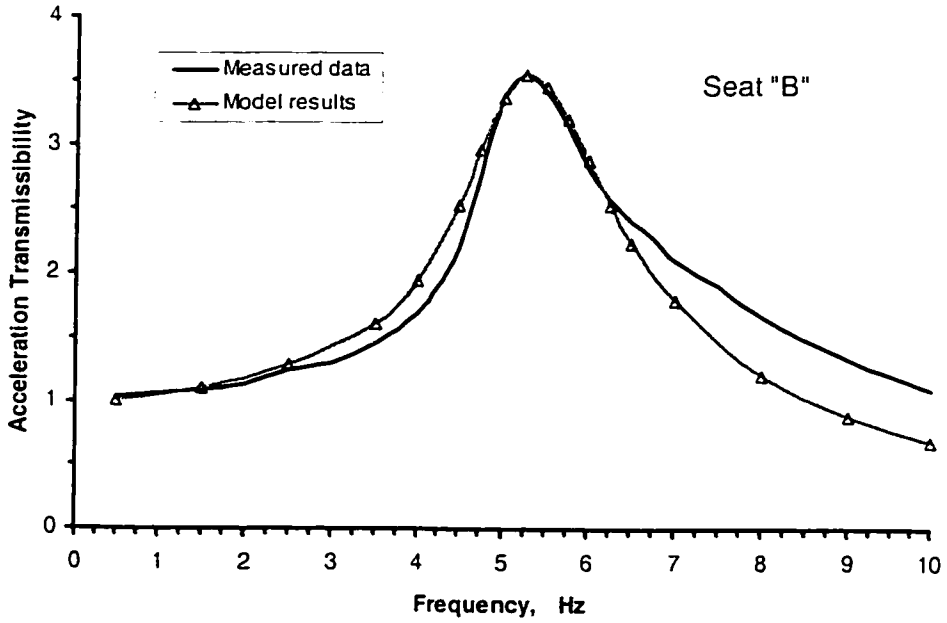

Figure 3.9: Comparison between modeled and measured acceleration transmissibility amplitude and phase of seat "B" under excitation displacement amplitude of 6.35 mm and preload of 55 kg.

Figures 3.10 to 3.12 depict respectively the predicted and measured acceleration transmissibility characteristics of seat "C" with preload of 55 kg corresponding to three different excitations. For excitation displacement amplitude of 2.54 mm, as shown in Figure 3.10, the amplitude and phase of the predicted transmissibility match the measured data very well below 5 Hz. Then the predicted amplitude increases more rapidly than the measured amplitude. The two curves have same peak value of 5.5. After the two curves reach peak value, both of them start to decrease. The measured amplitude declines faster than the predicted. This phenomenon leads to two results. One is that the predicted resonant frequency shift to left by 0.25 Hz. The other is that the predicted amplitude comes to be equal to the measured at 7.5 Hz. Finally, the two curves will get close above 7.5 Hz. For excitation displacement amplitude of 12.7 mm, shown in Figure 3.12, the resonant frequency shifts to right by 0.25 Hz. The resonant peak of the model is higher than the measure data. The error of peak value is up to 8%. The rest of curves are very close. For excitation displacement amplitude of 6.35 mm, shown in Figure 3.11, the model response reveals very good agreement with the measured data in terms of peak acceleration transmissibility and the resonant frequency in the entire frequency range.

For the above three cases, the phase curves of transmissibility show the same trend as the amplitude curves of transmissibility. In the case of small excitation amplitude of 2.54 mm, as shown in Figure 3.10, the predicted phase shift to left by 0.25 Hz. When middle excitation amplitude of 6.35 mm, shown in Figure 3.11, is applied, the predicted phase fit the measured very well. For the large excitation amplitude of 12.7 mm, as shown in Figure 3.12, the predicted phase shift to right by 0.25 Hz.

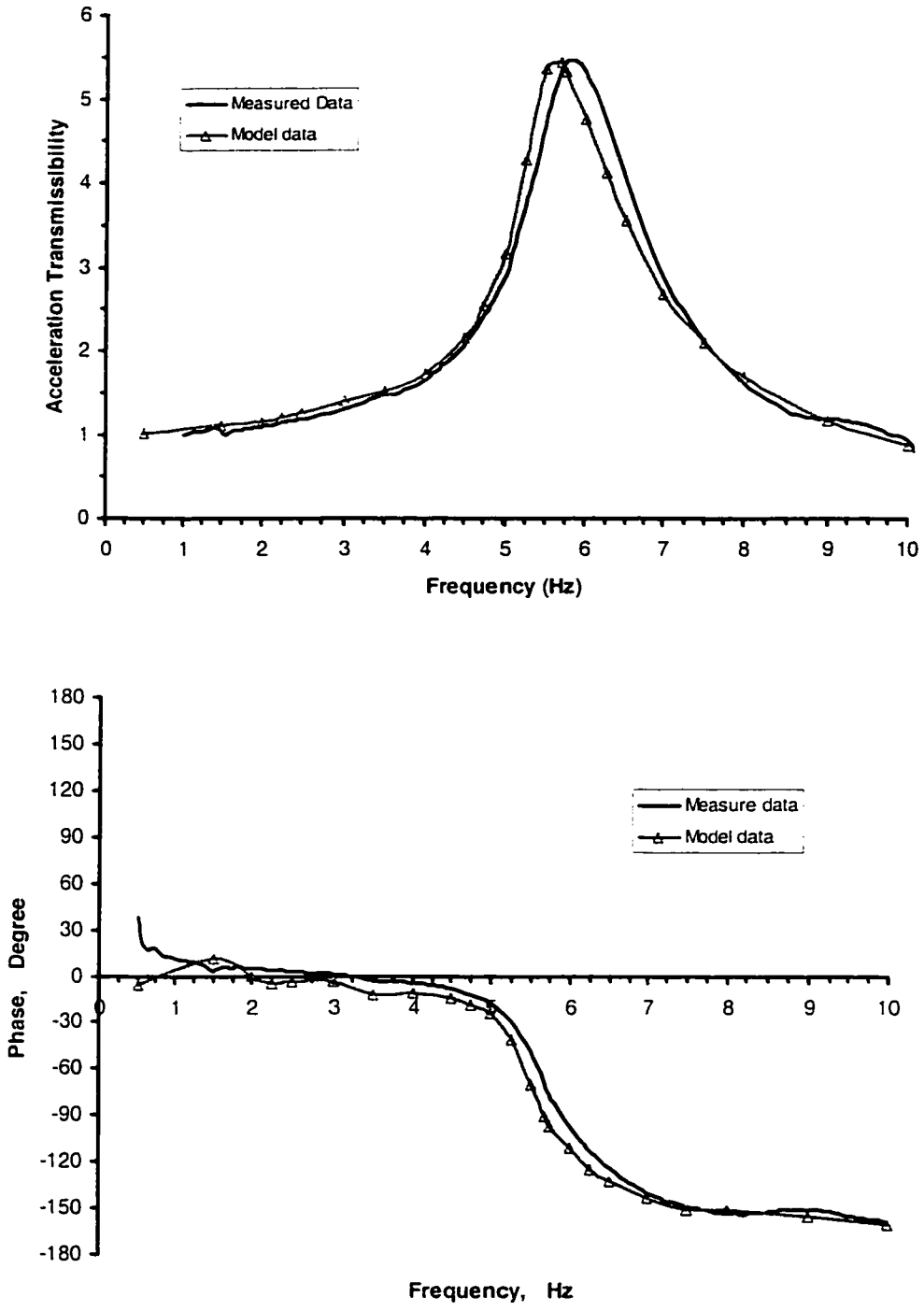

Figure 3.10: Comparison between modeled and measured acceleration transmissibility amplitude and phase of seat "C" under excitation displacement amplitude of 2.54mm and preload of 55 kg.

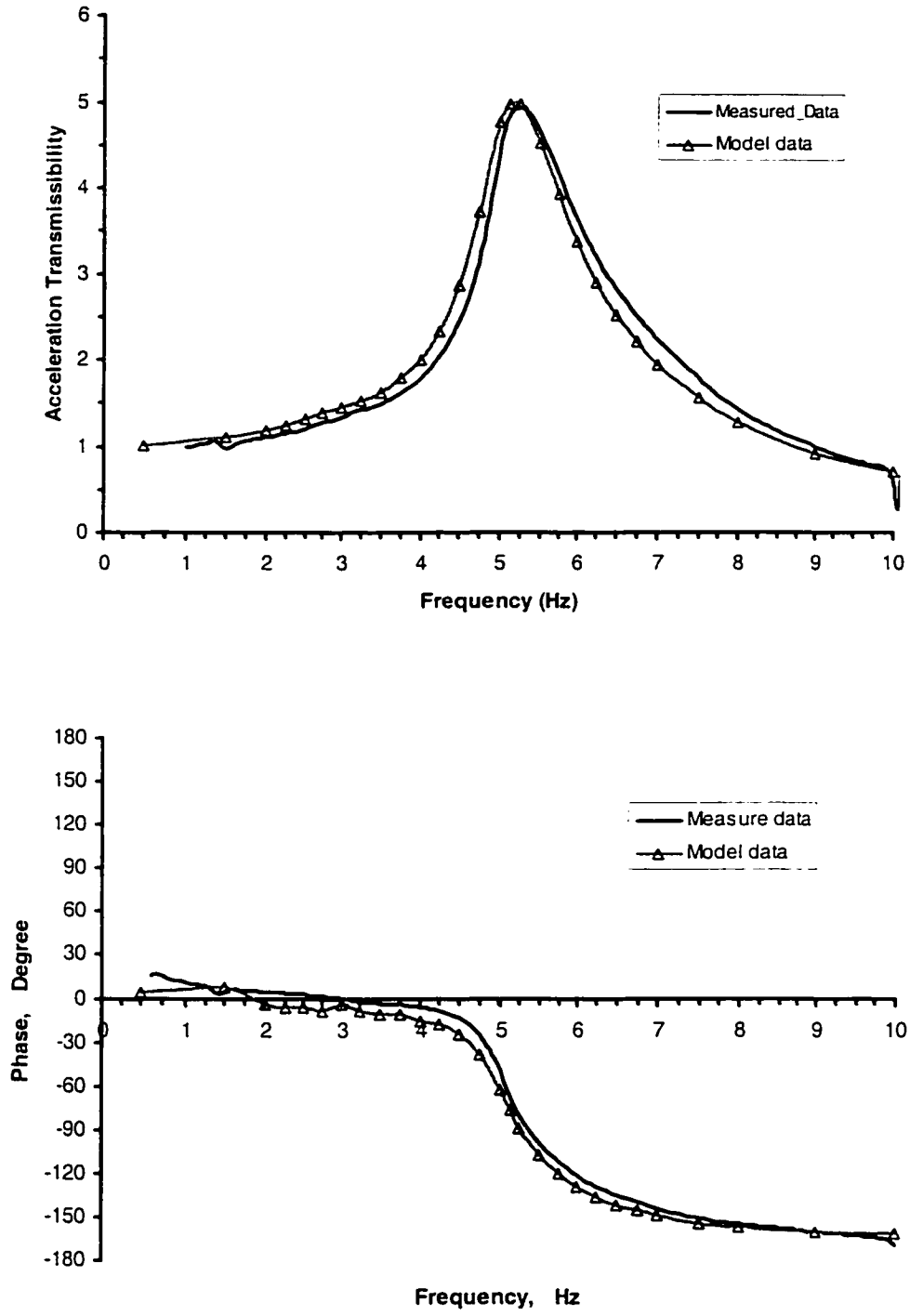

Figure 3.11: Comparison between modeled and measured acceleration transmissibility amplitude and phase of seat "C" under excitation displacement amplitude of 6.35mm and preload of 55 kg.

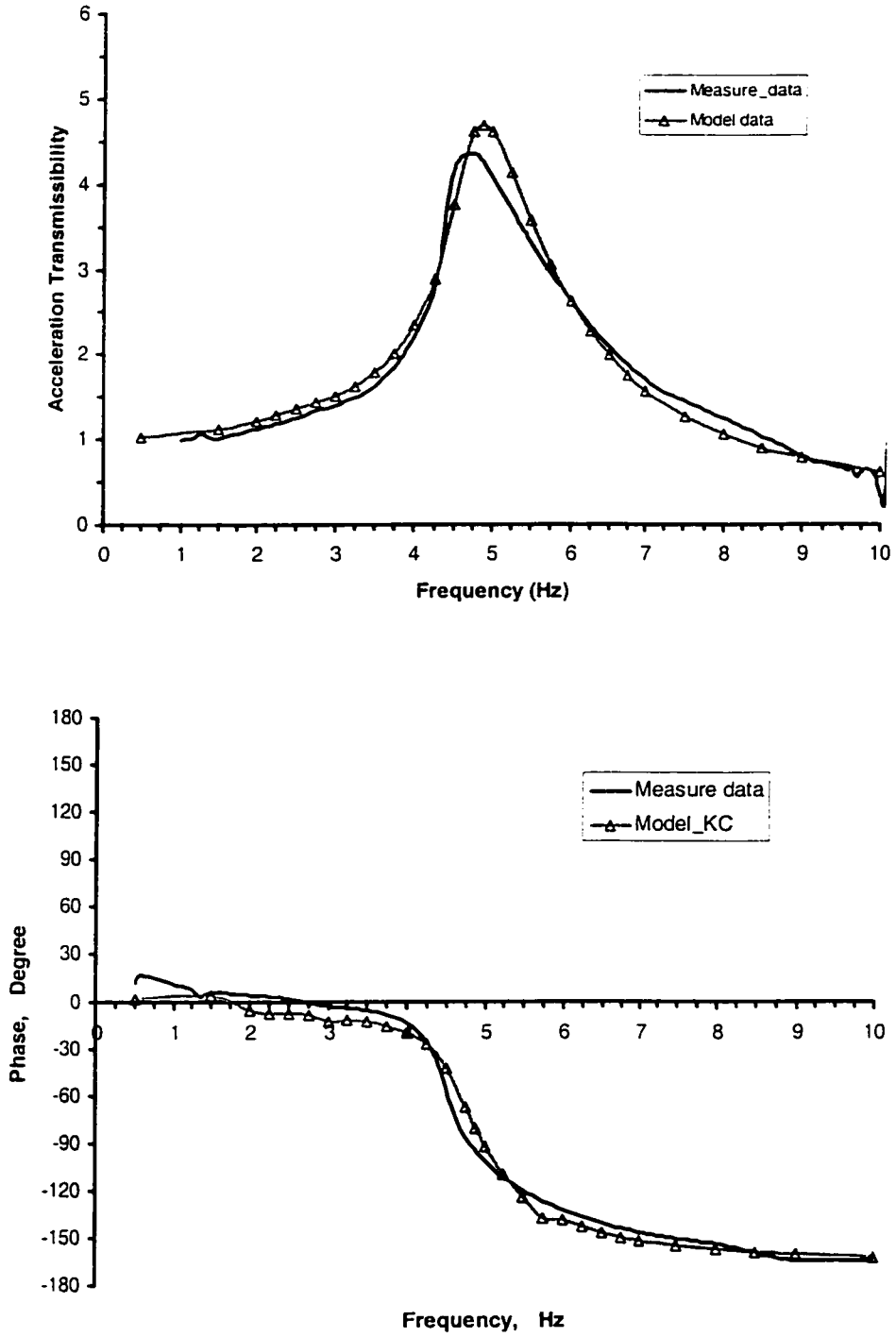

Figure 3.12: Comparison between modeled and measured acceleration transmissibility amplitude and phase of seat "C" under excitation displacement amplitude of 12.7mm and preload of 55 kg.

3.5 Summary

In this chapter, the results of seat cushion transmissibility measurements are reported when using a rigid mass as the load. The transmissibility characteristics are observed to be strongly dependent on the excitation amplitude. The peak transmissibility value decreases with the increase in excitation displacement amplitude and the resonant frequency of transmissibility also decreases with the increase in excitation amplitude. Based on the seat cushion model described in Chapter 2, a non-linear theoretical vertical vibration model of the car seats is derived. The fundamental theory of dynamic mechanical behavior and hydraulics of flexible open-celled foam material is used during the development of the model. The seat model includes linear and nonlinear stiffness, which shows characteristic of mechanical properties of the open-celled foam in various strain phases and contribution of the seat's frame. Linear and nonlinear damping coefficients are applied to obtain the results, which presents hydraulics of the confined gas in the foam matrix that flows under load.

Finally, the stiffness and damping models are combined with a rigid mass to construct a seat-rigid mass system. The vertical acceleration transmissibility of the seat cushion model is computed under different amplitudes of excitation, and compared with the measurements performed with three seat cushions. The validity of the models is demonstrated by comparing the model results with the measured data. The results show reasonably good agreement between the model results and the measured data over the entire frequency range for three different inputs provided to seat "C" and one input provided to other two seats.

4 VIBRATION PERFORMANCE AND PARAMETER SENSTTIVITY ANALYSIS OF THE SEAT-RIGID MASS SYSTEM

4.1 Introduction

Ride quality is concerned with the sensation or feel of the driver or passenger in the environment of a moving vehicle. Apart from many other factors, the ride comfort is related to the vibration transmitted to the seated body, which may be influenced by a variety of sources, including surface irregularities, aerodynamic forces, engine and driveline vibration, and non-uniformities (unbalances) of the tire/wheel assembly. Usually, surface irregularities, ranging from potholes to random vibration of the surface elevation profile, act as the major source that excite the vibration of the vehicle body through the tire/wheel assembly and suspension system. Exposure to whole-body vehicle vibration may cause a complex distribution of oscillatory motions and forces within the body [1]. The complex nature of vibration transmitted through the seat determines the perception of the whole-body vibration and effects on the ride comfort.

The comfort characteristics of automotive seats are frequently assessed through subjective and objective ride performance tests. While subjective evaluations yield considerable data on relative ride ranking, they can be effectively used to obtain ride perception, but do not provide quantitative information to the designer. Alternatively, objective assessments of seats provide important quantitative information on the design. The objective assessments may be performed in the field or in the laboratory under representative vibration conditions. There are two types of methods for evaluating vibration performance in an objective manner. They are measures based upon physical

quantities obtained from the experiments and measures based upon simulation quantities attained from analysis of proven system models. The former is primarily used to evaluate the properties or performance of specific designs or properties, while the latter is generally employed to predict the performance potentials and to formulate desirable design parameters.

In this chapter, different performance measures are formulated to assess the comfort performance of automotive seats and influence of selected design parameters. The influence of variations in various design factors on the performance characteristics are investigated through parametric sensitivity studies.

4.2 Performance measures

Evaluation of human exposure to whole-body vibration (WBV) can be carried out by examining different response quantities, such as displacement, velocity and acceleration responses of the human-seat or load-seat interface. Many studies have established that the acceleration is the most suitable parameter to assess the vibration attenuation performance of seats and human perception of vibration [46,52]. Several response quantities based on acceleration include overall (i.e. 0.5-80 Hz) rms acceleration, frequency-weighted rms acceleration, root-mean quad acceleration, and peak acceleration which may be used to define parameters to assess the relative performance of the seats. Some of these performance measures are described below.

The peak acceleration response of a seat could be effectively used to assess its vibration as well as shock isolation performance. Furthermore, the human perception and response to vibration can also be related to peak acceleration [1,71]. The influence of

model or design parameters on the seat performance is thus assessed in terms of peak acceleration, defined as the peak deviation from the mean value in the time-domain.

4.2.1 S.E.A.T.

The S.E.A.T. (Seat Effective Amplitude Transmissibility) value is defined as to measure the efficiency of a seat in isolating the body from vibration. It provides a simple numerical assessment of the seat isolation efficiency, as described earlier in Chapter 1. In order to measure a S.E.A.T. and frequency-weighted S.E.A.T. value of a seat, rms acceleration and the frequency-weighted rms acceleration are introduced firstly.

The spectral components of the response acceleration may also be evaluated in terms of rms acceleration spectra. Both the International (ISO 2631-1) and British Standard (BS 6841) suggest the use of frequency-weighted rms acceleration and provide the weighting filter constants corresponding to center frequencies of the one-third octave bands [1,71]. The ratio of the rms acceleration spectra measured on the seat and at the base in one-third octave frequency bands may thus be used to assess the vibration transmission performance of the seats. Both the ISO-2631 [1] and BS 6841 [71] provide weighting filter networks, W_k and W_b, respectively, that are applicable to whole-body vertical acceleration.

The rms of acceleration may be computed either in the time domain or in the frequency domain. The time domain method permits the derivation of overall rms acceleration over an exposure duration T in the following manner:

$$a_{rms\_time} = \sqrt{\frac{1}{T}\int_0^T \ddot{x}^2(t)dt} \tag{4.1}$$

where $\ddot{x}(t)$ is the instantaneous acceleration in m/s^2.

The computation in the frequency-domain permits the analysis of rms acceleration spectra or distribution in specific frequency bands. One-third octave band analysis is widely used to study the ride performance in automotive applications since it is considered to have sufficiently fine resolution and it yields manageable number of values. The rms in the frequency-domain corresponding to center frequency of one-third octave band may be calculated by integrating the power spectral density of acceleration over the desired frequency band:

$$a_{rms}(f_c) = \sqrt{\int_{f_l}^{f_u} PSD_{\ddot{z}(t)} df} \tag{4.2}$$

where $PSD_{\ddot{z}(t)}$ is the power spectral density of acceleration in $(m/s^2)^2/Hz$, f_l and f_u are the lower and upper limits of the frequency band in Hz, and a_{rms} is rms acceleration corresponding to center frequency f_c in m/s^2.

The rms value in the frequency domain over the entire range of frequency of interest may be obtained by computing:

$$a_{rms\_freq} = \sqrt{\sum_{i=1}^{N} \left(a^2_{f_c}\right)_i} \tag{4.3}$$

where N is the total number of frequency bands considered and $(a_{f_c})_i$ is rms acceleration of i^{th} component centered at one-third octave component f_c.

When evaluating vibration with respect to its possible effects on the human body, the frequency weightings are required. The International Standard ISO 2631-1 (1997) [1] defines principal frequency weighting W_k for assessing exposure to vertical vibration in the frequency range of 0.5 to 80 Hz. The Standard defines a frequency-weighting transfer function $H_w(s)$ that is applied to derive the time history of the weighted acceleration using

the Convolution method, as shown in Figure 4.1. The frequency-weighted overall rms acceleration $a_{w.rms}$, in the time domain is thus obtained from:

$$a_{w.rms\_time} = \sqrt{\frac{1}{T}\int_0^T \ddot{x}_w^2(t)dt} \tag{4.4}$$

where T is the measurement duration in seconds and $\ddot{x}_w(t)$ is the instantaneous frequency-weighted acceleration in m/s^2.

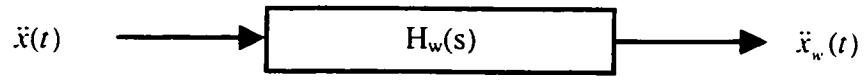

Figure 4.1: Application of frequency-weighting function defined in ISO-2631 [1].

The frequency-weighted rms acceleration corresponding to each one-third octave band can also be computed using the magnitudes of the frequency-weighting filter defined in ISO-2631 [1]. The overall value of frequency-weighted rms acceleration is then computed from:

$$a_{w.rms\_freq} = \sqrt{\sum_{i=1}^{N}\left(W_k(f_c)a_{f_c}\right)_i^2} \tag{4.5}$$

where W_i is the magnitude of the frequency weighting function corresponding to center frequency f_c of the i-th frequency band; $(a_{f_c})_i$ is the rms acceleration for i-th one-third octave frequency band centered at f_{c_i}; and N is the total number of frequency bands considered.

The frequency-weighted rms acceleration can also be calculated directly from acceleration power spectral density:

$$a_{w.rms\_freq} = \sqrt{\int_{f_l}^{f_u} |H_w(jf)|^2 PSD_{\ddot{x}(t)} df} \tag{4.6}$$

where f_l and f_u are the lower and upper limits of the frequency range of interest.

The crest factor is defined as the ratio of the frequency-weighted instantaneous peak value of the frequency-weighted acceleration signal to the frequency-weighted overall rms acceleration [4]. The peak value shall be determined over the duration of measurement, T. The crest factor yields a measure of the shock contents of the measured signal. For vibration with crest factors below or equal to 9, the basic evaluation method using weighted rms of acceleration is normally sufficient [1]. For the passenger cars, the crest factor of acceleration signal is often below 9. For vibration with crest factor above 9, the basic evaluation method may underestimate the effects of vibration exposure due to presence of occasional shocks, and transient vibration.

4.2.2 Acceleration transmissibility

The steady-state vibration transmission characteristics of a seat-rigid mass system can be conveniently evaluated in terms of acceleration transmissibility, which is defined

as the ratio of acceleration magnitude transmitted to the seat-rigid mass interface to the magnitude of excitation acceleration at the seat base, in the frequency range of interest. The vertical vibration transmissibility can provide significant information related to vibration attenuation characteristics and probable frequency range of vibration isolation.

4.3 Synthesis of a road-measured excitation

Owing to highly nonlinear properties of the automotive seat, the vibration isolation effectiveness and the vibration comfort performance of seats would strongly depend upon the nature of excitation (magnitude and frequency contents). It is thus vital to characterize the vibration excitations encountered at the seat base of a specific vehicle. For laboratory assessment studies, it would be essential to synthesize respective excitations using a motion generator. The vertical vibration encountered at the seat base of an automobile are predominant in the vicinity of vertical mode resonance of the sprung and unsprung masses, as evident from power spectral density of acceleration measured on the floor of passenger car [57], shown in Figure 4.2. The acceleration spectra measured at floor was performed under the condition, which is an automobile over a given medium roadway at constant speed (85 km/h). The human body sensitivity to vibration is strongly related to the vibration frequency. The vibration in the0.5 to 0.75 Hz frequency range tend to cause dizziness and motion sickness, while those in the 4 to 8 Hz range cause whole-body resonance. The human head and neck are known to be sensitive to vibration in the 18 to 20 Hz range [57]. The rule of good ride quality in a passenger car is that the natural frequency of the car body should be near 1 Hz in order to avoid the sensitive frequency region of human body, and to provide effective attenuation of vibration

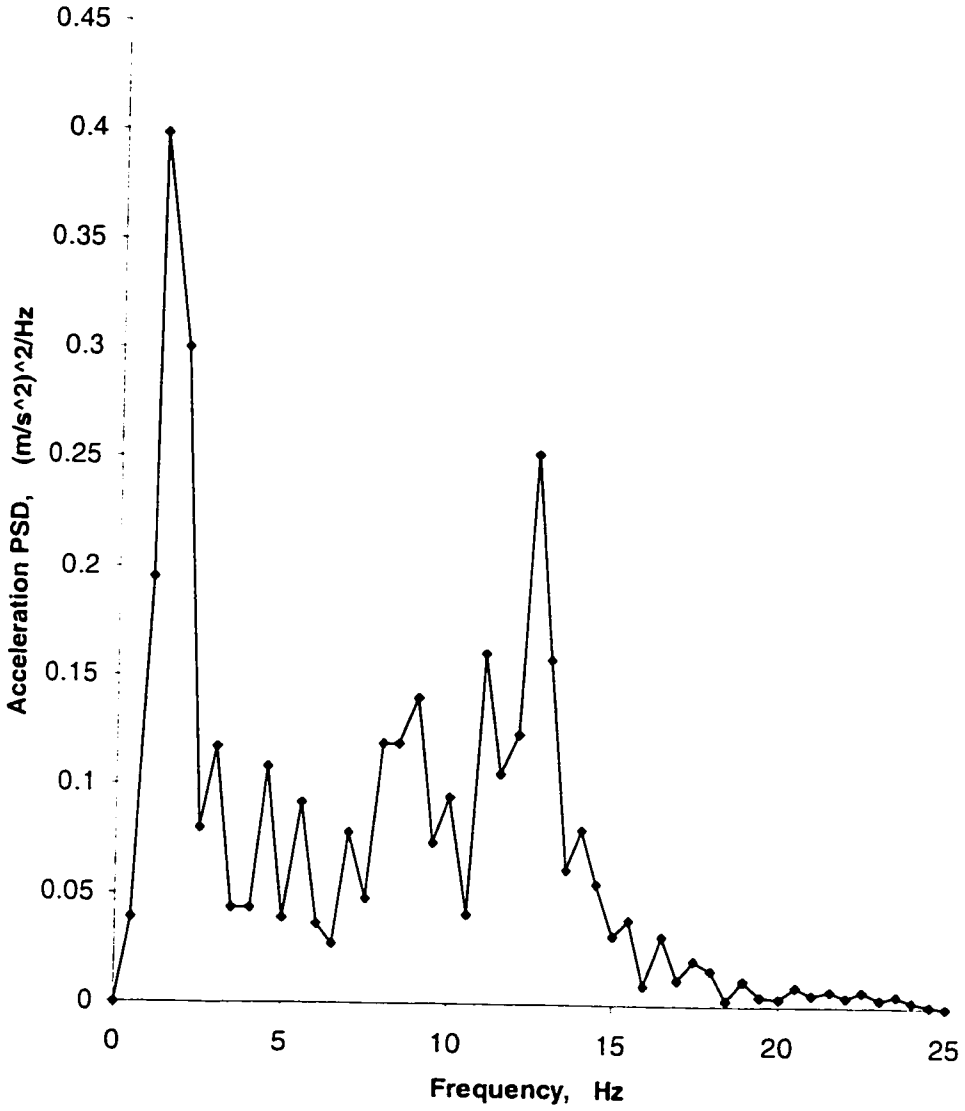

Figure 4.2: Acceleration PSD measured at the floor of a passenger car [57].

in the 4 to 8 Hz range. The PSD of acceleration measured at the floor reveals two peaks: near 1 Hz and 12 Hz, respectively, which are attributed to the vertical mode resonances of the sprung and unsprung masses. For a typical passenger car, the peak amplitude associated with the sprung mass resonance is an order of magnitude higher than the unsprung mass [54,55,56].

A measured 'representative' vibration signal can be conveniently synthesized in the laboratory to assess the vibration isolation performance of seats under controlled conditions. Considering that $y(t)$ is a white noise random signal and $x(t)$ is the time history of the synthesized acceleration signal corresponding to the measured acceleration $PSD(S_x(f))$, a frequency response function relating the two may be derived using the relationship for single-input-single-out (SISO) single-DOF system [58,59]:

$$|H(jf)|^2 = \frac{S_x(jf)}{S_y(jf)} \tag{4.7}$$

where $S_x(jf)$ is the power spectral density of the measured/synthesized acceleration; $S_y(jf)$ is the power spectral density of the white noise excitation, such that:.

$$S_y(jf) = S_0 \tag{4.8}$$

Assuming $S_0 = 1$, the frequency response function required to synthesize the measured acceleration PSD, $H(jf)$, may be derived from:

$$|H_x(jf)| = \sqrt{S_x(jf)} \tag{4.9}$$

A frequency response function is formulated to express the measured acceleration PSD illustrated in Figure 4.2, using a frequency response function similar to that of a 2-DOF system, as follows:

$$H^*(s) = \frac{d_1 s(s^2 + d_2 s + d_3)}{(s^2 + d_4 s + d_5)(s^2 + d_6 s + d_7)} \tag{4.10}$$

where the coefficients d_1 to d_7 are identified through parametric optimization. An objective function is defined to minimize the error between the predicted and the measured values of the frequency response function:

$$U(x) = \sum_{f=0.1}^{20} (|H_e(j2\pi f)| - |H^*(j2\pi f)|)^2 \tag{4.11}$$

where x is a vector of model parameters to be identified, expressed as:

$$x = \{d_1, d_2, d_3, d_4, d_5, d_6, d_7\}^T ; \; d_i > 0 \tag{4.12}$$

$H_e(jf)$ *and* $H^*(s)$ are the derived and identified functions, respectively. In order to ensure somewhat comparable contributions of error in the objective function in different frequency ranges, the weighting factors are introduced. A weighting factor of 5 is selected in the vicinity of two peaks occurring in the frequency ranges of 0.6 to 1.4 Hz and 10.1 to 14 Hz. The value of the weighting factor is maintained as 1 in the remaining frequency range. The equation (4.11) is thus rewritten as:

$$\begin{aligned} U(x) = & \sum_{f=0.1}^{0.5} (|H(j2\pi f)| - |H^*(j2\pi f)|)^2 + 5 \sum_{f=0.6}^{1.4} (|H(j2\pi f)| - |H^*(j2\pi f)|)^2 \\ & + \sum_{f=1.5}^{10} (|H(j2\pi f)| - |H^*(j2\pi f)|)^2 + 5 \sum_{f=10.1}^{14} (|H(j2\pi f)| - |H^*(j2\pi f)|)^2 \\ & + \sum_{f=14.1}^{29} (|H(j2\pi f)| - |H^*(j2\pi f)|)^2 \end{aligned} \tag{4.13}$$

Optimization Toolbox [60,61] in MATLAB is used to solve the constrained optimization problem, defined in Equations (4.12) and (4.13). The solutions are obtained for different initial values of the parameters vector x. The model parameters identified corresponding to minimum error of the objective function are summarized below:

$$d_1 = 2.13;\quad d_2 = 325.33;\quad d_3 = 12288.21;\quad d_4 = 7.05;\quad d_5 = 52.67;$$

$$d_6 = 20.48;\quad d_7 = 6168.50; \tag{4.14}$$

The magnitude of the identified frequency response function, described in equation (4.10), is compared with that derived from the acceleration *PSD*, as shown in Figure 4.3. The results, in general, show a fairly good agreement between the measured and identified frequency response function. The magnitude of the computed function correlates very well with the measured data within 0 to 3 Hz and 10 to 20 Hz frequency ranges. The computed frequency response function reveals two resonant peaks respectively in the vicinity 1.15 Hz and 12.5 Hz, which are quite consistent with the measured data. The resonance in the vicinity of 1.15 Hz is primarily associated with the sprung mass of the car, while the resonance in the vicinity of 12.5 Hz is associated with the unsprung mass. The two peak values derived from the computed function, however, are slightly lower than those from the measured data. The largest error occurs in the 5 to 7 Hz range and approaches almost 17%.

The time history of the acceleration excitation signal is synthesized by applying the computed frequency response function to a white noise signal (Figure 4.4 (a)). The displacement and velocity of the synthesized signal are obtained by integrating, filtering and scaling the acceleration signal using the DSP (Digital Signal Processing) software.

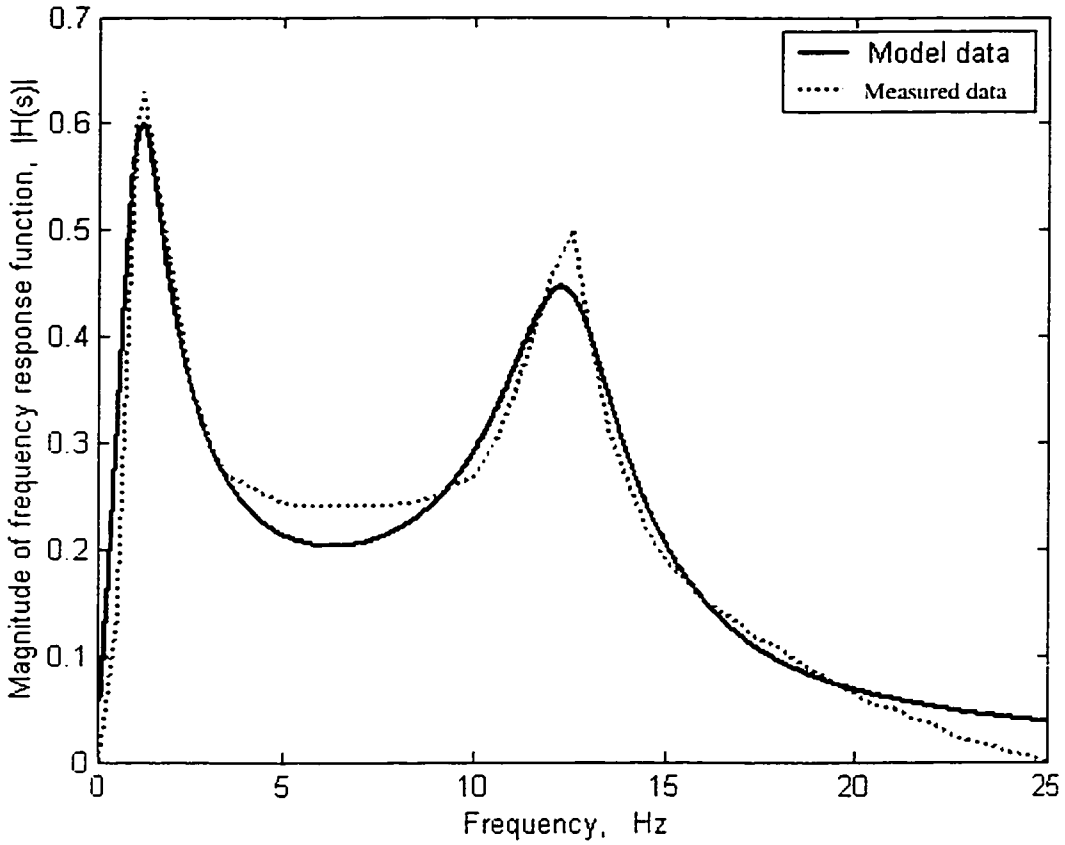

Figure 4.3: Comparison of the model to measured frequency response function.

The validity of the synthesized acceleration signal is further examined by comparing its PSD with the target or measured acceleration PSD, as illustrated in Figure 4.4 (*b*). The results show reasonably good agreement between the synthesized and measured acceleration PSD's. The computed acceleration PSD reveals two resonant peaks respectively in the vicinity 1.15 Hz and 12 Hz, which are consistent with those observed from the measured data.

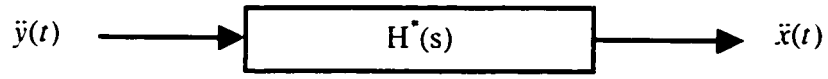

(*a*)

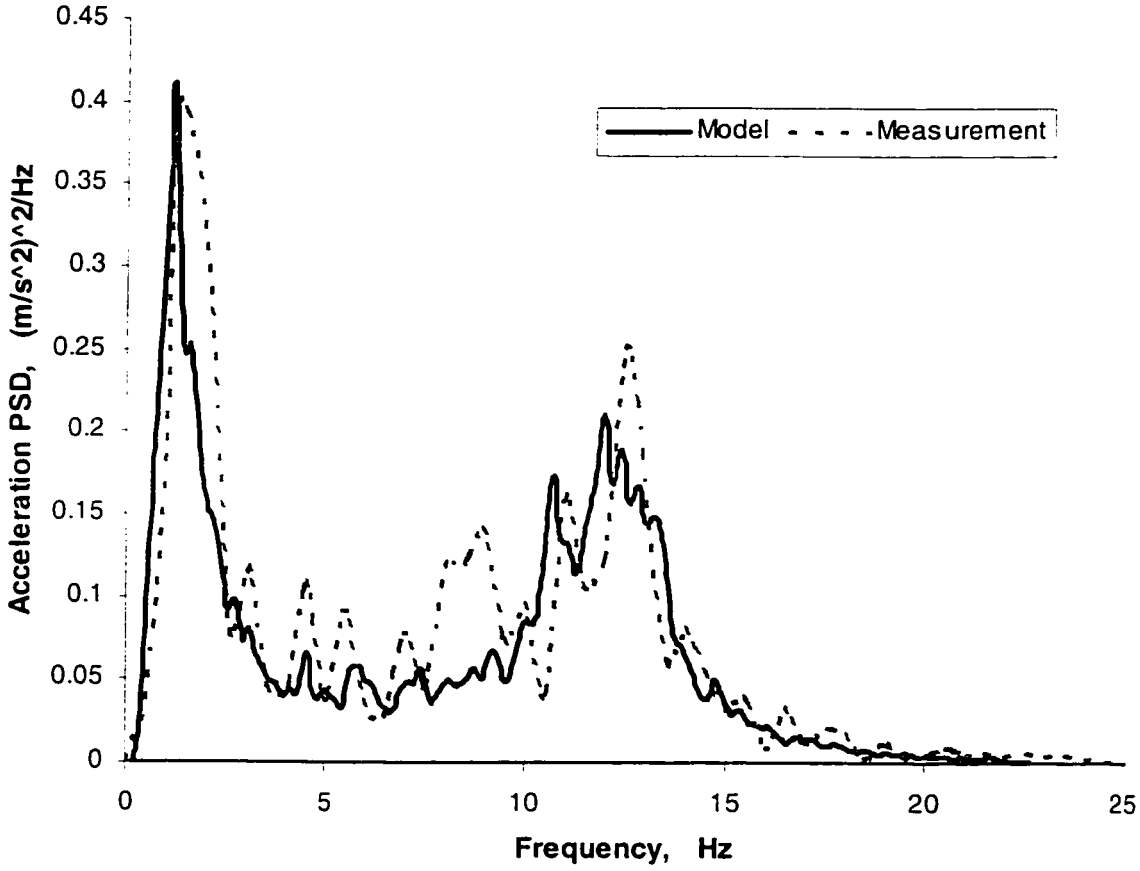

(*b*)

Figure 4.4: (*a*) Application of computed frequency response function for synthesis of acceleration time-history; and (*b*) Comparison of PSD of the synthesized acceleration signal with the measured acceleration PSD.

4.4 Analysis of vibration isolation characteristics

The analytical model of the seat-mass system, derived in Chapter 3, is analyzed to determine the vibration isolation characteristics of the candidate seats under different excitations. The analytical model includes nonlinear stiffness and damping effects of the PUF as function of the preload, and nature of excitation and response. The model simulations are performed under road measured excitation and white noise random excitation of different magnitudes. The overall rms acceleration of the road-measured or synthesized acceleration excitation, illustrated in Figure 4.4 (*b*), is computed as 1.2 m/s^2. Three different levels of white-noise random excitation are selected for the analysis with overall rms acceleration of 0.25, 0.5 and 1.0 m/s^2 to study the effect of magnitude of excitation. The simulations are performed for all three-candidate seats and the response characteristics are evaluated in terms of selected performance measures described in section 4.2. These include: unweighted and frequency-weighted S.E.A.T. values and acceleration transmissibility. The results are discussed in view of the vibration isolation performance of the seats.

Figures 4.5 and 4.6 illustrate the PSD of the acceleration excitation at the seat base and the acceleration response of the mass on seat "A" under synthesized and white noise excitations. The corresponding results for seats "B" and "C" are presented in Figures 4.7 to 4.10. Each figure presents a comparison of the excitation and response acceleration spectra to identify the vibration attenuation or amplification properties of the seats.

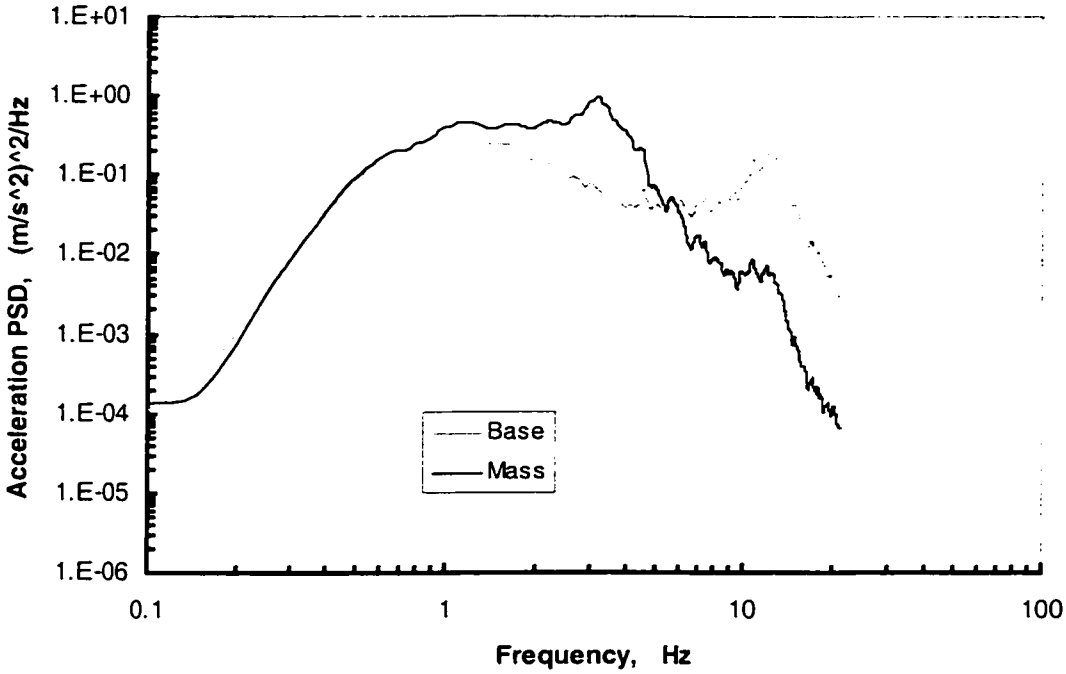

Figure 4.5: *PSD* of acceleration of mass and pan of seat "A" under road-measured random excitation.

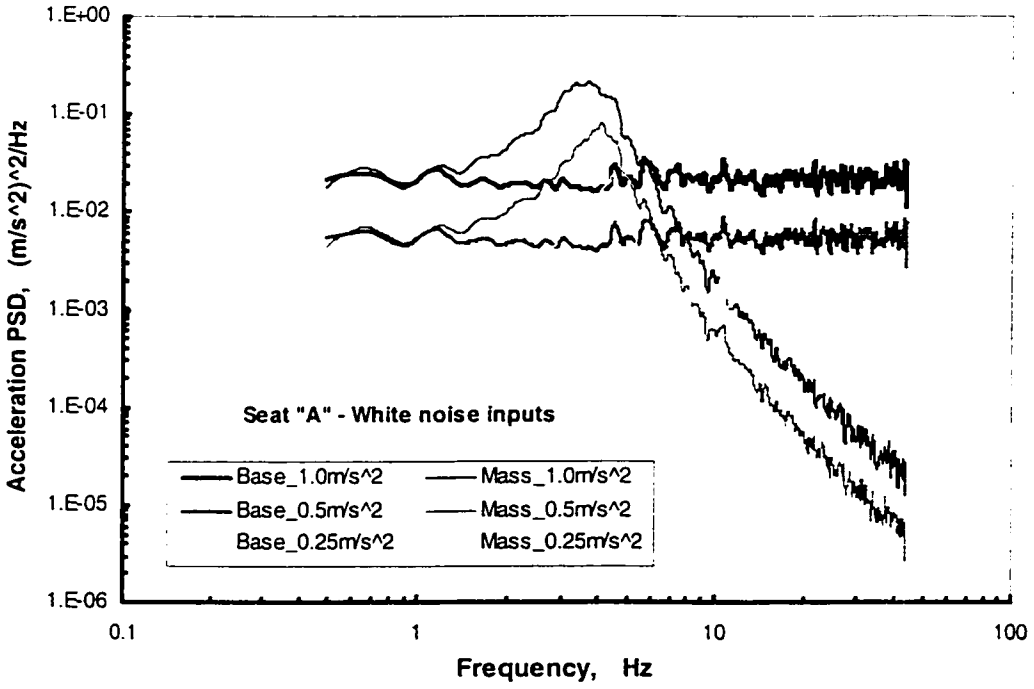

Figure 4.6: *PSD* of acceleration of mass and pan of seat "A" under white noise input.

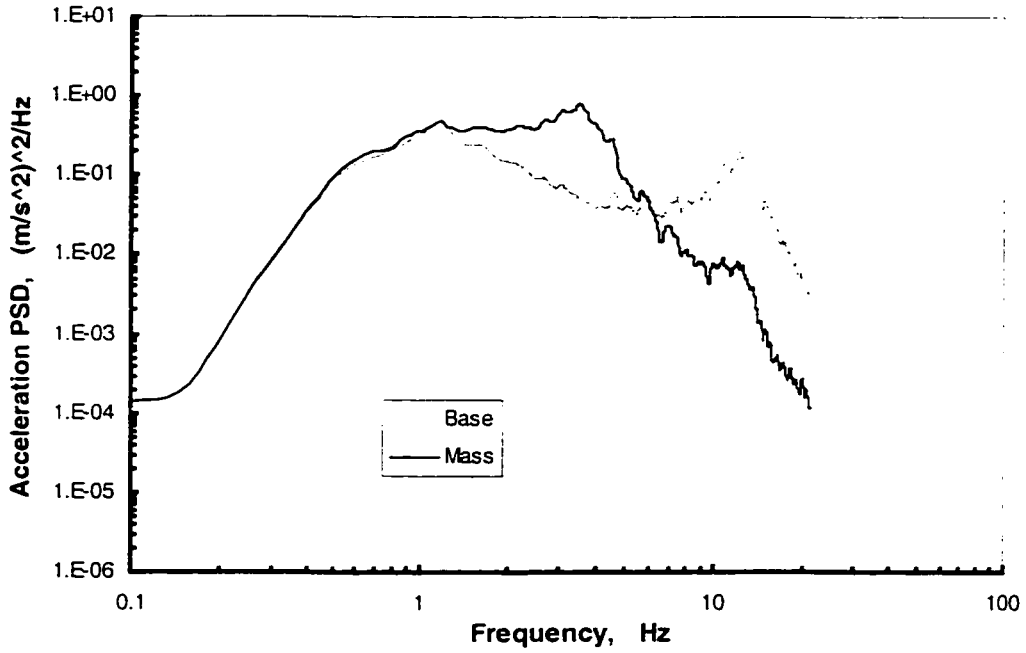

Figure 4.7: *PSD* of acceleration of mass and pan of seat "B" under road-measured random excitation.

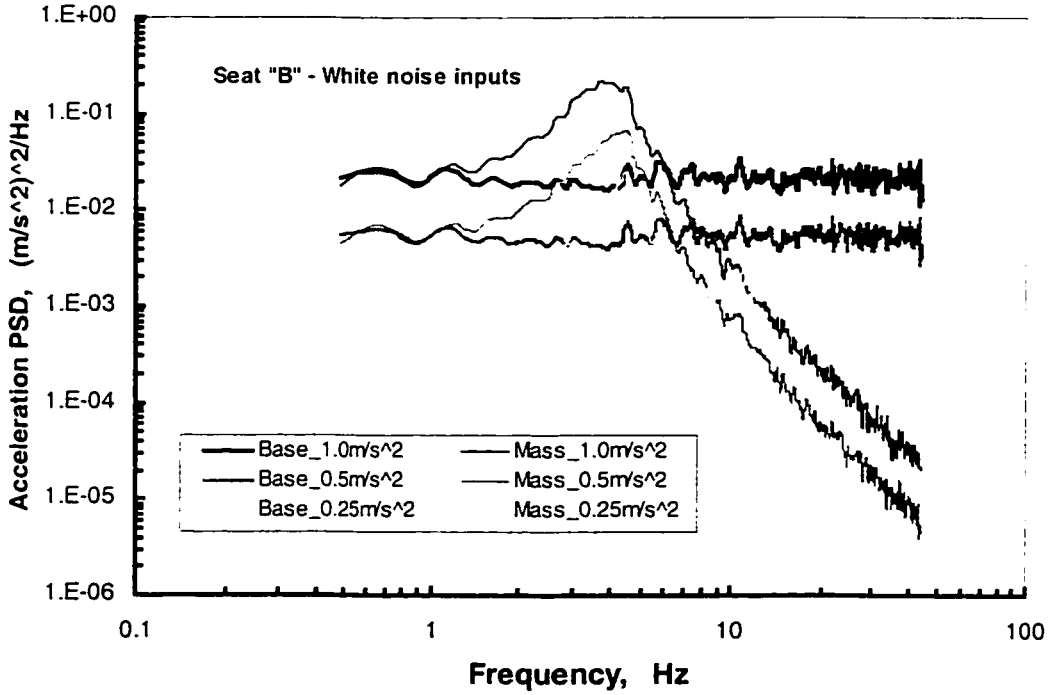

Figure 4.8: *PSD* of acceleration of mass and pan of seat "B" under white noise input.

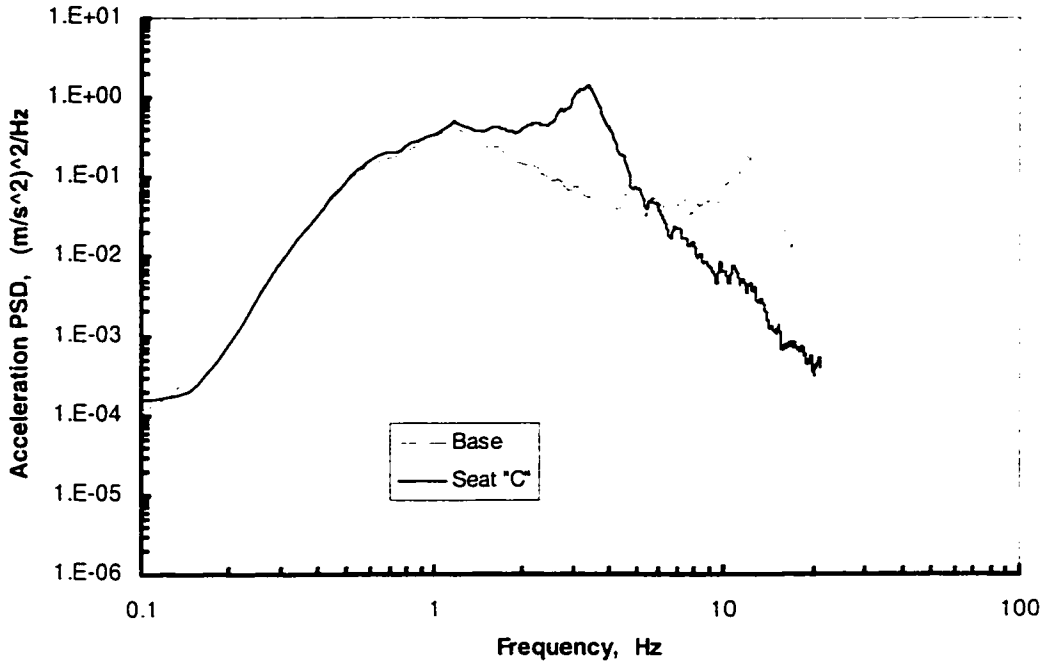

Figure 4.9: *PSD* of acceleration of mass and pan of seat "C" under road-measured random excitation.

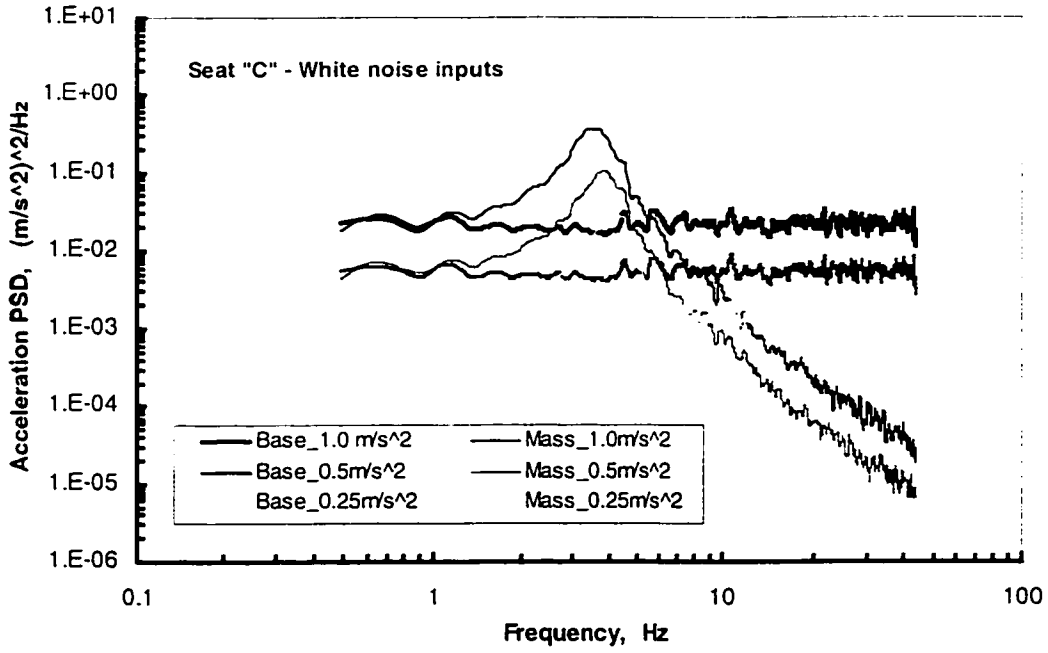

Figure 4.10: *PSD* of acceleration of mass and pan of seat "C" under three different white noise input.

The results under road-measured excitations show that all the seats tend to transmit pan vibration directly to the mass at frequencies below 1.0 Hz. The base-to-seat vibration transmission in the 1.0 Hz to 5 Hz range reveals amplification, while the vibration above 5 Hz is attenuated at the cushion-mass interface. The mass acceleration responses of all three seats exhibit two peaks in the vicinity of 3.0-3.5 Hz and 12 Hz, which are attributed to the resonant frequencies of the seat-mass system and excitation in the vicinity of the wheel-hop frequency. The seat "C", however, tends to suppress the peak response corresponding to wheel-hop frequency. A comparison of mass acceleration PSD responses of all three seats, illustrated in Figure 4.11, reveals their generally similar performance. The seat "C", however, yields highest amplification of vibration near 3.2 Hz and least attenuation at frequencies above 15 Hz. The results shown in Figures 4.6, 4.8 and 4.10 illustrate the influence of magnitude of white-noise excitation on the vibration isolation responses of the three seat-mass models. It can be seen that the acceleration response of the mass increases in the entire frequency range, with increasing input acceleration level. This trend is evident for all three seats. The frequency of peak acceleration response of the mass, however, decreases with increasing input acceleration. The resonance of the seat-mass system for seat "A" occurs near 3.7 Hz under 1.0 m/s^2 rms acceleration, 4.0 Hz under 0.5 m/s^2 and 4.5 Hz under 0.25 m/s^2. The frequency range in which vibration is attenuated through the seat "A" varies depending on the excitation level. The attenuation of vibration is attained above 5.5 Hz under 1.0 m/s^2 rms input, 6 Hz under 0.5 m/s^2 rms input, and 6.5 Hz under 0.25 m/s^2 rms input. Based on the results presented above, it can be seen that the frequency range of vibration isolation increases

under a higher input level. The seats "B" and "C" also reveal similar trends in mass acceleration response under white noise excitation.

Figure 4.12 depicts the mass acceleration PSD responses of three seat models under vertical white noise excitations of magnitude of 0.5 m/s^2 rms acceleration. It can be seen that the three seats yield almost identical response. The mass acceleration response exhibits insignificant changes in the frequency range below 1.5 Hz, amplification of vibration in frequency range between 1.5 and around 6 Hz, and attenuation in the frequency range above 6 Hz. Some differences in the responses of the seat-mass models are also evident although small. The magnitude of acceleration of the mass of seat "C" is slightly larger than those of the other two seats in the vicinity of 4 Hz. The peak acceleration response of seat "B" is slightly smaller than that of seat "C" but slightly larger than that of seat "A".

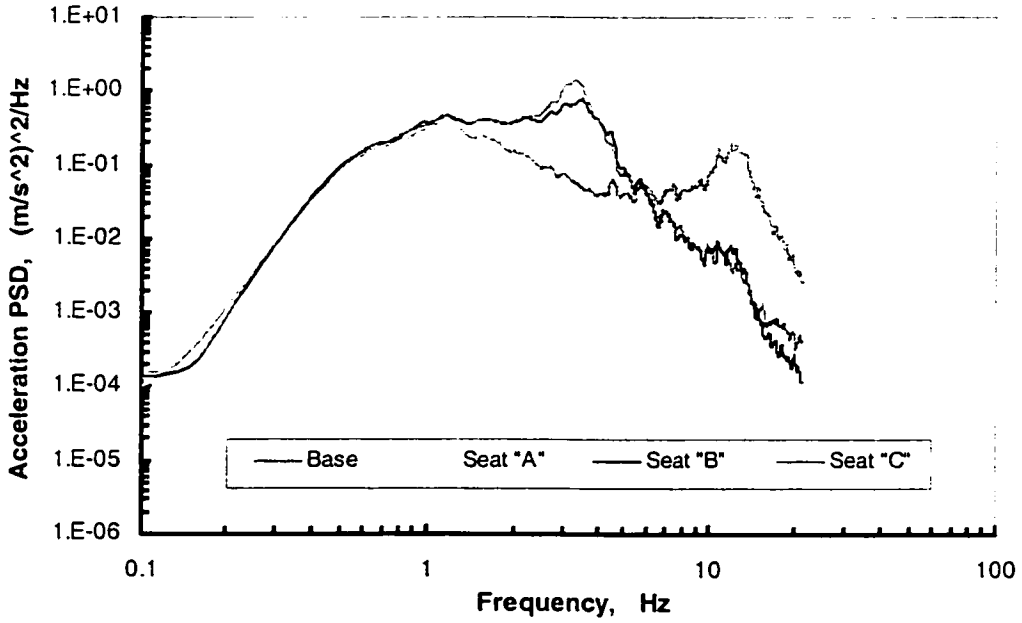

Figure 4.11: Comparison of acceleration PSD of three seats under road-measured random excitation.

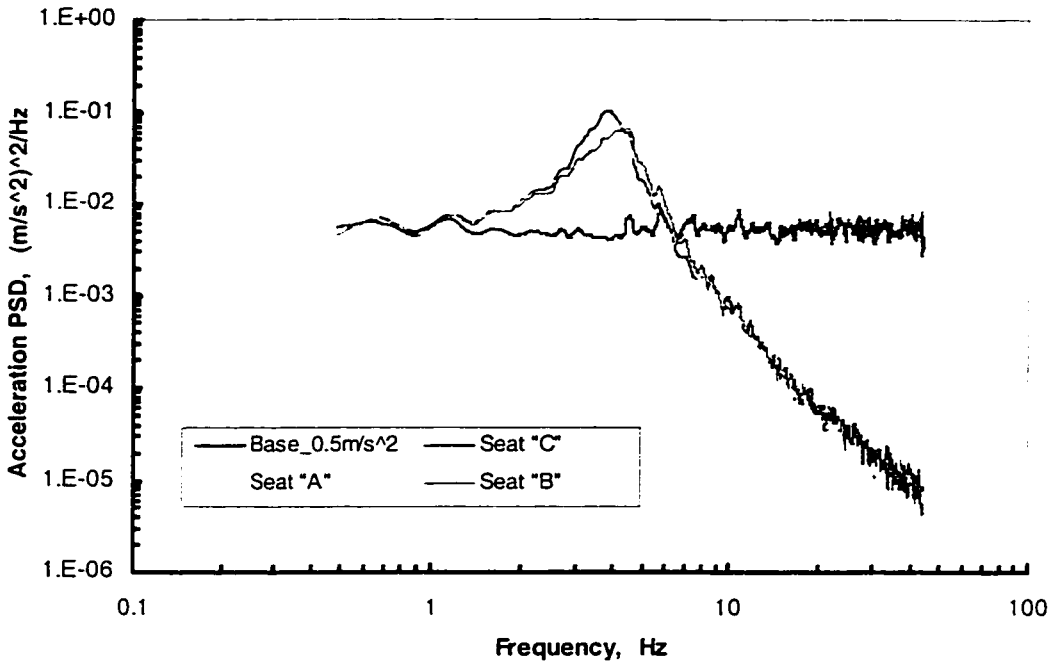

Figure 4.12: Comparison of acceleration PSD of three seats under three different white noise input.

The simulation results attained for the three seat-mass models are analyzed to derive a_{rms_freq}, a_{rms_time}, a_{w,rms_freq}, a_{w,rms_tim}, S.E.A.T.$_{freq}$, S.E.A.T.$_{time}$, S.E.A.T.$_{w,freq}$, S.E.A.T.$_{w,time}$, $a_{w,peak}$, and crest factors corresponding to road-measured random input and the white noise acceleration inputs of three different magnitudes. The results attained in the time domain and in the frequency domain revealed very small difference. The peak relative error between a_{rms_freq} and a_{rms_time}, and S.E.A.T.$_{freq}$ and S.E.A.T.$_{time}$ were observed to be well below 5%. These results suggested that the ride quality assessment of an automobile seat under road-measured and broad-band excitations could be conveniently accomplished in the frequency domain. The results are summarized in Tables 4.1 and 4.2 corresponding to road-measured and white-noise random excitations.

respectively. Owing to small difference in the measures computed in time- and frequency-domain, the values derived from the frequency-domain alone are presented. It has been suggested that the rms acceleration levels between 0 to 0.04g, 0.04 to 0.06g, and above 0.06g of automobiles correspond to smooth, medium and rough ride [56,70] for seat base.

The results attained under road-measured acceleration excitation suggest that all the three seats amplify the acceleration, as evident from the unweighted and weighted S.E.A.T. values (0.5 – 10 Hz) (Table 4.1). The application of frequency-weighting tends to lower the S.E.A.T. and a_{rms} values, which is attributed to the attenuation characteristics of the weighting function. The seat "C" yields highest values of a_{rms} (1.55 m/s^2) and $a_{w,rms}$ (1.19m/s^2), while the seat "A" (a_{rms} = 1.36 m/s^2; $a_{w,rms}$ =1.01m/s^2) yields slightly lower values than seat "B" (a_{rms} = 1.37 m/s^2; $a_{w,rms}$ =1.05m/s^2). The seat "C" also yields highest values of S.E.A.T. and S.E.A.T.$_w$, while the seat "A" yields lowest values. The results summarized in Table 4.1 support the trends observed in Figures 4.5 to 4.12.

Table 4.1: Vibration Isolation Performance of Three Seat-Mass Models under Road-Measured Acceleration Excitation (1.2 m/s^2 rms).

Seat	Performance Measure					
	a_{rms}	$a_{w,rms}$	S.E.A.T.	S.E.A.T.$_w$	$a_{w,peak}$	Crest Factors
"A"	1.36	1.01	1.13	1.02	3.65	3.6
"B"	1.37	1.05	1.14	1.07	3.90	3.7
"C"	1.55	1.19	1.29	1.20	5.60	4.7

The results attained under broad-band excitation are shown in Table 4.2. The S.E.A.T.$_w$ measures further confirm that all the three seats tend to amplify the vibration when loaded with a rigid mass. The seat "A" continues to yield lowest values of a_{rms}, a_{rms_w}, S.E.A.T. and S.E.A.T.$_w$, irrespective of the magnitude of broad band excitation. It is interesting to note that the S.E.A.T. values obtained on the basis of unweighted rms accelerations are lower than the unity values for all three seats, irrespective of the excitation magnitude. The S.E.A.T.$_w$ values, however, exceed the unity value in most cases. This is attributed to the frequency-weighting. The application of frequency weighting yields only slightly smaller value of the a_{rms_w} than the a_{rms} under 0.25 m/s^2 excitation. The difference between the a_{rms} and a_{rms_w}, however, tend to grow under higher magnitude excitations. This is attributed to reduce resonant frequency and increased frequency range of attenuation under high magnitude excitation. It also needs to be emphasized that the values 0.25, 0.5 and 1.0 m/s^2 represent the nominal values of rms accelerations due to three excitations employed in the study. The exact values of overall rms accelerations due to white-noise excitation varied slightly.

An examination of values of mass acceleration responses of the three models suggests that seats "A", "B", and "C" could yield peak acceleration of magnitudes of 3.65 m/s^2, 3.90 m/s^2 and 5.60 m/s^2, respectively under the road-measured excitation. The corresponding crest factor being 3.6, 3.7 and 4.7, respectively. The results suggest that seats "A" and "B" yield more comparable vibration isolation performance, while seat "C" yields the worse performance.

Table 4.2: Vibration Isolation Performance of Three Seat-Mass Models under Broad-Band Random Excitation.

Seat	White-noise excitations (m/s^2)	Performance Measure					
		a_{rms}	$a_{w,rms}$	S.E.A.T.	S.E.A.T.$_w$	$a_{w,peak}$	Crest Factors
"A"	0.25	0.20	0.19	0.82	1.17	0.60	3.2
	0.5	0.38	0.34	0.77	1.06	1.10	3.2
	1.0	0.72	0.63	0.73	0.97	1.88	3.0
"B"	0.25	0.21	0.19	0.84	1.20	0.66	3.4
	0.5	0.39	0.36	0.79	1.10	1.21	3.4
	1.0	0.74	0.66	0.75	1.02	2.10	3.2
"C"	0.25	0.22	0.21	0.91	1.29	0.73	3.5
	0.5	0.42	0.38	0.86	1.18	1.25	3.3
	1.0	0.80	0.70	0.81	1.08	2.23	3.2

4.5 Parameter sensitivity analysis

A parametric study is performed by using the combined seat-rigid mass model system to study the influence of variations in the seat model parameters on the vibration isolation performance. Although the stiffness and damping parameters of the PUF cushions are characterized using curve-fitting techniques, the identified coefficients could be related to the physical behavior to an extent, as discussed earlier in section 3.3.1. The

coefficients a_1, a_2, a_3 and a_4 employed in the stiffness model relate to stiffness gain, weight-dependence of stiffness, relative velocity and deflection dependence, and relative deflection dependence of the stiffness values, respectively. The coefficients b_1, b_2, b_3 and b_4 employed in the damping model relate to the damping coefficient gain, weight dependence of the damping coefficient, relative velocity and deflection dependence of the damping coefficient, and relative deflection dependence of the damping coefficient, respectively. A study of influence of variations in these coefficients may yield some insight into the role of physical properties of the PUF cushions, such as the preload, velocity and deflection dependence of the force-deflection and force-velocity characteristics. The parametric sensitivity analysis is performed by varying the coefficients between 0.75 to 1.25 times the identified values presented in Tables 2.5 and 2.6.

The steady-state vibration transmission characteristics of a seat-rigid mass system can be conveniently evaluated in terms of acceleration transmissibility, which is defined as the ratio of acceleration magnitude transmitted to the seat-rigid mass interface to the magnitude of excitation acceleration at the seat base, in the frequency range of interest. The vertical vibration transmissibility can provide significant information related to vibration attenuation characteristics and probable frequency range of vibration isolation. A study of the influence of variations in such parameters on the vibration transmissibility and the S.E.A.T. value can provide significant insight and provide a guideline in view of the most desirable design parameters of the seat. Owing to the considerable similarity of all the three seats, the analysis is performed for seat "C" alone loaded with a rigid mass.

4.5.1 Influence of excitation

The vertical vibration transmission performance of the seat-rigid mass system is strongly affected by the excitation magnitude due to the nonlinear properties arising from the seat model. Figure 4.13 illustrates the acceleration transmissibility of the seat computed under different excitations, including the road-measured acceleration (1.2 m/s^2 rms) and white noise acceleration (0.25 m/s^2, 0.5 m/s^2 and 1.0 m/s^2 rms) excitations. It can be seen that the magnitude of excitation has very little effect on the seat transmission performance in the frequency range below 2 Hz and above 7 Hz. Under low excitation magnitude (0.25m/s^2), the peak acceleration transmissibility of 4.75 occurs near 4 Hz, while the attenuation appears at frequencies above 6.5 Hz. An increase in excitation

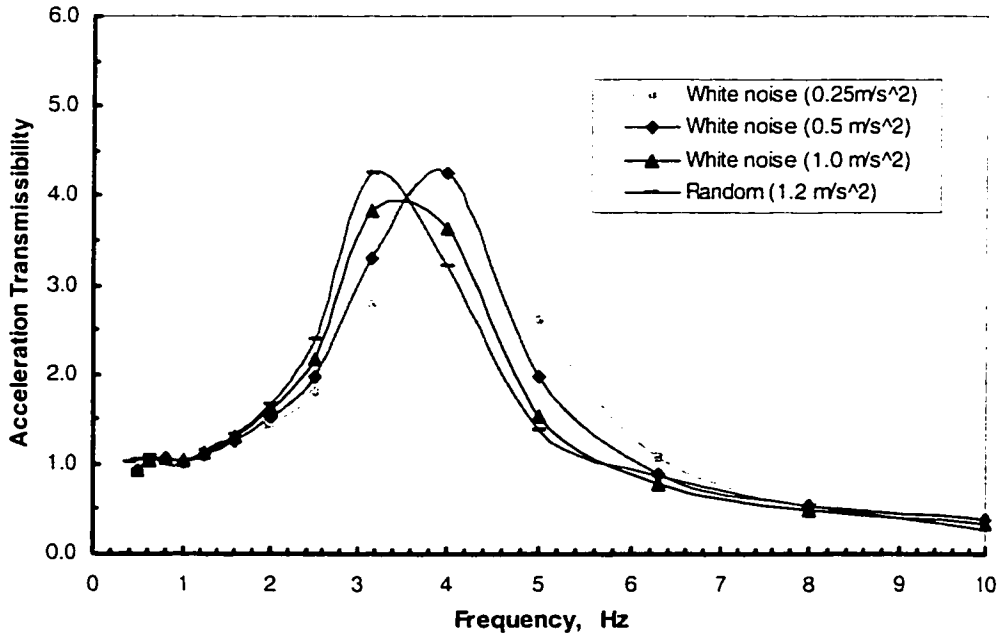

Figure 4.13: Influence of excitation on the seat acceleration transmissibility.

magnitude to 0.5m/s^2 yields a lower value of peak acceleration transmissibility of 4.25 occurring at a lower frequency of 3.75 Hz. Moreover, the seat tends to attenuate vibration at frequencies above 6.1 Hz. A further increase in the excitation magnitude to 1.0m/s^2 reveals similar tendency. The peak acceleration transmissibility reduces to 4, which occurs at a further lower frequency of 3.5 Hz, while the vibration attenuation appears at lower frequencies above 5.8 Hz. Under the road-measured acceleration excitation (1.2m/s^2 rms), the resonant frequency further decreases to 3.25 Hz, while the peak acceleration transmissibility increases to 4.25.

The results suggest that the vibration excitation level directly affects the acceleration transmission performance of the seat-rigid mass system. The influence of excitation magnitude on the vibration isolation performance is further evaluated in terms of S.E.A.T. and S.E.A.T.$_w$ values, as shown in Figure 4.14. It can be seen that the S.E.A.T.$_w$ value is smaller than the S.E.A.T. value under road-measured random input and the S.E.A.T.$_w$ values are larger than the S.E.A.T. values under broad-band random excitations. Under low excitation magnitude (0.25m/s^2), the S.E.A.T. and S.E.A.T.$_w$ values are 0.91 and 1.29, respectively. An increase in excitation magnitude (0.5m/s^2) yields relatively smaller values, of 0.86 and 1.17, respectively. A further increase in excitation magnitude (1.0m/s^2) reveals the same tendency, the S.E.A.T. and S.E.A.T.$_w$ values being 0.81 and 1.08, respectively. The response under road-measured random acceleration (1.2m/s^2) yields higher values of S.E.A.T. 1.28 and S.E.A.T.$_w$ 1.2, respectively.

Based on the results described above, it can be seen that the seat isolation efficiency increases (S.E.A.T. values decrease) with an increase in excitation magnitude

of a broad band excitation. In views of the strong dependence of the system performance on excitation level, the parametric analysis presented in the following section are restricted to excitation, magnitude of 0.5 m/s^2.

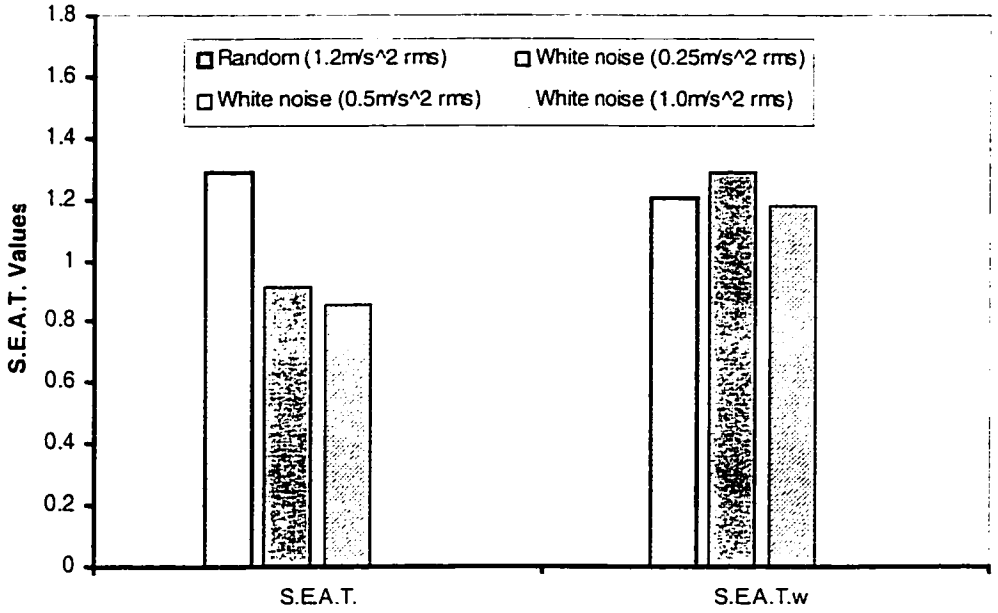

Figure 4.14: Influence of excitation on the S.E.A.T. values.

4.5.2 Influence of stiffness parameters

The influence of stiffness model parameters (a_1, a_2, a_3 and a_4) on the vibration isolation properties of seat "C" are evaluated in terms of acceleration transmissibility and S.E.A.T. responses. The analyses are performed under 0.5 m/s^2 rms broad-band excitation, while the seat mass is considered as 56 kg. Figure 4.15 to 4.18 illustrate the influence of variations in the model parameters a_1, a_2, a_3 and a_4, respectively on the acceleration transmissibility response. It should be noted that a higher value of a_1 would

yield higher stiffness of the PUF cushion. An increase in parameter a_1 yields higher peak transmissibility magnitude and a higher resonant frequency, which causes lower acceleration transmissibility in frequency range of 1.2 to 3.7 Hz and a higher acceleration transmissibility in the frequency range above 3.7 Hz (Figure 4.15). However, a decrease in parameter a_1 yields lower peak transmissibility magnitude and a lower resonant frequency, which causes higher acceleration transmissibility in the frequency range of 1.2 to 3.5 Hz and a lower acceleration transmissibility in frequency range above 3.5 Hz.

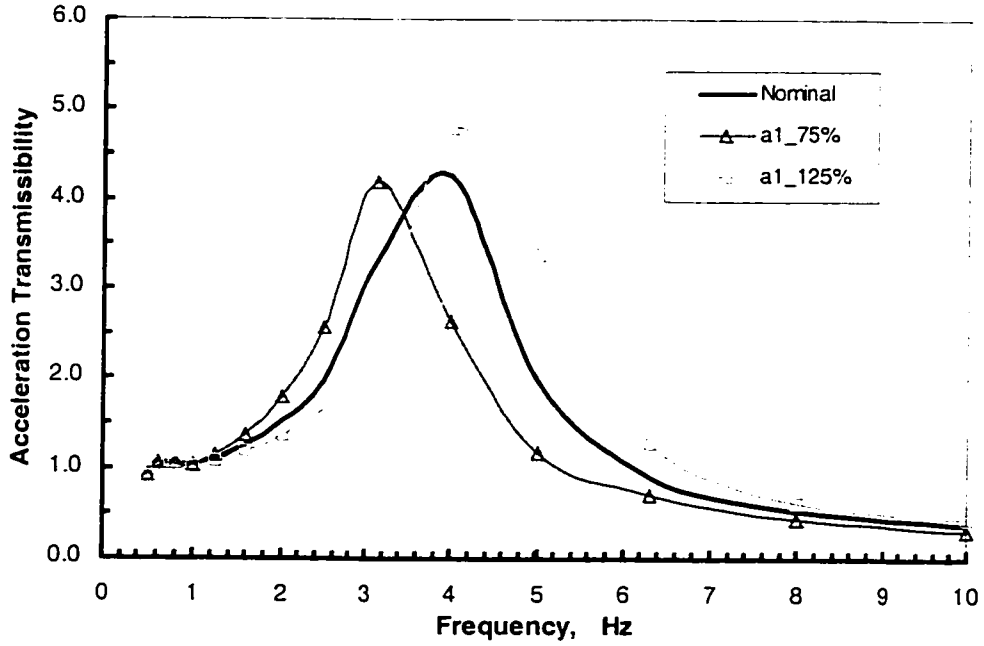

Figure 4.15: Influence of the stiffness gain (a_1) on the seat acceleration transmissibility.

Figure 4.16 indicates the influence of weight-dependent stiffness constant a_2 on the seat acceleration transmissibility under 0.5 m/s^2 rms acceleration excitation. The results show that a decrease in parameter a_2 yields lower peak transmissibility magnitude

and resonant frequency, which causes higher acceleration transmissibility in the frequency range of 1.2 to 3.4 Hz and a lower acceleration transmissibility in frequency range above 3.4 Hz. An increase in the parameter a_2 yields much higher peak transmissibility magnitude and resonant frequency. Based on the results described above, it can be seen that the resonant frequency and resonant peak value of the seat acceleration transmissibility increases as the seat stiffness dependence on the preload increases.

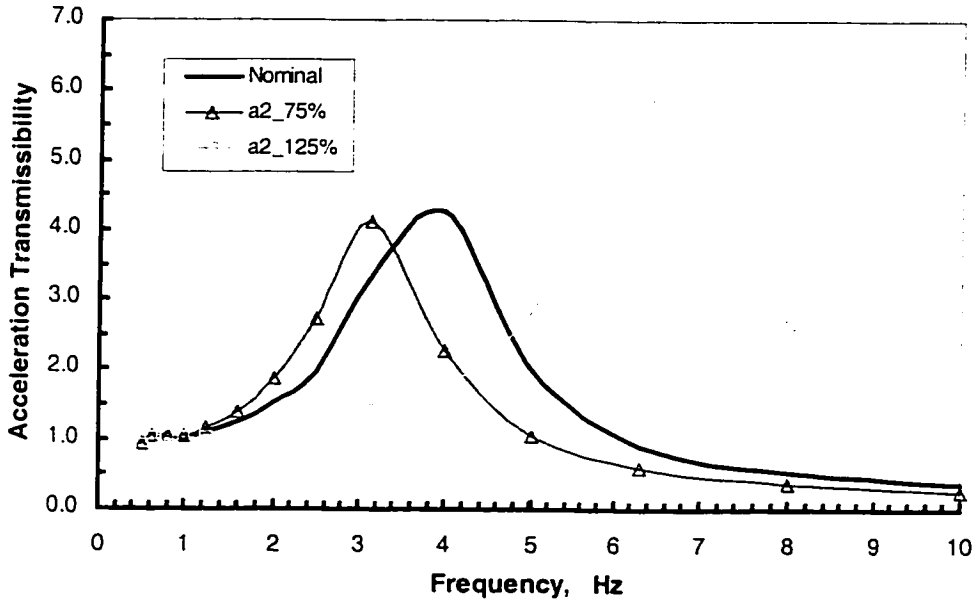

Figure 4.16: Influence of weight dependence of the stiffness (a_2) on the seat acceleration transmissibility.

Figure 4.17 depicts the influence of variation in parameter a_3 on the seat acceleration transmissibility under the 0.5 m/s^2 rms acceleration excitation. The parameter a_3 not only relates to the relative velocity dependence of the stiffness, but also

the relative deflection dependence of the stiffness. It may also be interpreted as the excitation frequency dependent stiffness constant, as described in Equation (3.2). The results show negligible effect of variation in parameter a_3 on the acceleration transmission properties. The dependence on the relative deflection alone is evident from the results attained under variation in parameter a_4 (Figure 4.18). An increase in parameter a_4 yields higher peak transmissibility magnitude and a slight higher resonant frequency. Conversely, a decrease in parameter a_4 yields lower peak transmissibility magnitude and a lower resonant frequency. The results suggest that the peak resonant response could be lowered by lowering the frequency dependence of the PUF material properties.

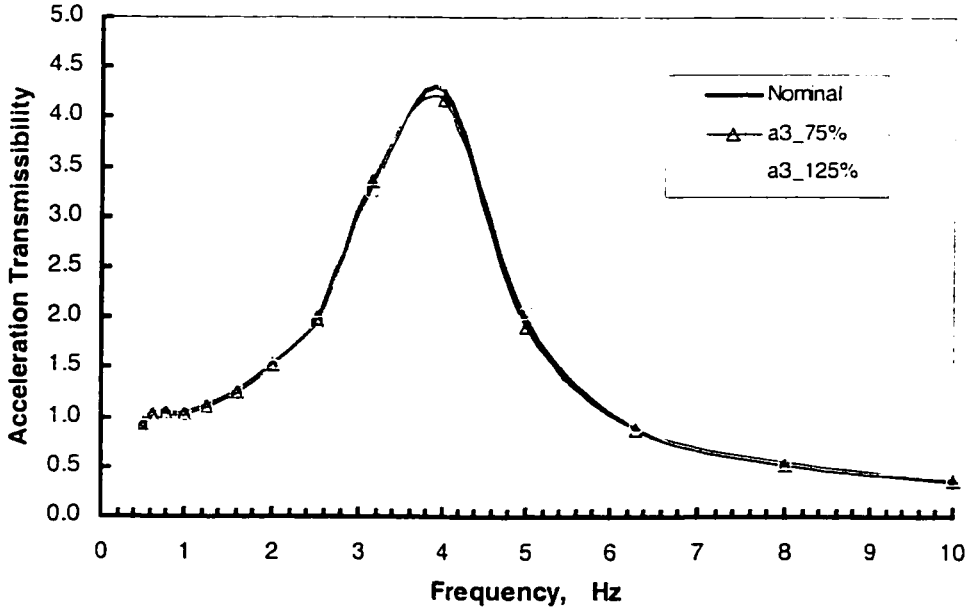

Figure 4.17: Influence of relative velocity and deflection dependence of the stiffness (a_3) on the seat acceleration transmissibility.

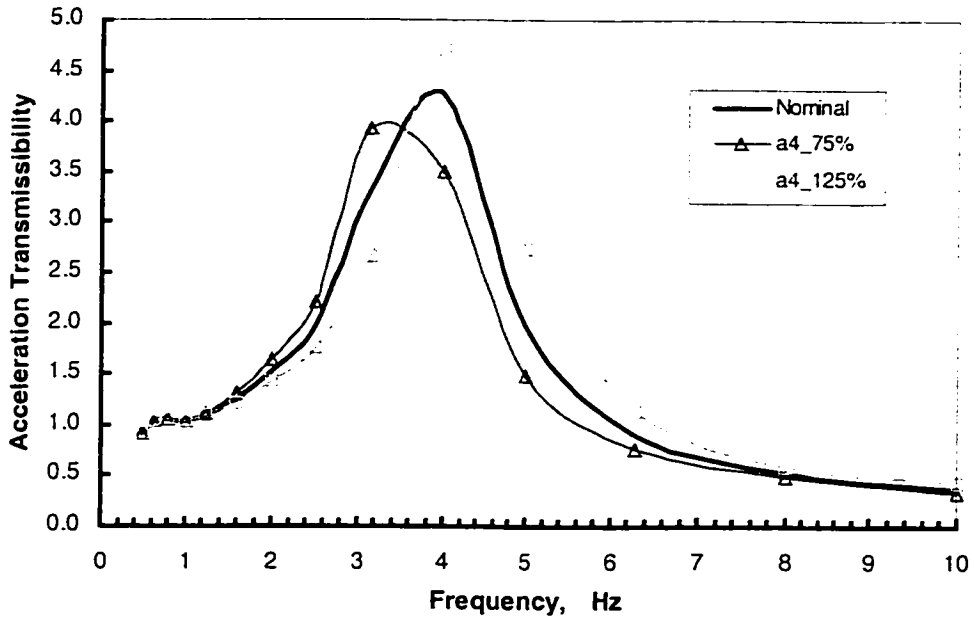

Figure 4.18: Influence of relative deflection dependence of the stiffness (a_4) on the seat acceleration transmissibility.

The influence of variation in stiffness model coefficients on the vibration isolation performance of the seat-mass system is further analyzed in terms of S.E.A.T. and S.E.A.T.$_w$ values, as shown in Figures 4.19 and 4.20. Both the unweighted and weighted values of S.E.A.T. exhibit identical trends with respect to variations in the model parameters. The frequency-weighted value of the S.E.A.T., however, is considerably larger than the unweighted values, as observed earlier from the results presented in Table 4.2.

An increase in the stiffness gain parameter a_1 causes an increase in the S.E.A.T. values. A lower value of a_1 provides better seat isolation efficiency. A lower value of a_2 related to preload dependency of the stiffness also yields considerably lower S.E.A.T. values. The parameter a_3 describing the dependence on the relative deflection and

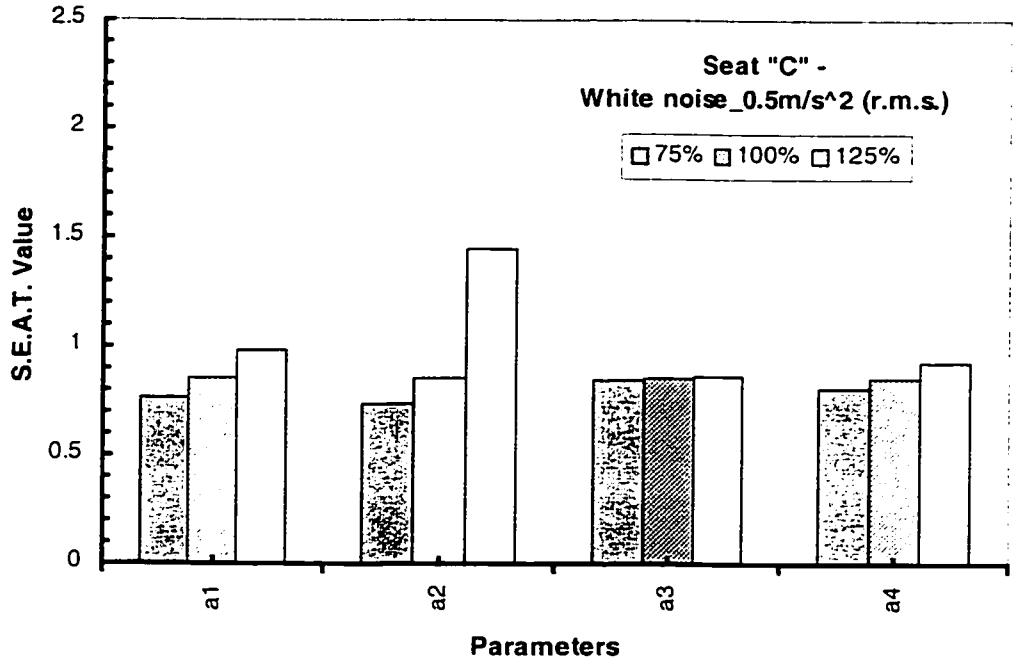

Figure 4.19: Influence of the stiffness parameters on the S.E.A.T. values.

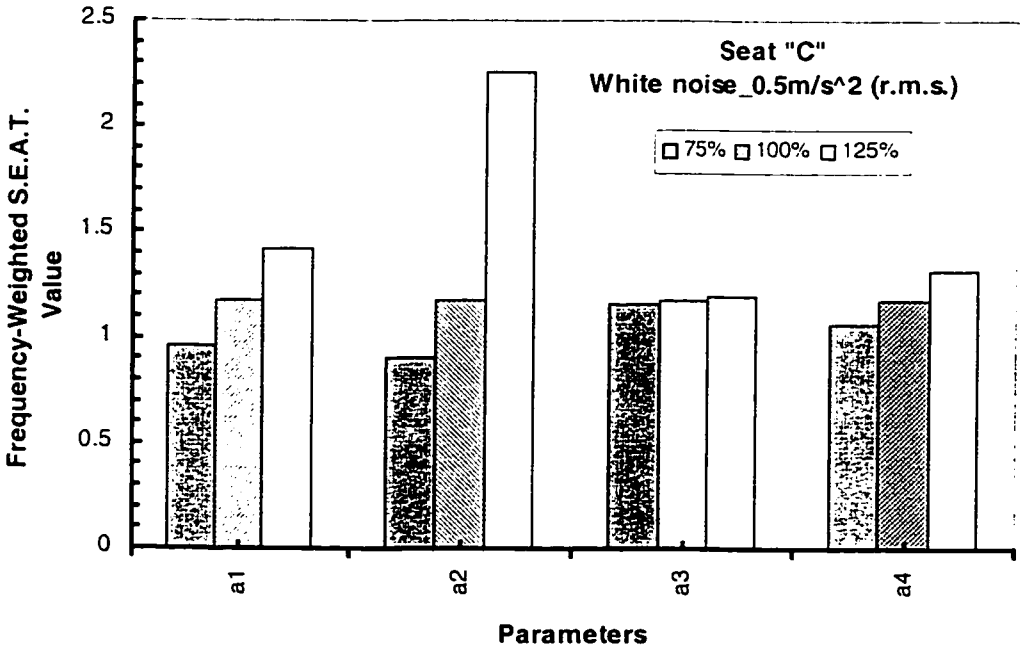

Figure 4.20: Influence of the stiffness parameters on the frequency-weighted S.E.A.T. values.

relative velocity response or the frequency does not influence the S.E.A.T. values. The influence of the relative deflection dependence parameter a_4 yields relatively small effect on the S.E.A.T. values; S.E.A.T. values being higher for higher values of a_4. These trends are quite similar to those observed from Figure 4.15 to 4.18.

The influence of variations in the stiffness model parameters are also quantified in terms of percent change normalized with the response corresponding to the nominal parameter value. The percentage variations in S.E.A.T. values attained for ± 25 % variations in the stiffness parameters are summarized in Table 4.3. The variation in

Table 4.3: Variation in S.E.A.T. value caused by the stiffness parameters.

Variation in Parameters	**Percentage change in S.E.A.T.$_W$ value (%)**			
	a_1	a_2	a_3	a_4
100% to 75%	-18.6	-23.6	-1.6	-9.9
100% to 125%	20.9	91.6	1.7	12.1

S.E.A.T. value caused by –25 % change in parameters is expressed as 100 % to 75 %, and that caused by +25 % change in parameters is defined as 100 % to 125 % variation. The percent change in the S.E.A.T. response is defined as:

$$100\% \text{ to } 75\ \% \text{ S.E.A.T. value variation } (\%) = \frac{SEAT_{75\%} - SEAT_{100\%}}{SEAT_{100\%}} \times 100\% \qquad (4.15)$$

$$100\% \text{ to } 125\ \% \text{ S.E.A.T. value variation } (\%) = \frac{SEAT_{125\%} - SEAT_{100\%}}{SEAT_{100\%}} \times 100\% \qquad (4.16)$$

where S.E.A.T.$_{75\%}$, S.E.A.T.$_{100\%}$ and S.E.A.T.$_{125\%}$ refer to the S.E.A.T. values corresponding to a parameters assuming 75 %, 100 % and 125 % of its nominal value,

respectively, while all other parameters assume their nominal values. The results show that reducing the weight dependence of the PUF could enhance the isolation efficiency of the seat.

4.5.3 Influence of damping parameters

The influence of damping model parameters (b_1, b_2, b_3 and b_4) on the vibration isolation properties of seat "C" is evaluated in terms of acceleration transmissibility and the S.E.A.T. responses. The analyses are performed under 0.5 m/s^2 rms broad-band excitation, while the seat mass is considered as 56 kg. Figures 4.21 to 4.24 illustrate the influence of variations in the model parameters b_1, b_2, b_3 *and* b_4, respectively on the acceleration transmissibility response. It should be noted that a higher value of b_1 would

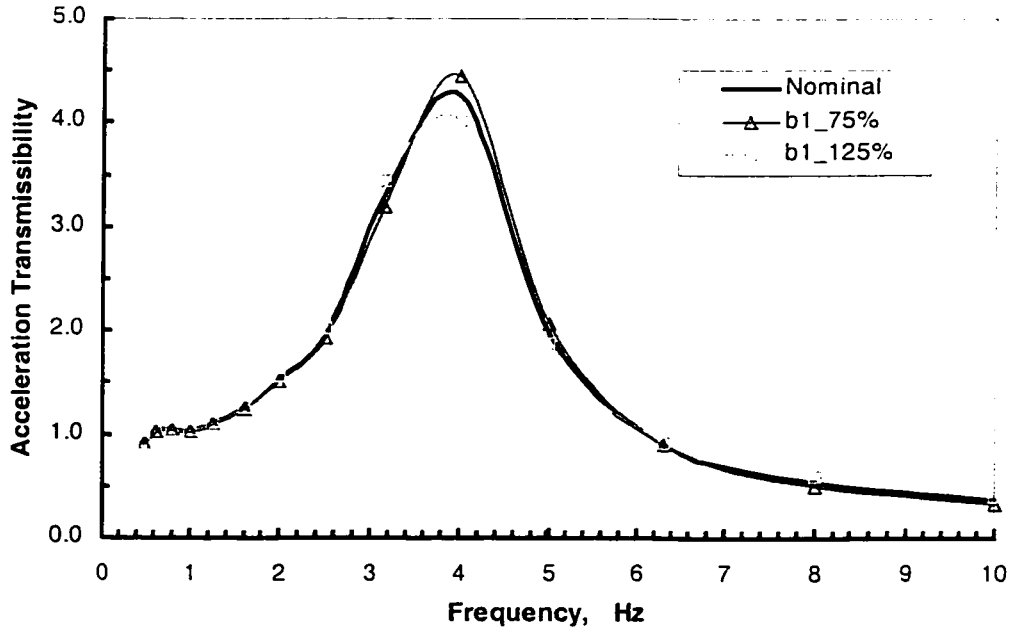

Figure 4.21: Influence of the damping coefficient gain (b_1)on the seat acceleration transmissibility.

yield higher damping coefficient of the PUF cushion. A 25% increase in parameter b_1 yields lower peak transmissibility magnitude and a slightly lower resonant frequency, while a 25% lower value of b_1 causes higher transmissibility magnitude and frequency (Figure 4.21). The variation in the damping coefficient gain influence the transmissibility response only in the vicinity of the resonant frequency. This is attributed to extremely light damping due to PUF cushions.

Figure 4.22 indicates the influence of weight-dependent damping constant b_2 on the seat acceleration transmissibility under 0.5 m/s^2 rms acceleration excitation. The results show that a decrease in parameter b_2 yields higher peak transmissibility magnitude and a slightly higher resonant frequency due to relatively lower effective damping. An

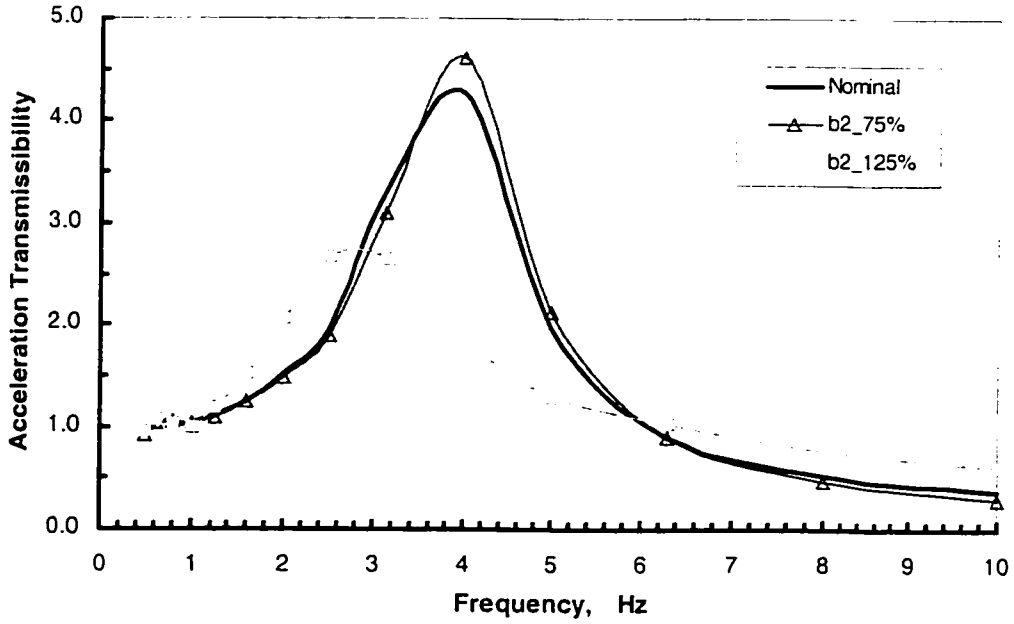

Figure 4.22: Influence of weight dependence of the damping coefficient (b_2) on the seat acceleration transmissibility.

increase in the parameter b_2 yields considerably lower peak transmissibility magnitude and resonant frequency. This is attributed to rather large increase in effective damping due to higher value of b_2.

Figure 4.23 depicts the influence of variation in parameter b_3 on the seat acceleration transmissibility under 0.5 m/s^2 rms acceleration excitation. The parameter b_3 not only relates to the relative velocity dependence of the damping coefficient, but also the relative deflection dependence of the damping coefficient. It may also be interpreted as the excitation frequency dependent damping constant, as described in Equation (3.3). It can be seen that increasing the parameter b_3 has only little effect on the seat

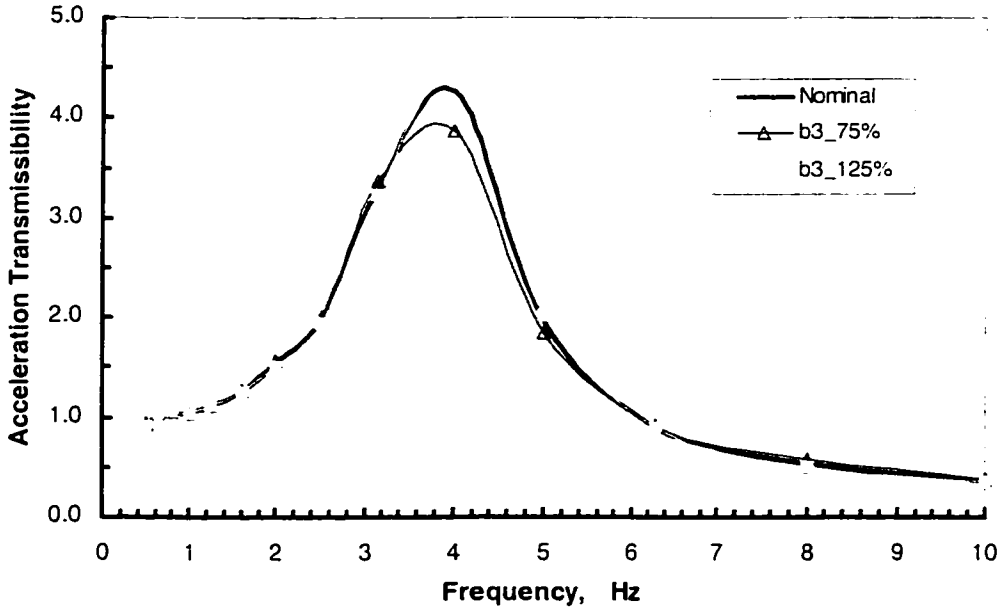

Figure 4.23: Influence of relative velocity and deflection dependence of the damping coefficient (b_3) on the seat acceleration transmissibility.

parameter b_3 yields lower peak transmissibility magnitude and a slightly lower resonant frequency. The results suggest that the peak resonant response could be lowered by lowering the frequency dependence of the PUF material properties. Figure 4.24 depicts the influence of variation in parameter b_4 on the seat acceleration transmissibility. The results show negligible effect of variation in parameter b_4 on the acceleration transmissibility over the entire frequency range., which is attributed to relative small dependence of the damping coefficient on the relative deflection response of the seat-mass model.

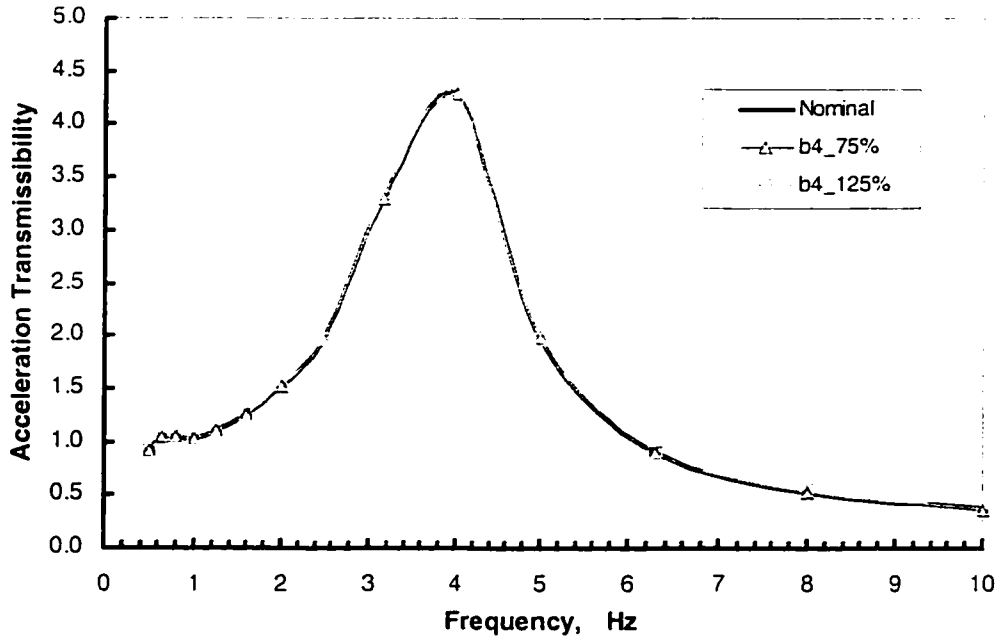

Figure 4.24: Influence of relative deflection dependence of the damping coefficient (b_4) on the seat acceleration transmissibility.

The influence of variation in damping model coefficients on the vibration isolation performance of the seat-mass system is further analyzed in terms of S.E.A.T. and S.E.A.T.$_w$ values, as shown in Figures 4.25 and 4.26. Both the unweighted and weighted values of S.E.A.T. exhibit identical trends with respect to variations in the model parameters. The frequency-weighted value of the S.E.A.T., however, is considerably larger than the unweighted values, as observed earlier from the results presented in Table 4.2. An increase in the damping gain parameter b_1 causes a slight decrease in the S.E.A.T. values. A higher value of parameter b_1 provides slightly better seat isolation efficiency. A lower value of parameter b_2 related to preload dependency of

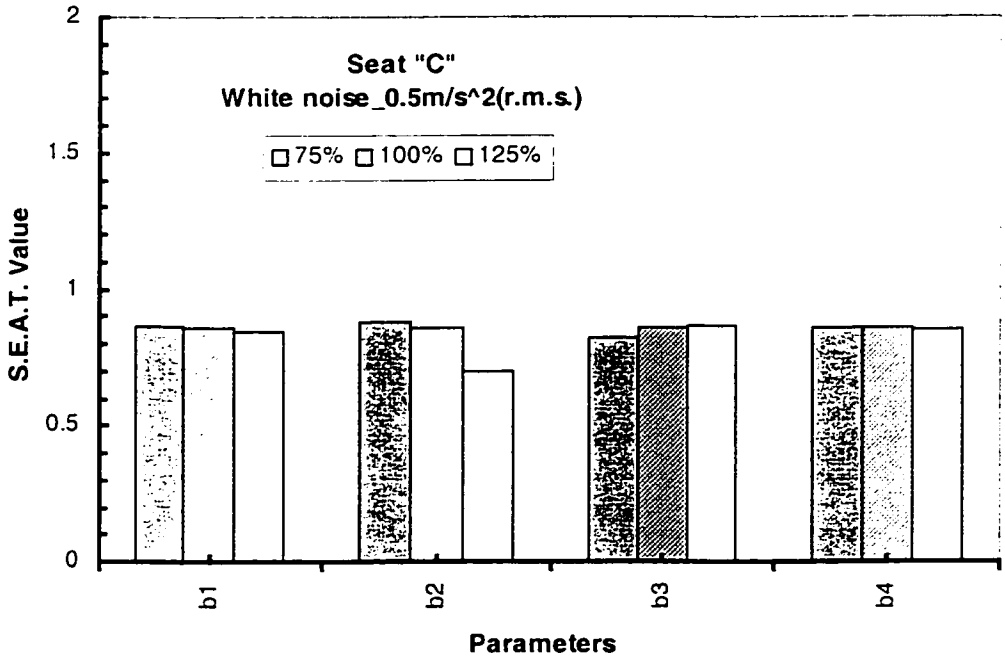

Figure 4.25: Influence of the damping parameters on the S.E.A.T. values.

the damping also yields slightly higher S.E.A.T. value. The influence of the frequency dependence parameter b_3 yields relatively small effect on the S.E.A.T. values; S.E.A.T. values being higher for higher values of b_3. The parameter b_4 describing the dependence on the relative deflection response does not influence the S.E.A.T. response. These trends are quite similar to those observed from Figure 4.21 to 4.24.

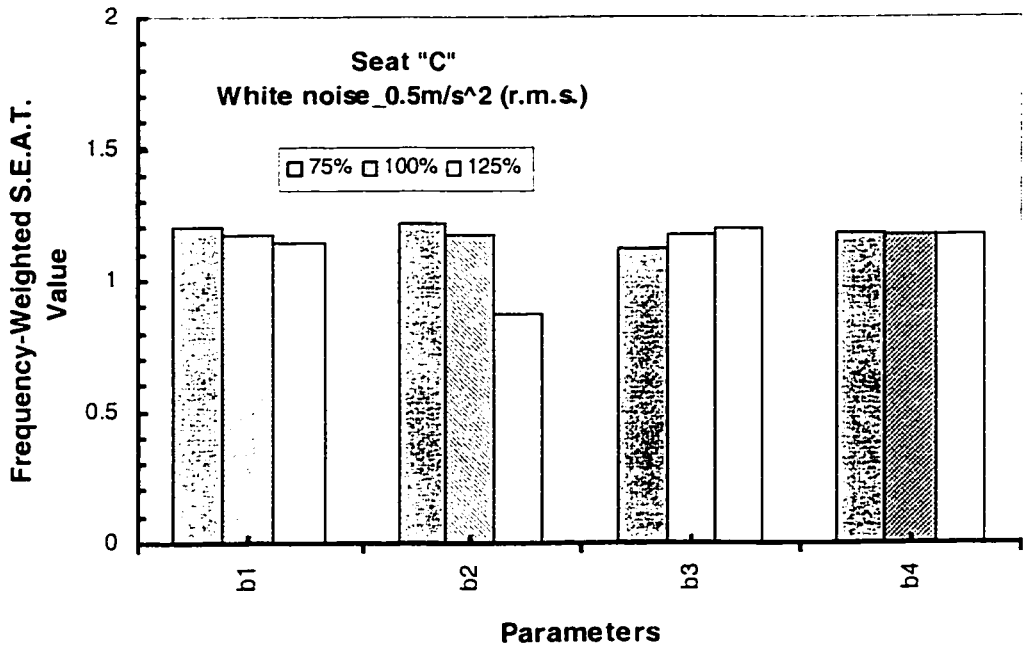

Figure 4.26: Influence of the damping parameters on the frequency-weighted S.E.A.T. values.

The influence of variations in the damping model parameters are also quantified in terms of percent change normalized with the response corresponding to the nominal parameter value, as defined in Equations (4.15) and (4.16). The percentage variations in S.E.A.T. values attained for ± 25 % variations in the damping parameters are

summarized in Table 4.4. The results show very small effect of variation in the damping parameters, except for the weight dependent parameter $b2$ of the PUF. A higher value of b_2 could enhance the isolation efficiency of the seat. The relative small effects of damping model parameters are attributed to light damping properties of the PUF. The $\pm 25\%$ variations in the coefficients yield only small change in the damping coefficient.

Table 4.4: Variation in S.E.A.T. value caused by the damping parameters.

Variation in Parameters	Percentage change in S.E.A.T.$_W$ value (%)			
	b_1	b_2	b_3	b_4
100% to 75%	2.1	3.8	-4.8	0.3
100% to 125%	-2.7	-25.6	1.6	-0.4

Figures 4.27 to 4.30 depict the influence of variations in the model parameters for seats "A" and "B" on the seat acceleration transmissibility. The results show quite similar tendencies, as to the effects of variation in the model parameters. Figures 4.31 and 4.32 illustrate the influence of body weight (preload) on the acceleration transmissibility of seats "A" and "B", respectively. The results show that a higher preload yields slightly higher resonant frequency and peak transmissibility. The seat "B" exhibits considerably more dependency on the preload.

The influence of variation in the model parameters on S.E.A.T. values of seat "A" and "B" are shown in Figures 4.33 and 4.34, respectively. The results show trends are similar to those observed for seat "C".

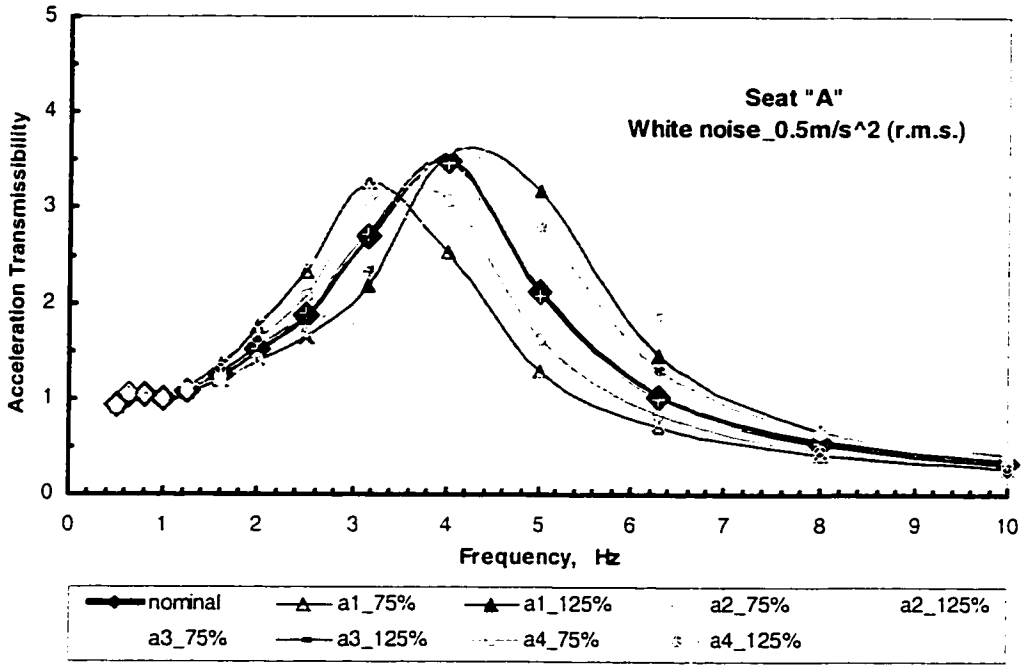

Figure 4.27: Influence of stiffness model parameters for seat "A" on the seat acceleration transmissibility.

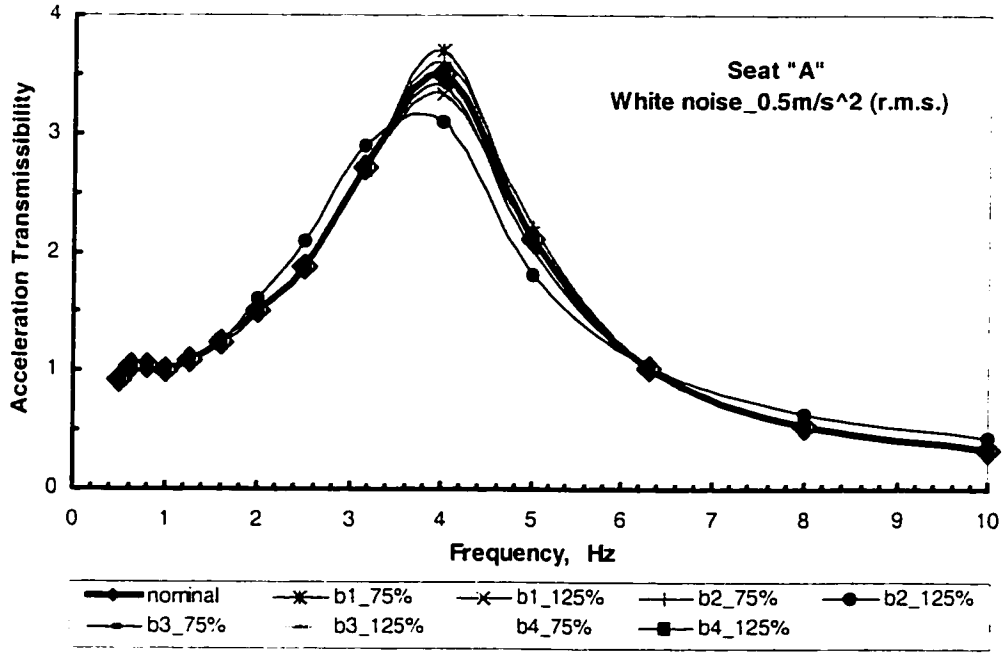

Figure 4.28: Influence of damping model parameters for seat "A" on the seat acceleration transmissibility.

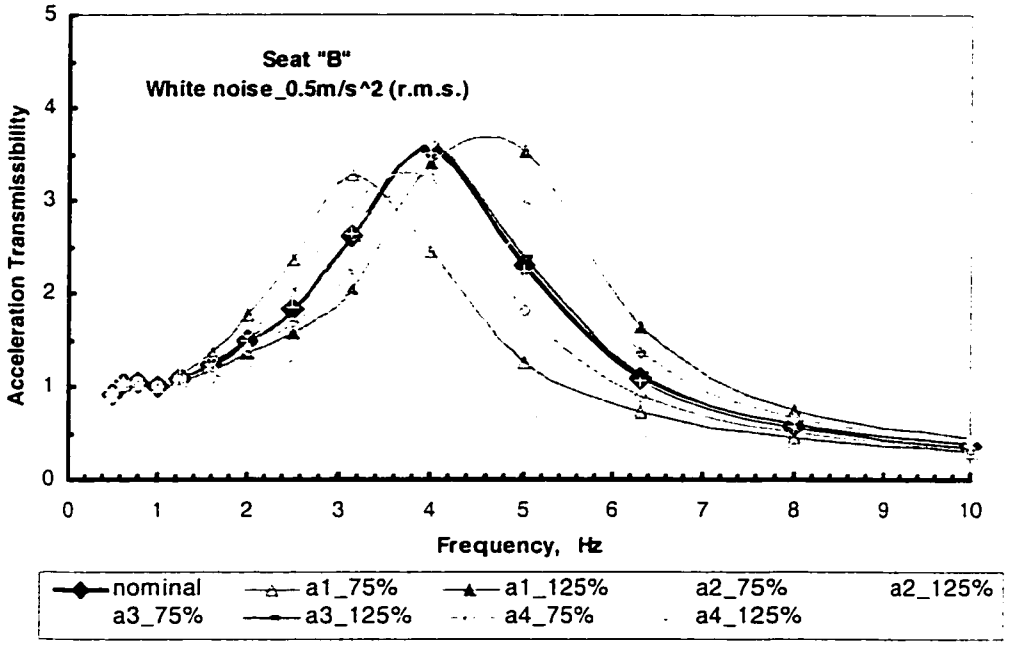

Figure 4.29: Influence of stiffness model parameters for seat "B" on the seat acceleration transmissibility.

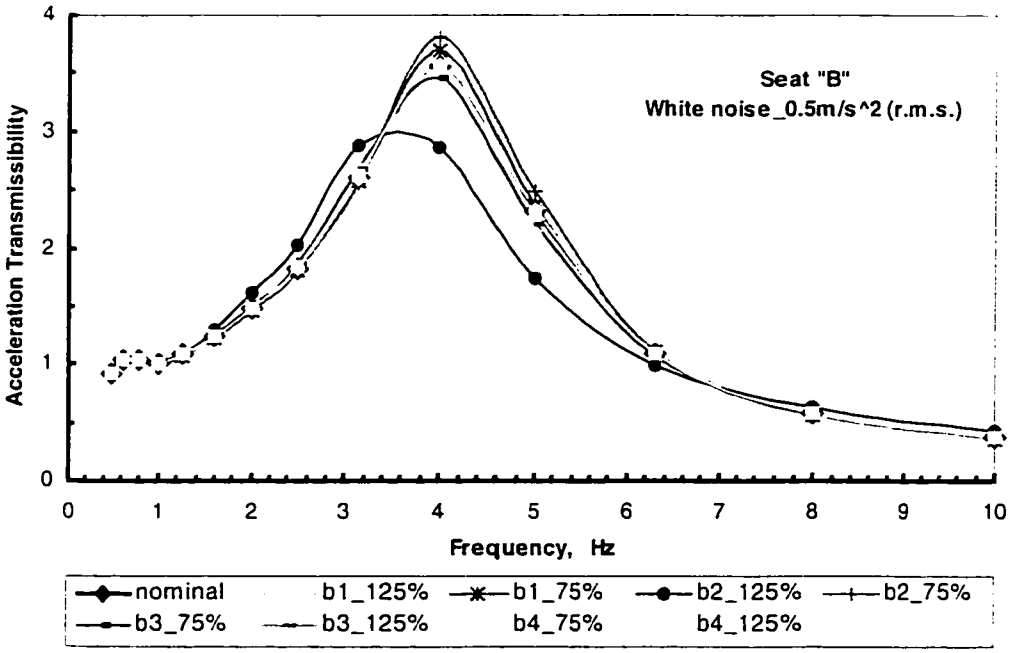

Figure 4.30: Influence of damping model parameters for seat "B" on the seat acceleration transmissibility.

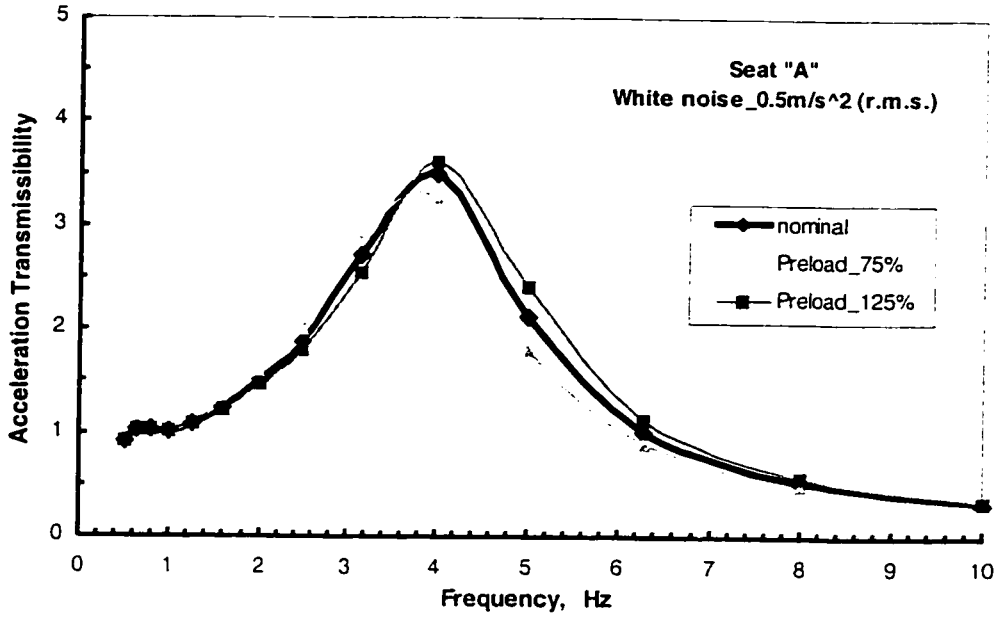

Figure 4.31: Influence of preload for seat "A" on the seat acceleration transmissibility.

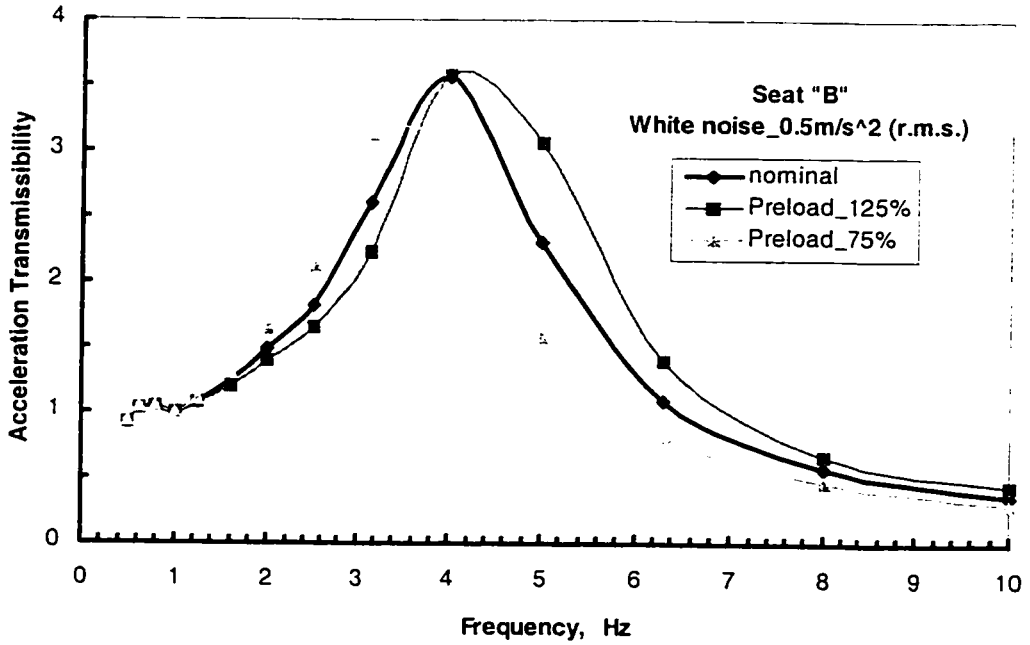

Figure 4.32: Influence of preload for seat "B" on the seat acceleration transmissibility.

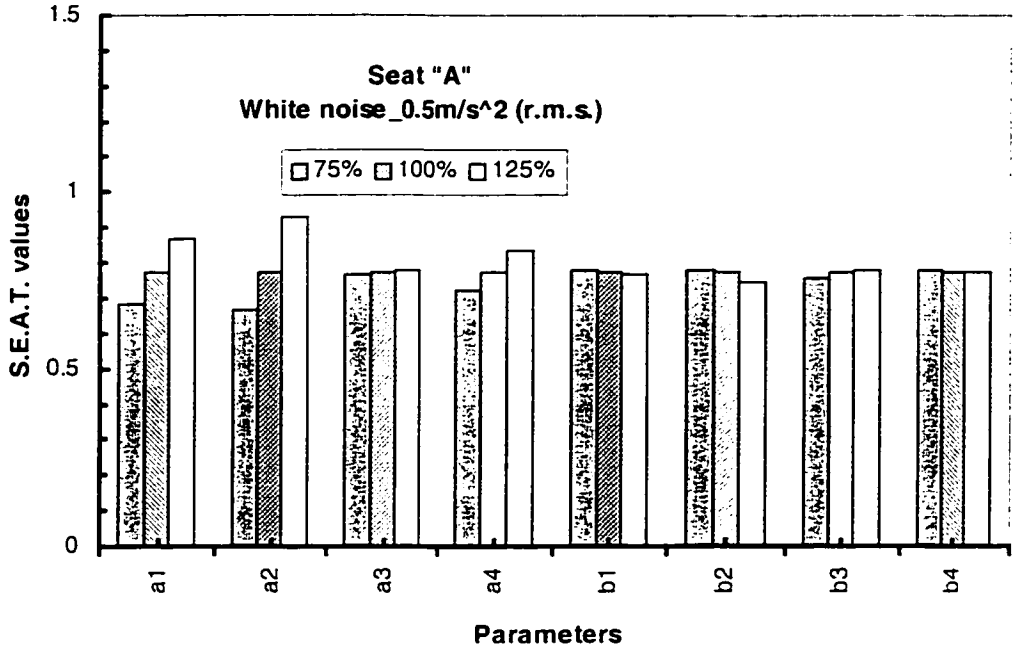

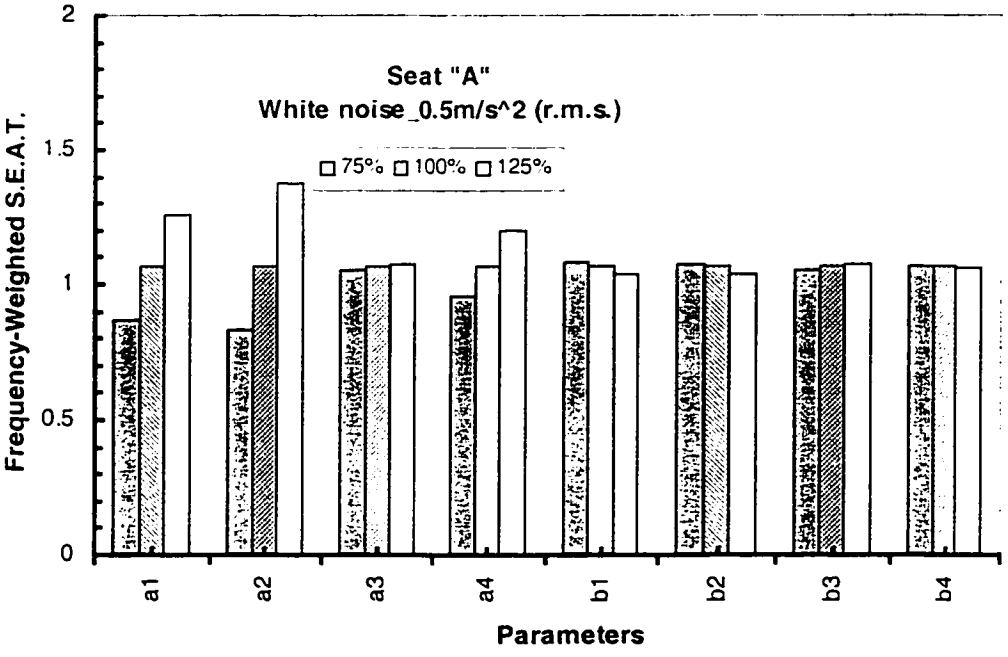

Figure 4.33: Influence of seat model parameters on S.E.A.T. values and frequency-weighted S.E.A.T. values for seat "A".

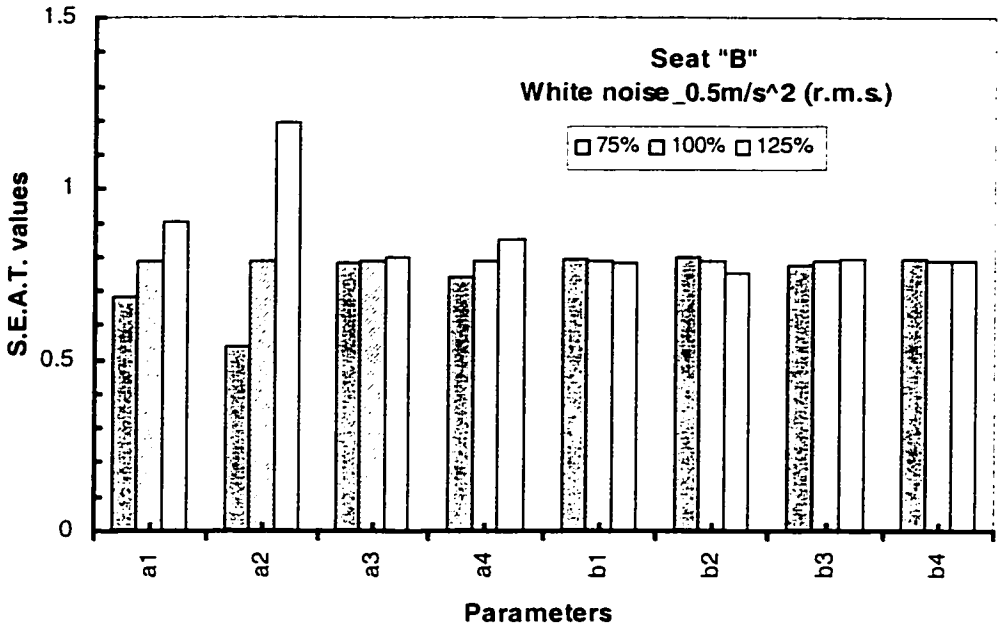

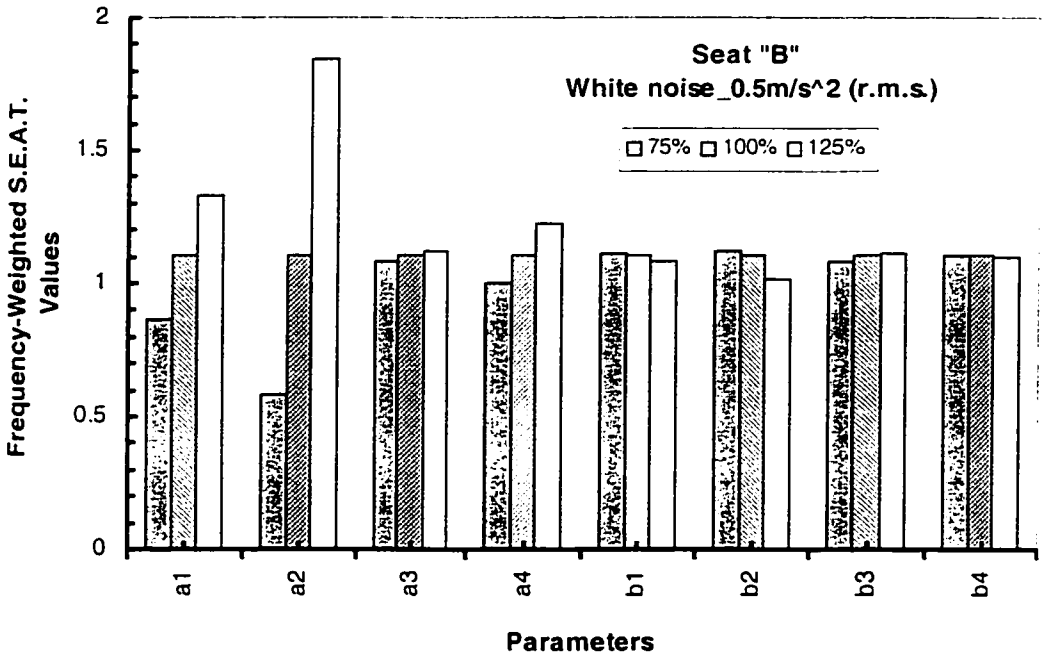

Figure 4.34: Influence of seat model parameters on S.E.A.T. values and frequency-weighted S.E.A.T. values for seat "B".

4.6 Summary

In this chapter, the concept of frequency weighting is introduced into vibration performance parameters, which include S.E.A.T value and acceleration transmissibility, in order to evaluate accurately and in truth the seat performance exposed to whole body vibration. A road-measured random excitation is created using optimization toolbox in MATLAB software based on the reported measure power spectral density at the car floor. A combined seat-rigid mass system is simulated under different excitations, including a road-measured random excitation with acceleration rms of $1.2m/s^2$ and white noise with acceleration rms of $0.25m/s^2$, $0.5m/s^2$ and $1.0m/s^2$, respectively. The various vibration performance parameters (S.E.A.T value and acceleration transmissibility) of the seats are obtained and evaluated. The results show that seat "A" has the smallest values of all vibration performance parameters, seat "B" rank the second, and seat "C" yields the worse performance. A comprehensive parametric study is performed to quantify the influence of various parameters on the overall vibration attenuation performance of the coupled seat-rigid mass system, in terms of both the vibration transmissibility and S.E.A.T. values. The results show quite similar tendencies for all the three seats. The seat isolation efficiency increase with an increase in excitation magnitude of a broad band excitation. An decrease in parameters a_1, a_2, a_4 and b_3 of stiffness and damping models yield lower peak transmissibility and resonant frequencies and could enhance the isolation efficiency of the seat. Inversely, a decrease in parameters b_1 and b_2 yield higher peak transmissibility and resonant frequencies and could weaken the isolation efficiency

of the seat. The results also show negligible effect of variation in parameters a_3 and b_4 on the acceleration transmissibility and the isolation efficiency of the seat.

5 DEVELOPMENT OF HUMAN BODY MODEL

5.1 Introduction

In Chapter 3, the models of the seats were developed and validated on the basis of a rigid mass used to represent the occupant. The biodynamic response behavior of the seated human occupant, however, is known to affect the overall vibration isolation performance of the seat [5,29,72]. It is thus essential to develop a model of the seat-occupant system that incorporates the biodynamic contributions due to the seated occupant. A suitable biodynamic model capable of representing the postural constraints encountered in automotive seating, however, is still lacking. The biodynamic response characteristics of the human body are known to be influenced by several factors, including subject weight, posture, backrest support, feet and hand position, vibration excitation type and level, etc. While most of the current biodynamic models have been derived on the basis of measured biodynamic response functions, the conditions associated with the development of these models have often been very different from those that would apply to automobile drivers. The dynamic responses of seated subjects exposed to whole-body vibration have been investigated and characterized in terms of 'to-the-body' and 'through-the-body' functions, such as driving-point mechanical impedance (DPMI), or apparent mass (APMS) and seat-to-head transmissibility (STHT) functions [4,25]. The ranges of biodynamic response of seated occupants with no back support and exposed to whole-body vibration have been defined in the recent International Standard, ISO-5982 (2001) [25]. The ISO-10326 [62] specifies the basic requirements for the laboratory testing of vibration transmission through a vehicle seat to the occupant in order to test the performance of seats. Hinz et al. [63] performed

laboratory testing of operator seat vibration with 37 subjects seated erect without back support in order to study the influence of subjects' posture, type of seat and various inputs, on the performance of the seats. Wei and Griffin [64] developed mathematical models of the driving point impedance of the human body by measuring the apparent masses of 60 subjects including men, women and children. Rakheja and Boileau [52] identified the biodynamic responses of seated human body through laboratory tests conducted on 22 subjects, including 12 male and 10 female subjects, under different sitting postures (back support, hands portion, feet position) and excitations.

A number of the seated occupant models have been derived from the measured biodynamic responses of subjects seated with no back support and exposed to vibration [17,18,27,30,48]. The majority of the models, however, are derived from the data acquired under relatively high magnitudes of vibration. The reported models may thus be considered not likely applicable to automobile occupants which involve a seated posture with body supported by an inclined backrest and seat pan, with hands either in lap or on the steering wheel, and subjected to significantly lower vibration levels. Furthermore, these models were derived on the basis of the measured driving-point mechanical impedance or apparent mass and seat-to-head transmissibility magnitude and phase responses of subjects seated on a rigid platform. The nonlinear properties of the seat and the effects of coupling between the seat and the occupant are not considered in developing the model. The validity of an occupant model for automotive seats has not yet been proven.

In this Chapter, vibration attenuation properties of automotive seats with human occupants are evaluated in the laboratory. The measured data are presented in terms of

frequency response characteristics of the seat-occupant system. Coupled seat-occupant models are formulated upon integrating the reported biodynamic models to the seat model proposed in Chapter 3. The analytical acceleration transmissibility characteristics of the coupled model are compared with those obtained from the laboratory measurements to examine the validity the model. In addition, an optimization problem is formulated and solved to identify the biodynamic model of the seated body that attempts to account for contributions due to seat-occupant coupling.

5.2 Experiments

Owing to the potential health and safety risks and ethical concerns, associated with vibration exposure of test subjects involved in experimental assessment of seats, considerable efforts are being made in developing anthropodynamic dummies that could replace the human occupant participation in such studies [19,20,35,52,66]. Alternatively, a number of studies have attempted to analyze the vibration isolation performance of seats using biodynamic models. These studies, however, have been mostly directed for suspension seats [17,18,35]. In this study, similar attempts are made to study the vibration attenuation properties of automotive seats.

The vibration transmission characteristics of seat "C" loaded with a human subject were investigated using the whole-body vehicular vibration simulator (WBVVS). The test set-up is described in section 3.2.1. A male subject with total body mass of 75 kg and height of 1.75m participated in the experiments. The subject was considered to represent 50^{th} percentile adult population. The mass of the occupant supported by the seat cushion was estimated as 54.75 kg since approximately 73 percent of the human mass is

supported by the seat, with the remainder supported by the feet interface with the floor pan [43]. It must be emphasized that emergency safety switches were provided to the subject and to the operator to ensure safety of test subject.

The vibration transmission performance of seat "C" was evaluated under sinusoidal excitations of magnitudes varying from 2.54 mm to 12.7 mm in the frequency range of 0.625 to 10 Hz swept at a rate of 1 octave per minute. The excitation signal was configured to provide constant amplitude displacement excitation in the frequency range of 0.625 to 2 Hz and constant acceleration amplitude in the frequency range of 2 to 10 Hz. The test matrix, illustrating the range of amplitude and frequencies, is defined in Table 5.1.

Table 5.1: Test matrix of the range of excitation stroke and frequency for seat "C".

Excitation	Subject Mass (kg)	Constant Peak Displacement (mm)	Frequency range (Hz)	Constant Peak Acceleration (m/s^2)	Frequency range (Hz)
Swept Sinusoidal	75	2.54	0.625 – 2	0.4	2 – 10
		6.35	0.625 – 2	1.0	2 – 10
		12.7	0.625 – 2	2.0	2 – 10

The seated subject was advised to assume two different postures in two tests. In the first test, the subject was seated with fully supported back with an inclined backrest and seat pan, and with hands in lap. In the second test, the subject was seated erect

without backrest and with hands on a steering wheel. An accelerometer was mounted between the body and the seat cushion to measure the vertical acceleration response of the seat. Another accelerometer was mounted on the seat track to measure the excitation. The measured acceleration signals were amplified and supplied to a two-channel signal analyzer, B&K2035. The analyzer-based software was used to compute the vertical acceleration transmissibility of the seat, and the power spectral density of response and excitation accelerations. The acceleration transmissibility characteristics revealed two peaks over the frequency range of 0.625-10 Hz, with predominant vibration occurring near the principal resonance of the seat-occupant system [19,20,67].

Figure 5.1 presents the measured transmission characteristics of seat "C" with subject seated without backrest support under three different amplitudes of excitation, which are described in Table 5.1. The results show principal resonance in the frequency range of 3.0 to 4.25 Hz, depending upon the magnitude of excitation. The second peak occurs in frequency region of 8 to 10 Hz, whose magnitude is relatively small. Considering that the seat-mass resonance occurs near 5 Hz (Figure 3.2), the response characteristics of the seat-occupant system suggest complex contributions due to the human subject. The presence of the secondary small peak also suggests more complex couplings within the anatomical structures, possibly between the legs and the upper torso [49]. The results clearly show that the excitation amplitude lays obvious effects on the transmissibility magnitude. The transmissibility magnitudes attained under different excitations are very close below 1.5 Hz. The transmissibility magnitudes increase rapidly with increasing frequency and approach the resonant peak value of 2.1 at resonant frequency of 3.0 Hz under the excitation amplitude of 12.7 mm. The response

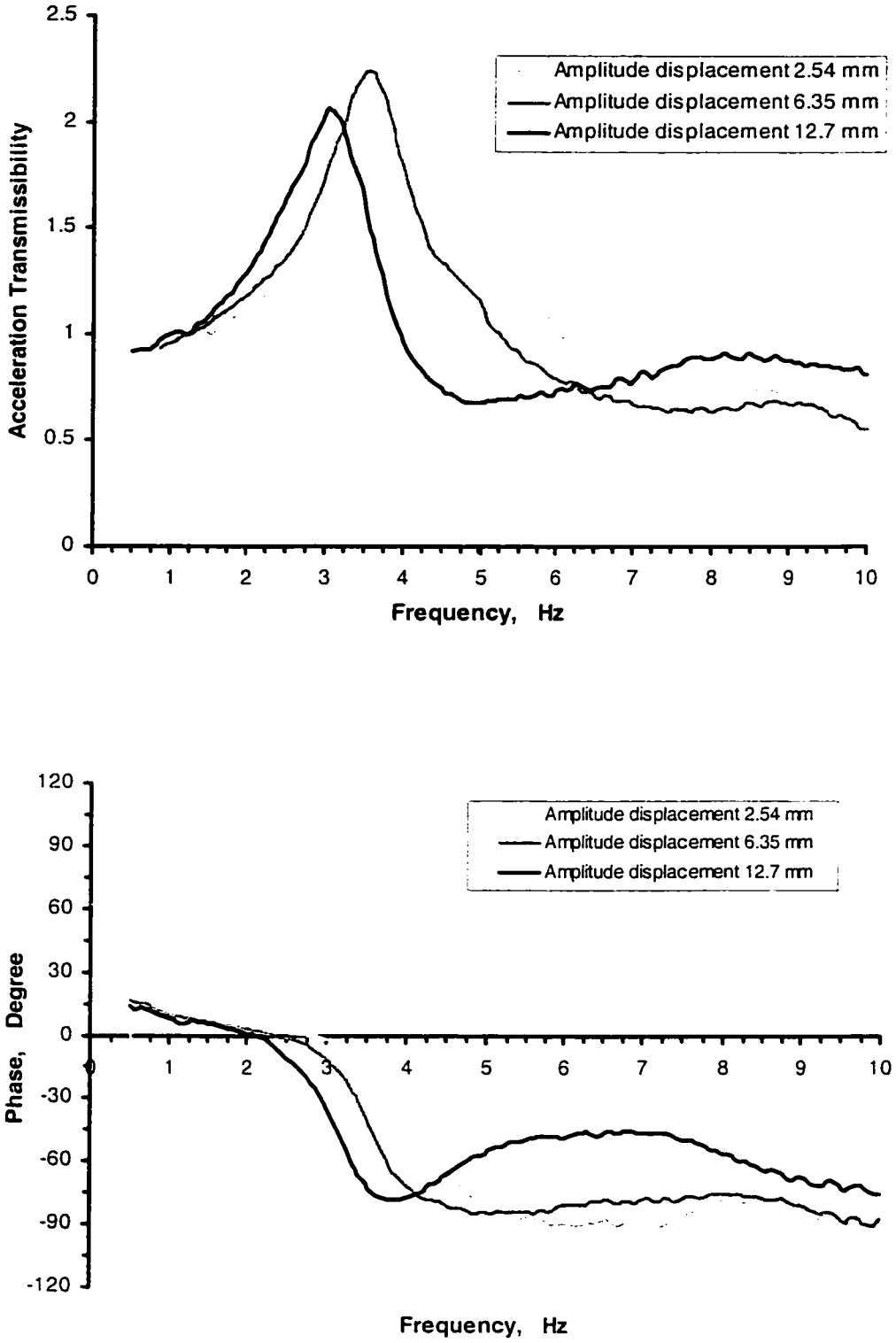

Figure 5.1: Measured acceleration transmissibility of seat "C" with a subject seated without back support.

magnitude then decreases in the 3.0 to 4.75 Hz frequency range approaching a value of 0.7 near 4.75 Hz. The transmissibility magnitude tends to increase with further increase in the frequency and approaches the second peak value of 0.9 near 8.25 Hz. Both the principle resonant frequency and the corresponding resonant magnitude increase as the excitation amplitude is decreased. These trends were also evident from both the measured and simulation results attained for the seat-mass system. Under the excitation amplitude of 6.35 mm, the magnitudes of transmissibility approaches the resonant peak value of 2.25 at resonant frequency of 3.5 Hz, and it yields attenuation of vibration above 5.25 Hz. An increase in displacement amplitude to 12.7 mm causes the resonant amplitude of nearly 2.1 at a frequency of 3 Hz. The higher amplitude excitation yields a more distinct peak near 8 Hz, most likely attributed to the seated body. The resonant frequency increases to 4.25 Hz when the amplitude of excitation is reduced to 2.54 mm, while the resonant amplitude also increases to 2.3. From Figure 5.1, it can be seen that the phase characteristics of acceleration transmissibility vary considerably with the magnitude of excitation. The positive phase values at lower frequencies are most likely caused by the signal noise, which tends to be higher at lower frequencies. The experimental results suggest nonlinear behavior of the automotive seat and occupant system, as both the peak amplitude and the resonant frequency decrease with increasing seat track input.

Figure 5.2 presents the measured transmission characteristics of seat "C" with a subject with and without back support under the excitation amplitude of 12.7 mm. It indicates that the subject's posture lays obvious effects on the magnitude properties of the transmissibility. Both the transmissibility peak and the resonant frequency for the subject with back support are smaller than that for the subject without back support. The

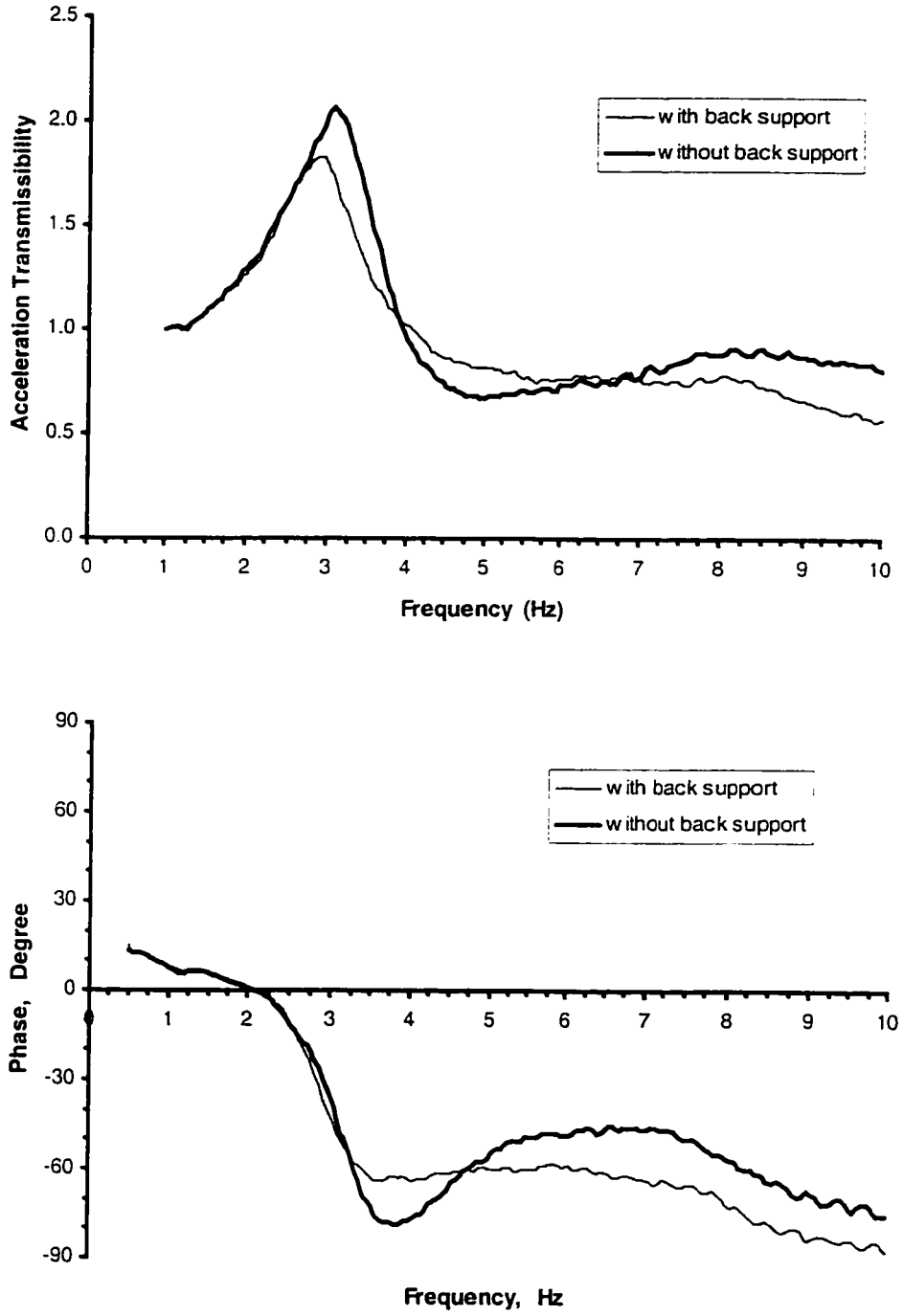

Figure 5.2: Measured acceleration transmissibility of seat "C" with subject seated with and without back support (Excitation: 12.7 mm peak displacement).

magnitudes of the transmissibility are very close below 2.5 Hz. While the magnitude of the transmissibility reaches the peak value of 1.8 at resonant frequency of 3.0 Hz in the case of the subject with back support, the magnitude of the transmissibility continues to increase and approaches the peak value of 2.1 at resonant frequency of 3.25 Hz in the case of the subject without backrest. With the increase of the frequency, the magnitude of the transmissibility decreases rapidly in frequency range of 3.25 to 5 Hz and then slowly above 5 Hz, which a secondary peak appears near 8 Hz. The subject's posture also affects the transmissibility phase response, as shown in Figure 5.2.

The reported measurements of vibration transmission performance of the seat-human system for seats "A" and "B" were also considered to study the validity of the models of seats "A" and "B". The measurements of vibration transmission performance were performed under sinusoidal excitations in the frequency range of 0.625 to 10 Hz swept at a rate of 1 octave per minute [52]. The test results were obtained with a total of 22 subjects, including 12 male and 10 female subjects. The experimental data were analyzed and shown in Figures 5.3 and 5.4. The experimental results further indicate that the human body affects the transmissibility characteristics of the seat. For seat "A", the transmissibility curves corresponding to the different subjects, as shown in Figure 5.3, suggest that the resonant frequencies vary from 2.75 to 3.25 Hz, while the resonant amplitudes vary from 2.2 to 4.0. The transmissibility amplitude in the vicinity of the secondary resonance appears to be considerably small. For seat "B", as shown in Figure 5.4, the resonant frequencies vary from 3 to 4 Hz and the resonant amplitudes vary from 1.8 to 2.7. The transmissibility amplitudes near the secondary resonance (frequency range of 6 to 9 Hz) tends to be considerably higher than those observed for seat "A".

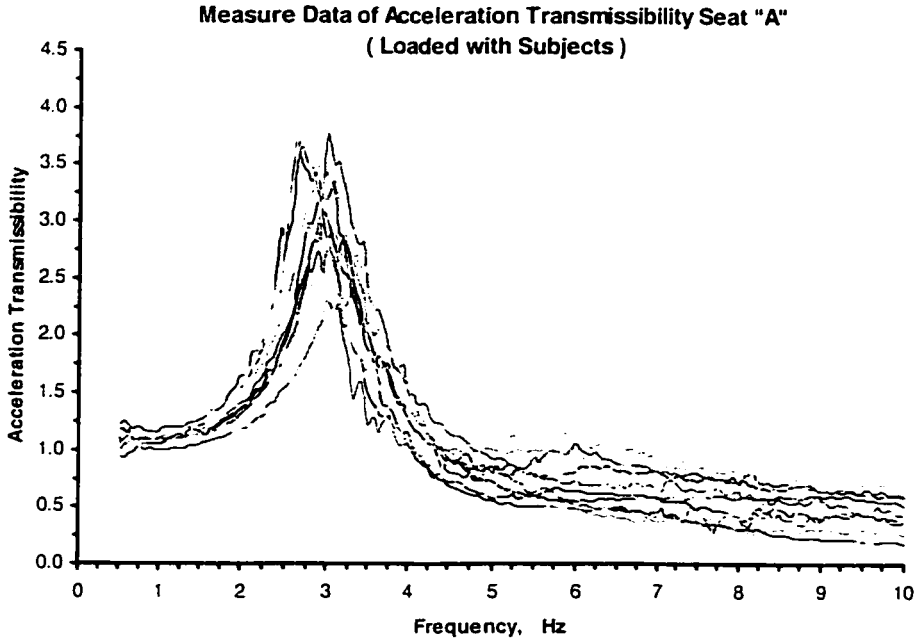

Figure 5.3: Measured acceleration transmissibility for seat "A" (22 subjects).

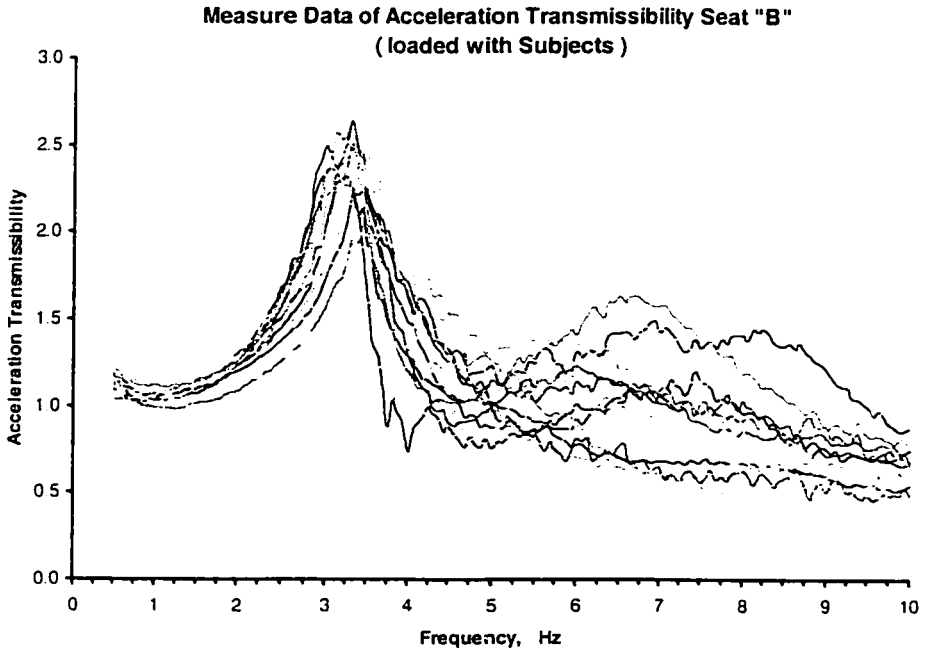

Figure 5.4: Measured acceleration transmissibility for seat "B" (22 subjects).

In summary, the seats "A" and "C" tend to provide some attenuation of the vertical vibration arising from the seat track in the frequency range of 4 to 8 Hz, where the human body is known to be sensitive. In contrast, seat "B" provides some amplification within the same range.

5.3 Seat-occupant models

A number of biodynamic vibration models for a seated human occupant have been reported in the literatures, which have been described in Chapter 1. The effectiveness of these models to characterize the biodynamic responses of seated occupants in terms of apparent mass or driving-point mechanical impedance and seat-to-head transmissibility under whole-body vibration has also been widely reported [17,18,25-32,37]. In this study, four different linear vibration models are selected to study the vibration comfort performance of the occupant-seat system. These include single-DOF system model proposed by Fairly and Griffin [29], two-DOF model proposed by Suggs *et al.* [30], three-DOF model proposed by Wu [18], and four-DOF human body model proposed by Boileau [17]. The proposed occupant models are integrated to the validated nonlinear seat model to study the response characteristics of the coupled model.

The single-DOF seated human body model proposed by Fairly and Griffin [29] was integrated to the seat model to construct an occupant-seat system, as shown in Figure 5.5. The proposed seated body involves two masses: m_1 being the mass of the upper body moving relative to the platform supporting the subject, and m_2 being the mass of the lower body. The mass of the legs m_3 was ignored. The model parameters were identified to fit the measured mean APMS of 60 subjects, including male, female and children,

sitting erect without back support. The APMS was measured under 1.0 m/s^2 random vibration. The differential equations of motion of the resulting coupled seated-occupant system are obtained and expressed as below:

$$\begin{aligned} &m_1\ddot{x}_1 + c_B(\dot{x}_1 - \dot{x}_0) + k_B(x_1 - x_0) = 0 \\ &m_2\ddot{x}_0 + c_B(\dot{x}_0 - \dot{x}_1) + k_B(x_0 - x_1) + F_{seat} = 0 \\ &F_{seat} = k(x_o - x_i) + c(\dot{x}_o - \dot{x}_i) \end{aligned} \tag{5.1}$$

where k_B and c_B represent the restoring and dissipative properties of the occupant model, and k and c are the nonlinear stiffness and damping coefficients of the seat, as described in Chapter 3.

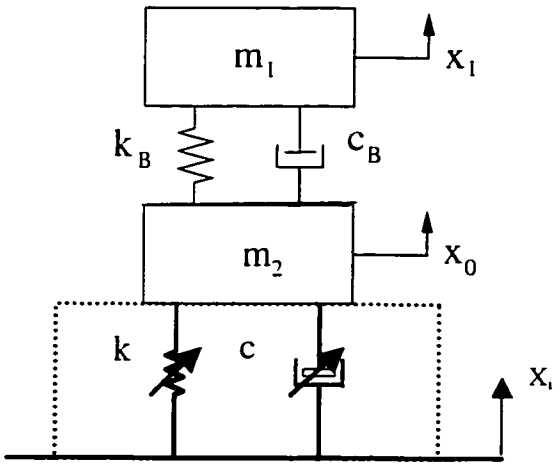

Figure 5.5: Occupant-seat system model with single-DOF human body model.

A two-DOF biodynamic model of the human body proposed by Suggs *et al.* [30] was integrated to the seat model to form a three-DOF occupant-seat system model, as shown in Figure 5.6. The lumped masses of the model consisted of m_1, representing the

lower torso; and m_2, representing the head and the neck. The coefficients k_1, k_2, c_1, and c_2 represent the stiffness and damping constants of the occupant model. The differential equations of motion of the coupled system are obtained and expressed as below:

$$
\begin{aligned}
&m_1\ddot{x}_1 + c_1(\dot{x}_1 - \dot{x}_0) + k_1(x_1 - x_0) = 0 \\
&m_2\ddot{x}_2 + c_2(\dot{x}_2 - \dot{x}_0) + k_2(x_2 - x_0) = 0 \\
&c_1(\dot{x}_0 - \dot{x}_1) + k_1(x_0 - x_1) + c_2(\dot{x}_0 - \dot{x}_2) + k_2(x_0 - x_2) + F_{seat} = 0 \\
&F_{seat} = k(x_o - x_i) + c(\dot{x}_o - \dot{x}_i)
\end{aligned}
\tag{5.2}
$$

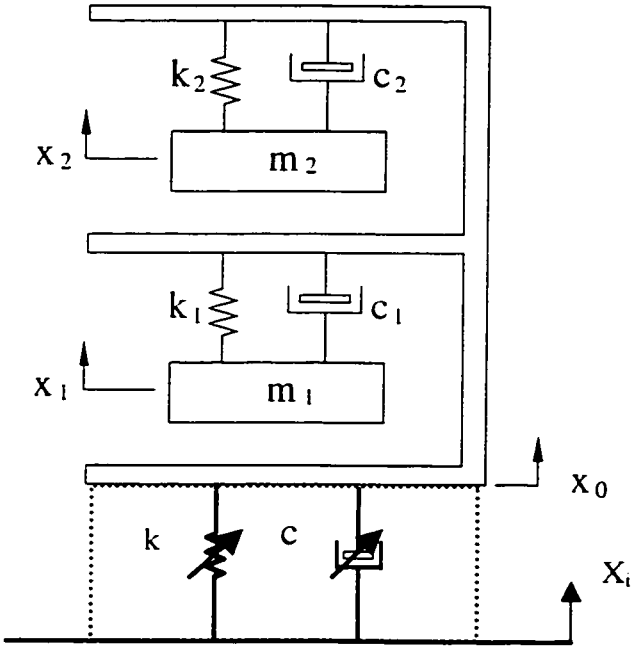

Figure 5.6: Occupant-seat system model with two-DOF human body model.

The three-DOF model proposed by Wu et al. [18], has been adopted into the ISO –5982 [25]. The model derived as the basis of both the APMS and the STHT consists of

three mass (m_1, m_2 and m_3) and constant stiffness (k_1, k_2 and k_3) and damping (c_1, c_2 and c_3) coefficients. A four-DOF coupled seat-occupant model is realized by integrating proposed occupant model to the nonlinear model of the seat, as shown in Figure 5.7. The masses m_o to m_3 used in the model have no explicit physical meaning. The masses m_1 to m_3 are introduced with an objective to describe the biodynamic behavior related to two resonant peaks observed in the APMS and STHT magnitude response near frequencies of 5 Hz and 10 Hz, respectively. The lower mass m_o is used to increase the flexibility for

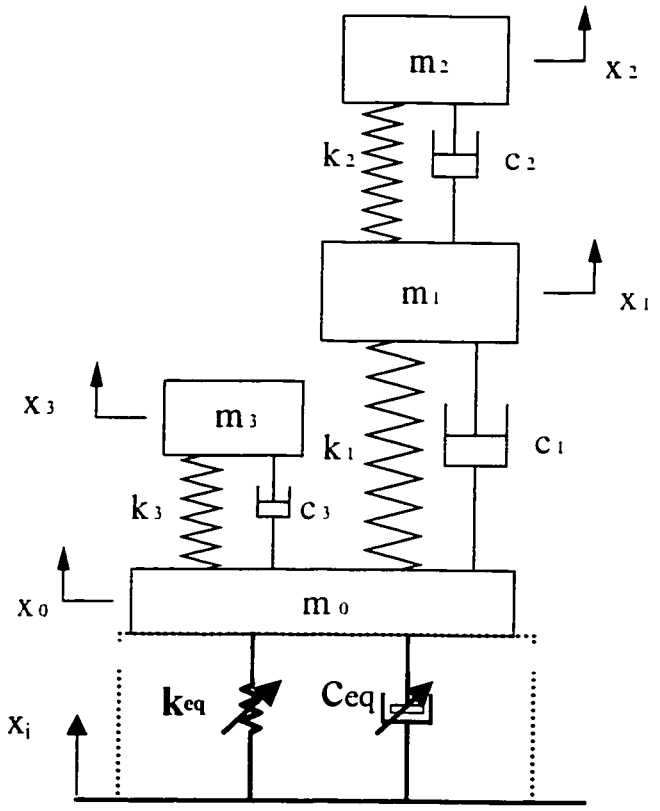

Figure 5.7: Occupant-seat system model with three-DOF human body model.

tuning the model parameters without increasing the number of DOF. This mass specifically affects the APMS response with only negligible effect on the STHT response. The differential equation of motion of the resulting coupled system are obtained as:

$$
\begin{aligned}
&m_1\ddot{x}_1 + c_1(\dot{x}_1 - \dot{x}_0) + k_1(x_1 - x_0) + c_2(\dot{x}_1 - \dot{x}_2) + k_2(x_1 - x_2) = 0 \\
&m_2\ddot{x}_2 + c_2(\dot{x}_2 - \dot{x}_1) + k_2(x_2 - x_1) = 0 \\
&m_3\ddot{x}_3 + c_3(\dot{x}_3 - \dot{x}_0) + k_3(x_3 - x_0) = 0 \\
&m_0\ddot{x}_0 + c_1(\dot{x}_0 - \dot{x}_1) + k_1(x_0 - x_1) + c_3(\dot{x}_0 - \dot{x}_3) + k_2(x_0 - x_3) + F_{seat} = 0 \\
&F_{seat} = k(x_o - x_t) + c(\dot{x}_o - \dot{x}_t)
\end{aligned}
\tag{5.3}
$$

The four-DOF model, proposed by Boileau [17], is also integrated to the nonlinear seat model to form an occupant-seat system, shown in Figure 5.8. This model consists of four masses, coupled by linear elastic spring and viscous-damper elements. In this model, however, the masses m_1 to m_4 have explicit physical meaning. The mass m_1 represents the head and neck; the mass m_2 represents the chest and upper torso; the mass m_3 represents the lower torso; and the mass m_4 represents the thighs and pelvis in contact with the seat. The mass of lower legs and the feet are not considered in this model, assuming their negligible contributions to the biodynamic response of the seated human body. The model proposed is for a seated subject that maintains a back not supported posture. The model parameters were identified such that the model response correlates with both the target DPMI and STHT magnitude and phase responses. The differential equation of motion of the coupled five-DOF model system are obtained as:

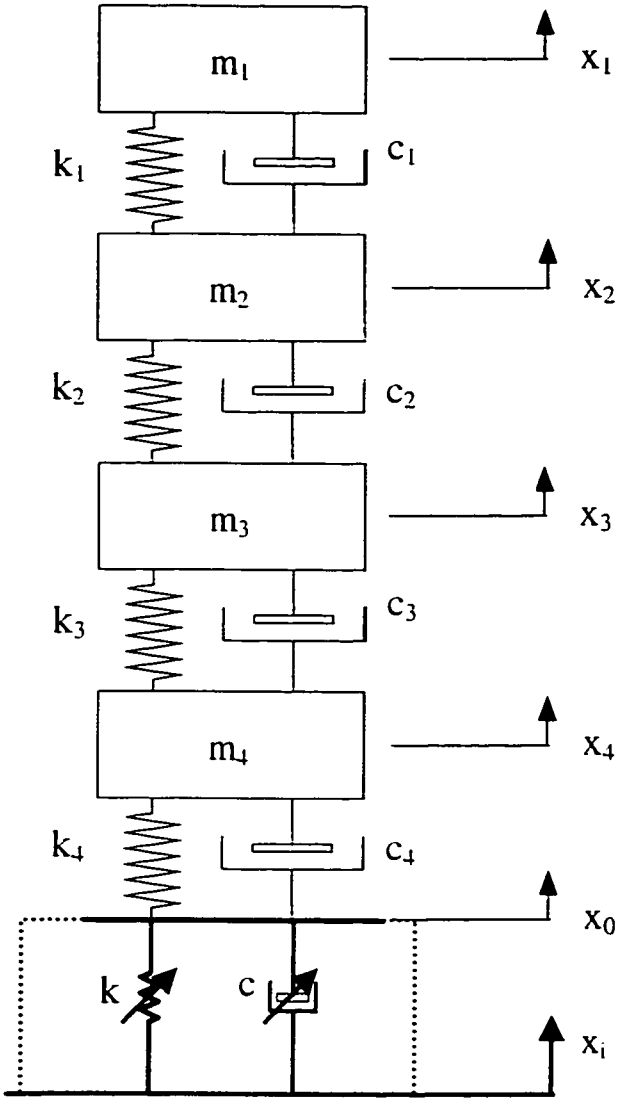

Figure 5.8: Occupant-seat system model with four-DOF human body model.

$$
\begin{aligned}
&m_1\ddot{x}_1 + c_1(\dot{x}_1 - \dot{x}_2) + k_1(x_1 - x_2) = 0 \\
&m_2\ddot{x}_2 + c_2(\dot{x}_2 - \dot{x}_3) + k_2(x_2 - x_3) + c_1(\dot{x}_2 - \dot{x}_1) + k_1(x_2 - x_1) = 0 \\
&m_3\ddot{x}_3 + c_3(\dot{x}_3 - \dot{x}_4) + k_3(x_3 - x_4) + c_2(\dot{x}_3 - \dot{x}_2) + k_2(x_3 - x_2) = 0 \\
&m_4\ddot{x}_4 + c_4(\dot{x}_4 - \dot{x}_0) + k_4(x_4 - x_0) + c_3(\dot{x}_4 - \dot{x}_3) + k_3(x_4 - x_3) = 0 \\
&c_4(\dot{x}_0 - \dot{x}_4) + k_4(x_0 - x_4) + F_{seat} = 0 \\
&F_{seat} = k(x_o - x_i) + c(\dot{x}_o - \dot{x}_i)
\end{aligned}
\tag{5.4}
$$

F_{seat} in equations (5.1) to (5.4) is the nonlinear dynamic force due to seat, where k and c are nonlinear stiffness and damping coefficients described in Chapter 3.

5.4 Response analysis of the occupant-seat system models

The nonlinear occupant-seat system models for three seats considered in the study are respectively constructed using Equations (5.1) to (5.4). Each seat model is combined with the selected four different human body models. The nonlinear occupant-seat system models described by coupled differential equations of motion are simulated in the SimuLink Toolbox of the MATLAB software under swept sinusoidal excitations to derive the seat-to-base acceleration transmissibility responses in the frequency range of 0.625 to 10 Hz. These excitations are identical to those in the experimental study. The simulation results are composed with the measured data to explore the validity of the proposed occupant models and the coupled seat-occupant system models.

Figures 5.9 to 5.11 present a comparison of acceleration transmissibility characteristics of the four different seat-occupant models with the measured data acquired for seat "C" under three different levels of excitation, respectively. The results show that the four occupant models yield considerably different magnitude and phase response of

the seat "C", irrespective of the level of excitation. Figure 5.9 presents the magnitude and phase response characteristics of acceleration transmissibility under sinusoidal excitations of amplitude of 2.54 mm. The results suggest that the two-DOF occupant model, proposed by Suggs *et al.* [30], yields relatively good agreement between the computed and measured acceleration transmissibility below 7 Hz. The three-DOF seat occupant model yields its resonant frequency near 4.25 Hz and peak acceleration transmissibility in the order of 2.35, which are slightly higher than the measured resonant frequency and transmissibility magnitude. At excitation frequencies higher than 5.75 Hz, seat "C" with two-DOF occupant model tends to underestimate the acceleration transmissibility by much as 40 %. The phase response of seat "C" with the two-DOF occupant model also agrees quite well with the measured response up to 7 Hz (Figure 5.9).

The response characteristics of the seat "C" employing single-DOF, three-DOF and four-DOF human body models are observed to be considerably different from the measured response above 3.75 Hz. The resonant frequency and peak magnitude response of all these models are considerably lower than those attained from the measured data. The results presented in Figure 5.9.

From Figure 5.9, it can be also seen that all the four models yield relatively good agreement between the computed and measured phase of acceleration transmissibility below 4.5 Hz. At excitation frequencies higher than 4.5 Hz, all the four models underestimate the measured phase of transmissibility. The differences between computed and measured data depend on the human body model.

Figure 5.9 suggest that only two-DOF occupant model, present by Suggs et al.[30], could provide an effective evaluation of the vibration comfort performance of the

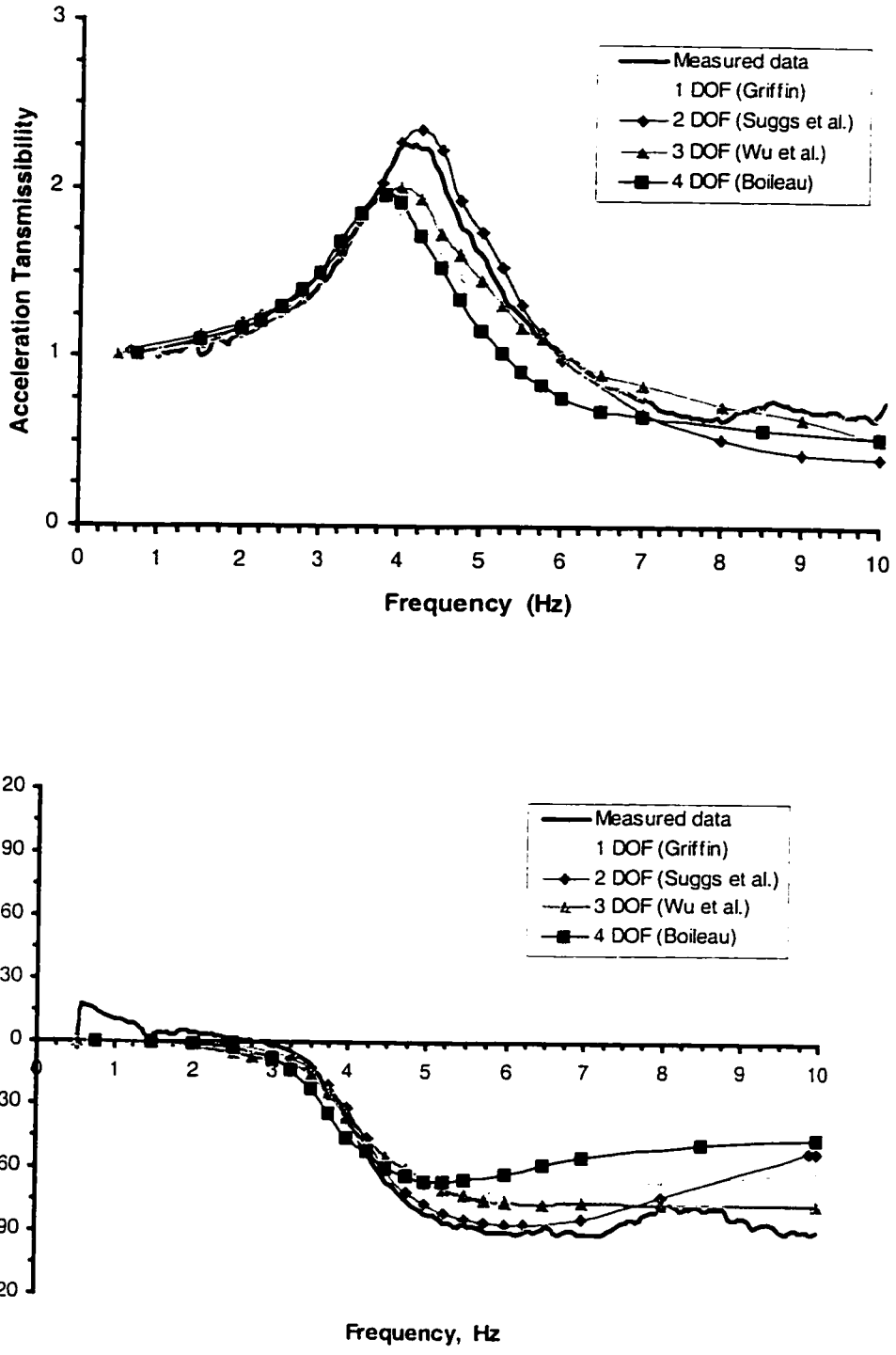

Figure 5.9: Comparison of the analytical and measured acceleration transmissibility response of seat "C" coupled with different occupant models (Excitation: 2.54 mm).

seat-occupant system exposed to low level of vertical vibration (2.54 mm peak). It is essential to mention that vast majority of the occupant models have been derived on the basis of biodynamic responses of seated occupants exposed to relatively higher magnitudes of vibration.

Figure 5.10, illustrates a comparison of acceleration transmissibility characteristics of seat "C" coupled with the four human body model and exposed to sinusoidal excitation of 6.35 mm peak amplitude. The results show trends that are somewhat opposite to those observed in Figure 5.9. The single-, three- and four-DOF occupant models provide seat acceleration transmissibility magnitudes that are comparable with the mean measured data in the entire frequency range. The seat response with the two-DOF occupant model is considerably higher than the measured data. The some occupant model, however, yields reasonably good agreement with the measured data under 2.54 mm excitation, as demonstrated in Figure 5.9. The results, therefore, suggest that biodynamic response behavior of human occupant is nonlinear. The studies conducted by Fairly and Griffin [29], Suggs *et al.* [30], Wu [18], and Boileau [17] have also concluded that the biodynamic behavior is dependent upon the amplitude of excitation, apart from many other anthropometric and postural factors, while the four-DOF occupant model, coupled with seat "C", yields reasonably good agreement with the measured transmissibility magnitude, its phase response derivates considerably from the measured data. The phase responses of the seat with the remaining occupant models, however, are observed to be comparable with the measured response.

Figure 5.11 presents the amplitude and phase characteristics of acceleration transmissibility of seat "C" coupled with the selected occupant models under the

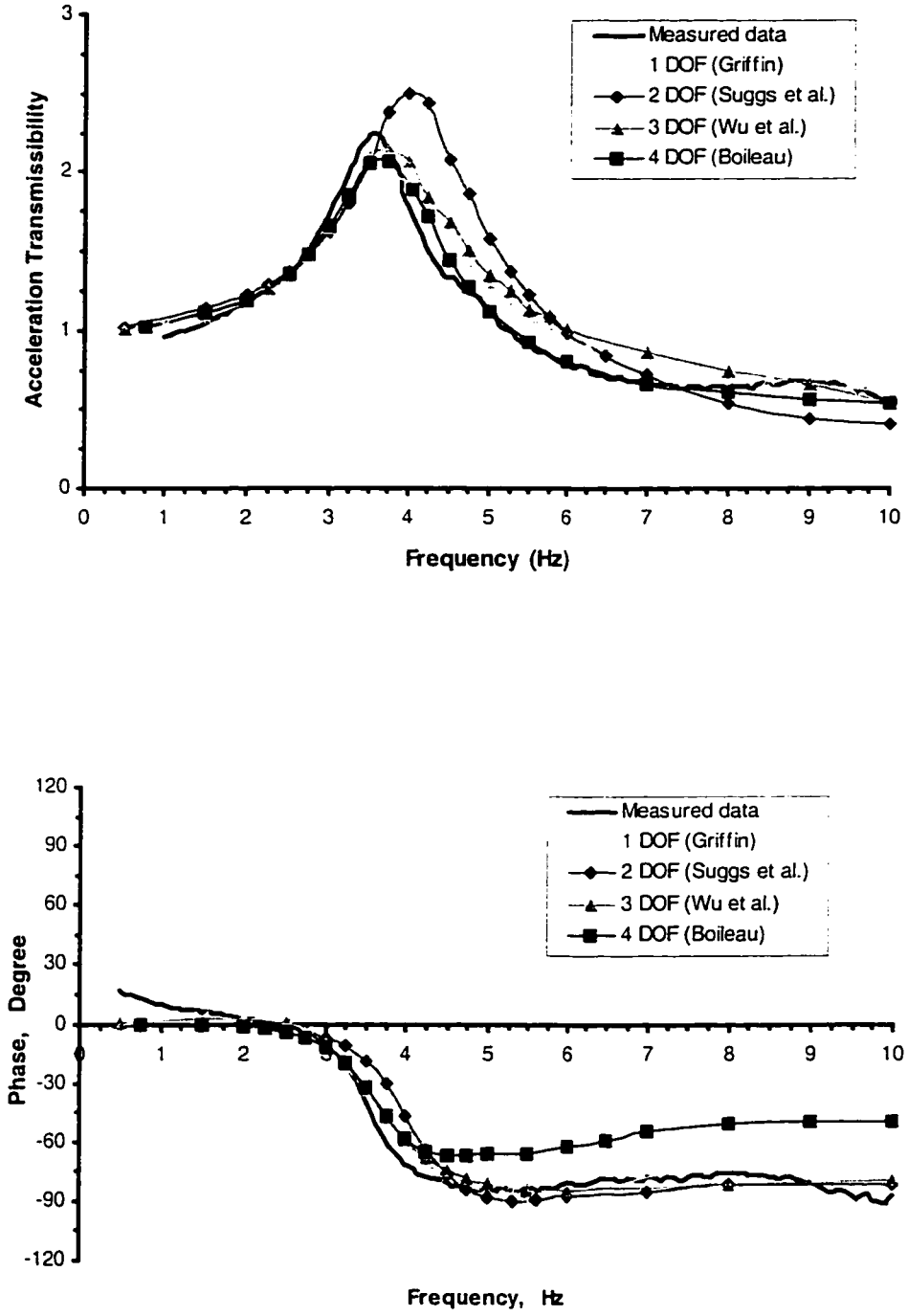

Figure 5.10: Comparison of the analytical and measured acceleration transmissibility response of seat "C" coupled with different occupant models (Excitation: 6.35 mm).

excitation amplitude of 12.7 mm. The response characteristics of the seat-occupant model employing all the four human body models result in transmissibility curves which differ considerably from the measured response over the entire frequency range, both magnitude and phase. Both the resonant frequencies and the magnitudes of transmissibility of the seat "C" with all the occupant models are observed to be considerably larger than measured data. The results further suggest the nonlinearity in the occupant biodynamic response and that the limitation of the proposed linear models in seating dynamics application.

The measured acceleration transmissibility of seats "A" and "B" with human occupants have been reported in an earlier study [83]. Figures 5.3 and 5.4. depict the mean acceleration transmissibility characteristics of the seats "A" and "B" that are derived from measurements performed with 22 human subjects under 6.35 mm excitation amplitude. The weight and height of selected subjects varies considerably to represent a wide population. The weight of the male subjects ranges from 118 lbs to 211 lbs, with mean weight of 166.5 lbs. The mean weights of the male subjects representing 5^{th}, 50^{th} and 95^{th} percentile groups are approximately 128 lbs, 163 lbs and 208 lbs, respectively. The weight of the female subjects ranges from 110 lbs to 181 lbs, with mean weight of 139.3 lbs. The mean weights of the female subjects representing 5^{th}, 50^{th} and 95^{th} percentile groups are approximately 107.6 lbs, 132.6 lbs and 179.5 lbs, respectively. The height of the male subjects selected for the study ranges from 64 inches to 74.8 inches, while that of the female subjects varied from 62.9 inches to 70 inches. The age of the subjects varied from 23 years to 50 years, with mean age of 30.1 years. Each subject was seated in the seat with feet supported on the vibrating platform and hands on the steering

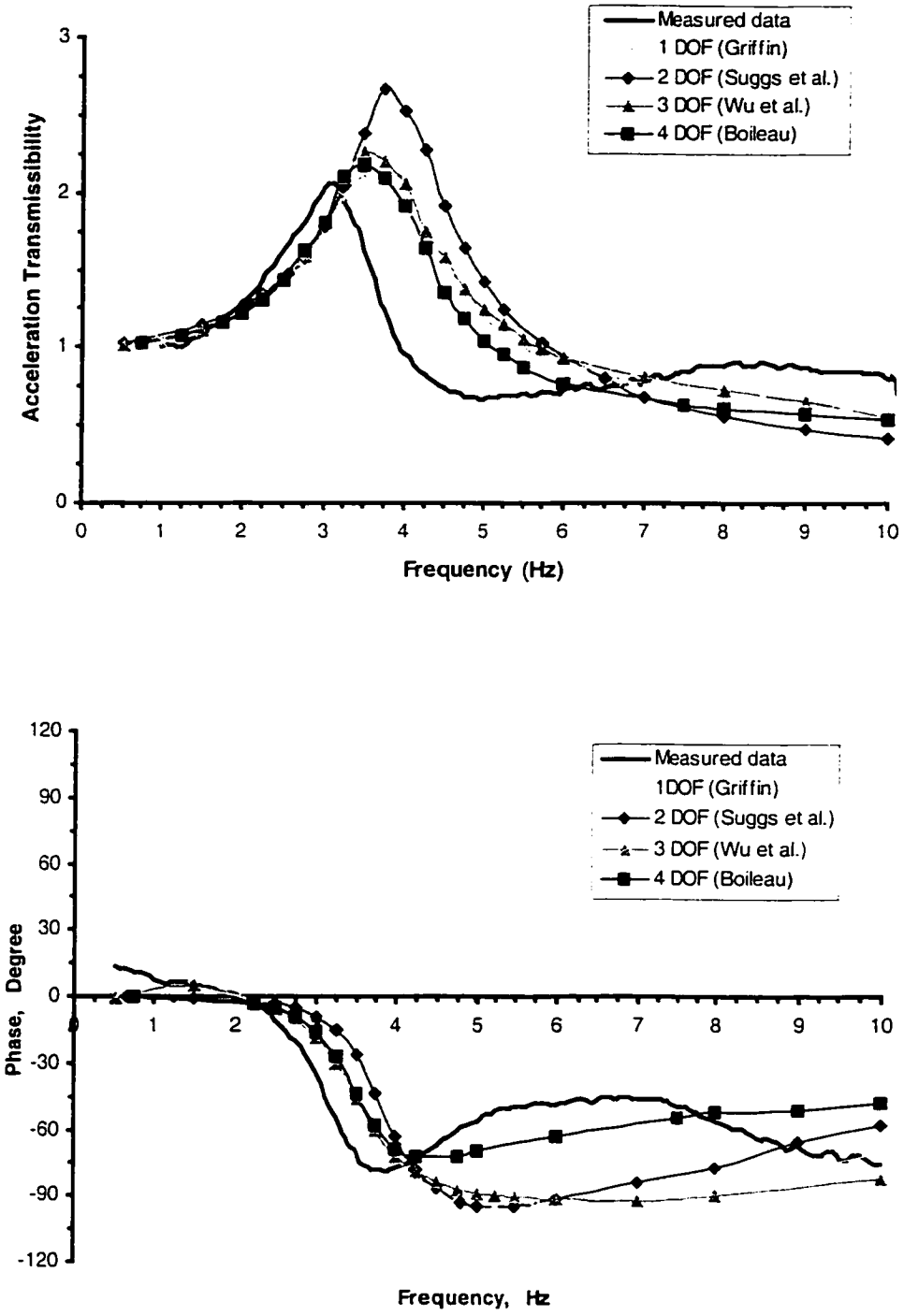

Figure 5.11: Comparison of the analytical and measured acceleration transmissibility response of seat "C" coupled with different occupant models (Excitation: 12.7 mm).

wheel. The subjects were advised to assume a driving posture considered most comfortable by the individuals. It was observed that most subjects assumed almost erect posture, while making adequate use of the back support. The sinusoidal vibration spectra swept at a rate of 1 octave/minute comprised constant displacement excitation of 6.35 mm magnitude in the 0.625-2 Hz frequency range, and constant acceleration of approximately 0.1 g (1 m/s^2) magnitude in the frequency range. The results clearly show that the results attained with all of the selected occupant models differ considerably from the mean measured data for both seats.

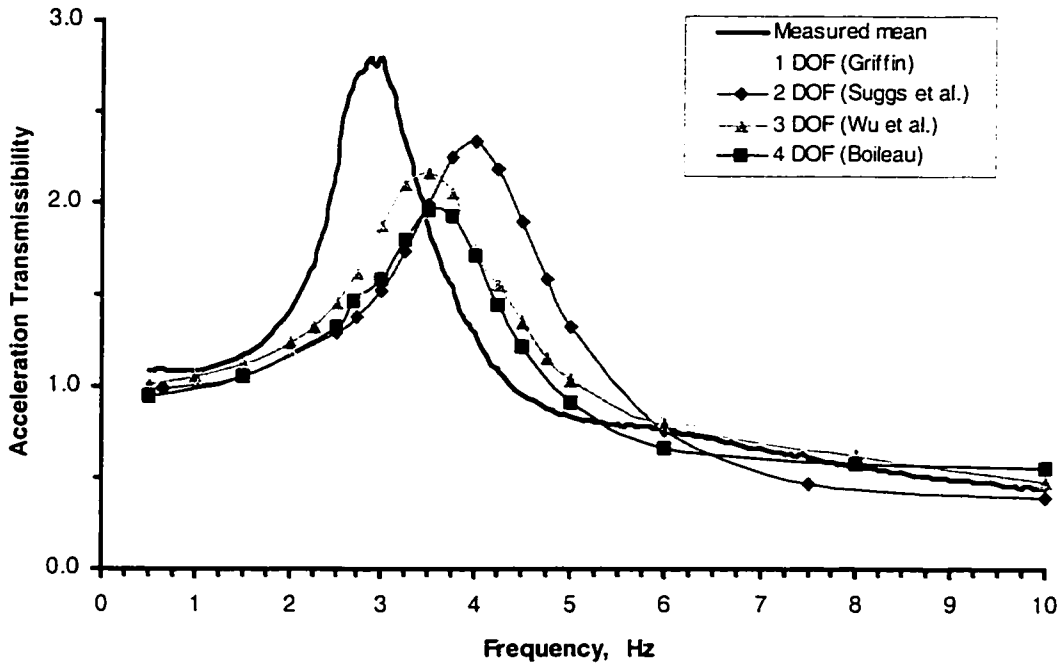

Figure 5.12: Comparison of the analytical and measured acceleration transmissibility response of seat "A" coupled with different occupant models (Excitation: 6.35 mm).

For seat "A", the resonant frequencies of all the models are observed to be higher than that observed from the measured mean data and the magnitude of transmissibility of all the models are considerably smaller than the measured mean data. Similar tendencies are also observed for seat "B". The results further show that the two-DOF model, proposed by Suggs et al. [30], yields considerably higher transmissibility magnitude and resonant frequency.

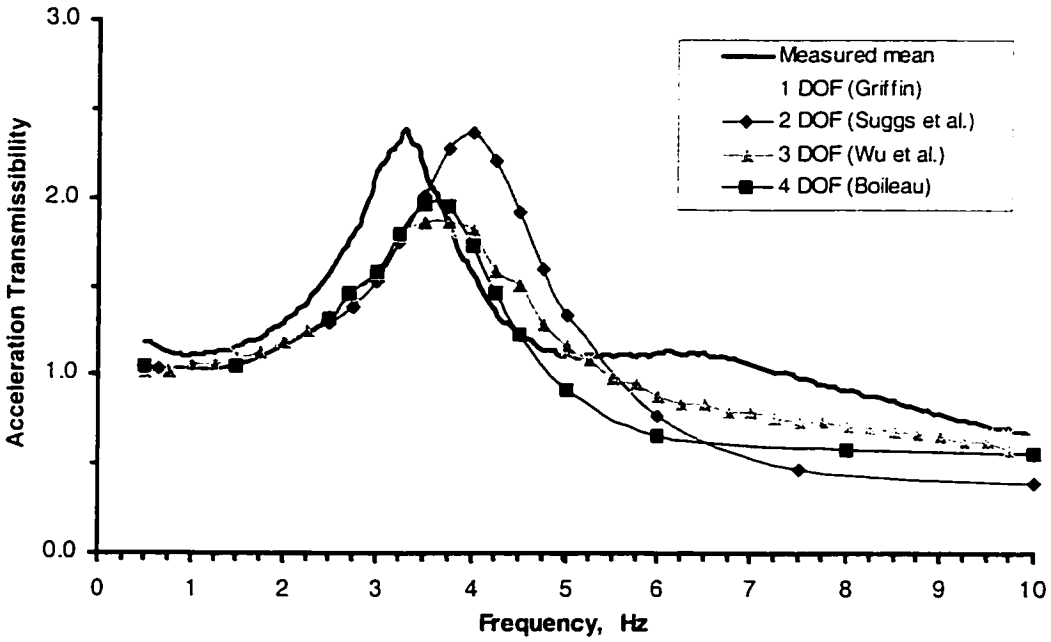

Figure 5.13: Comparison of the analytical and measured acceleration transmissibility response of seat "B" coupled with different occupant models (Excitation: 6.35 mm).

5.5 Development of Human body Model

The results presented in Figures 5.9 to 5.13 suggest that the application of a linear seated occupant model to an automobile seat could yield considerable error in the overall

vibration response of the seat-occupant system. Such error could be attributed to an array of contributing factors. The reported models have been described on the basis of the measured apparent mass or driving-point mechanical impedance and the seat-to-head transmissibility, while the nonlinear effects of the body have been ignored. A number of studies have shown considerable influence of the amplitude of the excitation of the measured biodynamic response [18,25,26,35], which is ignored in the formulation of linear biodynamic models. Furthermore, the models have been mostly derived on the basis of the data acquired for a sitting posture with no back support. The results presented in Figures 5.9 to 5.11 clearly illustrate the nonlinear behavior of the coupled seat-occupant system. The results presented in Figures 5.11 and 5.12 for seats "A" and "B", respectively, however could not support this finding, since the data were available for a single level of excitation (6.35 mm peak). A comparison of results attained for seats "A", "B" and "C" also suggests that the response behavior of the coupled seat-occupant system could also depend upon the properties of the seat. It should be noted that the occupant models have been formulated on the basis of the measured data on a flat rigid surface and exposed to whole-body vibration. It is perceived that a body seated on an elastic seat could yield somewhat different responses due to elastic body-seat coupling. The difference in the response characteristics of the three seats could be attained to this phenomenon.

In this section, the parameters of the three degree-of-freedom linear human body model, proposed by Wu [18], is identified on the basis of measured acceleration transmissibility and the APMS data in an attempt to account for the body-seat coupling effects. Wu [18] identified the model parameters through minimizing an error function

comprising the measured and model response in terms of magnitude and phase characteristics of the APMS and the STHT of occupants seated on a rigid flat surface exposed to whole-body vibration. The proposed model, shown in Figure 5.14, comprises four masses, coupled by linear spring and damping elements. The lower mass m_0 is introduced to increase the flexibility for tuning the model parameters without increasing the number of degree-of-freedom. While the model masses, and stiffness and damping elements do not represent any specific body segments, it was suggested that mass m_1 may be considered to represent the lower torso and pelvis in contact with the seat. The mass m_2 may be considered to represent the upper torso, the neck and the head and the mass m_3 to represent the thighs in contact with the seat.

In this study, the model parameters are identified to satisfy two different response functions: (i) biodynamic response in terms of APMS magnitude and phase of the body seated on a hard surface; and (ii) measured seat acceleration transmissibility of the coupled seat-occupant system.

The equations of motion for the occupant model shown in Figure 5.14 are rewritten as:

$$\begin{cases} m_1\ddot{x}_1 + c_1(\dot{x}_1 - \dot{x}_0) + k_1(x_1 - x_0) + c_2(\dot{x}_1 - \dot{x}_2) + k_2(x_1 - x_2) = 0 \\ m_2\ddot{x}_2 + c_2(\dot{x}_2 - \dot{x}_1) + k_2(x_2 - x_1) = 0 \\ m_3\ddot{x}_3 + c_3(\dot{x}_3 - \dot{x}_0) + k_3(x_3 - x_0) = 0 \end{cases} \tag{5.5}$$

where m_i, c_i and k_i (i = 1, 2, 3) are the masses, damping coefficients and stiffness coefficients, respectively, of the model; x_0 is the displacement of the driving point; and x_1, x_2, and x_3 are displacement coordinates of the three model masses.

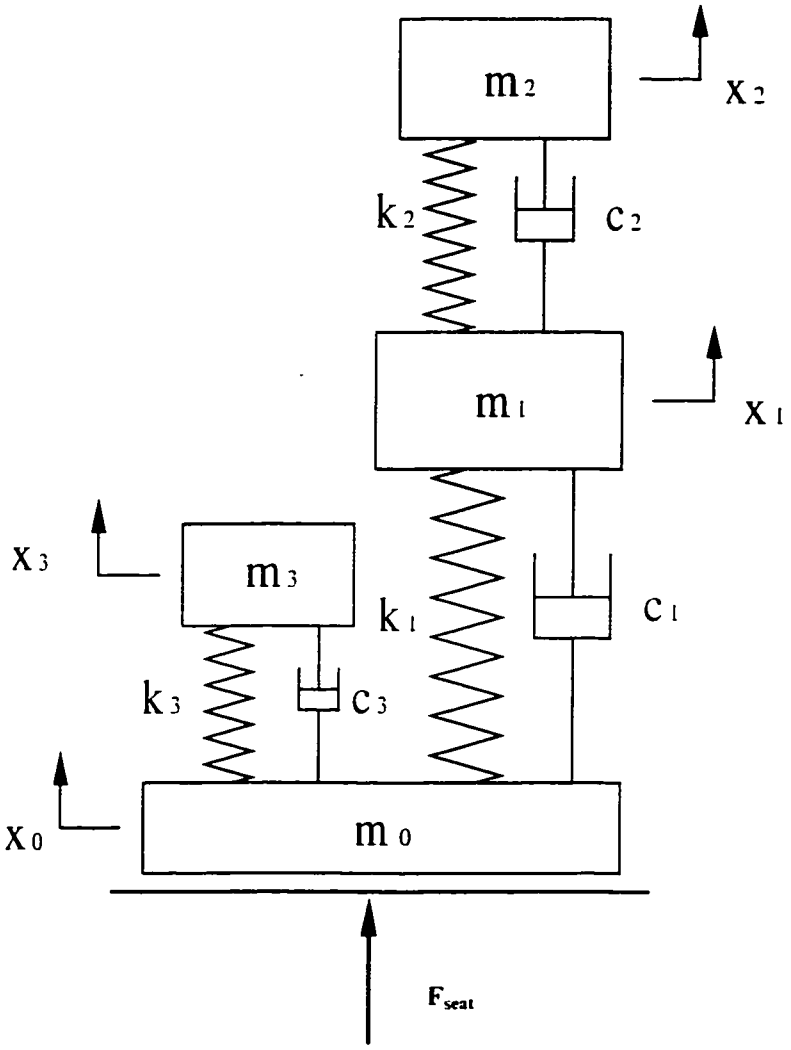

Figure 5.14: Biodynamic model of the seated occupant, proposed by Wu [18].

Laplace transform of Equations (5.5) yields the following expressions for the transfer functions, where each function relates to the ratio of a mass response to the base motion:

$$\begin{cases} \dfrac{X_1(s)}{X_0(s)} = \dfrac{(c_1 s + k_1)(m_2 s^2 + c_2 s + k_2)}{\Delta(s)} \\ \dfrac{X_2(s)}{X_0(s)} = \dfrac{(c_1 s + k_1)(c_2 s + k_2)}{\Delta(s)} \\ \dfrac{X_3(s)}{X_0(s)} = \dfrac{c_3 s + k_3}{m_3 s^2 + c_3 s + k_3} \end{cases} \tag{5.6}$$

where

$$\Delta(s) = [m_1 s^2 + (c_1 + c_2)s + (k_1 + k_2)](m_2 s^2 + c_2 s + k_2) - (c_2 s + k_2)^2 \tag{5.7}$$

In the presence of an elastic seat cushion, the force acting at the driving-point (mass m_0) could be derived from the visco-elastic model of the seat. The apparent mass (APMS) response on a rigid seat may be derived from the resultant force at mass m_0 and the driving-point acceleration $\ddot{x}_0$, in the following manner:

$$m_0 \ddot{x}_0 + c_1(\dot{x}_0 - \dot{x}_1) + k_1(x_0 - x_1) + c_3(\dot{x}_0 - \dot{x}_3) + k_3(x_0 - x_3) = F_{seat} \tag{5.8}$$

The solution of Equations (5.5) and (5.8) yields:

$$F_{seat} = m_0 \ddot{x}_0 + m_1 \ddot{x}_1 + m_2 \ddot{x}_2 + m_3 \ddot{x}_3 \tag{5.9}$$

The APMS response of the occupant model can then be derived as follows:

$$M(s) = \frac{F_{seat}(s)}{s^2 X_0(s)} = m_0 + m_1 \frac{X_1(s)}{X_0(s)} + m_2 \frac{X_2(s)}{X_0(s)} + m_3 \frac{X_3(s)}{X_0(s)} \tag{5.10}$$

The acceleration transmissibility of the seat-occupant system model, shown in Figure 5.15, is computed from the ratio of acceleration response $\ddot{x}_0$ of the mass m_0 and the seat-track acceleration $\ddot{x}_i$. In this study, the multi-parameter error minimization algorithm is applied to minimize a weighted error function of the occupant APMS response and the acceleration transmissibility response of the occupant-seat system.

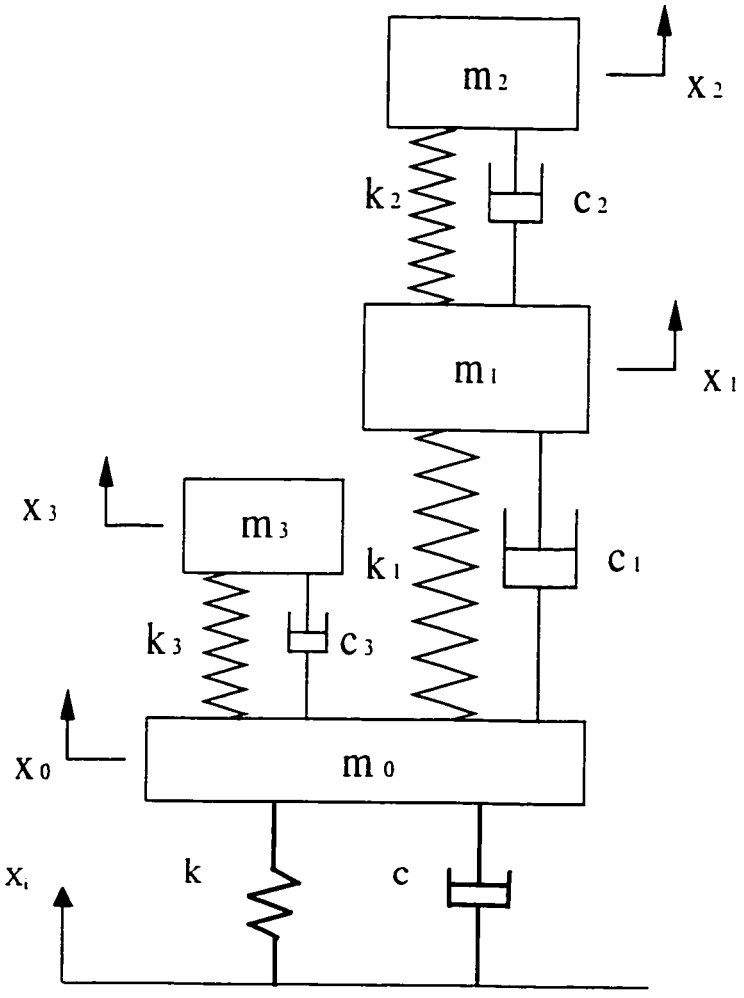

Figure 5.15: Coupled model of the seat-occupant system.

For the purpose of minimization, the nonlinear seat model is represented by its linear equivalent properties about an operating point. Equations (2.16) and (2.19) describing the nonlinear seat properties are linearized for a preload (w) of 55 kg in vicinity of the seat resonant frequency of 3.5 Hz, while the amplitude of deflection (A) is assumed to be 6.35 mm.

The equations of motion of the linear coupled seat-occupant model (Figure 5.15) can be expressed as:

$$\begin{cases} m_1\ddot{x}_1 + c_1(\dot{x}_1 - \dot{x}_0) + k_1(x_1 - x_0) + c_2(\dot{x}_1 - \dot{x}_2) + k_2(x_1 - x_2) = 0 \\ m_2\ddot{x}_2 + c_2(\dot{x}_2 - \dot{x}_1) + k_2(x_2 - x_1) = 0 \\ m_3\ddot{x}_3 + c_3(\dot{x}_3 - \dot{x}_0) + k_3(x_3 - x_0) = 0 \\ m_0\ddot{x}_0 + c_1(\dot{x}_0 - \dot{x}_1) + k_1(x_0 - x_1) + c_3(\dot{x}_0 - \dot{x}_3) + k_2(x_0 - x_3) \\ \qquad + k_{eq}(x_o - x_i) + c_{eq}(\dot{x}_o - \dot{x}_i) = 0 \end{cases} \tag{5.11}$$

where k_{eq} and c_{eq} are the linearized stiffness and damping coefficients of the seat.

Laplace transform of Equations (5.11) yields the following expressions for the transmissibility:

$$T(s) = \frac{X_0(s)}{X_i(s)} = \frac{cs + k}{(m_0 s^2 + cs + k) + m_1 \dfrac{X_1(s)}{X_0(s)} s^2 + m_2 \dfrac{X_2(s)}{X_0(s)} s^2 + m_3 \dfrac{X_3(s)}{X_0(s)} s^2} \tag{5.12}$$

5.5.1 Parameter Identification of human body model

The parameters of the human body model shown in Figure 5.14 are identified through a curve-fitting algorithm with an objective to achieve a close match of the apparent mass and the base-to-seat transmissibility response functions computed from

Equations (5.10) and (5.12), respectively, with the corresponding measured data. A multi-parameter optimization technique is employed to identify the model parameters. An objective function is defined to minimize the error between the computed and the measured values of the apparent mass and the base-to-seat transmissibility response in the frequency range of 0.1 to 10 Hz. The sum of squared error resulting from the frequency response functions is expressed as:

$$\begin{aligned} U(x) &= \sum_{f=0.1}^{10} (|M_m(s)| - |M(s)|)^2 + \sum_{f=0.1}^{10} (|\phi_m(s)| - |\phi(s)|)^2 + \sum_{f=0.1}^{10} (|T_m(s)| - |T(s)|)^2 \\ &= \sum_{f=0.1}^{10} (|M_m(j2\pi f)| - |M(j2\pi f)|)^2 + \sum_{f=0.1}^{10} (|\phi_m(j2\pi f)| - |\phi(j2\pi f)|)^2 \\ &\quad + \sum_{f=0.1}^{10} (|T_m(j2\pi f)| - |T(j2\pi f)|)^2 \end{aligned} \tag{5.13}$$

where $M_m(s)\,and\,\phi_m(s)$ are the measured apparent mass modulus and phase, respectively; and $M(s)\,and\,\phi(s)$ are the apparent mass modulus and phase responses of the model, respectively, derived from Equation (5.10). $T_m(s)\,and\,T(s)$ are the measured and computed base-to-seat transmissibility responses, respectively. The operator s in Equations (5.10) and (5.13) is represented by $j2\pi f$, and the design vector x of the model parameters is given by:

$$x = \{m_0, m_1, m_2, m_3, c_1, c_2, c_3, k_1, k_2, k_3\}^T \tag{5.14}$$

where 'T' designates the transpose.

In order to ensure somewhat comparable contributions of error in the objective function corresponding to different excitation frequencies, different weighting factors are introduced to rewrite the weighted error function as:

$$U(x) = \sum_{f=0.1}^{10} \lambda_1 (|M_m(s)| - |M(s)|)^2 + \sum_{f=0.1}^{10} \lambda_2 (|\phi_m(s)| - |\phi(s)|)^2 + \sum_{f=0.1}^{10} \psi (|T_m(s)| - |T(s)|)^2$$
$$= \sum_{f=0.1}^{10} \lambda_1 (|M_m(j2\pi f)| - |M(j2\pi f)|)^2 + \sum_{f=0.1}^{10} \lambda_2 (|\phi_m(j2\pi f)| - |\phi(j2\pi f)|)^2$$
$$+ \sum_{f=0.1}^{10} \psi (|T_m(j2\pi f)| - |T(j2\pi f)|)^2 \qquad (5.15)$$

In the above expression, λ_1 *and* λ_2 are the weighting factors applied to the apparent mass modulus and phase error functions, respectively, and ψ is the corresponding weighting factor applied to the base-to-seat transmissibility error function. Table 5.2 lists the values of the weighting factors used in minimization of the error function.

Table 5.2: Weighting factor values used in the error function.

λ_1	$\lambda_1 = 1$: 0.1 to 3.4 Hz and 5.6 to 10 Hz. $\lambda_1 = 5$: 3.5 to 5.5 Hz.
λ_2	$\lambda_2 = 1$: 0.1 to 3.9 Hz. $\lambda_2 = 5$: 4.0 to 10 Hz.
ψ	$\psi = 1$: 0.1 to 2.4 Hz and 4.6 to 7.9 Hz. $\psi = 5$: 2.5 to 4.5 Hz and 8.0 to 10 Hz.

The weighted error function utilizes the measured base-to-seat acceleration transmissibility magnitudes for seat "C" presented in Figure 5.10 for a 6.35 mm

excitation. The measured values for the APMS magnitudes and phase response are taken from the mean idealized values presented in ISO-5982 [25].

The weighted error function described in Equation (5.15), is minimized subject to following constraints applied to the model parameters:

$$\begin{cases} m_0 > 0;\ m_1 > 0;\ m_2 > 0;\ m_3 > 0; \\ k_1 > 0;\ k_2 > 0;\ k_3 > 0; \\ c_1 > 0;\ c_2 > 0;\ c_3 > 0; \end{cases} \tag{5.16}$$

Since the reported data and measured data relate to a total body mass of 75 Kg, it is estimated that 54.8 kg (i.e. 73% of total body mass) would actually be supported by the seat. A limit constraints is thus further applied to the total body mass supported by the seat, such that the total coupled model mass would vary within a narrow band of $\pm 4\%$:

$$52.8 \le \sum_{i=0}^{3} m_i \le 57 \tag{5.17}$$

Optimization Toolbox [60,61] in MATLAB is used to solve the constrained optimization problem, defined in Equations (5.15) to (5.17). The solutions are obtained for a number of different initial values of the parameters vector x, and the resulting model parameters are examined to obtain optimal and minimum error of the objective function. Different optimization runs corresponding to different initial values of the parameters vector x converged to similar values of the human body model parameters and the error magnitude. The resulting values of the human body model are summarized in Table 5.3.

Table 5.3: Parameters identified for the occupant model.

Parameters	Value	Parameters	Value	Parameters	Value
m_0 (kg)	12.6	k_1 (N/m)	31280	c_1 (Ns/m)	1441
m_1 (kg)	11.4	k_2 (N/m)	48970	c_2 (Ns/m)	311
m_2 (kg)	22.3	k_3 (N/m)	10000	c_3 (Ns/m)	561
m_3 (kg)	9.7				

The validity of the resulting occupant model is examined by comparing both the APMS and seat transmissibility responses of the model with the target data. Equations (5.10) and (5.12) are solved to compute the APMS and seat acceleration transmissibility responses, respectively, of the coupled model using the identified occupant

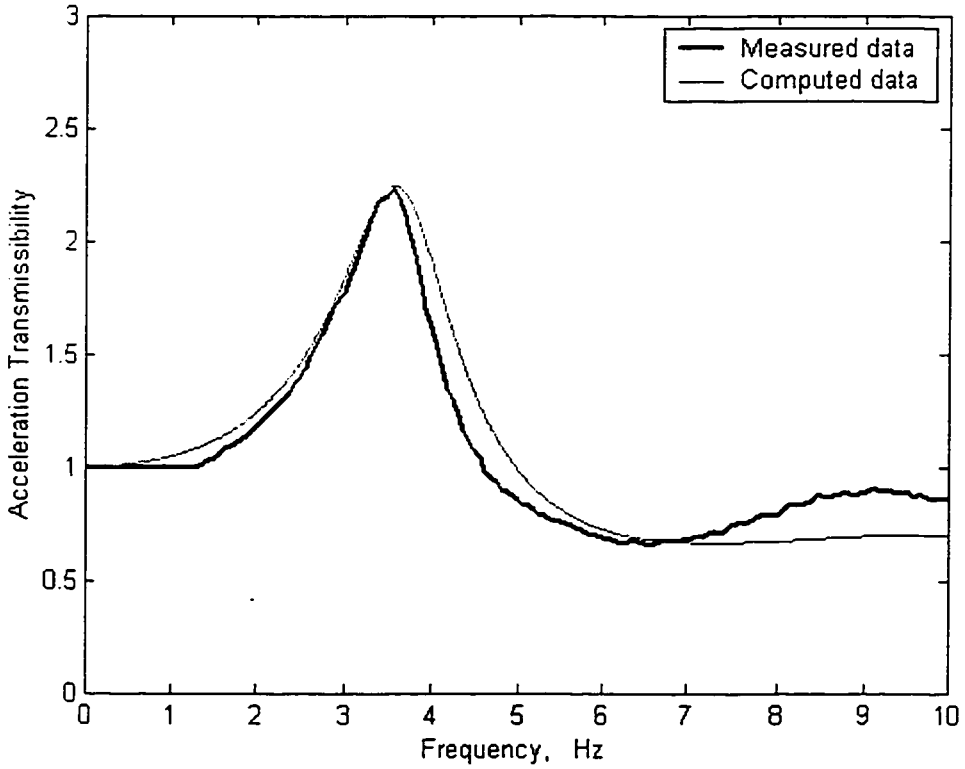

Figure 5.16: Comparison of the computed base-to-seat acceleration transmissibility response with the measured data (Excitation: 6.35 mm).

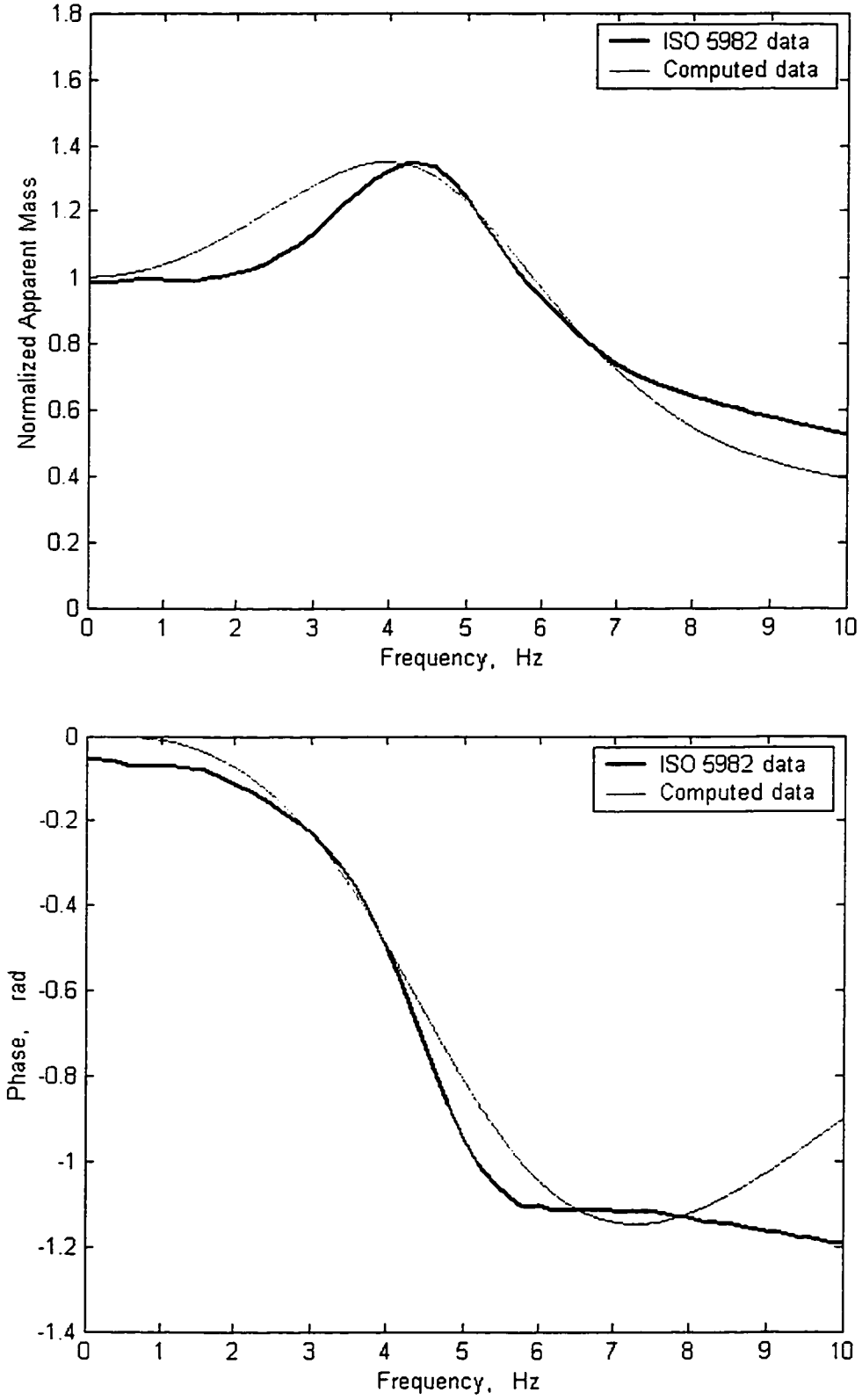

Figure 5.17: Comparison of the computed normalized APMS response with the mean ISO 5982 data.

model parameters. Figure 5.16 illustrates a comparison of the acceleration transmissibility response of the seat "C" with the occupant model with the corresponding measured data.

Generally, the results show a reasonably good agreement between the measured and the computed base-to-seat transmissibility response characteristics. While the base-to-seat transmissibility response, computed from the model, correlates very well with the measured data up to 7 Hz, the normalized APMS response exhibits deviations from the target ISO 5982 data in the 1-3 Hz frequency range and at frequencies above 7 Hz. The peak value of the computed normalized APMS magnitude is in the order of 1.35, which a very similar to the target value. The peak magnitudes, however, occur at slightly different frequencies. The target peak magnitude occurs at a frequency of 4.3 Hz, while the computed peak response reveals peak magnitude near 3.9 Hz. The computed phase response of the model correlates very well with the target data up to 8 Hz.

An eigenvalue analysis performed on the human body model with the identified parameters revealed three modes. The undamped natural frequencies and damping ratios corresponding to these three modes are (i) 4.9 Hz and 0.889; (ii) 5.0 Hz and 0.464; and (iii) 12.1 Hz and 0.899. All of the three modes can be related to the damped response of masses m_3, m_1 and m_2. The larger damping ratios are caused by corresponding to larger damping coefficients or smaller mass.

5.5.2 Response Analysis of the coupled seat-occupant model

The nonlinear occupant-seat systems are analyzed in the SimuLink Toolbox of the MATLAB software to derive the acceleration transmissibility characteristics under

different sinusoidal excitations. The model for seat "C" is analyzed under 2.54 mm, 6.35 mm and 12.7 mm amplitudes of excitation, as described earlier. The analysis of seats "A" and "B" models, however, was limited to 6.35 mm excitation amplitude, as the measured data available only for this excitation.

Figures 5.18 to 5.20 illustrate a comparison of the computed acceleration transmissibility responses of the seat "C" coupled with the identified occupant model under 2.54 mm, 6.35 mm and 12.7 mm excitation amplitudes, respectively, with the corresponding measured data. The Figures also illustrate the responses attained with the reported single-, two-, three- and four-DOF occupant models. The results show that the coupled model with the identified occupant model yields considerably lower resonant frequency under 2.54 mm and 6.35 mm excitations (Figures 5.18 and 5.19). The results

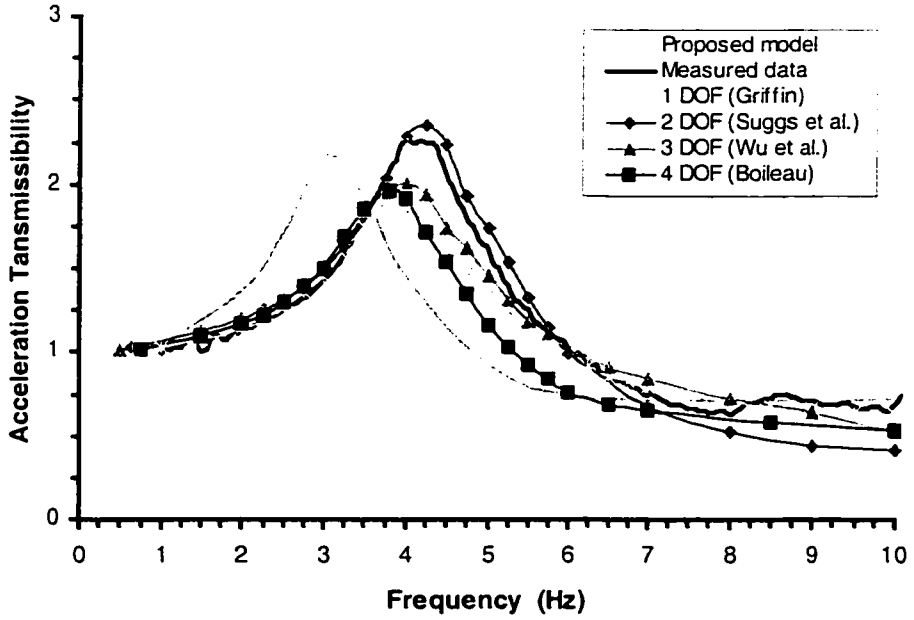

Figure 5.18: Comparison of the model results with measured acceleration transmissibility response of seat "C" (Amplitude: 2.54 mm).

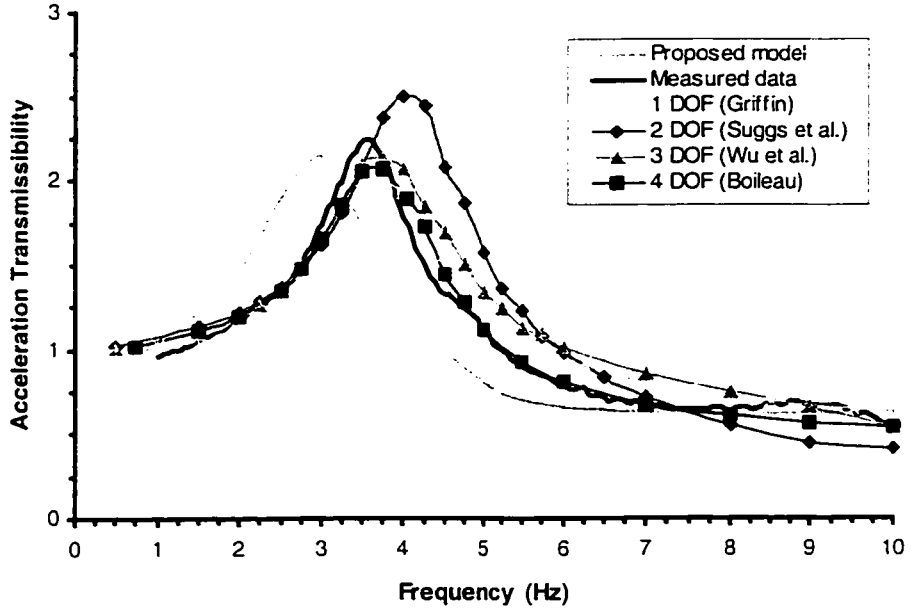

Figure 5.19: Comparison of the model results with measured acceleration transmissibility response of seat "C" (Amplitude: 6.35 mm).

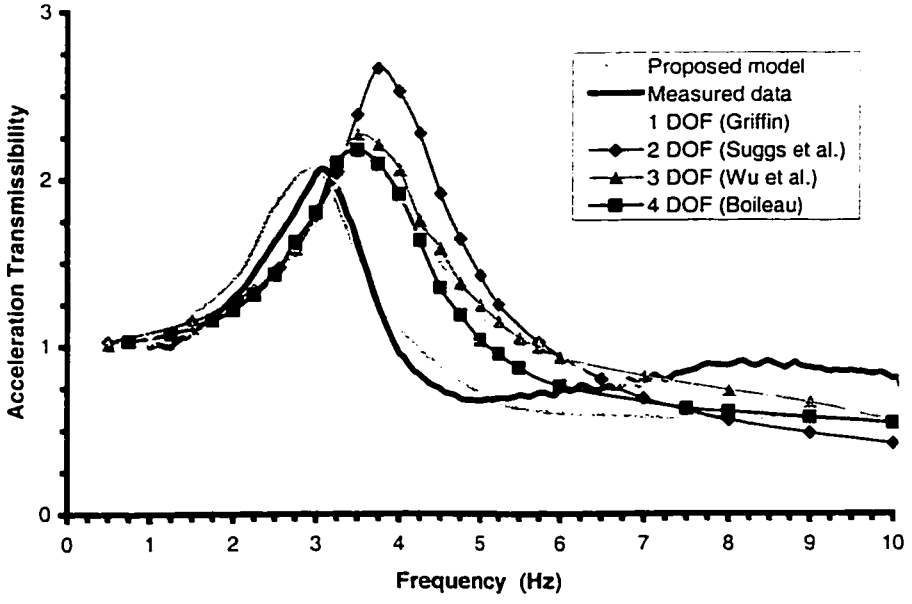

Figure 5.20: Comparison of the model results with measured acceleration transmissibility response of seat "C" (Amplitude: 12.7 mm).

under 12.7 mm excitation, however, are somewhat comparable to the measured data. Such discrepancies between the identified and proposed models and the measured data could be due to two factors. Firstly, the assumption of cushion deflection (A = 6.35 mm) in the operator-point linearization of the seat in error minimization and identification occupant model parameters could contribute to considerable error under lower amplitudes of excitation, where the cushion deflection response could be considerably lower. Secondly, the nonlinearity associated with biodynamic response of the human occupant could yield considerable error in the overall seat-occupant system response.

Figures 5.21 and 5.22 illustrate the comparison of acceleration transmissibility response of seats "A" and "B" models with the corresponding measured data. The

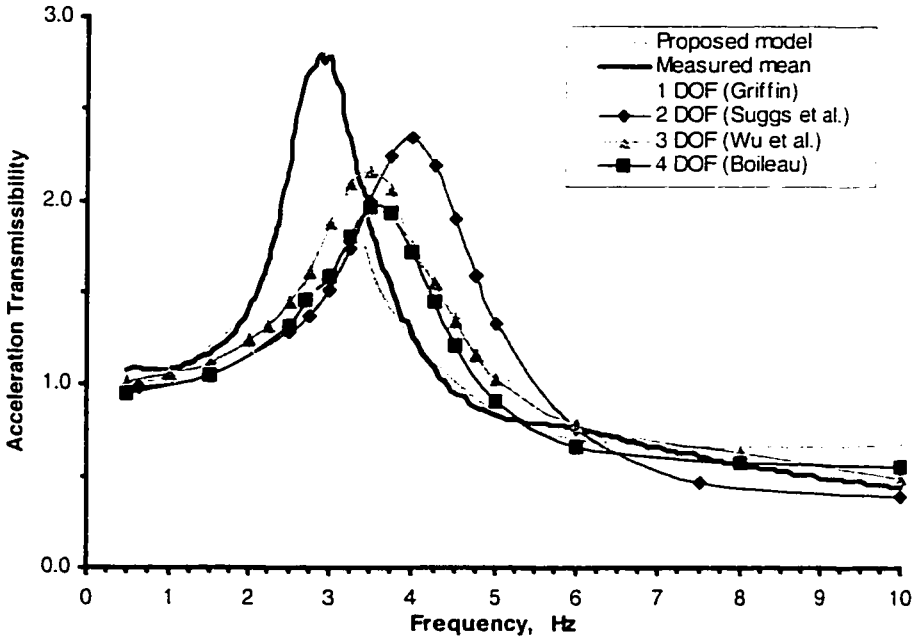

Figure 5.21: Comparison of the model results with measured acceleration transmissibility response of seat "A" (Amplitude: 6.35 mm).

Figures also illustrate the computed responses obtained with the selected reported occupant models and the identified occupant model. In general, the resonant frequencies of the seats "A" and "B" coupled with the identified occupant model are observed to be consistent with the measured mean data. The magnitudes of transmissibility response of those models, however, are observed to be smaller than the corresponding measured mean data. Those derivations could be attained to the operating-point linearization of the seat model about relatively higher deflection amplitude of 6.35 mm.

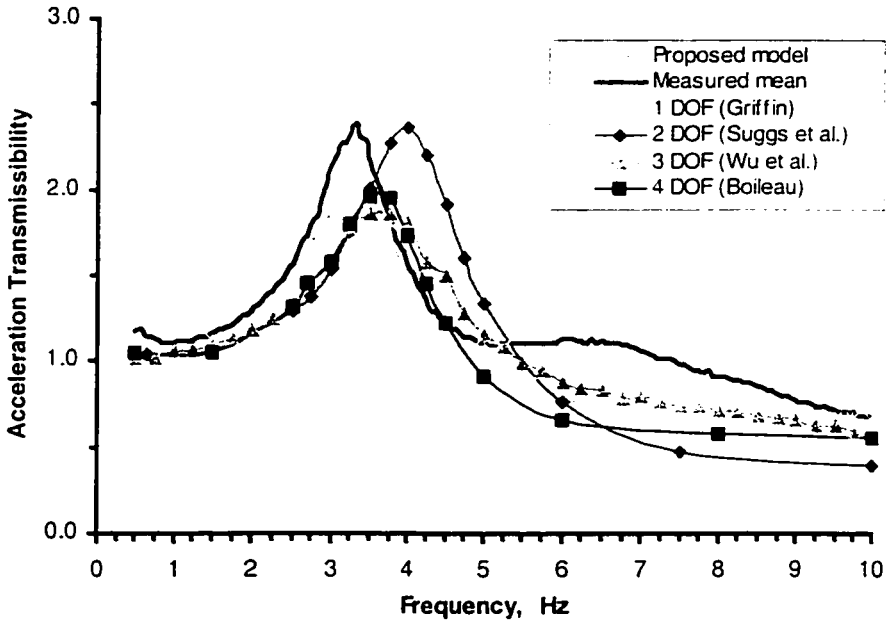

Figure 5.22: Comparison of the model results with measured acceleration transmissibility response of seat "B" (Amplitude: 6.35 mm).

5.6 Summary

In this chapter, the acceleration transmissibility characteristics of seat "C" loaded with a human subject, representing 50th percentile adult population, are measured and

discussed. The transmissibility characteristics are observed to be strongly dependent on the excitation amplitude and posture of the seated human body. The peak transmissibility value decreases with the increase in excitation displacement amplitude and the resonant frequency decreased with the increase in excitation displacement amplitude. Both the peak transmissibility value and the resonant frequency of transmissibility for the subject with back support were smaller than those obtained for the subject without back support.

The seat-occupant system models are formulated by combining the seat models with four different reported human body models, which were derived on the basis of the measured driving-point mechanical impedance or apparent mass and seat-to-head transmissibility responses of the subjects seated on a rigid platform. The vertical seat acceleration transmissibility of the coupled system models are derived under different amplitudes of excitation, and compared with the measurements performed with seat-subject system. The results showed that the coupled-occupant models cannot predict the vibration responses over the selected range of excitation amplitudes and frequencies. The results suggested nonlinearities associated with the biodynamic behavior of the seated human occupant exposed to whole-body vibration. It was further perceived that the body coupling with an elastic seat could also contribute to such deviations. Consequently, an alternate model was identified on the basis of reported APMS data for the subjects seated on a rigid platform and the measured acceleration transmissibility of the seat-occupant system under a specific level of excitation.

Reasonable agreements were observed between the computed and the measured APMS and base-to-seat transmissibility, when a linearized model of the seat was considered under a specific level of excitation. The seated human body model, when

coupled with the nonlinear seat model, however, resulted in acceleration transmissibility considerably different from the measured data under the different levels of excitations. Such deviations were due to the nonlinearities associated with the biodynamic behavior of the occupant and the assumption associated with the operating point linearization of the seat model.

6 CONCLUSION AND RECOMMENDATIONS FOR FUTURE WORK

6.1 Highlights and contributions of the Study

The primary focus of this dissertation research is to study vibration ride comfort performance of occupants seated on car seats and exposed to whole-body vibration. The dissertation research is conducted in six systematic phases including: (i) experimental characterization of seats in terms of force-deflection and force-velocity characteristics as functions of seated load, and nature of excitations; (ii) development and validation of the seat cushion model; (iii) development of the seat model and validation of the seat-rigid mass system model; (iv) parametric sensitivity analysis; (v) development and validation of a coupled human-seat system model by integrating the selected reported biodynamic models of the occupant to the validated seat model; (vi) development and analysis of a three degree-of-freedom linear seated human body model. The major highlights and contributions of this investigation are summarized as follows:

a) Perform laboratory tests to derive the static and dynamic properties of seat cushions as functions of the seated load, excitation frequency and deflection amplitude.

b) Derive a nonlinear seat cushion model based on the measured static and dynamic properties by using least square method and examine the model validity by comparing the computed data with the measured data.

c) Perform laboratory measurements to derive vibration transmissibility characteristics of a car seat loaded with a rigid mass and a subject under three

different amplitudes of swept sinusoidal excitation in the 0.625 – 10 Hz frequency range.

d) Develop an analytical seat model of the seat-mass system for general application and perform simulation to examine the model validity when loaded with a rigid mass.

e) Synthesize a road-measured random excitation of vehicle floor vibration based on a road-measured acceleration power spectral density at the floor of a passenger car.

f) Assess vibration performance of the seat loaded with a rigid mass in terms of various performance measures described in related standards and published studies.

g) Conduct parametric sensitivity analysis for the coupled seat-rigid mass system to study the influence of variations of the seat model parameters on the transmissibility and isolation efficiency under road-measured as well as white noise random excitations of three different amplitudes.

h) Analyze the vibration transmissibility characteristics of the coupled seat-occupant systems, which are derived by combining the three seat models with the four reported biodynamic models of the occupant, and examine the validity of the seat-occupant model by comparing the analytical results with the measured data of acceleration transmissibility.

i) Develop a three degree-of-freedom biodynamic model by minimizing errors between the computed data and standardized data of the biodynamic response

function APMS and the measured seat vibration transmissibility of the coupled occupant-seat system in an attempt to incorporate the coupling effects of the body and the elastic seat.

j) Analyze the acceleration transmissibility characteristics of the coupled seat-occupant systems, which are derived by combining the three seat models with the identified biodynamic model of the occupant, and examine its validity by comparing the model responses with the measured data under different amplitudes of excitation.

6.2 Conclusions

On the basis of the results attained in this dissertation, following major conclusions are drawn:

a) The static stiffness and the hysteresis of a seat cushion are nonlinearly dependent upon the seat deflection and the preload.

b) The dynamic properties of the seat cushion are a strong nonlinear function of the frequency and amplitude of excitation and preload. The amplitude of excitation and preload lay great influence on the dynamic stiffness. The influence of the excitation frequency on the dynamic stiffness, however, is relatively small. Inversely, the equivalent damping coefficients are strongly dependent upon the excitation frequency, while the dependency upon the preload and amplitude of excitation is relatively small.

c) The influences of excitation frequency and amplitude, and the preload on the dynamic properties of a seat cushion depend upon the type of seat, namely the nature of the polyurethane foam.

d) In an effort to develop a seat model for general application, the dynamic properties of the seat are characterized as a nonlinear function of the preload, relative velocity and relative deflection of the cushion.

e) A nonlinear seat cushion model for general application, which accounts for all the three phases of the stress-strain characteristic of the cushion and the cushion bottoming, is successfully developed. The coupled seat-rigid mass system revealed good agreement with the measured data of acceleration transmissibility.

f) A comparison of the acceleration transmissibility characteristics of the seat-rigid mass system with the acceleration transmissibility of the seat-human system revealed significant contributions of the human body to the overall comfort performance of the seat. The vibration attenuation performance of the seat is further enhanced when dynamic interactions of the human body are incorporated.

g) The acceleration transmissibility characteristics of both seat-rigid system and seat-occupant system are influenced strongly by the amplitude of excitation. Both the peak transmissibility value and the resonant frequency of the seat-rigid mass system and the seat-occupant system decrease with increase in the amplitude of excitation.

h) The time-history of a representative random seat-track excitation is synthesized on the basis of the road-measured acceleration power spectral density at the floor of a passenger car. The synthesized excitation could serve as an input in evaluating the seat performance and parametric sensitivity analysis.

i) A coupled seat-rigid mass system, developed upon incorporating the proposed nonlinear seat model and the rigid mass, can serve as an analysis and assessment tool.

j) The results of parametric sensitivity analyses show that an increase in parameters a_1, a_2, a_4 and b_3 cause an increase of peak transmissibility and resonant frequency and a decrease of isolation efficiency.

k) Inversely, an increase in parameters b_1 and b_2, cause a decrease of peak transmissibility and resonant frequency and an increase of isolation efficiency.

l) The results of parametric sensitivity analyses show also negligible effect variation in parameters a_3 and b_4 *on* peak transmissibility, resonant frequency and isolation efficiency.

m) Analyses of acceleration transmissibility of seat-occupant system show that the published human body models, which were derived on the basis of the measured driving-point mechanical impedance or apparent mass and seat-to-head transmissibility responses of subjects seated on a rigid platform, do not account for overall vibration attenuation analysis of the coupled car seat-occupant systems under the conditions investigated in this study.

n) The deviations between the measured and model responses could be attributed to two factors: (i) nonlinearities associated with the biodynamic behavior of the seated occupant that cannot be characterized by the linear biodynamic models; and (ii) the lack of consideration of the elastic interface between the seated body and an elastic seat.

o) The biodynamic model of the seated occupant, identified using the acceleration transmissibility of the coupled seat-occupant system and the APMS of the occupant, provided reasonably good agreements with the measured data under the condition considered for the operating point linearization.

p) The identified occupant model, coupled with nonlinear seat model, however, did not yield notable improvements in the vibration responses of the coupled system. The results thus suggested that nonlinearities associated with the biodynamic behavior of the seated occupants under whole-body vibration need to be considered for the analysis.

q) In an attempt to consider the influence of elastic coupling between the seat and the human body, a three degree-of-freedom linear seated human body model is developed on the basis of both APMS data and the vibration transmissibility characteristics of the coupled system. The use of optimization based error minimization necessitated the operating-point linearization of the seat.

6.3 Recommendations for Future Studies

The following described studies are recommended for future research:

a) In order to minimize the error of the seat cushion model, more than three same band seats are tested and mean of measured data are employed as the basis of characterizing the property of the seat. More candidate seats are involved in the experiments to examine the effectiveness of the methodology. Likewise, more human subjects, who are divided into various kind for representing different preload corresponding to 5^{th}, 50^{th} and 95^{th} percentile body weight, different height corresponding to 5^{th}, 50^{th} and 95^{th} percentile body height, and different shape corresponding to 5^{th}, 50^{th} and 95^{th} percentile body shape, participate in the experiments to obtain more richly and precisely measured data.

b) Further studies in the human body model should consider nonlinearity of the seat model when identifying the parameters of the human body model. Furthermore, FEA linear model and nonlinear model may be studied in developing human body model in order to make more precise human model.

c) Except for the ride comfort performance along vertical direction, horizontal ride comfort performance of seat in the frequency range of interest should be also studied.

d) Study APMS with the coupling effect of the body and the elastic seat.

e) In order to study further the performance characteristics of the seat-human body system in a realistic environment of multiple axes vibration, studies incorporating a full-scale vehicle model are recommended.

REFERENCES

1. International Standard Origination ISO 2631-1. "Mechanical Vibration and Shock– Evaluation of Human Exposure to Whole-Body Vibration", Part 1: General Requirements, Second Edition, 1997, 30pp.

2. J. Ick, "The Application of Flexible Polyurethane foam for automotive Seating.", *Cellular Plastics in Transportation*, 1975.

3. Neil J. Manficld, Michael J. Griffin, "Non-linear in Apparent Mass and Transmissibility During Exposure to Whole-Body Vertical Vibration", *Journal of Biomechanics*, 33, 2000.

4. Griffin, M. J., "Handbook of Human Vibration", *Academic Press*, 1990.

5. Paddan, G.S. and Griffin, M.J., "The Transmission of translational Seat Vibration to the Head. 1. Vertical Seat Vibration", *Journal of Biomechanics 21*, pp191-197, 1988.

6. Dupuis, H. and Zerlett, G., "The Effects of Whole-Body Vibration", *Springer-Verlag*, New York, (1986), 162 pp.

7. Seidel, H. and Heide, R., "Long-term Effects of Whole-Body Vibration: a Critical survey of the Literature", *Int Arch Occup Environ Health*, Vol 58, (1986), 1-26.

8. Hilyard, N.C., Collier, P. and Care, C.M., "Dynamic Mechanical Behavior of Flexible Foam Cushion Materials and Its Influence on Ride Comfort", *The UK Informal Group Meeting on Human Response to Vibration*, The National Institute of Agriculture Engineering, Silsoe, Bedfordshire, England, 14-16 September, 1983.

9. Hilyyard, N.C., "Mechanics of Cellular Plastics", *Macmillan Publishing Co., Inc.*, New York, 1982.

10. Woods, G., "Flexible Polyurethane Foam: Chemistry and Technology", *Applied Science Publishers, Ltd.*, England, 1982.

11. Gibson, L.J. and Ashby, M. F., " Cellular Solids Structure and Properties.", *Pergramon Press*, Inc., New York, 1988.

12. Lee, J. and Ferraiuolo, P., "Seat Comfort.", *SAE Paper 930105*, 1993.

13. Diebschlag, W., Heidinger, F., Kurz, B. and Heiberger, R., " Recommendation for ergonomic and climatic physiological vehicle seat design.", SAE *Paper 880055*, 1988.

14. Rakheja, S., "Computer-Aided Dynamic Analysis and Optimal Design of Suspension System for Off-Road Tractors", *Ph.D. Thesis, Concordia University*, Montreal, Cnanda, 1983.

15. Smith, S. D., "The Effect of Military Aircraft Seat Cushion on Human Vibration Response", The UK Informal Group Meeting on Human Response to Vibration, The Institute of Naval, Medicine, Alverstoke, Gosport, Hants, England, 19-21 September, 1994.

16. Wu, X. and Griffin, M. J., "Simulation Study of factors Inflencing The Serverity of Suspension Seat End-Stop Impacts", *The UK Informal Group Meeting on Human Response to Vibration*, Silsoe Research Institute , Wrest Park, Silsoe, Bedfordshire, England, 18-20 September, 1995.

17. Boileau, P.E. "A Study of Secondary Suspension and Human Driver Response to Whole-Body Vehicular Vibration and Shock", *Ph.D. Thesis, Concordia University*, Montreal, 1995.

18. X. Wu, "Study of Driver-Seat Interactions and Enhancement of Vehicular Ride Vibration Environment ", *Ph.D. Thesis, Concordia University*, Montreal, Canada, 1998.

19. W.N. Patten, S. Sha and C. Mo, "Vibration Model of Open Celled Polyurethane Foam Automotive Seat Cushions", *Journal of Sound and Vibration*, 217(1), pp145-161, 1998.

20. W.N. Patten, and Jian Pang, "Validation of a Nonlinear Automotive Seat Cushion Vibration Model", *Vehicle System Dynamics*, 30, pp55-68, 1998.

21. Tchermychouk, V., "Objective Assessment of Static and Dynamic Seats under Vehicular Vibrations", *M.A.Sc. Thesis, Concordia University*, Montreal, 1999.

22. J.W. Leenslag, E. Huygens and A. Tan, "Recent Advances in the Development and Characterization of Automotive Comfort Seating Foams", *ICI Polyurethane: Polyurethane World Congress 97*, Amsterdam, The Netherlands, 29th September to 1st October 1997.

23. S. Murakami, K. Saiki, M. Hayashi, T. Satou and T. Fukami, "A Newly Developed MDI-Based Polyurethane Flexible Foam for Automotive Seat Cushion Having Both Superior Static and Dynamic Properties", *Journal of Cellular Plastics*, Volume 37-May 2001.

24. Kazushige Ebe and Michael J. Griffin, "Factors Affecting Static Seat Cushion Comfort", *Ergonomics*, vol. 44, NO. 10, pp901-921, 2001.

25. International Standard for Standardization 5982, "Mechanical Vibration and Shock – Range of Idealized Values to Characterize Seated-Body Biodynamic Response Under Vertical Vibration", 2000.

26. P.E. Boileau, S. Rakheja, X.Yang and I. Stiharu, "Comparsion of Biodynamic Response Characteristics of Various Human Body Models as Applied to Seated Vehicle Drivers", *Noise & Vibration Worldwide*, October, 1997.

27. Coermann R. R. , "The Mechanical Impedance of the Human Body in Sitting and Standing Position at low frequencies", *Human Factors*, pp227-253, 1962.

28. Payne, P.R. "Methode to Quantify Ride Comfort and Allowable Accelerations", *Aviation, Space, and Environmental Medicine*, pp262-269, 1978.

29. Fairley, T.E. and Griffin, M.J., "The Apparent Mass of the Seated Human Body: Vertical Vibration ", *Journal Biomechanics*, Vol. 22, No. 2, pp 81-94, 1989.

30. Suggs, C.W., Stikeleather, L.F., et al., "Application of a Dynamic Simulator in Seat Testing", *Trans, of ASAE*, Vol.13, pp378-381, 1970.

31. International Standard for Standardization 5982, "Vibration and Shock – Mechanical Driving Point Impedance of the Human Body", 1982.

32. Allen, G., "A critical Look at Biodynamic Modeling in Relation to Specifications for Human Tolerance of Vibration and Shock", *AGARD Conference Proceedings, Models and Analogues for the Evaluation of Human Biodynamic Response, Performance and Protection*, ppA25.5-15, Paris, France, 6th-10th November.1978.

33. William T. Thomson, "Theory of Vibration with Applications", *Prentice-Hall,Inc.* 1998.

34. Ahmed, A. and S. Rakhejia, "An equivalent Liberalization Technique for Frequency Response Analysis of Asymmetric Dampers", *J. of Sound and Vibration*, 153(3): 1992.

35. Rakheja, S, Boileau, P.-E. and Xuting Wu, "Laboratory Characterization of and Development of Component Models", *CONCAVE 17 - 99, CONCAVE Research Center*, Concordia University, 1999.

36. Amirouche, F.M. and Ider, S.K., "Simulation and Analysis of a Biodynamic Human model Subjected to Low Accelerations – a Correlation Study", *Journal of Sound and Vibration*, 123, pp281-292, 1988.

37. P.R. Payne and E.G.U. Band, "A Four-Degree-of-Freedom Lumped Parameter model of the Seated Human Body", *Aerospace Medal Research Laboratory, Wright-Patterson Air Force Base, Ohio, Report No. AMRL-TR-70-35*, 1971

38. W. Qassem, "Model Prediction of Vibration Effects on Human Subject Seated on Various Cushions", *Medical Engineering and Physics*, V.18, N.5, pp350-358, 1996.

39. Demic, M., "Investigate ion of Human Body Oscillatory Parameters under the Action of Shock Excitations", *ISO document TC 108/SC 4/WG 2 N 158*, 15pp, 1987.

40. T. Belytschko and E. Privitzer, "Refinement and Validation of a Three-dimensional Head-Spine Model", *Aerospace Medical Research Laboratory, Wright-Patterson Air Force Base, Ohio, Report No. AMRL-TR-78-7*, 1971.

41. S. Kitazaki and M.J. Griffin, "A Model Analysis of Whole-Body Vertical Vibration, Using a Finite Element Model of the Human Body", Journal of Sound and Vibration, 200(1), pp83-103, 1997.

42. SAE J1051, "Force Deflection Measurement of Cushioned Components of Seats for Off-Road Work Machines", *Society of Automotive Engineers*, J1051, December 1988.

43. Xuting Wu, Rakheja, and S, Boileau, P.-E. "Study of Human-Seat Interface Pressure Distribution under Vertical Vibration", *International Journal of Industrial Ergonomics*, 21(6), pp433-449, 1998.

44. Rakheja, S.,Peijun Liu, A.K.W. Ahmed and H. Su, "Analysis of An Interlinked Hydro-Pneumatic Suspension", Advanced Automotive Technologies, DSC-Vol. 52, Proceedings of AMSE Winter Ann. Meet., New Orleans, Nov., pp279-288, 1993.

45. Meinecke, E.A. and Clark, R.C., "Mechanical Properties of Polymeric foam", Technomic Publishing Co., 1973.

46. "Static and Dynamic Characterization of Automotive Seats", *CONCAVE Research Center*, Concordia University, Jan. 1997.

47. Smith, S.D., "Nonlinear Resonance Behavior in the Human Exposed to Whole-Body Vibration.", *Shock and Vibration*, 1(5), pp439-450, 1994.

48. Smith, S.D., "Modeling Female vs Male Whole-Body Vibration Response.", *The Twenty-First Annual Meeting of the American Society of Biomechanics , Clemson University, South Carolina, September 24-27*, 1997.

49. Smith, S.D., "Modeling differences in the vibration response characteristics of the human body." *Journal of Biomechanics* , 33, pp1513-1516, 2000.

50. K.Shen, L. Liu, C.Mo, M. Sunwoo and W.N. Patten, "Predictive Feed Forward Control of an Electro-Hydraulic Automotive Seat Motion Simulator", *13th IFAC World Congress. San Francisco*, 1996.

51. L.J.Gibson and M.F. Ashby, "Cellular Solids Structure & Properties", New York, Pergamon Press. 1988.

52. "Estimation of Vibration Transmission of the Seat-Human System Though Measurements of the Seat-Load System", *CONCAVE Research Center*, Concordia University, Jan. 1997.

53. Michael J. Griffin, "Evaluation of Vibration with Respect to Human Response", *Technical paper series 860047, pp11-34, The engineering resource for advancing mobility*, 1978.

54. Wong, J.Y. , "Theory of Ground Vehicle", 2nd.ed. John Wiley & Sons, Inc., 1993.

55. 余志生, "汽车理论", 第二版, 机械工业出版社, 1990.

56. Smith, C.C., McGehee, D.Y., and Healey, A.J., "The Prediction of Passenger Riding Comfort from Acceleration Data", *Journal of Dynamic Systems, Measurement, and Control, Trans. ASME, Vol.100, Series G, No.1, pp34-41*, 1978.

57. Pinhas Barak, "Magic Numbers in Design of Suspension for Passenger Cars.", *SAE Paper 911921*, 1991.

58. Paul H.Wirsching, Thomas L. Paez and Keith Ortiz, "Random Vibration - Theory and Practice", New York : John Wiley & Sons, c1995.

59. 李杰敏, "汽车拖拉机试验学", 第二版, 机械工业出版社, 1996.

60. "MATLAB Application Toolbox – Users' Manual", The MATH WORKS Inc. 1997.

61. "Optimization Toolbox for Use with MATLAB", The MATH WORKS Inc. 1997

62. International Standard Origination ISO 10326. "Mechanical Vibration–Laboratory Method for Evaluating Vehicle Seat Vibration", Part 1: Basic Requirements, 1992.

63. B.Hinz, G.Menzel, R. Bluthner and H.Seidel, "Laboratory Testing of Operator Seat Vibration with 37 Subjects-Critical Comment on ISO/DIS 7096", *Journal of Sound and Vibration*, 215(4), pp977-988, 1998.

64. L. Wei and M. J. Griffin, " Mathematical Models For the Apparent Mass of the Seated Human Body Exposed to Vertical Vibration", *J. of Sound and Vibration*, 212(5), 1998.

65. L. Wei and M. J. Griffin, " The Prediction of Seat Transmissibility from Measures of Seat Impedance", *J. of Sound and Vibration*, 214(1), pp121-137, 1998.

66. C.W. Suggs, C.F. Abrams and L.F. Stikeleather, "Application of a Damped Spring-Mass Human Vibration Simulator in Vibration Testing of Vehicle Seats.", *Ergonomics 12*, pp79-90, 1969.

67. Y.Matsumoto and M.J.Griffin, "Movement of the Upper-Body of Seated Subjects Exposed to Vertical Whole-Body Vibration at the Principal Resonance Frequency", *J. of Sound and Vibration*, 215(4), pp743-762, 1998.

68. H.Brger and B.J.Gilmore, "The Effects of Whole-Body Vibration", New York: Springer, 1986.

69. International Standard Origination ISO 5982. "Vibration and Shock–Mechanical Driving Point Impedance of the Human Body", First Edition, 1981.

70. Barake, P., and Sachs, H., "On the Optimal Ride Control of a Dynamic Model for an Automotive Vehicle System", The Dynamics of Vehicles on Roads and Tracks. Proceedings 9th IAVSD-Symposium Linkoping, Sweden, Jun 24-28, 1985.

71. British Standard Guide to "Measurement and Evaluation of Human Exposure to Whole-Body Mechanical Vibration and Repeated Shock", BS 6841:1987.

72. Paddan, G.S. and Griffin, M.J., "A Review of the Transmission of translational Seat Vibration to the Head.", *J. Sound and Vibration, 215,* pp863-882, 1998.

73. R. Ranganathan and Mudumba Vamsi Mohan, "A Review of the General Effects Whole-Body Vibration", *J. of Vehicle Design*, Vol. 4, 1997.

74. Suzanne D.Smith, "Cushions and Suspensions: Predicting Their Effects on the Biodynamic Responses of Humans Exposed to Vertical Vibration", *J. of Vehicle Design*, Vol.4, 1997.

75. Mats Berg, "A Non-linear Rubber Spring Model for Rail Vehicle Dynamics Analysis", *Vehicle System Dynamics*, 30, 1998.

76. P.Holmlund, R. Lundstrom, L.Lindberg, "Mechanical Impedance of the Human Body in Vertical Direction", *Applied Ergonomics*, 31, 2000.

77. X. Wu, S. Rakheja, and P.-E. Boileau, "Analysis of Relationships Between Biodynamic Response Functions", *J. of Sound and Vibration*, 1999.

78. N.J.Mansfield and M.J. Griffin, "Biodynamic Response of the Seated Person to Vibration: Effect of Posture and Magnitude", *Pare presented at the 12th Conference of the European Society of Biomechanics, Dublin, Ireland.*

79. S.D.Smith, "Factors Influencing the Effects of Seat Cushion Concepts on Human Body Vibration Response", *Presented at North American Congress on Biomechanics*, 1998.

80. P.-E. Boileau, and S. Rakheja, "Whole-Body Vertical Biodynamic Response Characteristics of the Seated Vehicle Driver Measurement and Model Development", *International Journal of Industrial Ergonomics*, 22, 1998.

81. P.-E. Boileau, X. Wu, and S. Rakheja, "Definition of a Range of Idealized Values to Characterize Seated Body Biodynamic Response Under Vertical Vibration", *J. of Sound and Vibration*, V215, 1998.

82. Wu, Xuting, S. Rakheja, and P.-E. Boileau , "Study of human-seat seat interface pressure distribution under vertical vibration". *International J. of Industrial Ergonomics*, 21(6), pp433-449, 1998.

83. Rakeheja, S., V. Tchernychouk and I. Stiharu, "Measurement of vibration transmissibility and ride performance analysis of the seat-human system" CONCAVE report 15-96, submitted to Lear Corporation and GM Corporation, October 1996.